5-1997

Stratigraphy and Structure of Part of the Western Blue Ridge Foothills near Tellico Plains, Southeastern Tennessee

Steven L. Martin
University of Tennessee, Knoxville

To the Graduate Council:

I am submitting herewith a thesis written by Steven L. Martin entitled "Stratigraphy and Structure of Part of the Western Blue Ridge Foothills near Tellico Plains, Southeastern Tennessee." I have examined the final electronic copy of this thesis for form and content and recommend that it be accepted in partial fulfillment of the requirements for the degree of Master of Science, with a major in Geology.

Robert D. Hatcher, Jr., Major Professor

We have read this thesis and recommend its acceptance:

William M. Dunne, Thomas W. Broadhead, G. Michael Clark

Accepted for the Council:
Dixie L. Thompson

Vice Provost and Dean of the Graduate School

(Original signatures are on file with official student records.)

To the Graduate Council:

I am submitting herewith a thesis written by Steven L. Martin entitled "Stratigraphy and structure of part of the western Blue Ridge Foothills near Tellico Plains, southeastern Tennessee." I have examined the final copy of this thesis for form and content and recommend that it be accepted in partial fulfillment of the requirements for the degree of Master of Science, with a major in Geology.

Robert D. Hatcher, Jr., Major Professor

We have read this thesis
and recommend its acceptance:

Accepted for the Council:

Associate Vice Chancellor and
Dean of The Graduate School

Stratigraphy and structure of part of the western Blue Ridge Foothills near Tellico Plains, southeastern Tennessee

A Thesis

Presented for the

Master of Science

Degree

The University of Tennessee, Knoxville

Steven Lee Martin

May, 1997

Dedication

This thesis is dedicated to my parents
for their love and support in helping
me accomplish my goals.

Acknowledgments

Numerous people, both directly and indirectly, were involved in the creation of this thesis. Foremost, I am forever thankful to my major advisor, Prof. Robert D. Hatcher, Jr., for his insight, encouragement, and support throughout this project. I am very fortunate to have had the opportunity to work under his guidance. I would also like to thank my other committee members Dr. William M. Dunne, Dr. G. Michael Clark, and Dr. Thomas W. Broadhead for their comments and assistance during this project. I am also thankful for the Department of Geological Sciences Graduate Teaching Assistantship and the U. T. K. Science Alliance Center of Excellence Distinguished Scientist Stipend for financial support during my graduate enrollment. Additional support from the George D. Swingle Memorial Fellowship Award is also greatly appreciated.

I am very grateful to Mark Carter and Don Geddes for their friendship, field assistance, and discussions on the geology of the Western Blue Ridge. I would also like to thank Camilo Montes for his computer assistance, and to the many other Hatcher students I have had the pleasure of working with. A special thanks to Nancy Meadows and Gina Keeling for their invaluable help and friendships. Thanks also to Leonard Wiener and Carl Merschat (North Carolina Geological Survey), and Dr. Kauko Laajoki (University of Oulu, Finland) for sharing their work and interpretations in some of the same rocks. I would also like to thank Dr. Don W. Byerly for his advice and employment during my undergraduate degree. Many thanks to the many geology students (both graduate and undergraduate) I have had the pleasure of working with and knowing during my undergraduate and graduate degrees at the University of Tennessee. Your friendships have made this experience enjoyable. I am also very grateful to the department office staff (Melody, Cindy, and Denise) who are always willing to help.

Thanks to the rangers and staff at the Tellico and Hiwassee Ranger Districts for keys to gain access to some of the Forest Service roads and maps. Many thanks to the folks of Tellico Plains for their hospitality and access on their property during field work.

A very special thank you to my parents Chuck and Shirley Martin, and the rest of my family. Your love, encouragement, and support have made this endeavor possible. I am especially grateful to Dr. Dan Walker (National Research Council and UT graduate) for his friendship, encouragement, and advise throughout my undergraduate and graduate degrees. Dan, I cannot thank you enough for all you have done for me.

Abstract

The Upper Proterozoic Walden Creek and Great Smoky Groups (Ocoee Supergroup) are a thick sequence of metasedimentary rocks that underlies the western Blue Ridge Foothills in southeastern Tennessee. These rocks represent synrift sedimentation along the Late Proterozoic to Early Cambrian Laurentian margin. They were subsequently deformed and metamorphosed during the Taconic orogeny (Ordovician), then brittlely deformed by northwestward thrusting during the Alleghanian orogeny (Permian). Rejected alternative interpretations suggest that the Walden Creek Group may be Middle Ordovician to Mississippian in age, and deposited in a post-Taconic successor basin, possibly during the Acadian orogeny. Those interpretations require that these rocks were metamorphosed and deformed only during the Alleghanian orogeny.

Detailed geologic mapping (1:12,000 and 1:24,000) of a 191 km^2 (~74 mi^2) area indicates the western Blue Ridge Foothills in southeastern Tennessee consist of Chilhowee Group (Lower Cambrian), Walden Creek Group, and Great Smoky Group lithologies broken by late Paleozoic brittle faults. Rocks assigned to the Great Smoky Group are correlated with the Ammons and Dean formations, whereas rocks of the Walden Creek Group are correlated with the Wilhite and Sandsuck formations. A klippe of quartz arenite on Groundhog Mountain is correlated with the Hesse Quartzite (Chilhowee Group). The contact between the overlying Walden Creek Group (Wilhite Formation) and Great Smoky Group (Dean Formation) is conformable, thus providing an upper bound for the age of the Walden Creek Group. This contact previously has been interpreted as the southern continuation of the Greenbrier fault, as a Middle Ordovician unconformity, and more recently as conformable. The only other conformable contact between formations in the study area is between the Dean Formation and the underlying Ammons Formation (Great Smoky Group); all others are faults. In the Walden Creek

Group, the Wilhite Formation is thrust (Miller Cove fault) onto the Sandsuck Formation, which is thrust (Great Smoky fault) onto Valley and Ridge units.

Rocks within the study area were metamorphosed once, and cut by six regional thrust faults, and four generations of folds and cleavages. Metamorphism during the Taconic orogeny reached chlorite and biotite grade in the study area. During this orogeny, F_1 folds with axial-planar slaty cleavage (S_1) formed along with pressure-solution cleavage (S_{1a}). Brittle Alleghanian deformation resulted in emplacement of the Bullet Mountain, Great Smoky, Maggies Mill, Miller Cove, Rabbit Creek and Oconaluftee faults. These faults separate the western Blue Ridge Foothills in the study area into three thrust sheets (Great Smoky, Miller Cove, and Rabbit Creek thrust sheets). The Bullet Mountain thrust sheet is located in the Valley and Ridge and is interpreted to have been transported northwestward beneath the Great Smoky thrust sheet. F_2 kink folds and S_2 crenulation cleavage formed as a result of this Alleghanian deformation in the Miller Cove thrust sheet. F_3 folds and axial-planar slaty cleavage (S_3) formed in the Great Smoky thrust sheet. Folding of these western Blue Ridge thrust sheets by duplexing of Valley and Ridge footwall units represents the F_4 folding event.

Strain analysis (R_f/ϕ and normalized Fry methods) of ten oriented sandstones from the Walden Creek Group and the Great Smoky Group in three western Blue Ridge thrust sheets yield mean strain ratios (R_{xy}, R_{xz}, R_{yz}) of 1.33, 1.71, 1.3 ($X \geq Y \geq Z$) and 1.61, 2.27, 1.43 ($X \geq Y \geq Z$), respectively. Strains appear to be the result of one or two western Blue Ridge deformation events. The highest strain values occur near Alleghanian brittle faults, and toward the southeast in the direction of increasing metamorphic grade and deformation.

An environmental assessment for a hypothetical residential development within the Sixmile Creek and Rocky Branch watersheds in the study area indicates slope instabilities exist due to mechanical discontinuity characteristics in bedrock, recognition of previous landslides, topography, and climate. Previous landslides within this area are classified as debris slides and debris flows, and were possibly triggered by heavy rainfall events. Extensive development is not recommended in most of the assessment area.

Table of Contents

List of Figures

List of Tables

List of Plates

Chapter I
Introduction

The Ocoee Supergroup is the principal lithostratigraphic unit in the western Blue Ridge of eastern Tennessee, western North Carolina, and northern Georgia (Fig. I-1). It has been interpreted as the product of Late Proterozoic to Early Cambrian synrift sedimentation along the southeastern Laurentian margin (Stose and Stose, 1949; King and others, 1958; DeWindt, 1975; Rankin, 1975; Hatcher, 1972, 1978; Rast and Kohles, 1986). King and others (1958) defined the Ocoee Supergroup in the Great Smoky Mountains National Park as consisting of the Snowbird, Great Smoky, and Walden Creek groups. The sequence was subsequently deformed and metamorphosed during the Taconic orogeny (Ordovician), and deformed again during the Alleghanian orogeny (Permian) (Butler, 1972; Rankin, 1975; Hatcher, 1972, 1978; Kish, 1989; Connelly and Dallmeyer, 1990; Kish, 1991; Woodward and others, 1991; Connelly and Woodward, 1992). Recent hypotheses based on paleontological data suggest that all or part of the Ocoee Supergroup may be younger (Middle Ordovician to Mississippian) than originally thought (Tull and Groszos, 1988, 1990; Unrug and Unrug, 1990; Thompson and Tull, 1991; Unrug and others, 1991; Tull and others, 1993). According to these hypotheses, those units were deposited in a post-Taconic successor basin (possibly during the Acadian orogeny), then were deformed and metamorphosed during the Alleghanian orogeny.

The western Blue Ridge Foothills near Tellico Plains in southeastern Tennessee is a critical area for determining important stratigraphic and structural relationships between groups of the Ocoee Supergroup (Fig. I-2). The bedrock geology here consists of faulted and tightly folded metasedimentary rocks of the Walden Creek and Great Smoky groups. The rolling hills and low mountains of the Foothills belt are underlain by the dominantly fine-grained clastic strata of the Walden Creek Group, whereas the dominantly coarse-

Figure I-1. Geologic map of the western Blue Ridge in southeastern Tennessee, western North Carolina, and northern Georgia. Field area is represented by polygon outlined by heavy black line. Modified from Carter and others (1995a).

Geologic abbreviations: DCF-Dunn Creek fault; GF-Greenbrier fault; GSF-Great Smoky fault; MCF-Miller Cove fault; MMF-Maggies Mill fault; OF-Oconaluftee fault; RCF-Rabbit Creek fault.

Geographic abbreviations: GSMNP BDY-Great Smoky Mountains National Park boundary.

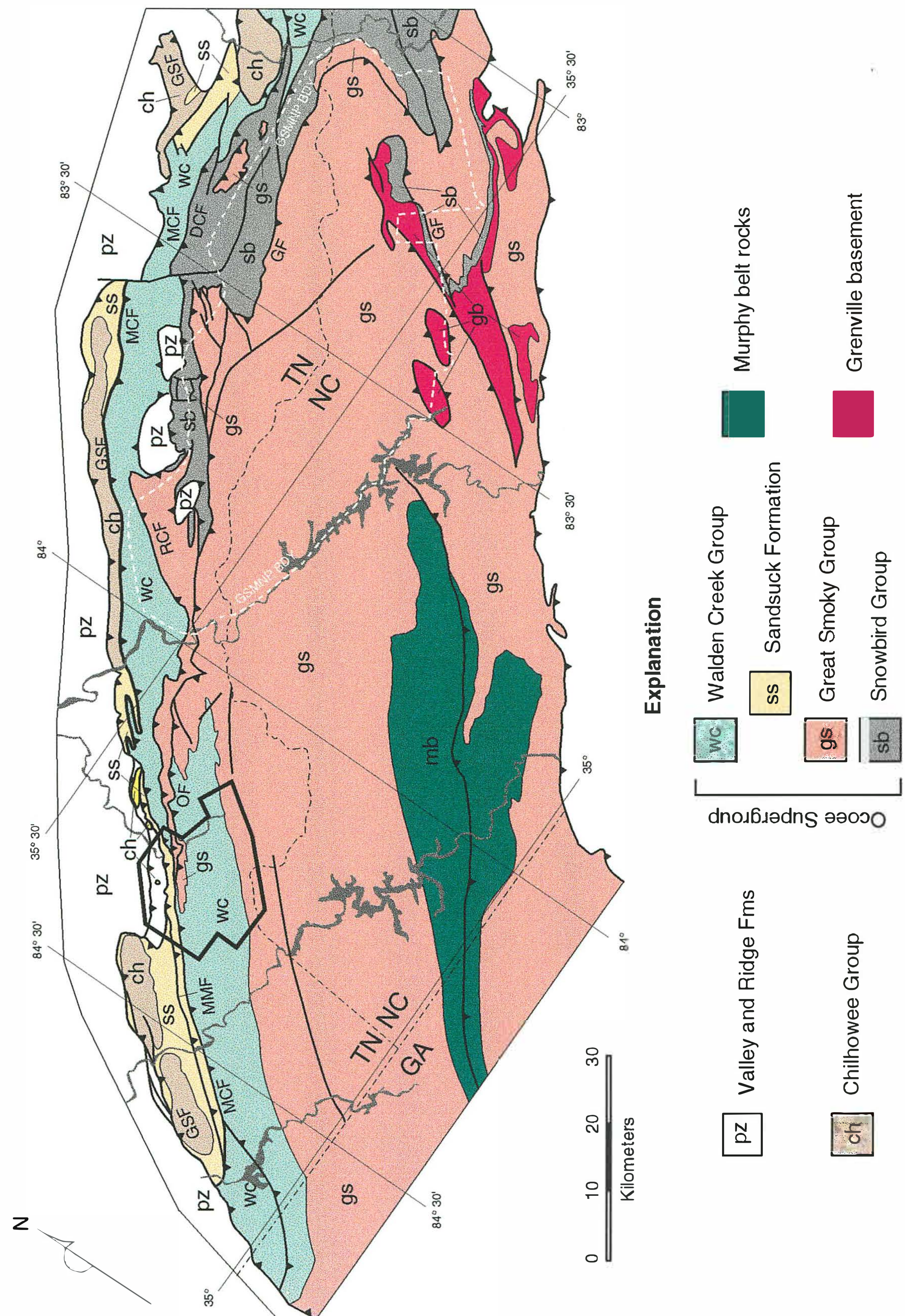
N
Kilometers
0
10
20
30
35°
35° 30'
84° 30'
84°
83° 30'
83°
TN
NC
GA
GSMNP Bdy
pz
ch
ss
wc
gs
sb
mb
gb
GSF
MCF
MMF
OF
RCF
DCF
GF
Explanation
Valley and Ridge Fms
Chilhowee Group
Walden Creek Group
Sandsuck Formation
Great Smoky Group
Snowbird Group
Ocoee Supergroup
Murphy belt rocks
Grenville basement

Figure I-2. Regional geologic map of the western Blue Ridge in southeastern Tennessee showing location of study area (heavy black line) and quadrangle locations. Heavy dashed lines represent the study areas of Carter (1994) and Geddes (1995) to the southwest and northeast of the study area, respectively. Modified from Carter and others (1995a).

Geologic abbreviations: GSF-Great Smoky fault; MCF-Miller Cove fault; MMF-Maggies Mill fault; OF-Oconaluftee fault; RCF-Rabbit Creek fault.

Geographic abbreviations: HR-Hiwassee River; R-Rafter; TP-Tellico Plains; TR-Tellico River.

Quadrangle abbreviations: BJ-Big Junction; BRF-Bald River Falls; FAR-Farner; MCF-McFarland; MEC-Mecca; RAF-Rafter; TP-Tellico Plains; WOF-Whiteoak Flats.

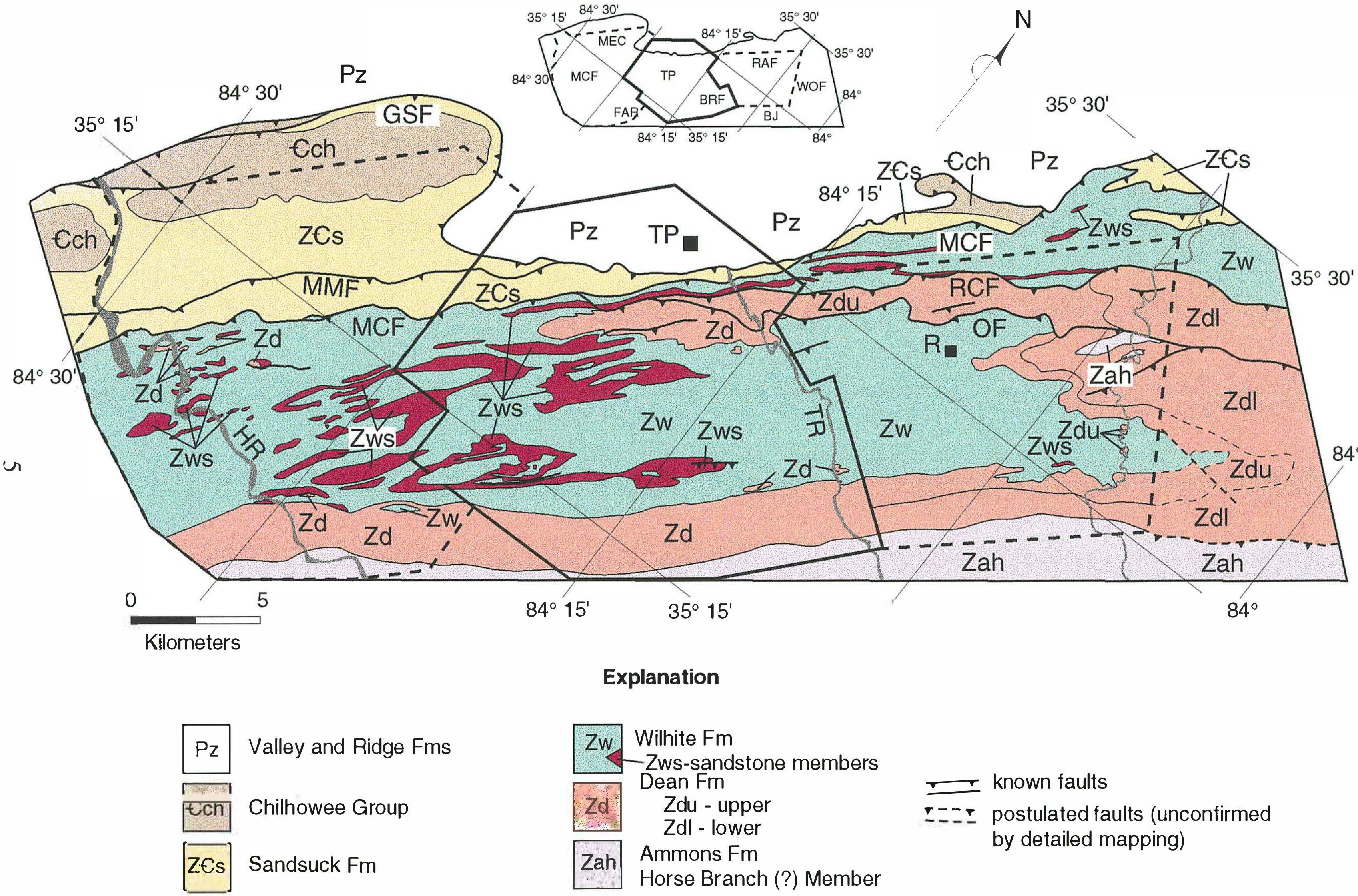
N
35° 15'
84° 30'
MEC
MCF
FAF
TP
BRF
RAF
WOF
BJ
84° 15'
35° 30'
84°
Pz
GSF
Ꞓch
ZꞒs
MMF
MCF
TP
RCF
OF
R
Zdu
Zd
Zdl
Zah
Zw
Zws
HR
TR
0
5
Kilometers
Explanation
Pz Valley and Ridge Fms
Ꞓch Chilhowee Group
ZꞒs Sandsuck Fm
Zw Wilhite Fm
Zws-sandstone members
Zd Dean Fm
Zdu - upper
Zdl - lower
Zah Ammons Fm
Horse Branch (?) Member
known faults
postulated faults (unconfirmed by detailed mapping)

grained clastic strata of the Great Smoky Group underlie the Unaka Mountains belt, which includes the high peaks of the Great Smoky Mountains, and the Unaka Mountains along the state line in southeastern Tennessee and southwestern North Carolina (Fig. I-2; Plate I).

This study focuses mainly on the stratigraphic and structural relationships between the Walden Creek and Great Smoky groups to determine the age and tectonic setting of the sequence. Reports of Silurian to early Mississippian microfossils from the Walden Creek Group (Unrug and Unrug, 1990; Unrug and others, 1991) have raised questions concerning the nature of the contacts between the Walden Creek Group and other units in the western Blue Ridge, as well as the age of these units. This suggestion also affects the interpretations of depositional and tectonic setting for the Walden Creek Group (Tull and Groszos, 1988, 1990; Thompson and Tull, 1991; Tull and others, 1993). The purpose of this study is to provide new data that will help define the stratigraphic and structural relationships, and structural chronologies of the Walden Creek Group in a portion of the western Blue Ridge foothills in southeastern Tennessee.

Location of study area

The western Blue Ridge of eastern Tennessee and western North Carolina can be subdivided into three physiographic subprovinces: (1) the westernmost frontal Blue Ridge fault blocks; (2) the Foothills belt; and (3) the Unaka Mountains belt (Rodgers, 1953). The study area spans part of the Valley and Ridge, the Foothills belt, and includes the westernmost mountain range of the Unaka Mountains belt to the southeast. The area encompasses approximately 191 km^2 (~74 mi^2) near Tellico Plains, Tennessee, and includes portions of the Tellico Plains, Bald River Falls, Farner and Unaka 7.5-minute quadrangles (Fig. I-2). The area is bounded to the northwest by Mocking Crow Mountain, to the northeast by the Tellico River, to the southeast by the Unicoi Mountains, and to the southwest by the Tellico Plains/Mecca 7.5-minute quadrangle boundary (Fig. I-2; Plate I).

Previous work

Some of the most significant geologic investigations of the Ocoee Supergroup in southeast Tennessee have been conducted along the Ocoee River Gorge south of the study area (Fig. I-3). Here, Safford (1856) originally defined the type sections of the Ocoee as the "Ocoee conglomerates and slates," while Hurst and Schlee (1962) were able to distinguish important stratigraphic continuities between major units within the Ocoee Supergroup. These stratigraphic continuities were recently reconfirmed in the Ocoee Gorge (Costello and Hatcher, 1986; Costello, 1993). King and others (1958) provided the modern stratigraphic framework of the Ocoee Supergroup in an extensive study of the geology of the Great Smoky Mountains National Park. Most of the previous geologic investigations near this study area were masters theses by University of Tennessee graduate students: McKinney (1964), Poppelreiter (1980), Carter (1994), and Geddes (1995). Other geologic investigations were conducted by Hale (1974), Merschat and Wiener (1973), Wiener and Merschat (1978, 1981, 1992), and Merschat and Hale (1983) (Fig. I-3).

One of the earliest modern detailed geologic investigations in the Tellico Plains area of southeastern Tennessee was by McKinney (1964), who mapped early Paleozoic strata in the Groundhog Mountain area near Tellico Plains. This area is within the Bullet Mountain thrust sheet and consists of Lower Cambrian Shady Dolomite and Rome Formation thrust northwest over Middle to Upper Cambrian Conasauga Group and Upper Cambrian to Lower Ordovician Knox Group of the Valley and Ridge. Within this area is Groundhog Mountain, which is capped by a clean, medium-grained quartzite. The mountain was previously postulated by Rodgers (1953) to have formed by tight folding of

Figure I-3. Previous geologic investigations in the western Blue Ridge of southeastern Tennessee, southwestern North Carolina, and northern Georgia. Study area is shaded.

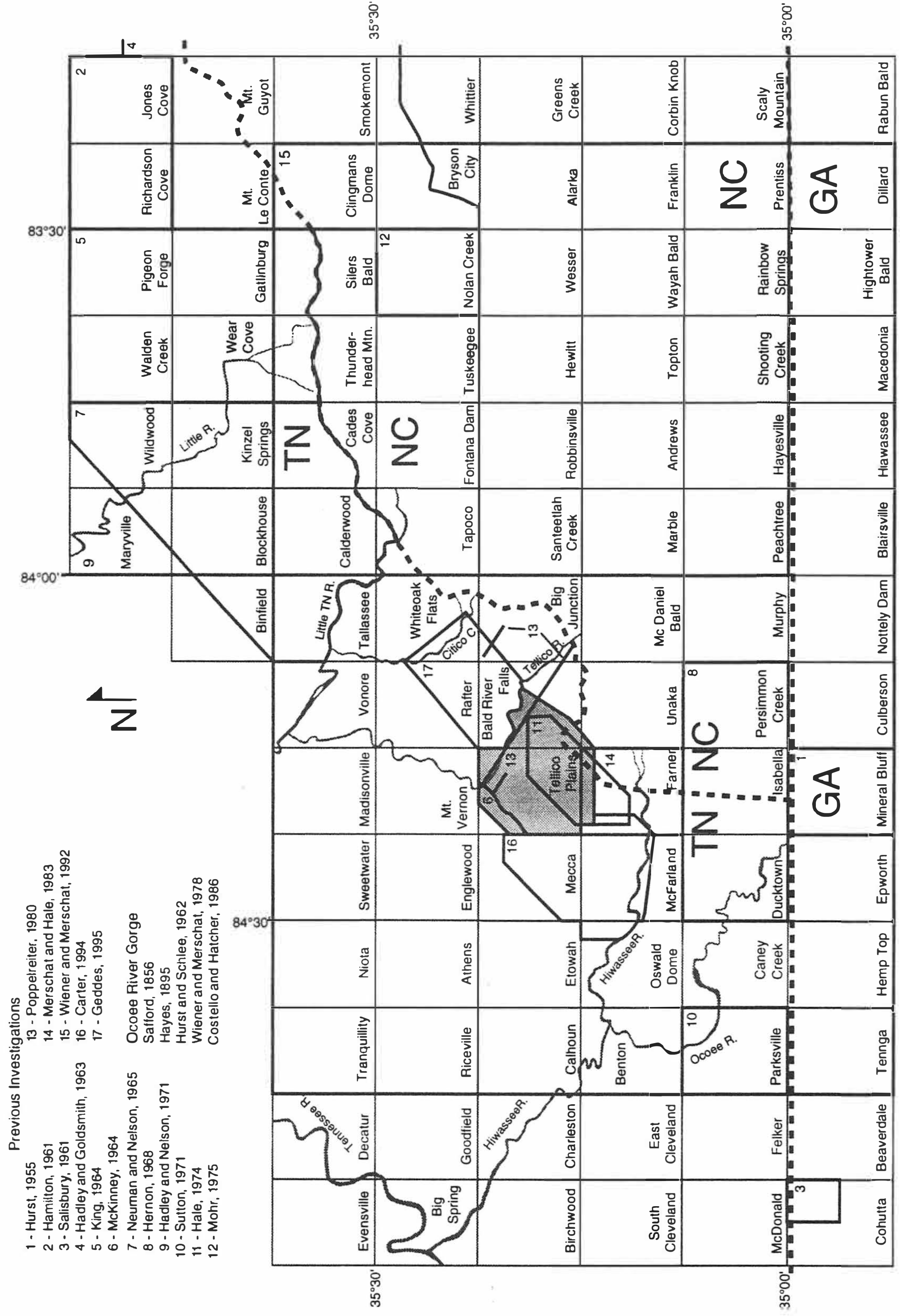
Previous Investigations
1 - Hurst, 1955
2 - Hamilton, 1961
3 - Salisbury, 1961
4 - Hadley and Goldsmith, 1963
5 - King, 1964
6 - McKinney, 1964
7 - Neuman and Nelson, 1965
8 - Hernon, 1968
9 - Hadley and Nelson, 1971
10 - Sutton, 1971
11 - Hale, 1974
12 - Mohr, 1975
13 - Poppelreiter, 1980
14 - Merschat and Hale, 1983
15 - Wiener and Merschat, 1992
16 - Carter, 1994
17 - Geddes, 1995
Ocoee River Gorge
Safford, 1856
Hayes, 1895
Hurst and Schlee, 1962
Wiener and Merschat, 1978
Costello and Hatcher, 1986
N
35°30'
35°00'
84°30'
84°00'
83°30'
TN
NC
GA
Evensville
Decatur
Tranquillity
Niota
Sweetwater
Madisonville
Vonore
Tallassee
Binfield
Big Spring
Goodfield
Riceville
Athens
Englewood
Mt. Vernon
Rafter
Whiteoak Flats
Blockhouse
Calderwood
Maryville
Wildwood
Kinzel Springs
Cades Cove
Walden Creek
Wear Cove
Thunder-head Mtn.
Pigeon Forge
Gatlinburg
Silers Bald
Richardson Cove
Mt. Le Conte
Clingmans Dome
Jones Cove
Mt. Guyot
Smokemont
Birchwood
Charleston
Calhoun
Etowah
Mecca
Bald River Falls
Tellico Plains
Big Junction
Tapoco
Fontana Dam
Tuskeegee
Nolan Creek
Bryson City
Whittier
South Cleveland
East Cleveland
Benton
Oswald Dome
McFarland
Farner
Unaka
Mc Daniel Bald
Santeetlah Creek
Robbinsville
Hewitt
Wesser
Alarka
Greens Creek
McDonald
Felker
Parksville
Caney Creek
Ducktown
Isabella
Persimmon Creek
Murphy
Peachtree
Marble
Andrews
Hayesville
Topton
Shooting Creek
Wayah Bald
Rainbow Springs
Franklin
Prentiss
Corbin Knob
Scaly Mountain
Cohutta
Beaverdale
Tennga
Hemp Top
Epworth
Mineral Bluff
Culberson
Nottely Dam
Blairsville
Hiawassee
Macedonia
Hightower Bald
Dillard
Rabun Bald
Tennessee R.
Hiwassee R.
Ocoee R.
Little TN R.
Little R.
Citico C.
Tellico R.

Lower Cambrian strata with subsequent erosion exposing Chilhowee Group lithologies, which are probably analogous to Glade and Lick Mountains in southwestern Virginia. The Groundhog Mountain klippe may be associated with the Great Smoky fault, either to the main fault surface or to an intermediate slice related to the Great Smoky fault system. McKinney (1964) concluded that the quartzite capping Groundhog Mountain is a klippe of Hesse Sandstone (Chilhowee Group) that has been thrust onto younger Shady Dolomite and Rome Formation. McKinney also interpreted the klippe to be an intermediate slice of upper Chilhowee Group rocks related to the Great Smoky fault system. If this klippe is related to the Great Smoky fault, the fault surface would be warped due to a later stage of deformation, and the strata in the upper plate would be overturned to the southeast. A portion of the southern part of the study area was mapped by Hale (1974), who observed a conformable stratigraphic relationship between the coarser-grained lithologies of the Great Smoky Group and the overlying banded metasiltstones of the lower Walden Creek Group. Hale also mapped sequences of arkosic sandstone within the banded metasiltstones. Poppelreiter (1980) made regional correlations between major structures in the area, and concluded that the contact between the Great Smoky Group and the Walden Creek Group is conformable.

Merschat and Wiener (Merschat and Wiener, 1973; Wiener and Merschat, 1978, 1981; Merschat and Hale, 1983; and Wiener and Merschat, 1992) made alternative interpretations for some of the contact relationships and correlations between major units of the Ocoee Supergroup in southeast Tennessee, southwest North Carolina, and north Georgia. Principally, they interpreted the contact between the Great Smoky Group and the Walden Creek Group to be the southern continuation of the Greenbrier fault, which changes the facing direction or tops of bedding and stratigraphic nomenclature across the contact.

Recently, Carter (1994) and Geddes (1995) mapped and interpreted the geology of the western Blue Ridge Foothills to the southwest and northeast of the study area (Fig. I-2). Detailed geologic mapping by Carter delineated the stratigraphic sequence of the uppermost formations of the Great Smoky Group, the Walden Creek Group, and the lower formations of the Chilhowee Group northeast of the Hiwasee River and southeast of Starr Mountain. Important results of this study included: (1) a stratigraphic contact between the underlying Great Smoky Group and underlying Walden Creek Group in doubly plunging anticlines cored by Great Smoky Group strata; (2) mappable metasandstone units within the metasiltstone lithofacies of the Wilhite Formation (Walden Creek Group); (3) carbonate lithologies in the Sandsuck Formation in the footwall of the Miller Cove fault; (4) a conformable relationship between the underlying Sandsuck Formation and the overlying Chilhowee Group; and (5) regional correlations for the area. Geddes (1995) mapped the area northeast of the study area between Citico Creek and the Tellico River. He delineated the uppermost formations of the Great Smoky Group and Walden Creek lithologies southeast of the Miller Cove fault, and was also able to demonstrate the stratigraphic relationship between the Great Smoky Group and Walden Creek Group. This relationship is present in southwest-plunging second-order anticlines that expose the upper formations of the Great Smoky Group and the overlying Walden Creek Group. An important correlation made in this thesis is the correlation of the upper part of the Cades Sandstone with the Dean Formation of the Great Smoky Group. Both Carter (1994) and Geddes (1995) integrated seismic reflection data (Cook and others, 1983) with surface data to provide evidence for the Foothills duplex beneath the Great Smoky overthrust.

Objectives

The main objectives of this thesis are: (1) determine the lithologies and areal extent of Walden Creek Group and upper Great Smoky Group formations; (2) determine the stratigraphic and structural relationships between the Walden Creek Group and the Great Smoky Group; (3) provide evidence in order to constrain an age interpretation for the Walden Creek Group; (4) determine the amount of internal strain in these units; and (5) complete a hypothetical applied problem that involved evaluation of an area for potential residential development using lithologic, structural, and geomorphic data. Achieving the first four objectives will help formulate conclusions about the age of the Walden Creek Group and model the chronology of tectonic events that have shaped the western Blue Ridge Foothills of the southern Appalachians. Objective five was completed by applying many of the bedrock data, along with additional surficial geologic data, to a problem.

Methodology

This research involved detailed geologic mapping (1:12,000) of the study area (Plate I). Field work was begun, while still an undergraduate in mid-July, 1992, and continued until mid-August, 1992. Mapping resumed in January, 1993, as a graduate student and continued with interruptions to August, 1995, and involved foot traverses along streams, ridges, roads, and highways. Most traverses were across regional strike, spaced closedly enough to permit tracing contacts along strike. Structural measurements of bedding, cleavages, folds, lineations, and fractures were collected from more than 2,300 stations throughout the study area (Plate II) using a Sylva Ranger™ compass. Structural analyses were aided using Stereonet software, developed by R. W. Allmendinger (Cornell University) for the Macintosh personal computer. Petrographic studies were conducted using a Leitz Orthoplan Pol polarizing microscope. Strain studies, using both the R_f/ϕ and normalized Fry method, were performed using software developed by Adolph Yonkee (University of Utah) for the Macintosh personal computer.

Chapter II
Lithostratigraphy

Introduction

The Ocoee Supergroup forms most of the western Blue Ridge province of the southern Appalachians in southeastern Tennessee, southwestern North Carolina, and northeastern Georgia (King and others, 1958) (Fig. I-1). Its thickness has been estimated to be approximately 15 km (50,000 ft), which is dominated by terrigenous clastic sedimentary rocks deposited nonconformably on Middle Proterozoic (Grenvillian) crystalline basement (Hayes, 1900; Keith, 1907a, 1907b; Stose and Stose, 1949; King and others, 1958; Odom and others, 1973; Costello, 1978; McConnell and Costello, 1982, 1984; Costello, 1986; Rankin and others, 1989). The Ocoee Supergroup is overlain by two separate groups of strata. In southeast Tennessee along the western Blue Ridge boundary, the Ocoee Supergroup is conformably overlain by the Lower Cambrian Chilhowee Group (King and others, 1958; King, 1964; Neuman and Nelson, 1965; Walker and Driese, 1991) (Figs. I-1, II-1). To the east in the central Blue Ridge, the Ocoee Supergroup is conformably overlain by the rocks of the Murphy belt (Keith, 1907a; Hurst, 1955; King and others, 1958; Hadley, 1970; Mohr, 1975) (Figs. I-1, II-1).

The Ocoee is divided into three groups; the Snowbird, the Great Smoky, and the Walden Creek Groups (King and others, 1958). An unbroken continuous stratigraphic sequence of the Ocoee Supergroup does not exist due to faulting and probable complexity of the depositional basin geometry. Reconstruction of the Ocoee stratigraphic sequence requires correlation of similar formations across faults, but King and others (1958), Hamilton (1961), and Unrug and Unrug (1990) had problems correlating formations from a hanging wall with similar units in the subjacent footwall. Traditionally, the large body of fine-grained rocks underlying most of the study area is interpreted as belonging to the

Figure II-1. Regional correlations of Late Proterozoic to early Paleozoic stratigraphy in eastern Tennessee and southwestern North Carolina. Number key denotes authors(s) and contributor(s) who defined the stratigraphic unit. No thickness or time durations are indicated by the size of individual blocks. Modified from Carter (1994).

Number key index: 1-Safford (1856); 2-Safford (1869); 3-Hayes (1891); 4-Keith (1895); 5-Campbell (1899); 6-Keith (1903); 7-Keith (1904); 8-Keith (1907a); 9-King and others (1944); 10-Hurst (1955); 11-King and others (1958); 12-King and Furguson (1960); 13-Hurst and Schlee (1962); 14-King (1964); 15-Fairly (1965); 16-Neuman and Nelson (1965); 17-Hernon (1968); 18-Merschat and Wiener (1973); 19-Mohr (1975); 20-Wiener and Merschat (1978); 21-Keller (1980); 22-Wiener and Merschat (1981); 23-Ausburn (1983); 24-Walters and Woodward (1987); 25-Lewis (1988); 26-Unrug and Unrug (1990); 27-Tull and others (1991); 28-Woodward and others (1991); 29-Carter (1994); 30-Geddes (1995).

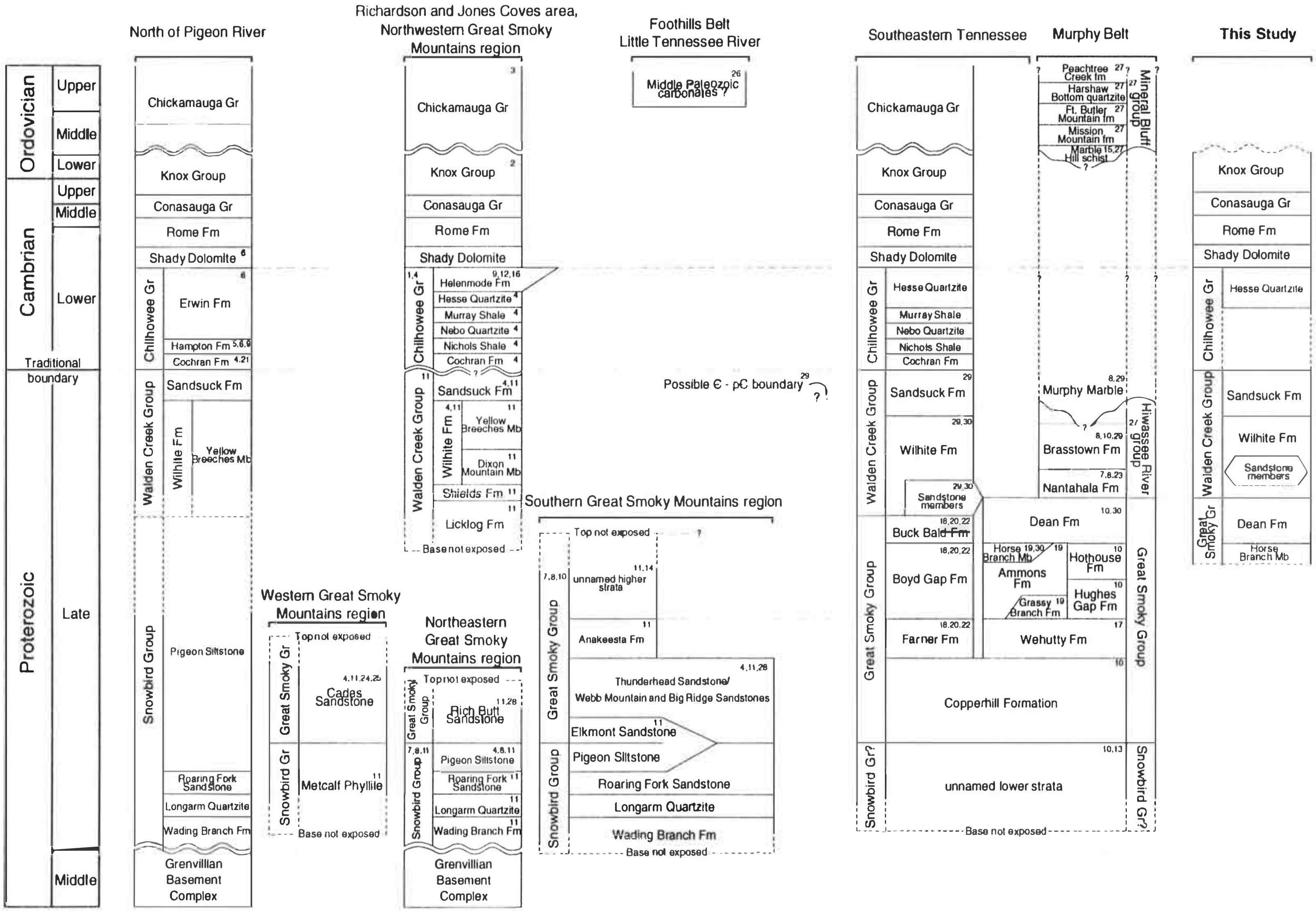

North of Pigeon River
Richardson and Jones Coves area, Northwestern Great Smoky Mountains region
Foothills Belt Little Tennessee River
Southeastern Tennessee
Murphy Belt
This Study
Ordovician
Upper
Middle
Lower
Cambrian
Upper
Middle
Lower
Traditional boundary
Proterozoic
Late
Middle
Chickamauga Gr
Knox Group
Conasauga Gr
Rome Fm
Shady Dolomite
Chilhowee Gr
Erwin Fm
Hampton Fm
Cochran Fm
Walden Creek Group
Sandsuck Fm
Wilhite Fm
Yellow Breeches Mb
Snowbird Group
Pigeon Siltstone
Roaring Fork Sandstone
Longarm Quartzite
Wading Branch Fm
Grenvillian Basement Complex
Helenmode Fm
Hesse Quartzite
Murray Shale
Nebo Quartzite
Nichols Shale
Dixon Mountain Mb
Shields Fm
Licklog Fm
Base not exposed
Middle Paleozoic carbonates ?
Possible Є - pЄ boundary
Western Great Smoky Mountains region
Top not exposed
Great Smoky Gr
Cades Sandstone
Snowbird Gr
Metcalf Phyllite
Northeastern Great Smoky Mountains region
Great Smoky Group
Rich Butt Sandstone
Southern Great Smoky Mountains region
unnamed higher strata
Anakeesta Fm
Thunderhead Sandstone/ Webb Mountain and Big Ridge Sandstones
Elkmont Sandstone
Sandstone members
Buck Bald Fm
Boyd Gap Fm
Farner Fm
Copperhill Formation
Snowbird Gr?
unnamed lower strata
Peachtree Creek fm
Harshaw Bottom quartzite
Ft. Butler Mountain fm
Mission Mountain fm
Marble Hill schist
Mineral Bluff group
Murphy Marble
Brasstown Fm
Nantahala Fm
Hiwassee River group
Dean Fm
Horse Branch Mb
Ammons Fm
Grassy Branch Fm
Hothouse Fm
Hughes Gap Fm
Wehutty Fm

Walden Creek Group. Wiener and Merschat (1978), Merschat and Hale (1983), and Wiener and Merschat (1992) have correlated this body with the Snowbird Group. Detailed accounts of the history of previous stratigraphic investigations of the Ocoee Supergroup were presented by Rodgers (1991) and Carter (1994).

Description of rock units

The following sections are lithologic descriptions of mappable rock units present in the study area, as well as descriptions of the correlated formations as defined by previous investigators. The stratigraphic nomenclature employed here follows that of King and others (1958) for Walden Creek Group strata, and of Hurst (1955) and Mohr (1975) for Great Smoky Group strata (Figs. II-1, II-1; Plate I). Murphy belt nomenclature for Great Smoky Group formations is used here to emphasize the stratigraphic relationship that exists between the rocks that overlie the Great Smoky Group in the western Blue Ridge of southeastern Tennessee and in the central Blue Ridge in southwestern North Carolina. The lowest mappable stratigraphic unit exposed in the field area is the Ammons Formation (Great Smoky Group), which is overlain by the Dean Formation (Great Smoky Group) (Fig. II-1). The Wilhite Formation (Walden Creek Group) follows in the sequence, and conformably overlies the Dean Formation. The Wilhite metasiltstone is the most dominant lithology exposed in the study area (Fig. II-2; Plate I). The Sandsuck Formation (Walden Creek Group) is the highest mappable stratigraphic unit in the field area, and is separated from the Wilhite Formation by the Miller Cove fault. A lithologic description of early Paleozoic strata in the Groundhog Mountain area, as mapped by McKinney (1964), is also included.

Great Smoky Group

The Great Smoky Group is the thickest unit in the Ocoee Supergroup, at an

Figure II-2. Simplified geologic map of study area. See Plate I for detail. Cross sections (Plate III) located along lines A-A', B-B', and C-C'.

Geologic abbreviations: BMF-Bullet Mountain fault; ES-Epperson synclinorium; GRA-Grindstone Ridge anticlinorium; GSF-Great Smoky fault; HBF-Hunt Branch fault; KHA-Kirkland Hollow anticlinorium; MCF-Miller Cove fault; MMF-Maggies Mill fault; OF-Oconaluftee fault; PRA-Payne Ridge anticlinorium; RCF-Rabbit Creek fault; TMA-Tellico Mountain anticlinorium; TPS-Tellico Plains synclinorium; U-upthrown fault block; D-downthrown fault block.

Geographic abbreviation: TP-Tellico Plains.

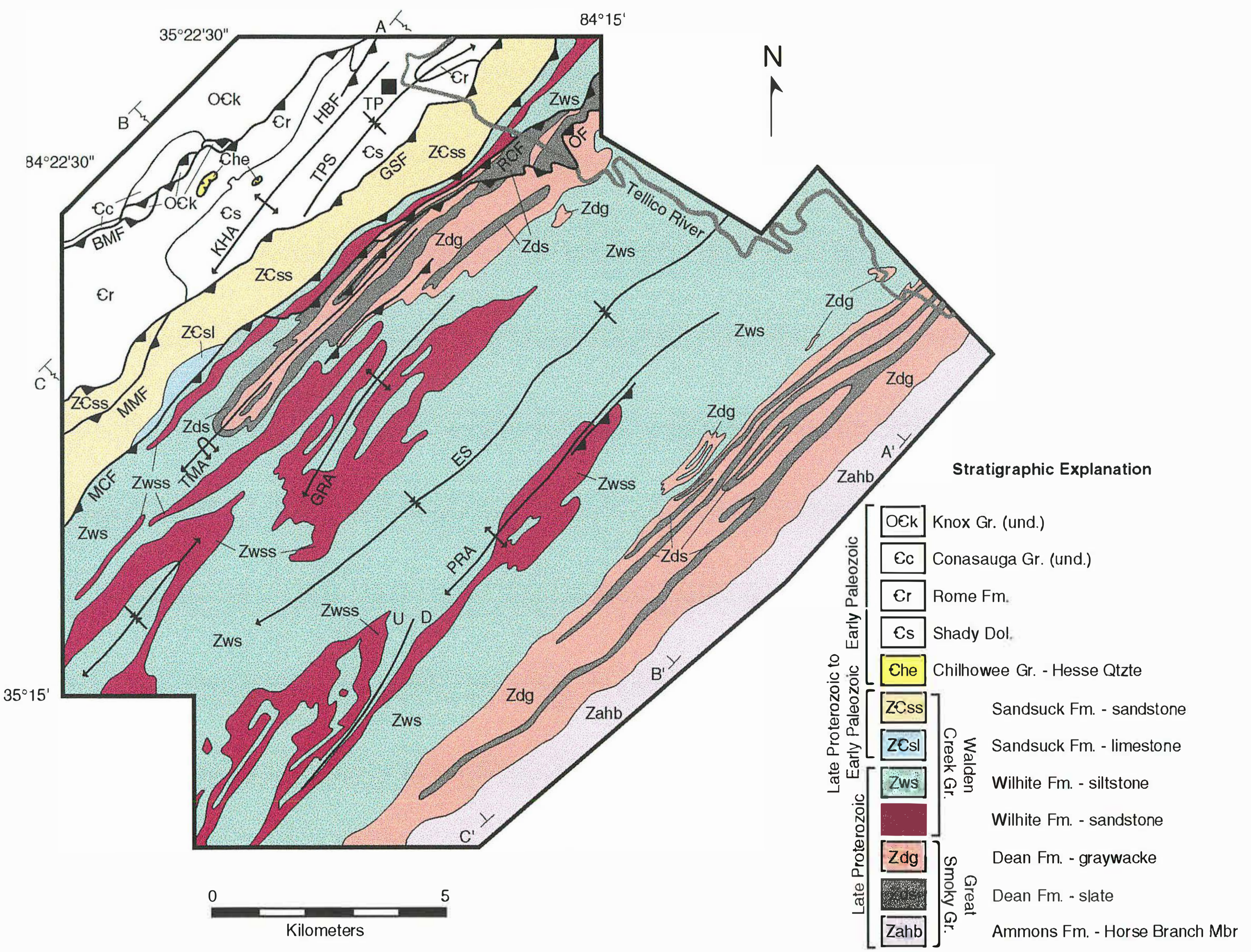

35°22'30"
84°15'
84°22'30"
35°15'
N
Tellico River
Stratigraphic Explanation
Early Paleozoic
OЄk Knox Gr. (und.)
Єc Conasauga Gr. (und.)
Єr Rome Fm.
Єs Shady Dol.
Єhe Chilhowee Gr. - Hesse Qtzte
Late Proterozoic to Early Paleozoic
Walden Creek Gr.
ZЄss Sandsuck Fm. - sandstone
ZЄsl Sandsuck Fm. - limestone
Late Proterozoic
Zws Wilhite Fm. - siltstone
Wilhite Fm. - sandstone
Great Smoky Gr.
Zdg Dean Fm. - graywacke
Dean Fm. - slate
Zahb Ammons Fm. - Horse Branch Mbr
0
5
Kilometers

estimated 8,000 m (25,000 ft) in the Great Smoky Mountains National Park region, and is generally composed of granule to pebble conglomerate, fine- to coarse-grained sandstone, dark silty or argillaceous slate, phyllite, and schist (King and others, 1958; Hadley and Goldsmith, 1963; King, 1964). This massive sequence extends 240 km (150 mi) along regional strike from the Pigeon River in eastern Tennessee southwestward into northern Georgia, and 65 km (40 mi) across regional strike from the foothills of southeastern Tennessee eastward to the flanks of the Murphy syncline of southwestern North Carolina and northern Georgia. The Great Smoky Group is also exposed in the Brasstown Bald and Shooting Creek windows beneath the Hayesville-Allatoona fault system in southwestern North Carolina (Hopson and others, 1989).

The base of the Great Smoky Group through most of its extent in the Great Smoky Mountains National Park is cut off by the Greenbrier fault. In the southeastern portion of Great Smoky Mountains National Park, however, the Great Smoky Group has been interpreted to conformably overlie the Snowbird Group (King and others, 1958). Montes (unpub. M.S. thesis) is currently reexamining the base of the Great Smoky Group near Bryson City, NC, to determine the contact relationship with the underlying Snowbird Group. In southeast Tennessee, along the Ocoee, Hiwassee, and Tellico Rivers, the top of the Great Smoky Group is conformably overlain by the Walden Creek Group (Hurst and Schlee, 1962; Hale, 1974; Poppelreiter, 1980; Costello and Hatcher, 1986, 1991; Carter, 1994; Geddes, 1995; this study). The Great Smoky Group is also conformably overlain by the Hiwassee River Group in the Murphy belt (Hurst, 1955; Tull and others, 1991).

Great Smoky Group lithologies generally consist of pebble conglomerate, graywacke, sandstone and slate (Hurst, 1955; King and others, 1958; Hernon, 1968; Mohr, 1975). The conglomerate is generally a coarser facies of the graywacke, and is characterized by graded beds and poor sorting. These rock types are repetitively interbedded throughout the Great Smoky Group sequence, and the formations are distinguished from each other by the relative abundance of each rock type.

Ammons Formation

The Ammons Formation is a sequence of well-oxidized mica schist, metasiltstone, and sandstone, with an atypical graphitic, laminated schist and metasiltstone member (Horse Branch Member) in the upper 300 m (990 ft) of the formation (Mohr, 1975; Ausburn, 1983). The oxidation state of this unit is greater than most units in the Great Smoky Group, because the mineral assemblages consist of magnetite, pyrite, and epidote rather than graphite, pyrrhotite, and zoisite (Mohr, 1975). The Ammons Formation conformably overlies the Grassy Branch Formation, and is stratigraphically equivalent to the Hothouse Formation of Hurst (1955) and Hernon (1968), and to the upper part of the Boyd Gap Formation of Merschat and Wiener (1973) and Wiener and Merschat (1978, 1981, 1992) (Fig. II-1). Mohr (1975) described the Ammons Formation as fine- to medium-grained felsic graywacke, metasiltstone, quartz-mica schist, and rare conglomerate. The upper 300 m (990 ft) of the Ammons Formation consist of a distinctive dark gray, graphitic, laminated schist, and dark laminated metasiltstone (Mohr, 1975; Ausburn, 1983; Geddes, 1995). The Hothouse Formation, as originally described by Hurst (1955), consists of interbedded graywacke and mica schist. with lesser amounts of conglomerate and quartzite. The thickness of the Ammons Formation is estimated to be 1,200 to 1, 500 m (3,900 to 4,900 ft) (Mohr, 1975), while the Hothouse Formation is estimated to be 2,440 to 3,350 m (8,000 to 11,000 ft) (Hurst, 1955).

Horse Branch Member

The lowest stratigraphic unit exposed in the study area occurs along the southeastern boundary on the southeastern slopes of the Unicoi Mountains in southeastern Tennessee and southwestern North Carolina (Fig. II-2). Lithologically, this unit consists of a medium gray to black, sulfidic and graphitic, medium- to coarse-grained feldspathic graywacke interbedded with dark gray to black, sulfidic. graphitic slate, and metasiltstone (Fig. II-3). Bed thicknesses range from 5.5 cm to 1.0 m for the graywackes, while the metasiltstone contains primary depositional dark and light bands that range from 0.7 to 1.5 cm. This unit is correlated with the Horse Branch Member of the Ammons Formation (Mohr, 1975; Ausburn, 1983; Geddes, 1995) (Figs. II-1, II-2). Mohr (1975) estimated the Horse Branch Member to be about 300 m (990 ft), while Ausburn (1983) estimated the thickness to range between 330 to 1300 m (1,090 to 4,265 ft). The thickness of the Horse Branch Member in the study area is estimated to be approximately 360 m (1,175 ft). Good exposures of this lithology are found along Bald River and U. S. Forest Service roads 126 and 44201 southeast of Basin Gap, Bald River Falls 7.5-minute quadrangle (Plate I).

Dean Formation

The Dean Formation conformably overlies the Ammons Formation, and is the uppermost unit of the Great Smoky Group in southeastern Tennessee and southwestern North Carolina (Hurst, 1955; Hernon, 1968; Mohr, 1975; Geddes, 1995). It is equivalent to the Buck Bald Formation of Merschat and Wiener (1973) and Wiener and Merschat (1978, 1981, 1992) (Fig. II-1). Hurst (1955) defined the Dean Formation as a unit consisting of staurolite-mica schist, cross-biotite schist, quartz metaconglomerate, quartzite, and pseudodiorite interbedded with lesser amounts of phyllite and sericite schist, with metagraywacke and metaarkosic sandstones locally present. These lithologies undergo horizontal and vertical variations along with many breaks in the lithologic sequence (Hurst, 1955). Mohr (1975) defined the Dean Formation as a unit consisting mostly of light gray, thinly bedded to laminated schist, and coarse-grained to conglomeratic felsic metagraywacke. Also occurring within this formation are beds of

Figure II-3. Schematic stratigraphic column for the lithologies exposed in the study area.

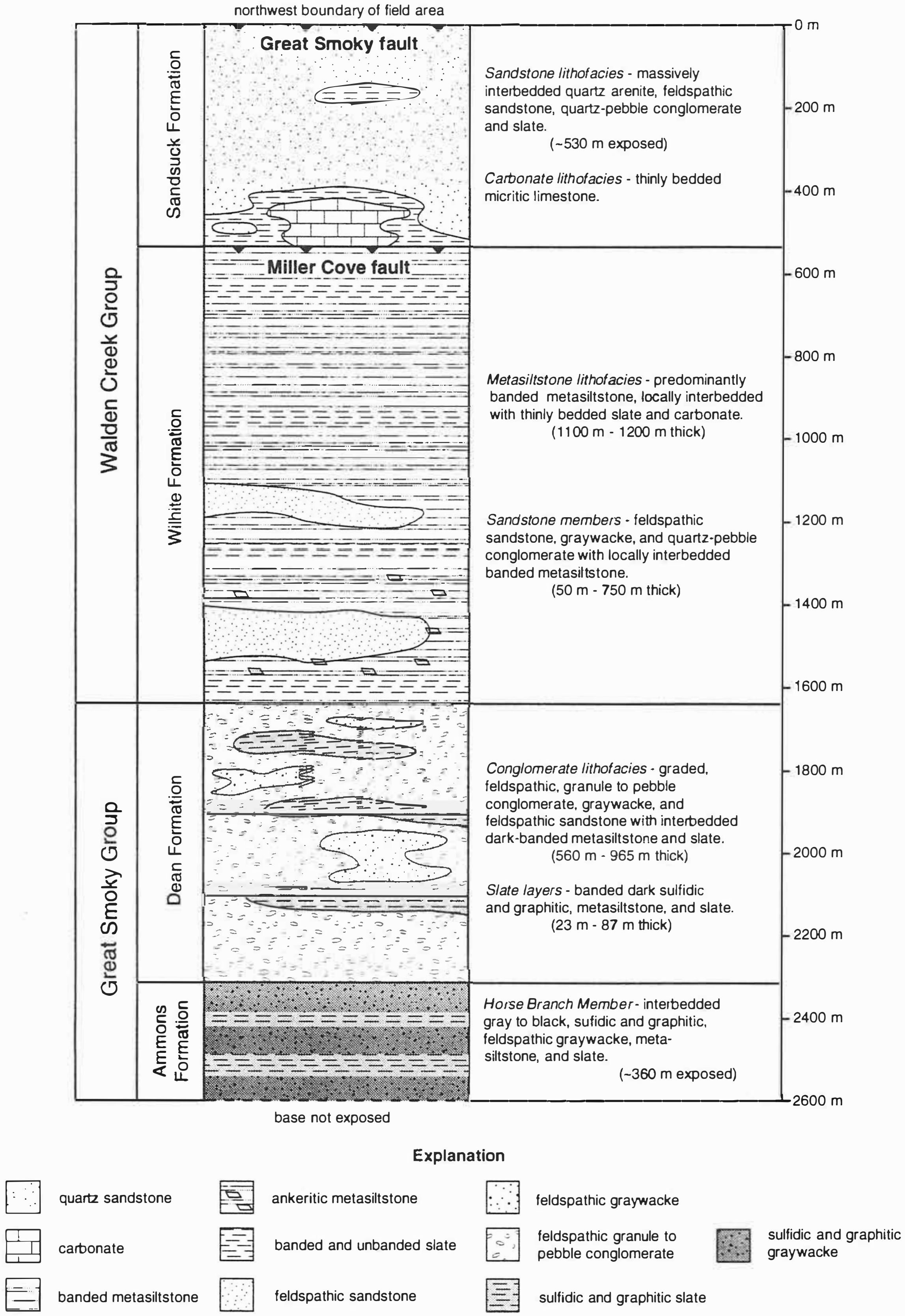
northwest boundary of field area
Great Smoky fault
Miller Cove fault
Walden Creek Group
Great Smoky Group
Sandsuck Formation
Wilhite Formation
Dean Formation
Ammons Formation
Sandstone lithofacies - massively interbedded quartz arenite, feldspathic sandstone, quartz-pebble conglomerate and slate.
(~530 m exposed)
Carbonate lithofacies - thinly bedded micritic limestone.
Metasiltstone lithofacies - predominantly banded metasiltstone, locally interbedded with thinly bedded slate and carbonate.
(1100 m - 1200 m thick)
Sandstone members - feldspathic sandstone, graywacke, and quartz-pebble conglomerate with locally interbedded banded metasiltstone.
(50 m - 750 m thick)
Conglomerate lithofacies - graded, feldspathic, granule to pebble conglomerate, graywacke, and feldspathic sandstone with interbedded dark-banded metasiltstone and slate.
(560 m - 965 m thick)
Slate layers - banded dark sulfidic and graphitic, metasiltstone, and slate.
(23 m - 87 m thick)
Horse Branch Member - interbedded gray to black, sufidic and graphitic, feldspathic graywacke, meta-siltstone, and slate.
(~360 m exposed)
0 m
200 m
400 m
600 m
800 m
1000 m
1200 m
1400 m
1600 m
1800 m
2000 m
2200 m
2400 m
2600 m
base not exposed
Explanation
quartz sandstone
carbonate
banded metasiltstone
ankeritic metasiltstone
banded and unbanded slate
feldspathic sandstone
feldspathic graywacke
feldspathic granule to pebble conglomerate
sulfidic and graphitic slate
sulfidic and graphitic graywacke

quartz-pebble metaconglomerate with minor amounts of metasiltstone and metaquartzite. Both Hurst (1955) and Mohr (1975) estimated the thickness of the Dean Formation to be 750 to 1,000 m (2,500 to 3,500 ft), while Ausburn (1983) estimated the thickness of the Dean Formation to be 1,100 to 1,300 m (3,600 to 4,265 ft).

In the study area, the coarse-grained, graded, granule to pebble conglomerate, feldspathic sandstone and graywacke, and slate exposed in strike belts along the northwest slopes of the Unicoi Mountains in the southeastern portion of the map and along Tellico Mountain in the upper northwest half of the map are correlated with the Dean Formation. These Great Smoky Group lithologies are also exposed in the cores of breached anticlines (whalebacks) beneath the Wilhite Formation to the northwest of the main strike belt mentioned above (Fig. II-2; Plate I). The Dean Formation is divided into two map units in the study area, a conglomerate lithofacies and slate lenses. The thickness of the Dean formation in the study area is estimated to range from 560 to 965 m (1,835 to 3,165 ft) thick.

Conglomerate lithofacies

This heterogeneous lithology consists of an irregularly interbedded succession of light- to dark-gray coarse-grained granule to pebble conglomerate, light gray medium- to coarse-grained graywacke and feldspathic sandstone, black slate, and dark gray metasiltstone (Fig. II-3). Bed thickness in the coarser-grained rocks ranges from 1 to 10 m, while the finer-grained, interbedded slates and metasiltstones have a thickness of less than 1.5 m. Many individual beds contain a complete graded sequence from conglomerate at the base to slate at the top. Other primary sedimentary structures include scour-and-fill features, cross bedding, and soft-sediment folds.

The most prominent lithology present is granule- to pebble-conglomerate and very coarse-grained sandstone (Figs. II-4A, II-4B). Conglomerate clasts consist of poorly to

Figure II-4. Characteristic lithologic features of the conglomerate lithofacies in the Dean Formation (Great Smoky Group). Sample location on top of Tellico Mountain on Tennessee State Highway 68 (station TP-563), Tellico Plains 7.5-minute quadrangle. (A) Granule- to pebble-conglomerate. Centimeter scale. (B) Enlarged image (plane light) of conglomerate thin section. Q=quartz, F=feldspar, and SL=slate clast. Field of view is approximately 3.5 cm wide.

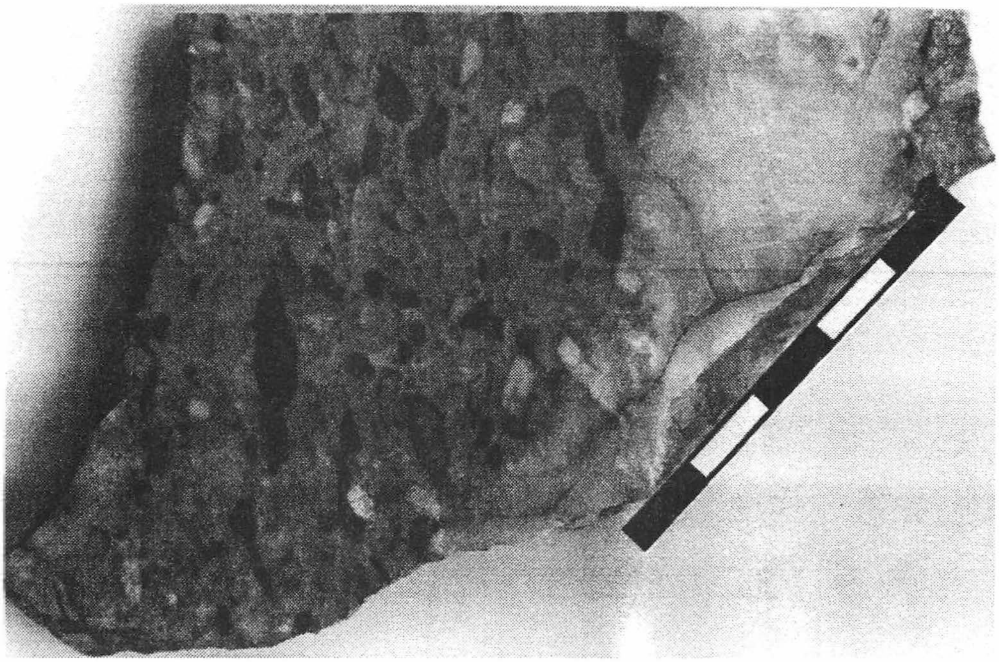

(A)

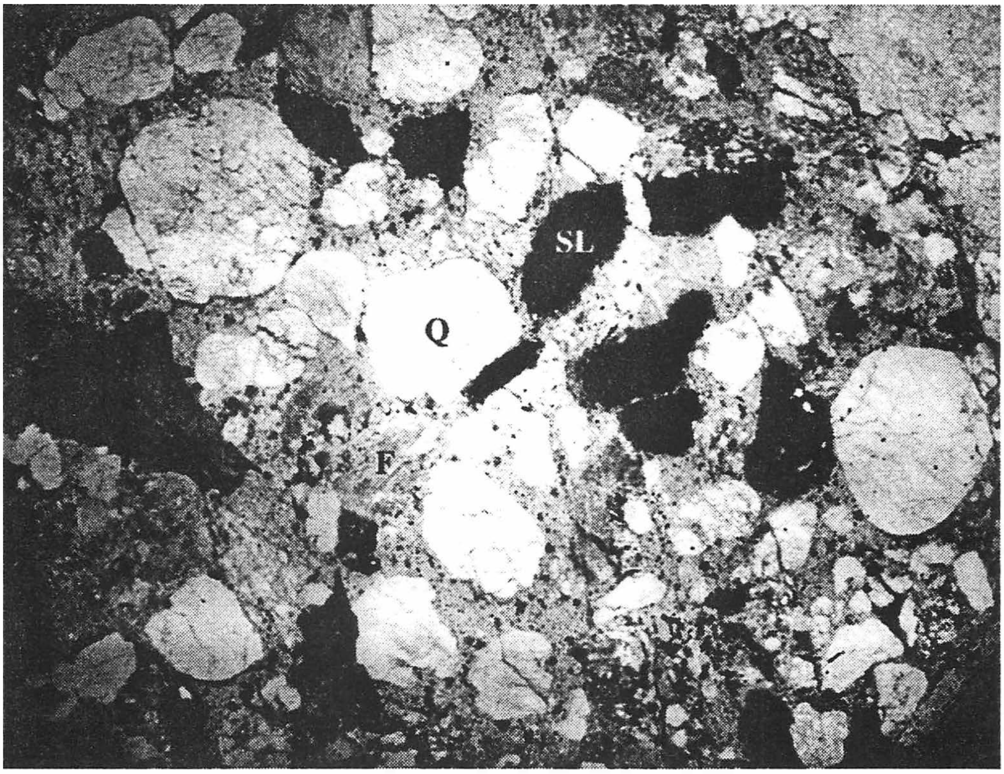

(B)

moderately sorted, rounded to sub-angular, quartz, feldspar, and rock fragments in a coarse sand matrix. Granule-size clasts consist of rounded bluish smoky quartz, and angular plagioclase and potassium feldspar, while pebble-sized clasts include well-rounded milky quartz, and slate chips (Appendix B). Cobble-size clasts are rare, but include limestone, dolomite, and quartzite, along with slate. Most of the medium- to coarse-grained feldspathic sandstones and graywackes are gradational downward into the underlying conglomerates. Other sandstones in this unit grade upward into metasiltstone and slate. The metasiltstone and slate in these graded sequences are commonly 6 cm thick with primary composition layering occurring as rippled bands or laminae. Much of the coarse-grained, graded sequences higher in the stratigraphic section contain greenish banded metasiltstone that is compositionally and texturally similar to the metasiltstone of the overlying Wilhite Formation, but without the ankerite that characterizes the Wilhite metasiltstones in this area. The sandstones consist principally of quartz and feldspar, and range from graywacke, subgraywacke, and feldspathic quartzite to quartzite (Fig. II-5). Matrix consists of metamorphic sericite, chlorite, and biotite that are present in various amounts, along with detrital muscovite and biotite.

Excellent exposures of the conglomerate lithofacies of the Dean Formation in the study area can be found along Tennessee Highway 165 (Tellico River road) at the eastern edge of the Tellico Plains 7.5-minute quadrangle, at Bald River Falls (Bald River Falls 7.5-minute quadrangle), along Tennessee Highway 68 at the top of Tellico Mountain (Tellico Plains 7.5-minute quadrangle), and on Forest Service road 126 leading to Basin Gap (Bald River Falls 7.5-minute quadrangle).

Slate lenses

Interbedded within the conglomerate lithofacies are mappable bodies of slate and metasiltstone. These lenticular units are exposed along the northwest slopes of the

Figure II-5. Classification of coarse-grained rocks of the Great Smoky Group. Present study (black circles) as compared to stratigraphically equivalent Great Smoky Group units (uppermost Great Smoky Group and Buck Bald Formation), and older Great Smoky Group units (Thunderhead Sandstone and Elkmont Sandstone). Diagram modified from Pettijohn (1949).

Number key:

1 - Sample TP-563; TN Hwy. 68 on top of Tellico Mountain, Tellico Plains 7.5-minute quadrangle.

2 - Sample TP-710; TN Hwy. 68 and Graves Mountain, Tellico Plains 7.5-minute quadrangle.

3 - Sample BRF-391; Tellico River 480 m southeast of Bald River Falls, Bald River Falls 7.5-minute quadrangle.

4 - Sample BRF-459; Tellico River 1.8 km southeast of Bald River Falls, Bald River Falls 7.5-minute quadrangle.

5 - Sample BRF-481; Tellico River 1.4 km northwest of Bald River Falls, Bald River Falls 7.5-minute quadrangle.

6 - Sample BRF-846; confluence of Tellico River and Wildcat Creek, Bald River Falls 7.5-minute quadrangle.

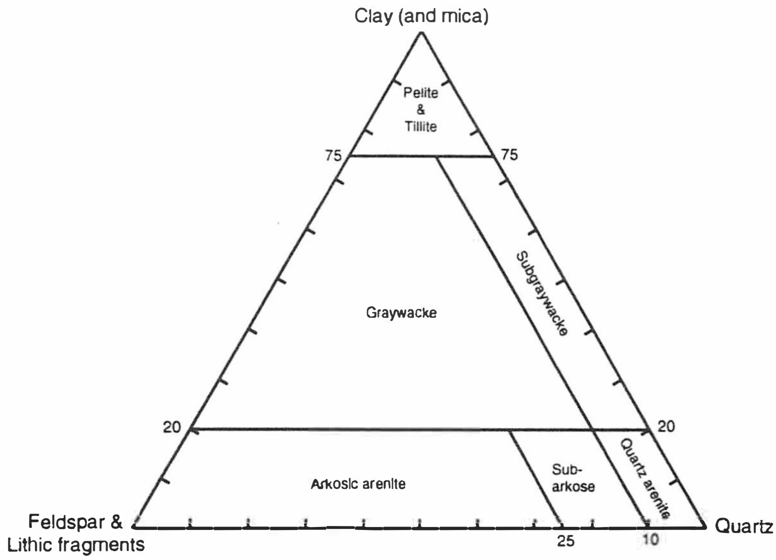

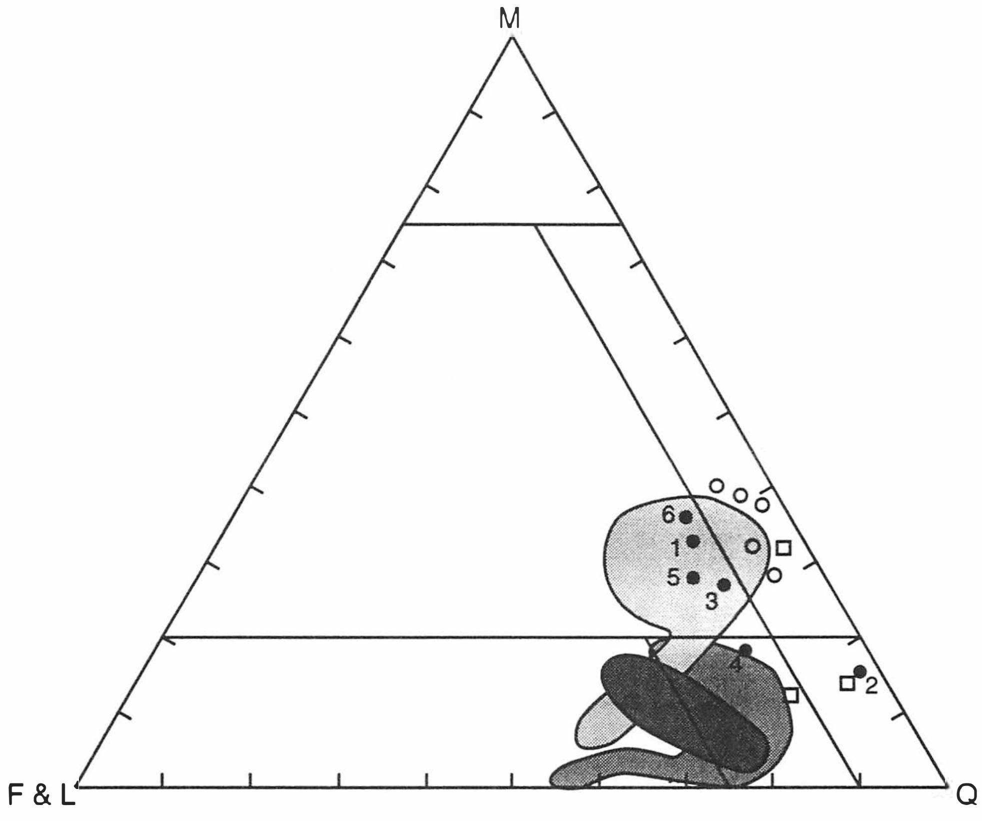

Explanation

- Uppermost Great Smoky Group - Salisbury (1961) (n=10)
- Thunderhead Sandstone - King (1964) (n=12)
- Elkmont Sandstone - King (1964) (n=3)
- □ Buck Bald Formation - Carter (1994) (n=3)
- ○ Dean Formation - Geddes (1995) (n=5)
- ● Dean Formation - this study (n=6)

Unicoi Mountains and along Tellico Mountain (Fig. II-2; Plate I). The slate bodies along Tellico Mountain are thicker than those along the Unicoi Mountains to the southeast, resulting either from original stratigraphic thickness changes or faulting. These fine-grained units consist of black, variably sulfidic and graphitic slate, and light to dark gray banded metasiltstone. The slate bodies located near the top of the unit contain a greater concentration of banded metasiltstone than do the slate bodies lower in the section, with much of the banded metasiltstone being very similar in appearance to the overlying banded metasiltstones of the Wilhite Formation. The upper slate and metasiltstone units are moderately well exposed along Forest Service road 126 northwest of Basin Gap, Bald River Falls 7.5-minute quadrangle. Other good exposures of black slate are located along Forest Service road 126 to Basin Gap, and along Tennessee Highway 68 as the road ascends Tellico Mountain, Tellico Plains 7.5-minute quadrangle. The thicknesses of these slate bodies range from 23 to 87 m (75 to 285 ft) along the southeastern portion of the study area, and to as great as approximately 190 m (630 ft) along Tellico Mountain to the northwest.

Walden Creek Group

The Walden Creek Group is the youngest and most lithologically diverse unit in the Ocoee Supergroup (King and others, 1958) (Fig. II-1). The Licklog, Shields, Wilhite, and Sandsuck formations (oldest to youngest) comprise the Walden Creek Group. It consists of a 2,500 m- (8,000 ft-) thick continuous succession of slate, metasiltstone, sandstone, conglomerate, and carbonate in the Foothills northwest of the Great Smoky Mountains (King and others, 1958; Hamilton, 1961; King, 1964). The Walden Creek Group can be traced from Jones Cove and Richardson Cove (Hamilton, 1961) through the Foothills belt of eastern Tennessee and into northeastern Georgia (McConnell and Costello, 1982). This sequence of strata is dismembered by faulting throughout the Foothills belt in southeastern Tennessee. South of the Little Tennessee River, and within the study area, lower Walden Creek strata (Wilhite Formation) are separated from the Sandsuck Formation by the Miller Cove fault (King, 1964; Neuman and Nelson, 1965; Carter, 1994; this study) (Fig. II-2; Plate I). In the study area, the Walden Creek conformably overlies the Great Smoky Group, while the top of the Walden Creek Group is cut off due to faulting (Great Smoky fault) and is thrust onto the Early Cambrian Shady Dolomite and Rome Formation.

Wilhite Formation

Most of the bedrock in the study area consists predominantly of a greenish-gray banded metasiltstone with intertonguing lenses of sandstone and conglomerate that are assigned to the Wilhite Formation of the Walden Creek Group (Figs. II-2, II-3; Plate I). These predominantly fine-grained rocks gradationally overlie the Dean Formation of the Great Smoky Group. King and others (1958) divided the Wilhite Formation into two members: the Dixon Mountain Member and the Yellow Breeches Member. The Dixon Mountain Member is the stratigraphically lowest member, and consists predominantly of micaceous and sandy siltstone with carbonate concentrated along laminae. The Yellow Breeches Member is characterized by sandy and conglomeratic limestone and dolomite interbedded with slate and metasiltstone. The thicknesses of the Dixon Mountain and Yellow Breeches members are about 450 m (1,500 ft) and 610 m (2,000 ft), respectively.

The Wilhite Formation in the study area is equivalent to the Dixon Mountain Member of the Wilhite Formation, the Shields Formation, and the Licklog Formation north of the Little Tennessee River in the Great Smoky Mountains (King and others, 1958; Hamilton, 1961; Hadley and Goldsmith, 1963; King, 1964; Neuman and Nelson, 1965), and to the Wilhite Formation in northwestern Georgia (McConnell and Costello, 1980, 1982, 1984). The Yellow Breeches Member of the Wilhite Formation is not present in the study area. The rocks correlated with the Wilhite Formation in this study have previously been correlated by Merschat and Wiener (1973), Wiener and Merschat (1978, 1981) Merschat and Hale (1983), and Wiener and Merschat (1992) with the Snowbird Group. Compositionally, the coarse-grained rocks of the Wilhite Formation are more quartz-rich, less feldspathic, and less micaceous than the coarse-grained rocks of the Snowbird Group (King and others, 1958) in the Great Smoky Mountains region (Carter, 1994; this study). Additionally, the fine-grained rocks of the Wilhite Formation are more argillaceous and less current-laminated than the more granular fine-grained Pigeon Siltstone (Snowbird Group) (King, 1964). Both the Wilhite Formation and the Pigeon Siltstone contain carbonate-bearing strata indicated by the occurrence of ankerite along laminae (King, 1964). These rocks are correlated with the Wilhite Formation rather than the Snowbird Group because of the compositional differences.

In the study area the Wilhite Formation consists of a metasiltstone lithofacies with interbedded sandstone (Figs. II-2, II-3; Plate I). The sandstone layers form discontinuous mappable units that consist mostly of coarse-grained rocks and generally lack finer-grained metasiltstone interbeds. The true thickness of the Wilhite Formation is indeterminate because faulting has cut off the top of the section. It is estimated that 1,100 to 1,200 m (3,600 to 4,000 ft) of Wilhite Formation strata is exposed in the study area.

Metasiltstone lithofacies

The metasiltstone lithofacies of the Wilhite Formation is the most dominant lithology exposed in the study area. It consists predominantly of metasiltstone, locally interbedded with slate and thinly-bedded fine-grained sandstone (Fig. II-3). The lower portions of the metasiltstone lithofacies are generally more darker gray, slaty, and calcareous than the upper part. The upper sequences of the metasiltstone lithofacies have more of an olive hue, and are locally sandy, especially in the southwestern portion of the field area. Excellent exposures of the entire sequence of the metasiltstone lithofacies occur along U. S. Forest Service road 210 (Tellico River road), Bald River Falls 7.5-minute quadrangle.

The most common lithology of the metasiltstone lithofacies is fine- to coarse-grained, greenish-gray to dark gray, banded metasiltstone (Figs. II-6A, II-6B). The banding represents primary deposition, and ranges in thickness from 0.2 to 4.0 cm. Bedding is characterized by rythmic, and graded, dark- and light-colored laminae. The fine-grained dark laminae consist predominantly of chlorite and sericite, and represent the more argillaceous parts of the metasiltstones. The coarser-grained light-colored laminae are comprised principally of silt- and very fine sand-size quartz and plagioclase grains, with subordinate amounts of chlorite, sericite, and local carbonate. Sedimentary structures preserved on many beds include ripple marks, dewatering structures, and scour and fill features. The metasiltstones commonly weather to various shades of brown, gray, and a very distinctive maroon or brick red color, which is due to a high concentration of iron (Fe) and manganese (Mn).

Dark-gray to greenish-gray, slightly banded slate and silty slate occur throughout the sandstone lithofacies, but are generally more abundant in the lower sections of the formation near the Great Smoky Group contact. Beds are commonly composed of thinner laminae (< 1.0 cm), which are less prominent and sometimes difficult to distinguish from the green metasiltstones higher in the section. The darker slate in the lower part of the formation is composed primarily of clay, muscovite, chlorite, and silt-sized particles with local occurrences of (and sometimes abundant) ankerite rhombs and pyrite cubes. Often the ankerite and pyrite are weathered and are altered to limonite and goethite pseudomorphs. Hurst and Schlee (1962) recognized similar, but more pyritic black slate above Great Smoky Group lithologies in the Ocoee River Gorge and

Figure II-6. Characteristic lithologic features of the metasiltstone lithofacies in the Wilhite Formation (Walden Creek Group). Sample location at the intersection of Forest Service roads 341 and 341C (station TP-75), Tellico Plains 7.5-minute quadrangle. (A) Primary depositional banding in metasiltstone. Centimeter scale. (B) Enlarged image (negative) of banded metasiltstone thin section. Field of view is approximately 2 cm.

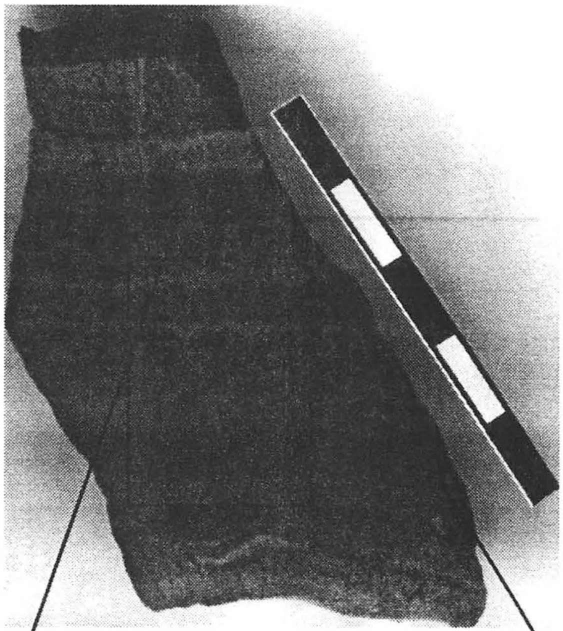

(A)

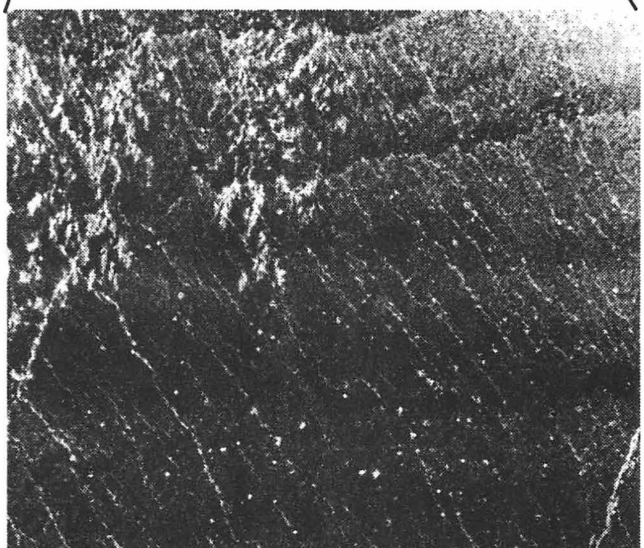

(B)

correlated it with the Nantahala Formation in the Murphy belt to the east. Although lacking the darker color and the abundance of pyrite, the thin black slates near the base of the Wilhite Formation near Bald River Falls have similar composition, texture, and stratigraphic position to the slates in the Ocoee River Gorge. Thus, the lower part of the Wilhite Formation in the study area may be correlative to the Nantahala Formation, possibly representing a distal western facies of that formation (Carter and others, 1993b; Carter, 1994). The best exposures of dark slates can be found in the southeastern portion of the study area along U. S. Forest Service road 210 near Turkey Creek Mountain and Bald River Falls, and U. S. Forest Service roads 126 and 384 at the base of the Gravelstand Top and Waucheesi Mountain, Bald River Falls 7.5-minute quadrangle (Plate I).

The lower sections of the metasiltstone lithofacies, and in minor amounts in the lower sandstone units, contain accessory ankerite (Figs. II-7A, II-7B). Ankerite occurs as aggregates and anhedral to euhedral rhombs, and when fresh has a cream to light tan color. The ankerite weathers rusty brown and may be completely weathered leaving rhomb-shaped voids. Ankerite can comprise as much as 25 percent of the rock mass, although the concentration varies laterally and vertically in a stratigraphic sequence. Ankeritic metasiltstone has previously been reported northeast and southwest of this study area in the Rafter, Whiteoak Flats, and Farner 7.5-minute quadrangles (Hale, 1974; Merschat and Hale, 1983; Carter, 1994; and Geddes, 1995). Geddes (1995) was able to distinguish mappable zones of ankeritic metasiltstone ranging from 120 to 520 m (400 to 1,700 ft) thick. Southwestward, into the present study area, the ankeritic metasiltstones occur as lateral discontinuous zones with the concentration of ankerite varying between each zone. For this reason, the ankerite-bearing metasiltstones are not designated as a mappable stratigraphic unit. The zones of ankeritic metasiltstone were used as marker beds during mapping, and are an indicator of stratigraphic positioning in the metasiltstone

Figure II-7. Characteristics of ankeritic metasiltstone in the Wilhite Formation (Walden Creek Group). Sample location along northwest slope of Tellico Mountain 1.5 km (0.9 mi) southwest of Tennessee State Highway 68 (station TP-343), Tellico Plains 7.5-minute quadrangle. (A) Ankeritic metasiltstone sample containing both fresh and weathered ankerite rhombs. (B) Enlarged image (negative) of ankeritic metasiltstone thin section. Field of view is approximately 7 mm wide. Photo courtesy of Prof. Robert D. Hatcher, Jr.

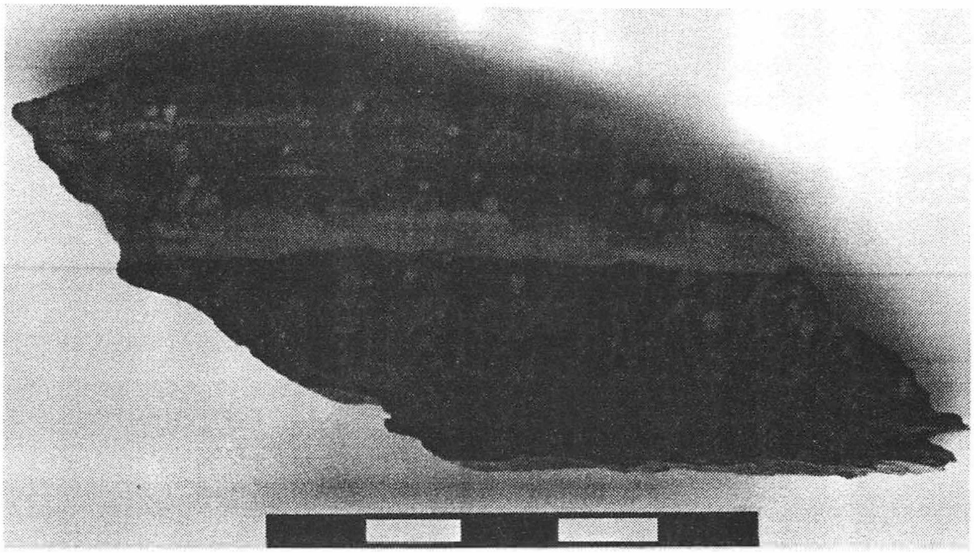

(A)

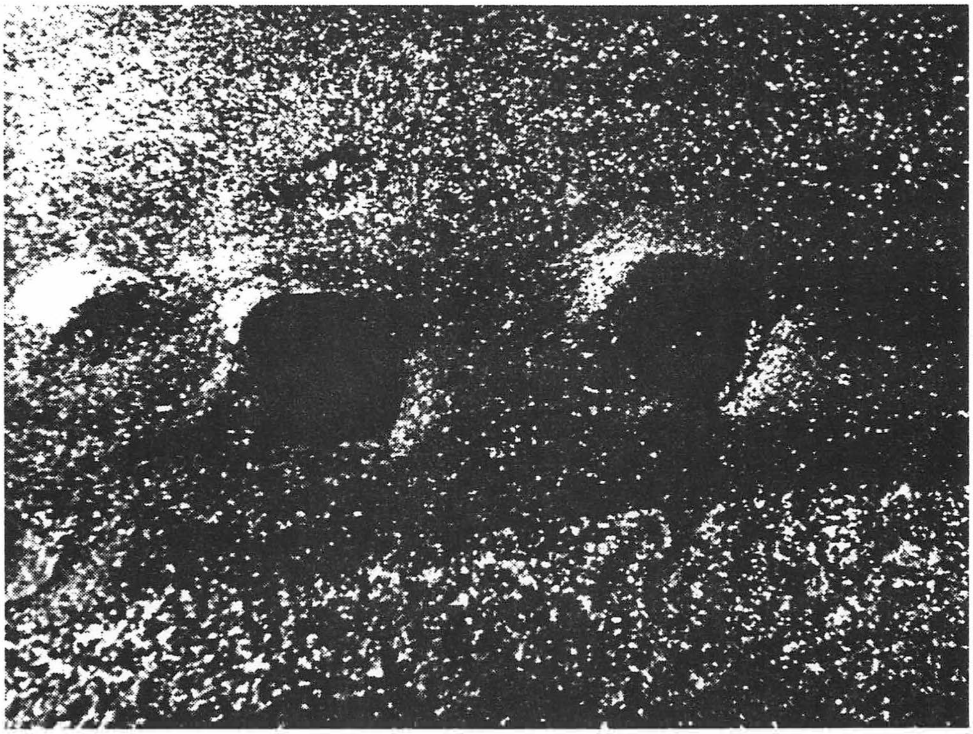

(B)

sequence. In the Coker Creek area of this study and into the Farner 7.5-minute quadrangle to the southwest, ankeritic metasiltstone was observed to have abundant, well-rounded, heavy mineral inclusions in the ankerite aggregates and rhombs (Hale, 1974; Merschat and Hale, 1983). They concluded the heavy mineral inclusions were of the same composition as the groundmass, thus indicating the carbonate was probably a post-depositional metamorphic feature. Good exposures of ankeritic metasiltstone can be found along U. S. Forest Service road 210 (Tellico River road) approximately 1.0 km (3,281 ft) southeast of the confluence of Turkey Creek and Tellico River, Bald River Falls 7.5-minute quadrangle, and at Hot Water Branch 450 m (1, 500 ft) west off Tennessee Highway 68 in the southern portion of the study area, Tellico Plains, 7.5-minute quadrangle.

Sandstone members

The sandstone members of the Wilhite Formation consist predominantly of pinkish-gray to tan, medium- to coarse-grained feldspathic sandstone, conglomerate, and rare metasiltstone in graded beds and interbedded lenses (Figs. II-2, II-3; Plate I). The sandstone members occur as mappable but discontinuous sheets or lenses that vary vertically and laterally in composition and thickness. The lowest sequence of sandstone occurs approximately 300 to 1,100 m (990 to 3,600 ft) above the contact with the Great Smoky Group, and underlies Payne Ridge in the southeastern portion of the study area. The same body of sandstone is also exposed on the northwest limb of the Epperson syncline, underlying the area around Grindstone Ridge and Tellico Mountain, where it is estimated to occur 90 to 150 m (300 to 500 ft) above the contact with the underlying Great Smoky Group (Plate I, Plate III). The southwestward plunging Epperson synclinorium preserves a younger sequence of sandstone bodies, approximately 110 m (360 ft) above the lower sequence of sandstone in the southwestern portion of the study area. These rocks underlie portions of the Coker Creek area, Black Mountain, and Borin Top.

The sandstone bodies are abundant in the central and southwestern portions of the map area and continue southwestward into the Farner and McFarland 7.5-minute quadrangles (Carter, 1994). These sandstone bodies pinch out rather abruptly to the northeast because of possible changes in the depositional environment and proximity to the source. Both the lower and upper sequences of sandstone contain a range of lithologies that are classified as graywacke, subarkose, and quartz arenite (Fig. II-8). The graywacke, subarkose, and quartz arenite lithologies are present in each lens, sheet, or body of sandstone. These lithologies grade vertically and laterally into each other, and do not form distinct mappable units. Each mappable sandstone body does, however, have unique sedimentological characteristics relative to its position in the section. Most of the sandstone bodies are conglomeratic at or near the base of the section. The sandstone units in the lower sequence consist of a quartz-pebble conglomerate with slate chips. The sandstones are generally graywacke with abundant subarkose and quartz arenite, some of which are calcareous. In the upper sequence of sandstones, the lower portion is conglomeratic, but clasts consist of quartz pebbles and lack the slate chips present in the lower sequences. The sandstones are also more lithologically subarkosic with lesser amounts of graywacke and quartz arenite. Metasiltstone is also more abundant in the upper sequences of sandstone. Here, metasiltstone occurs as mappable lenses within the sandstone, and as silty sandstone at the top of the section. The estimated thicknesses of the sandstone members range from 50 to 235 m (160 to 775 ft).

The best exposures of sandstone are found along creeks and near ridge tops. The sandstone beds are massive for the most part and range in thickness from 1 to 4 m. Quartz and feldspar are the primary constituents of the predominantly medium-grained sandstone (Fig. II-9A). Quartz is typically white, with lesser amounts of smoky quartz

Figure II-8. Classification of coarse-grained rocks of the Wilhite Formation. Present study (black circles) compared to other coarse-grained rocks of the Wilhite Formation, and to rocks of the Snowbird Group. Modified from Pettijohn (1949).

Number key:

1 - Sample TP-51v; confluence of Conasauga Creek and Wilson Branch, Tellico Plains 7.5-minute quadrangle.

2 - Sample TP-133; TN Hwy 68 (NW slope of Graves Mountain), Tellico Plains 7.5-minute quadrangle.

3 - Sample TP-289; U. S. Forest Service road 341 H, Tellico Plains 7.5-minute quadrangle.

4 - Sample TP-722; TN Hwy 68 (Coker Creek), Tellico Plains 7.5-minute quadrangle.

5 - Sample TP-928; Tellico River (1,500 ft NW of Tellico Beach), Tellico Plains 7.5-minute quadrangle.

6 - Sample TP-963v; Payne Ridge, Tellico Plains 7.5-minute quadrangle.

7 - Sample TP-998; 1,500 ft NW of the confluence of Conasauga Creek and Payne Branch, Tellico Plains 7.5-minute quadrangle.

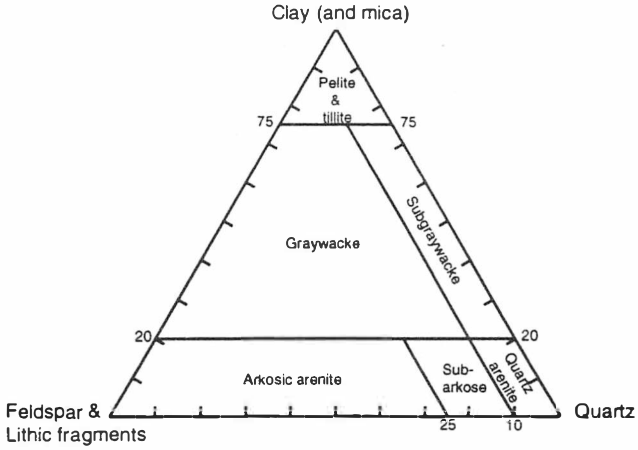

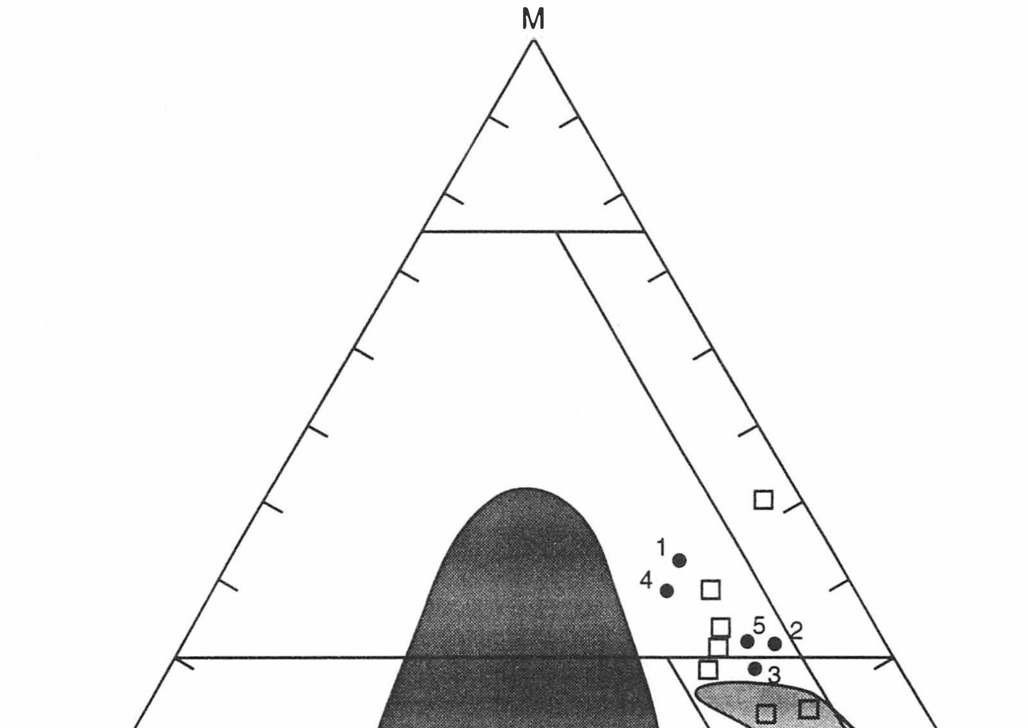

Explanation

- Snowbird Group - King (1964) (n=3)
- Wilhite sandstone - King (1964) (n=7)
- □ Wilhite sandstone - Carter (1994) (n=9)
- ● Wilhite sandstone - this study (n=7)

Figure II-9. Characteristic lithologic features of the sandstone member in the Wilhite Formation (Walden Creek Group). (A) Medium-grained sandstone exposure along Monroe County Highway 2342 (station TP-1097), Tellico Plains 7.5-minute quadrangle. Rock hammer is 32 cm in length. (B) Enlarged image (plane light) of sandstone thin section. Sample location at Grave Mountain on Tennessee State Highway 68 (station TP-133), Tellico Plains 7.5-minute quadrangle. Field of view is approximately 2 cm wide.

(A)

(B)

and rare occurrences of blue quartz. The feldspar (plagioclase) is rarely fresh, and weathers progressively from dirty white to a pinkish tan. Locally interbedded with the sandstone are pebble-size conglomerate that occur as thin- to thickly bedded lenses and graded channels. These lenses and channels are commonly about 1 m thick. The conglomerate consists predominantly of quartz pebbles, with subordinate quartzite, carbonate, and slate chips in a medium-grained subarkose to graywacke matrix. Sedimentary structures include local occurrences of cross bedding, graded bedding, and scour marks.

Petrographically, the sandstones are composed of moderately sorted, subangular to subrounded, quartz and feldspar (andesine) in a clay-rich matrix (Fig. II-9B). Quartz is the primary constituent with subequal amounts of feldspar and mica, warranting the designation of subarkose, graywacke, or quartz arenite, depending on the relative abundance of each constituent (Fig. II-8). Most quartz grains exhibit undulatory extinction, elongation, and flattening parallel to foliation, and, where closely packed, recrystallization occurs along grain boundaries. Feldspar grains are less abundant than quartz, but are similar in shape and size, and have undergone a greater degree of replacement by mica and carbonate. Many feldspar grains have been sericitized. The matrix consist mainly of sericite and chlorite with minor amounts of calcite, muscovite, and biotite. Accessory minerals include pyrite, hematite, magnetite, tourmaline, and zircon (Appendix B).

Sandsuck Formation

The Sandsuck Formation is the uppermost unit of the Walden Creek Group and, in the study area, is separated from the underlying Wilhite Formation by the Miller Cove fault (Figs. II-1, II-2; Plate I). In the study area, the Sandsuck Formation consists of sandstone, conglomerate, shale, and carbonate, and underlies Mocking Crow and Pine

Mountains and the adjacent valley to the southeast. These rocks are separated into sandstone and carbonate lithofacies, and are correlated with the lower member of the Sandsuck Formation of Carter (1994) (Figs, II-1, II-2; Plate I). The true thickness of the Sandsuck Formation is indeterminate here because the top and bottom of the formation are cut off by the Great Smoky and Miller Cove faults, respectively. The exposed thickness of the Sandsuck Formation in the study area is estimated to be 530 m (1,735 ft).

Sandstone lithofacies

The sandstone lithofacies of the Sandsuck Formation consists of massively interbedded quartz arenite and subarkosic sandstone, quartz-pebble conglomerate, and shale (Fig. II-3). The coarse-grained sandstone comprises most of the section and is more abundant and conglomeratic lower in the section. Shale and siltstone horizons are rare in the lower sections, but become more abundant higher in the section. The dominant lithology of parts of the sandstone lithofacies is a weathered, coarse-grained, light brown quartz arenite and grayish-brown, subarkosic sandstone (Fig. II-10). Fresh exposures of this lithofacies are rare, but when fresh the quartz arenites are tan, and the subarkosic sandstones are dark gray. These coarse-grained sandstones form massive beds up to about 2 m thick, and sedimentary structures, such as graded bedding and cross bedding, are rare. Locally interbedded with the coarse-grained sandstone is quartz-granule to pebble conglomerate. The conglomerate is moderately graded and discontinuous, with beds approximately 1 m thick. The siltstone and shale lithologies are medium gray when fresh, and weather to distinctive terra cotta brown chips. These fine-grained lithologies form thin beds about 5 to 10 cm thick, and commonly grade from shale and fine-grained siltstone to coarser-grained siltstone and fine-grained sandstone. The siltstone and shale are locally interbedded with the coarse-grained sandstone in the lower section of the sandstone lithofacies, but increase and thicken higher in the section enclosing the

Figure II-10. Classification of coarse-grained rocks of the Sandsuck Formation and Chilhowee Group. Present study (circles) compared to other coarse-grained rocks of the Sandsuck Formation and Chilhowee Group in southeastern Tennessee. Modified from Pettijohn (1949).

Number key: 1 - Sample TP-1388; TN Hwy 165 along the Tellico River, Tellico Plains 7.5-minute quadrangle.

2 - Sample GH-2; Groundhog Mountain, Tellico Plains 7.5-minute quadrangle.

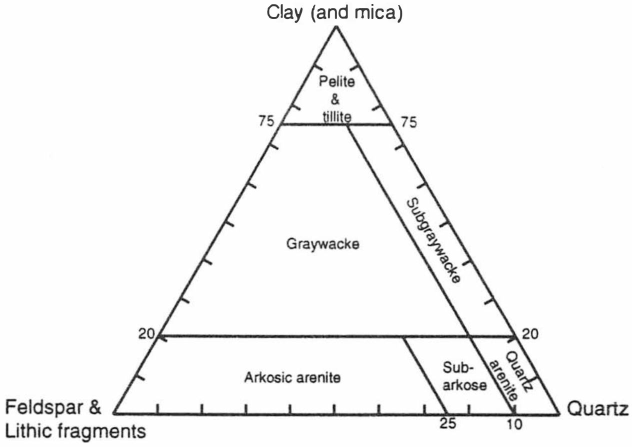

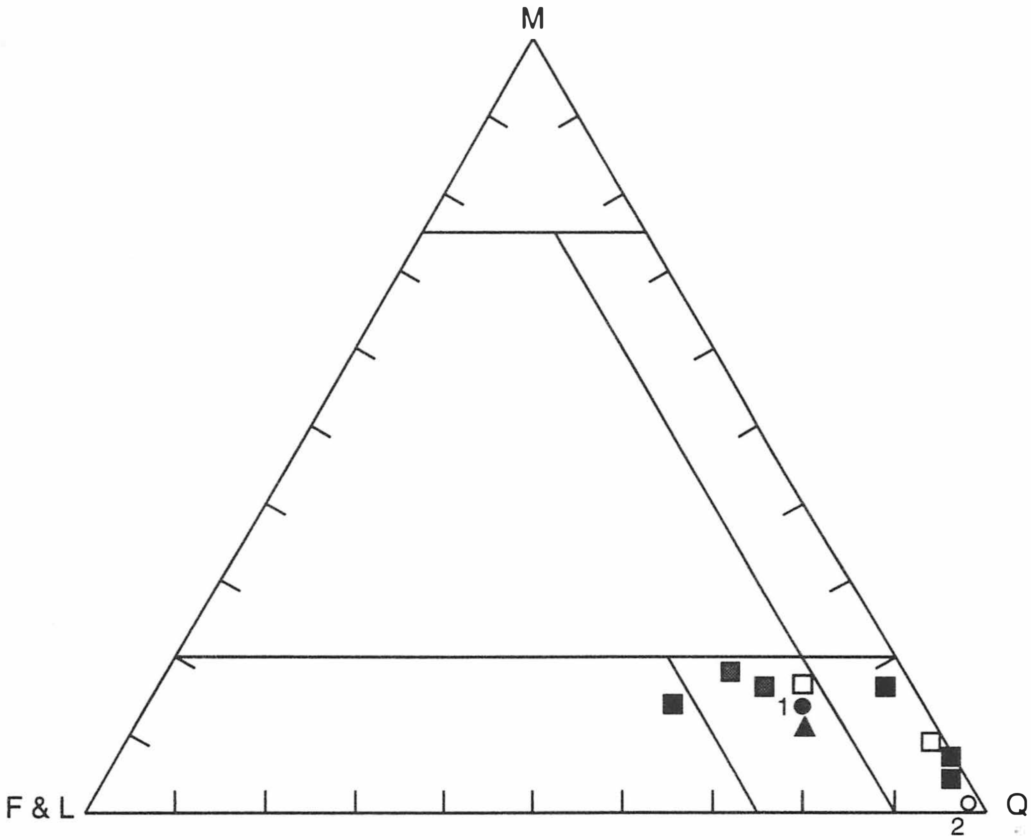

Explanation

- ■ Sandsuck Formation (lower member) - Carter (1994) (n=4)
- ■ Sandsuck Formation (middle member) - Carter (1994) (n=2)
- □ Sandsuck Formation (upper member) - Carter (1994) (n=2)
- ▲ Cochran Formation (Chilhowee Group) - Carter (1994) (n=1)
- ● Sandsuck Formation - this study (n=1)
- o Hesse Quartzite (Chilhowee Group) - this study (n=1)

carbonate at the top of the unit. Siltstone and shale are the dominant lithology underlying the valley southeast of Mocking Crow Mountain.

Compositionally, the rocks of the sandstone lithofacies consist of moderate to well-sorted, subrounded quartz, with minor amounts of feldspar and matrix-forming clays (Fig. II-11A). Quartz grains are typically monocrystalline with one type of detrital quartz, rather than the polycrystalline quartz grains common in the coarse-grained rocks of the Wilhite Formation. Unlike the coarse-grained rocks of the Wilhite Formation, the feldspar in the sandstone lithofacies is predominantly microcline with lesser concentrations of plagioclase. Accessory minerals include weathered hematite and/or pyrite, tourmaline, and zircon (Appendix B). The dominant constituent of the conglomerate is milky quartz, with subordinate feldspar (plagioclase) and various lithic fragments in a finer-grained, quartz-rich sandy matrix.

Carbonate lithofacies

The carbonate lithofacies of the Sandsuck Formation consists of a dark gray, fine-grained micritic limestone (Figs. II-2, II-3; Plate I). The carbonate is exposed only at the base of the northwest slope of Queens Mountain (Tellico Plains 7.5-minute quadrangle), and is interpreted to occupy a small, flat valley at the confluence of Conasauga Creek and Steer Creek. This discontinuous mappable lens of limestone is bounded at the top by the Miller Cove fault, and is interbedded with the shale and sandstone in the upper sections of the sandstone lithofacies This limestone unit is correlative with the limestone mapped by Carter (1994), because of similar lithologic and stratigraphic position of these rocks in the Maggies Mill fault block. Carter (1994) assigned the carbonate lithologies to the lower member of the Sandsuck Formation because: (1) the carbonate lithologies are enclosed by and interbedded with lithologies distinctly different from similar carbonates correlated with the Yellow Breeches Member of the Wilhite Formation (Hamilton, 1961;

Figure II-11. Characteristic lithologic features of the sandstone lithofacies in the Sandsuck Formation (Walden Creek Group) and quartz arenite in the Hesse Quartzite (Chilhowee Group). (A) Enlarged image (plane light) of sandstone thin section. Sample location along Tellico River on Tennessee State Highway 165 near Tellico Plains City Limits (station TP-1388), Tellico Plains 7.5-minute quadrangle. Field of view is approximately 2 cm wide. (B) Enlarged image (plane light) of quartz arenite thin section. Unoriented sample from Groundhog Mountain, Tellico Plains 7.5-minute quadrangle. Field of view is approximately 2 cm wide.

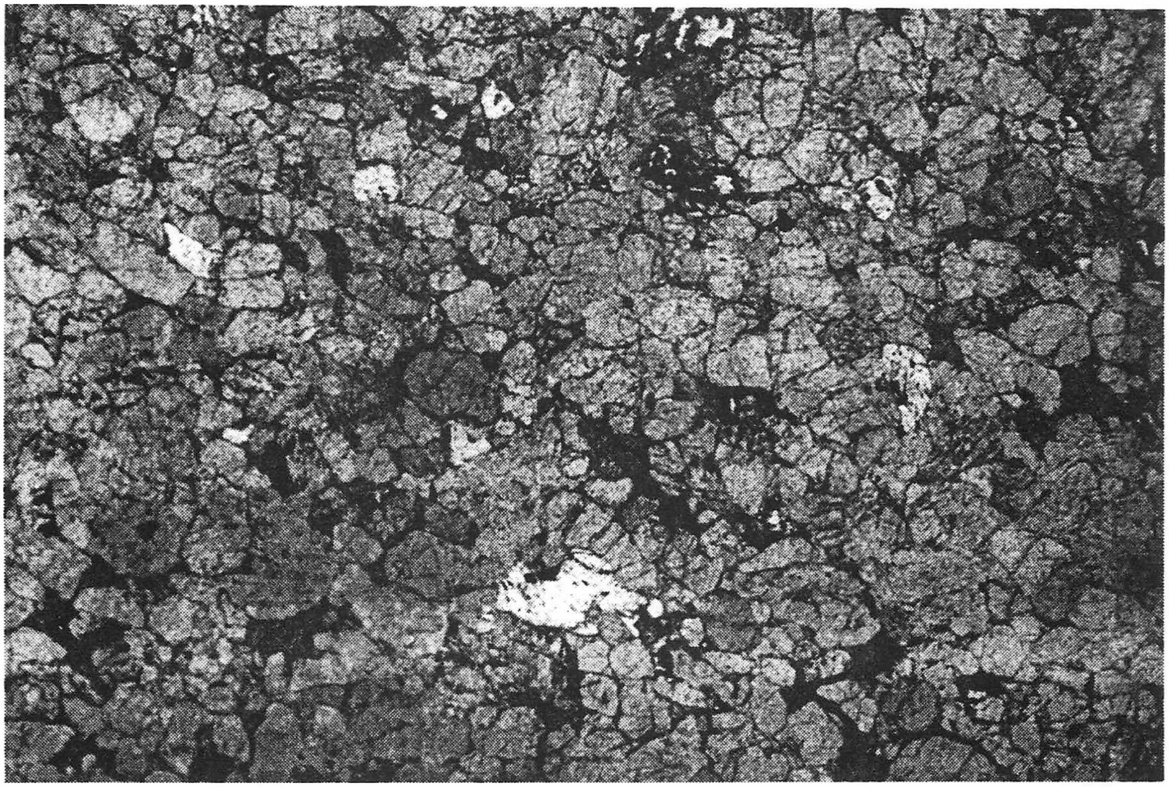

(A)

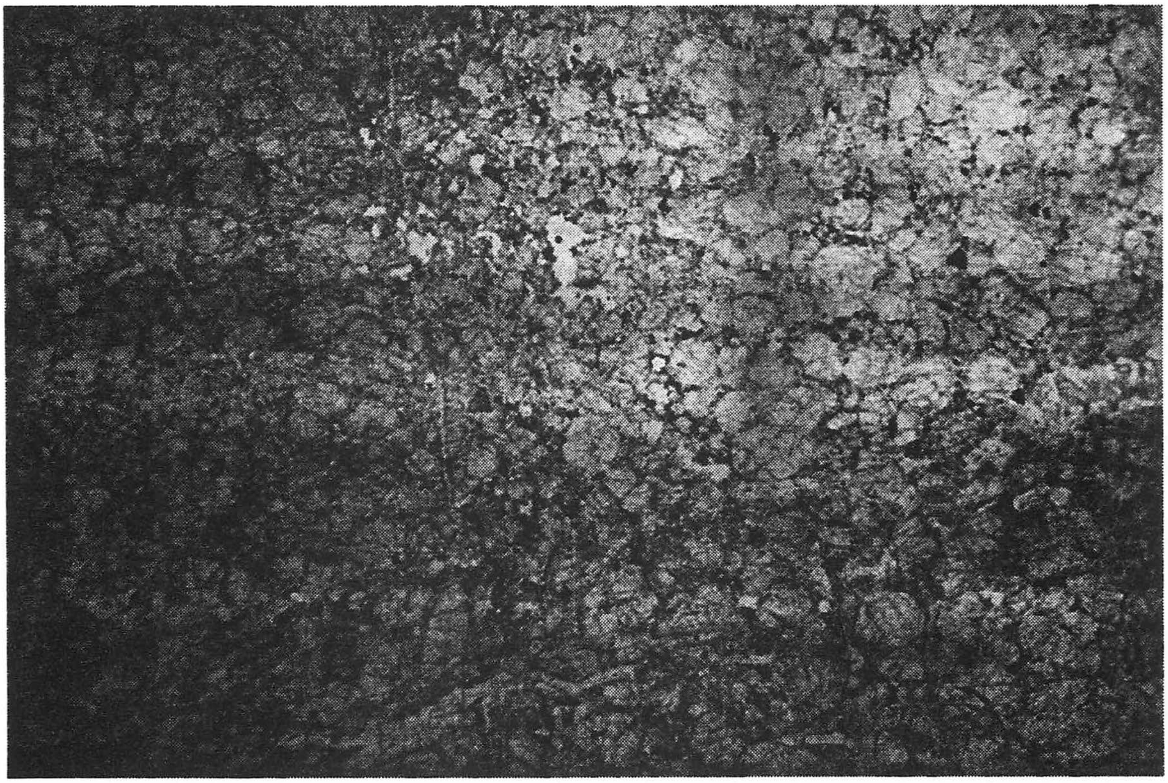

(B)

King 1964; Neuman and Nelson, 1965; Unrug and others, 1991); (2) the lack of lithologic similarities between the strata in the footwall of the Miller Cove fault and the strata in the hanging wall; and (3) similar carbonate lithologies assigned to the Sandsuck Formation in the Ocoee River Gorge (Hurst and Schlee, 1962; Sutton, 1971; Hatcher and others, 1991), in northwestern Georgia (Salisbury, 1961), and northeast of the study area near English Mountain (Hamilton, 1961).

The limestone is characterized by 0.5- to 1.0 m-thick beds locally interbedded with shale. Compositionally, the limestone consists predominantly of microcrystalline micrite and sparry calcite (Figs. II-12A, II-12B). Sub-rounded detrital quartz grains are common and are sporadically dispersed within the matrix, while feldspar grains are rare. Accessory minerals are opaque, and include magnetite and/or hematite (Appendix B).

Other units

Other units exposed in the study area include parts of the Chilhowee Group, Shady Dolomite, Rome Formation, Conasauga Group, and Knox Group (Figs. II-1, II-2; Plate I). These units occupy the northwestern portion of the study area near Groundhog Mountain and, with the exception of the Chilhowee Group, comprise Valley and Ridge footwall strata beneath the Great Smoky and Bullet Mountain faults. The Groundhog Mountain area was mapped and studied by McKinney (1964). His work is compiled into this study, and the stratigraphy is briefly discussed below (Fig. II-2; Plate I). The Groundhog Mountain area is included in this study in order to: (1) verify that the quartzite capping Groundhog Mountain is a klippe of Hesse Quartzite; and (2) provide continuity with the Early Cambrian to Late Proterozoic strata of the western Blue Ridge in the hanging wall of the Great Smoky fault. McKinney (1964) interpreted the klippe of Chilhowee Group quartzite to be located in an intermediate slice of strata related to the Great Smoky fault system, with the fault surface below the klippen corresponding to the lower surface of the

Figure II-12. Characteristic lithologic features of the carbonate lithofacies in the Sandsuck Formation (Walden Creek Group). Sample location near the confluence of Conasauga and Steer creeks (station TP-534), Tellico Plains 7.5-minute quadrangle. (A) Carbonate sample from the Sandsuck Formation. Centimeter scale. (B) Enlarged image (negative) of carbonate thin section. Field of view is approximately 4.5 cm wide.

(A)

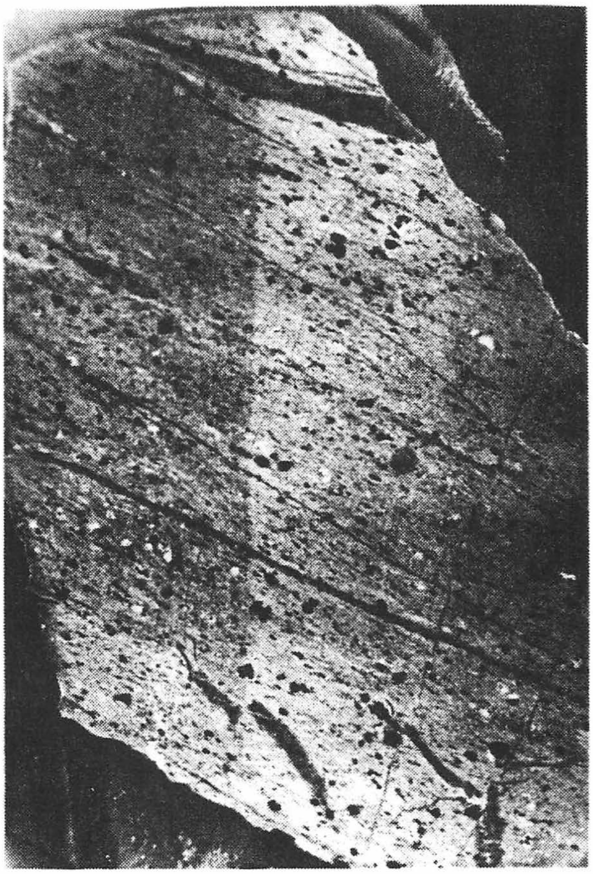

(B)

slice and the main Great Smoky fault surface overriding the lower slice surface. West of the study area, Early Cambrian Chilhowee Group rocks underlie Starr Mountain and comprise the hanging wall strata of the Great Smoky fault. The Shady Dolomite and Rome Formation are exposed in the Bullet Mountain thrust sheet, with slices of Knox Group exposed along the fault trace. Upper Conasauga Group and Knox Group strata are exposed in the footwall of the Bullet Mountain fault.

Chilhowee Group

Lower Cambrian Chilhowee Group rocks form a linear belt of mountains in east and southeast Tennessee, including Stone, English, Chilhowee, Starr, Chestnut, and Bean Mountains (Fig. I-1). Rocks of the Chilhowee Group cap the western Blue Ridge stratigraphic sequence, and consist of alternating coarse- and fine-grained formations. The coarse-grained lithologies in the upper formations are predominantly quartz arenite, while the lower formations consist of feldspathic sandstone and conglomerate. The Chilhowee Group is comprised of the (oldest to youngest) Cochran Formation, Nichols Shale, Nebo Quartzite, Murray Shale, Hesse Quartzite, and Helenmode Formation (Fig. II-1).

Hesse Quartzite

Two masses of quartz arenite are exposed on Groundhog Mountain and on a knob 915 m (3,000 ft) to the southeast, and are interpreted as klippes of Chilhowee Group rocks related to the Great Smoky fault (McKinney, 1964) (Fig. II-2; Plate I). I traversed the southeast slope of Groundhog Mountain to collect samples and to confirm McKinney's observations. These rocks consist of clean, well-sorted, white to tan or pink, medium- to coarse-grained quartz arenite (McKinney, 1964; this study) (Fig. II-11B). The slopes of Groundhog Mountain are covered with this lithology as talus or wash. The quartz arenite occupies the upper 30 m (100 ft) of Groundhog Mountain. Exposures are few and bedding is often massive. Compositionally, the orthoquartzite consists of over 90 percent quartz, with little or no feldspar and minor clay material (Fig. II-10; Appendix B). Assessory minerals include hematite, magnetite, and tourmaline. McKinney (1964) observed local *Skolithos* tubes in the quartzite that occurs as float or talus on the slopes of Groundhog Mountain.

Does the quartzite on Groundhog Mountain belong to the coarse-grained lithologies of the Chilhowee Group (Hesse Quartzite, Nebo Quartzite, Cochran Formation) or to the Sandsuck Formation? Compositionally, the sandstones of the Cochran and Sandsuck Formations are more feldspathic and conglomeratic than the Hesse and Nebo Quartzites (Figs. II-10, II-11A, II-11B). For this reason, the quartzite capping Groundhog Mountain should be correlated with either the Hesse or Nebo Quartzites. Lithologically, the Hesse and Nebo Quartzites are similar. Both formations are texturally mature quartzites that are cross-bedded and contain locally abundant *Skolithos* tubes (Neuman and Nelson, 1965; Walker and Driese, 1991). Typically, the Hesse Quartzite is more massively bedded, less cross-bedded, and has locally more abundance of *Skolithos* tubes than the Nebo Quartzite. McKinney (1964) tentatively correlated the quartz arenite on Groundhog Mountain with the Hesse Quartzite, because of the lithologic similarities to that unit. I also tentatively correlate the quartz arenite with the Hesse Quartzite based on lithologic similarities; massive bedding, composition, and similar texture. However, it is lithologically possible the quartz arenite could be correlated with the Nebo Quartzite. Additionally, the quartz arenite capping Groundhog Mountain is correlated with the Hesse Quartzite due to structural observations and implications (see Great Smoky fault section, Chapter III).

Shady Dolomite

The Lower Cambrian Shady Dolomite consists of two units in the study area: a lower dolomite unit and an upper shale-carbonate unit (McKinney, 1964). The dolomite unit consists of alternating, medium- to thick-bedded, light gray siliceous dolomite and medium dark-gray dolomite in the lower portion of the section, and thinly bedded, siliceous, yellowish brown and bluish-gray shaly dolomite in the upper section of the dolomite unit (McKinney, 1964). The shale-carbonate sequence consists of yellowish-gray, light green, and light bluish-gray shale and mudstone, chert, and a few interbedded carbonate beds in the upper part of the sequence. The shale-carbonate sequence underlies the valleys within the area of the Shady Dolomite with the best exposures in Kirkland Hollow, just beneath the Great Smoky fault (McKinney, 1964). The true thickness of the Shady Dolomite cannot be determined in the study area because of faulting and erosion. McKinney (1964) estimated a thickness between 60 to 90 m (200 to 300 ft), while Neuman and Nelson (1965) reported a thickness of approximately 330 m (1,100 ft) for the Shady Dolomite in Miller Cove.

Rome Formation

The Lower Cambrian Rome Formation consists mostly of maroon and red mudstone and silty shale with interbedded tan, red, and pink siltstone; fine-grained sandstone; and bluish-gray argillaceous carbonate (McKinney, 1964). Shale and mudstone dominate the section, but siltstone and associated sandstone are also abundant throughout the section. Bedding ranges from less than 20 cm thick for the shales and siltstones to less than 1 m thick for the interbedded sandstones. Intertidal sedimentary structures include mudcracks and flow casts, especially in the siltstones and sandstones (McKinney, 1964). Detrital mica is also locally present along siltstone bedding planes (McKinney, 1964). Shale and carbonate beds occur near the base of the formation and mark the conformable transition zone into the underlying Shady Dolomite. Poorly exposed carbonate beds are also occur elsewhere in the Rome Formation (Rodgers, 1953; McKinney, 1964). The top of the formation is not exposed in the study area due to faulting; therefore, the minimum thickness of the Rome is estimated to be 300 m (1,000 ft) thick (McKinney, 1964).

Conasauga Group

Only the upper part of the Middle Cambrian Conasauga Group is exposed in the study area. This unit is predominantly a yellowish-gray to light greenish-gray, fissile, clay shale with carbonate lithologies at the top (McKinney, 1964) A transition zone of medium dark-gray shaly limestone (about 5 cm thick) separates the clay shale and overlying light gray, massively bedded limestone (about 30 cm thick), which contains silty laminae and irregular silty dolomite layers that produce a ribboned appearance on weathered surfaces (McKinney, 1964). The Conasauga Group in this area is located in the footwall of the Bullet Mountain fault, with less than 190 m (600 ft) of the upper part being preserved (McKinney, 1964).

Knox Group

The Upper Cambrian to Lower Ordovician Knox Group conformably overlies the Conasauga Group. The Knox Group consists of medium to massively interbedded dark to light-gray limestone and dolomite that are characterized by a ribboned appearance similar to the underlying carbonates of the upper Conasauga Group (McKinney, 1964). The carbonates of the Knox Group are more cherty than the underlying Conasauga Group carbonates (McKinney, 1964), and the appearance of tan-weathering chert nodules in the soil marks the contact between the two groups. The carbonates in the study area are correlated with the southeastern phase of the Knox Group (McKinney, 1964) which regionally consists of a limestone-dominated package estimated to be more than 940 m (3,100 ft) thick (Rodgers, 1953).

Age of the Walden Creek Group - Stratigraphic evidence

The age of the Walden Creek Group and Ocoee Supergroup has been debated for more than a century (Hayes, 1891; Keith, 1895; Hayes, 1895; Keith, 1904; Stose and Stose, 1949; King and others, 1958; Tull and Groszos, 1990; Unrug and Unrug, 1990; Unrug and others, 1991; Tull and others, 1993). Traditionally, the age of the Ocoee Supergroup is considered to be Late Proterozoic (King and others, 1958). Unsubstantiated reports of fossils from the Wilhite Formation suggest that all or part of the Ocoee Supergroup is Silurian to early Mississippian (Unrug and Unrug, 1990; Unrug and others, 1991; Broadhead and others, 1991). Determining the age of the Walden Creek Group requires analysis of the units that are overlying, underlying, and possibly equivalent to the Walden Creek Group. The purpose of this section is to provide better evidence from the present study area to constrain the age of the Walden Creek Group.

The upper formations of the Chilhowee Group have been established as Early Cambrian from the presence of the crustacean *Isoxys chilhoweana* (Walcott, 1890), and the ostracode *Indiana tennesseensis* (Laurence and Palmer, 1963) in the Murray Shale. The base of the Cambrian is restricted to the units that have paleontological evidence available (King and others, 1958). Although much of the contact between the overlying Chilhowee Group and underlying Walden Creek Group is faulted, conformable contact relationships exist between the Cochran Formation (Chilhowee Group) and the Sandsuck Formation (Walden Creek Group) in several areas in southeastern and eastern Tennessee (Fig. I-1). These areas include: (1) Bean Mountain (Rackley, 1951), (2) Chestnut and Starr Mountains (Phillips, 1952; Carter, 1994), (3) southwestern slope of Chilhowee Mountain (Neuman and Nelson, 1965), (4) northwestern slope of English Mountain, and

(5) Del Rio district, north of the French Broad River (Keller, 1980). Additionally, Keller (1980) mapped a continuous section of the entire Walden Creek Group beneath the Chilhowee Group. The Walden Creek Group rocks in this study area, however, are separated from the main Walden Creek Group outcrop belt of the Foothills by several faults.

In the Foothills belt, the Sandsuck Formation is separated from the remainder of the Walden Creek Group by regional faults, except in the vicinity of English Mountain. Here, the constituent formations of the Walden Creek Group were defined by King and others (1958), and Hamilton (1961) mapped a continuous section of Walden Creek Group strata from the Licklog Formation to the Sandsuck Formation in the hanging wall of the Great Smoky fault. In the footwall, Hamilton (1961) observed Sandsuck Formation lithologies beneath the Chilhowee Group and tentatively correlated the Sandsuck Formation across the fault. The correlations of lithologically similar strata across faults have been used by many workers in the Foothills belt. Lithologic correlations across fault blocks are difficult, so these correlations must be made cautiously.

Paleontological data provide evidence to better constrain the age of the Walden Creek Group. Knoll and Keller (1979) reported occurrences of the Late Proterozoic to Paleozoic(?) acritarch *Bavlinella faveolata* in the Walden Creek Group throughout the Foothills belt. Additionally, soft-bodied metazoan macrofossils originally reported by Rackley (1951) and Phillips (1952) have been rediscovered along Ellis Branch in the Sandsuck Formation in the Mecca 7.5-minute quadrangle (Broadhead and others, 1991; Carter, 1994). In this region of southeastern Tennessee, the Sandsuck Formation is conformably overlain by fossiliferous Chilhowee Group rocks suggesting that the Sandsuck Formation is no younger than Early Cambrian, and may still be Late Proterozoic (Broadhead and others, 1991).

In the study area, no fossils were identified, so the age of the Walden Creek Group must be determined by analyzing stratigraphic relationships. The Chilhowee Group is preserved in the study area, but in klippes of the Great Smoky fault (McKinney, 1964), while the top of the Walden Creek Group is cut out by the Miller Cove and Great Smoky faults (Figs. II-2, II-3; Plate I, Plate III). The only independent evidence available locally for constraining the age of the Walden Creek Group is analysis of the stratigraphic relationships between the Walden Creek Group and the underlying Great Smoky Group.

The contact between the Walden Creek Group (Wilhite Formation) and the Great Smoky Group (Dean Formation) has been interpreted as: (1) the southern continuation of the Greenbrier fault (Merschat and Wiener, 1973; Wiener and Merschat, 1978, 1981; Merschat and Hale, 1983; Wiener and Merschat, 1992); (2) as a conformable contact (Hale, 1974; Poppelreiter, 1980; Costello and Hatcher, 1986, 1991; Carter and others, 1993b, 1995a, 1995c; Carter, 1994; Geddes, 1995; this study); and (3) an unconformity (Tull and Groszos, 1988, 1990; Thompson and Tull, 1991; Tull and others, 1993; Carter and others, 1995b). In the Great Smoky Mountains National Park, the Greenbrier fault juxtaposes Great Smoky Group rocks in the hanging wall onto Walden Creek Group and Snowbird Group rocks in the footwall. If the contact between the Walden Creek Group and Great Smoky Group in the study area is the southern continuation of the Greenbrier fault, a large portion of the metasiltstones and sandstones mapped as Wilhite Formation should be correlated with the Snowbird Group.

If the contact were a regional unconformity, all or part of the fine-grained metasedimentary rocks above the Great Smoky Group in the foothills belt in southeastern Tennessee would have been deposited in a post-Taconic successor basin. According to Tull and others (1993) an unconformity occurs in the Murphy syncline below the Mineral Bluff Group in southwestern North Carolina, and in the Talladega slate belt in Alabama. This interpretation requires deformation and metamorphism to have occurred during the Acadian (Silurian) and the Alleghanian (Permian) orogenies. Their tectonic scenario also permits the deposition of the middle Paleozoic fossil fragments reported by Unrug and Unrug (1990), and Unrug and others (1991). The pronounced lithologic change across the contact and the variable nature of the sediments beneath the Wilhite Formation could indicate, however, that an unconformity is present between the Walden Creek Group and the Great Smoky Group. Hurst (1955) reported the contact between the Dean Formation (Great Smoky Group) and Nantahala Formation (Hiwassee River Group) in the Mineral Bluff quadrangle in northern Georgia appeared gradational and concordant. However, Hurst (1955) suggested the contact may be unconformable because of the pronounced lithologic change across the contact, and the changing character of the metasediments beneath the Nantahala Formation. The Wilhite Formation is regionally equivalent to the Nantahala Formation because the contact relationship between the Wilhite and Dean formations in southeastern Tennessee is similar to the contact relationship between the Nantahala and Dean formations in the Murphy syncline.

Field evidence suggests a conformable contact between the Walden Creek and Great Smoky Groups. A conformable stratigraphic relationship for the Walden Creek and Great Smoky Groups has been reported along the Ocoee, Hiwassee, and Tellico Rivers in southeastern Tennessee (Hale, 1974; Poppelreiter, 1980; Costello and Hatcher, 1986, 1991; Carter, 1994). The boundary between the two units is exposed along the northwest slope of Unicoi Mountain in southeastern Tennessee. Here, the contact between the two units is variably gradational, intertonguing, and sometimes very sharp. No evidence of faulting, such as truncation of map units, gouge, small faults, or slickenlines, was observed. Moreover, none of the units appeared to be erosionally truncated, nor were there any Dean Formation clasts exposed in the Walden Creek Group sediments.

A transition zone consisting of Wilhite metasiltstone interbedded with Dean Formation lithologies, described by Poppelreiter (1980) in the upper part of the Dean Formation, was also recognized in this study. The transition zone occurs in the gradational conglomerate lithofacies and slate lenses in the Dean Formation, and consists of conglomeratic graywacke at the bottom of a sequence and greenish-gray banded metasiltstone and slate at the top. These metasiltstones occur in sequences of 1 to 3 m thick, and are distinguishable from the black laminated slate (~5 cm thick) at the top of most graded sequences in the Dean Formation. These metasiltstones are lithologically similar to those in the overlying Walden Creek Group and are also interbedded with dark slate of the conglomerate sequence. Additionally, the contact between the Walden Creek Group and the Great Smoky Group is complexly folded and overturned to the southeast (Carter and others, 1993a) (Plate I). Erosion has exposed many map-scale anticlines (whalebacks) cored by Great Smoky Group lithologies. In the study area, Great Smoky Group lithologies are exposed northwest of the main contact in the core of the Tellico Mountain anticlinorium (Plate I). The contact between the Walden Creek and Great Smoky Group here is relatively sharp (Figs. II-13A, II-13B). Other whalebacks occur southwest of the study area along the Ocoee (Hurst and Schlee, 1962) and Hiwassee (Carter, 1994) Rivers in southeastern Tennessee.

Modal analysis of coarse-grained lithologies from both groups reveals each group as being comprised essentially of the same constituents (Appendix B), but is texturally different. The coarse-grained lithologies of the sandstone units of the Wilhite Formation have smaller, better sorted, more rounded grains, and are less conglomeratic. This may represent a drastic change in the depositional environment such that the Wilhite and Dean Formations have similar sources, but the sandstones of the Wilhite Formation represent more distal sedimentation. Geddes (1995) suggested a map-scale gradation from older formations to younger formations between the uppermost fine-grained lithologies of the Dean Formation and the fine-grained lithologies of the Wilhite Formation. Rocks assigned to the lowermost Wilhite Formation are not as dark and sulfidic as the Dean Formation, yet are darker and more sulfidic than the fine-grained rocks higher in the

Figure II-13. Contact relationships between the Dean Formation (Great Smoky Group) and the Wilhite Formation (Walden Creek Group). Outcrop exposure located on top of Tellico Mountain on Tennessee State Highway 68. (A) Sharp contact between the thick-bedded, granule- to pebble-conglomerate of the Dean Formation and the thin-bedded, ankeritic, banded metasiltstone of the Wilhite Formation. (B) Close-up of photo above showing the sharpness of the contact between the Dean Formation and the Wilhite Formation. Rock hammer is 32 cm in length.

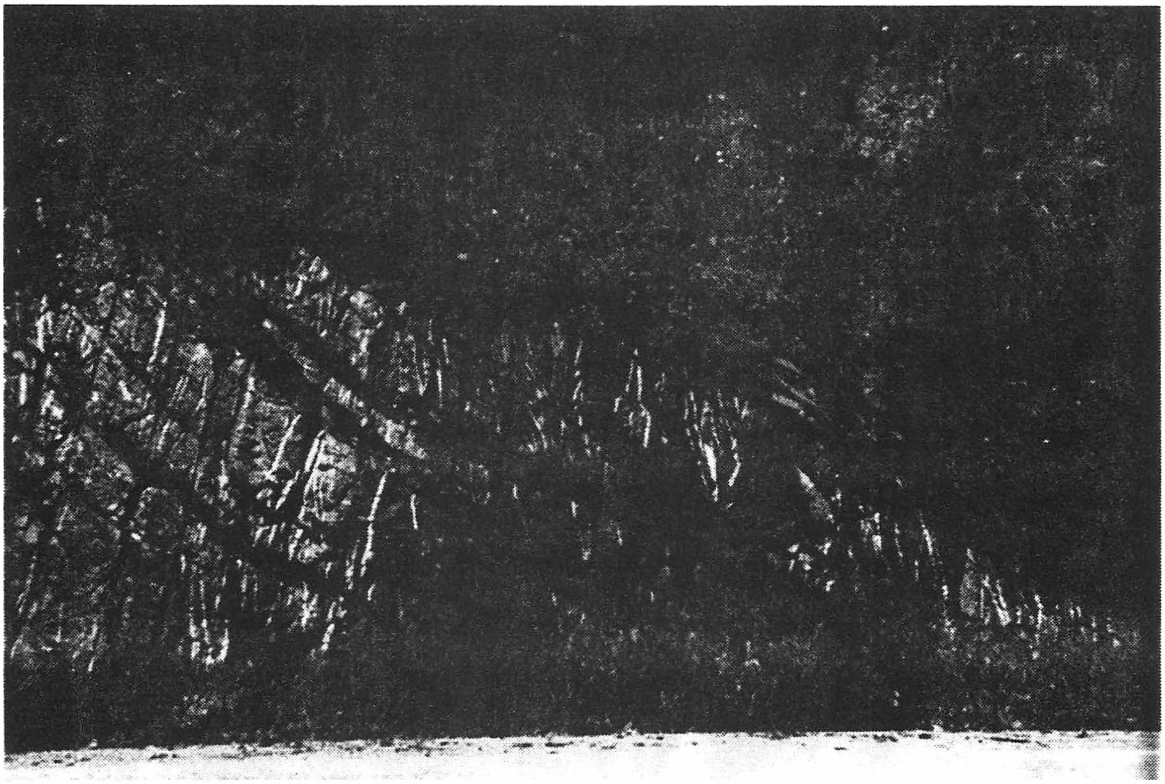

(A)

(B)

Wilhite Formation sequence. I thus believe the relationships between the Walden Creek Group and the Great Smoky Group strongly suggest that the contact between the two group is conformable.

Based on the evidence presented above, the age of Walden Creek Group is Late Proterozoic to Early Cambrian. The soft-bodied metazoans and acritarchs are the oldest reported fossils in the western Blue Ridge, and thus, the base of the Cambrian as defined by King (1949) might include at least the middle member of the Sandsuck Formation from which the fossils were recovered (Carter, 1994). A conformable stratigraphic relationship with the underlying Great Smoky Group results in a probable Late Proterozoic age for the oldest Walden Creek Group metasediments.

Chapter III
Structure

Introduction

The Ocoee Supergroup of the western Blue Ridge has undergone at least two deformational events during the Taconic (Ordovician) and Alleghanian (Permian) orogenies. The Taconic orogeny is characterized by folding, faulting, cleavage development, and Barrovian metamorphism, while the Alleghanian orogeny is characterized by brittle faulting and folding (Hamilton, 1961; Hadley and Goldsmith, 1963; King, 1964; Neuman and Nelson, 1965; Butler, 1972; Hatcher, 1972; Dallmeyer, 1975; Hatcher, 1978, 1989; Hatcher and others, 1989a; Connelly and Dallmeyer, 1991; Kish, 1991; Woodward and others, 1991). Structures observed in the field area related to these two events include thrust faults, folds, foliations, and joints. Thrust faults include meso- and macro-scale brittle structures, some of which are possibly reactivated pre- to synmetamorphic structures (King, 1964; Neuman and Nelson, 1965; Geddes, 1995). Several periods of deformation have produced folds ranging from centimeter- to kilometer-scale. Foliations include continuous (slaty) cleavage, pressure-solution cleavage, and crenulation cleavage. A chronology of previous structural studies in southeastern Tennessee is presented by Rodgers (1991) and Carter (1994).

Structures in the western Blue Ridge are the result of regional deformation. The amount of internal strain preserved in these rocks can be estimated using standard analytical and geometrical strain analysis techniques (R_f/ϕ and normalized Fry methods). The purpose of recent strain analyses of clastic rocks in the western Blue Ridge has been to quantify the amount of internal deformation (strain), and to relate this strain to regional structures and deformational history (Lewis, 1988; Walters, 1988; Connelly, 1993; Carter, 1994).

Faults

Six major faults are exposed in the study area: Bullet Mountain, Great Smoky, Maggies Mill, Miller Cove, Rabbit Creek, and Oconaluftee (Figs. II-2, III-1; Plate I). These faults juxtapose rocks of different age and metamorphic grade.

The northwesternmost fault exposed in the study area is the Bullet Mountain fault, which thrusts Lower Cambrian Shady Dolomite and Rome Formation strata onto younger Paleozoic Conasauga and Knox Groups (McKinney, 1964). McKinney (1964) interpreted the Bullet Mountain fault as an exposed slice of the frontal Blue Ridge fault system. The Bullet Mountain fault has also been interpreted as a floor thrust in a duplex beneath the Great Smoky fault (Carter, 1994). The Great Smoky fault is locally the frontal Blue Ridge fault, and thrust metamorphosed Lower Cambrian and Late Proterozoic rocks of the western Blue Ridge over unmetamorphosed Paleozoic rocks of the Valley and Ridge. The Maggies Mill fault is related to the Great Smoky fault, and separates lower Sandsuck Formation from the upper units of the Sandsuck Formation and Chilhowee Group (Carter, 1994). The Miller Cove fault juxtaposes chlorite grade, cleaved Wilhite Formation onto lower grade (anchizone) and less cleaved Sandsuck Formation of the Walden Creek Group. Southeast of the Miller Cove fault is the Rabbit Creek fault, which consists entirely of Great Smoky Group strata in the hanging wall, and Walden Creek Group strata in the footwall. The Rabbit Creek fault was originally mapped by Neuman and Nelson (1965) in the Great Smoky Mountains National Park, and traced southwestward to the study area by Wiener (unpub.) and Geddes (1995). The Rabbit Creek fault is interpreted as a reactivated syn- to premetamorphic structure (Neuman and Nelson, 1965; Geddes, 1995). The Oconaluftee fault consists of upper Great Smoky Group and lower Walden Creek Group hanging-wall strata which are penetratively cleaved and metamorphosed to chlorite and biotite grade. The footwall strata of the Oconaluftee fault consist of Great Smoky Group rocks that are present in the hanging wall of the Rabbit Creek fault, and

Figure III-1. Thrust sheets, bounding faults, and major folds in the study area. Refer to Fig. II-2 and Plate I for stratigraphic explanation. Cross-sections (Plates III, IIIa) located along lines A-A', B-B', and C-C'.

Geologic abbreviations: BMF-Bullet Mountain fault; ES-Epperson synclinorium; GRA-Grindstone Ridge anticlinorium; GSF-Great Smoky fault; HBF-Hunt Branch fault; KHA-Kirkland Hollow anticlinorium; MMF-Maggies Mill fault; MCF-Miller Cove fault; OF-Oconaluftee fault; PRA-Payne Ridge anticlinorium; RCF-Rabbit Creek fault; TMA-Tellico Mountain anticlinorium; TMF-Tellico Mountain fault; TPS-Tellico Plains synclinorium; U-upthown fault block; D-downthrown fault block; K-klippe.

Geographic abbreviation: TP-Tellico Plains.

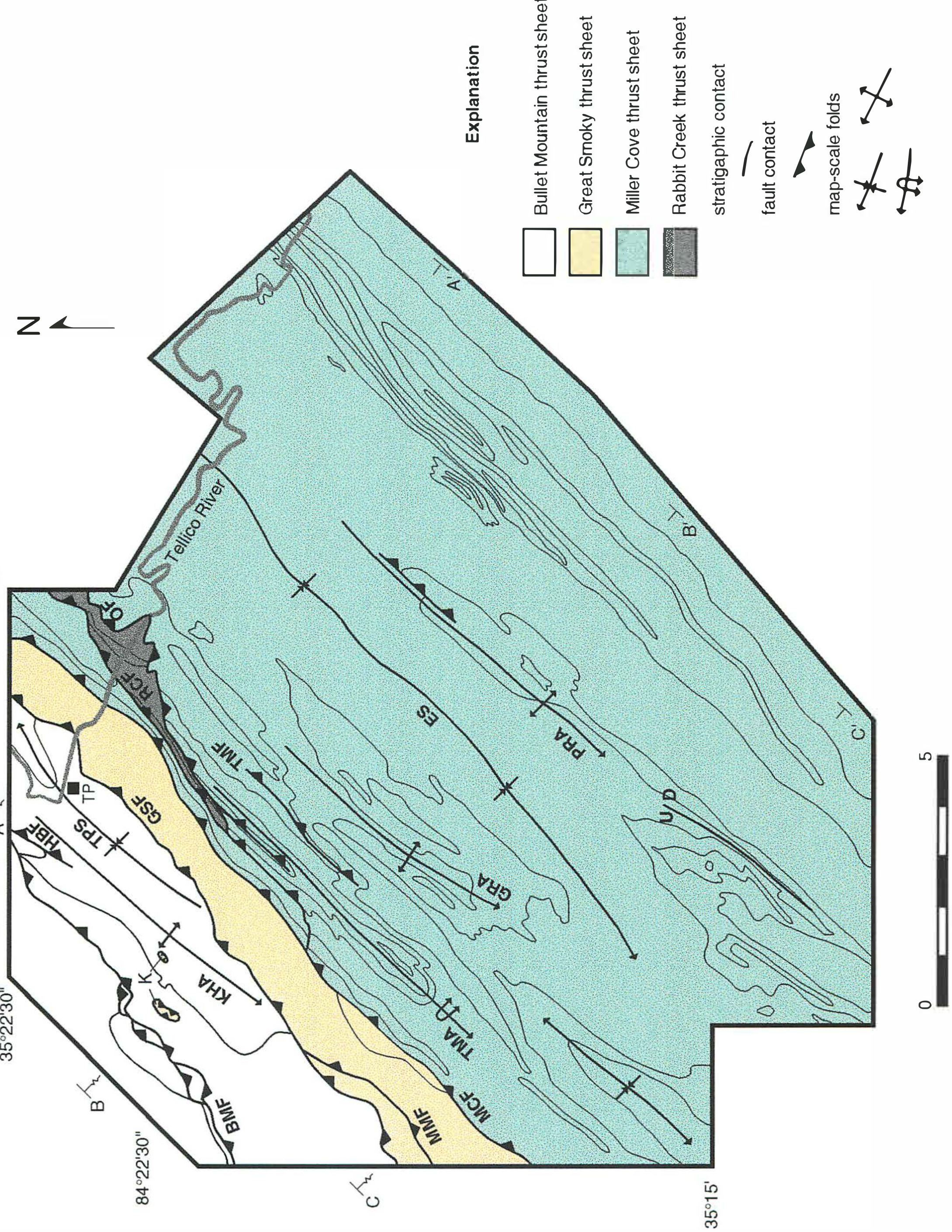
Explanation
Bullet Mountain thrust sheet
Great Smoky thrust sheet
Miller Cove thrust sheet
Rabbit Creek thrust sheet
stratigaphic contact
fault contact
map-scale folds
N
84°15'
35°22'30"
84°22'30"
35°15'
A
A'
B
B'
C
C'
Tellico River
BMF
MMF
MCF
TMA
KHA
K
HBF
TPS
TP
GSF
TMF
RCF
OF
GRA
ES
PRA
U
D
0
5
Kilometers

have been interpreted to represent a distal facies change within upper Great Smoky Group lithologies (Geddes, 1995). The Greenbrier fault is a large thrust that is transected by metamorphic isograds, and is interpreted to emplace younger rocks over older rocks everywhere along its trace (King and others, 1958; Neuman and Nelson, 1965). Neuman and Nelson (1965) interpreted the Oconaluftee fault as a postmetamorphic dextral strike-slip fault that obliquely cuts the Greenbrier fault, but then swings into parallelism with it, and either truncates or occupies the same movement plane as the Greenbrier. The trace of the Oconaluftee was mapped northeast of the study area by Geddes (1995). Geddes (1995) interpreted the Oconaluftee as a reactivated syn- to premetamorphic structure because this fault truncates older structures.

Bullet Mountain fault

The Bullet Mountain fault thrust rocks of the Chilhowee Group, Shady Dolomite, and Rome Formation over Conasauga Group and Knox Group (Rodgers, 1953; McKinney, 1964; Hardeman, 1966). In the study area, the trace of the Bullet Mountain fault is located along the contact between the maroon siltstones of the Rome Formation, and the tan shales of the Conasauga Group and the Knox Group carbonates. Three fault-bounded slices of Knox Dolomite also occur along the fault. The Bullet Mountain fault is exposed 1.4 km (4,500 ft) north of Rural Vale school at the Mecca/Tellico Plains 7.5-minute quadrangle boundary, and was traced northeastward by McKinney (1964) north of Groundhog Mountain, to the intersection of Tennessee State highways 39 and 68. The Bullet Mountain fault was estimated by McKinney (1964) to dip approximately 30° to 40° to the southeast.

McKinney (1964) interpreted the Bullet Mountain fault as a large intermediate slice of footwall rocks associated with the Great Smoky fault system that was transported northwestward beneath the Great Smoky fault. McKinney (1964) suggested that because structures within the Bullet Mountain thrust sheet closely coincide with structures associated with the emplacement of the klippe fault surface on Groundhog Mountain, the emplacement of the Bullet Mountain fault and klippe fault surface occurred during the same deformational event. Additionally, McKinney (1964) suggested the Bullet Mountain fault is a splay of the Great Smoky fault system because the Bullet Mountain fault is truncated by the Great Smoky fault along the northwestern side of the Conasauga reentrant. Carter (1994) suggested the Bullet Mountain fault may have been deformed into a duplex as it was transported beneath the Great Smoky fault, and that the Bullet Mountain fault is the floor thrust of a duplexed slice. Carter (1994) also interpreted the Bullet Mountain duplex as consisting of the Harrison Mill fault system in front of Bean Mountain south of the Hiwassee River.

In this study, the Bullet Mountain fault is interpreted as the floor thrust of the Bullet Mountain duplex, which has been transported northwestward beneath the Great Smoky fault (Plates III, IIIa). The roof thrust for this duplex is interpreted to be the Great Smoky fault. Lithologies in this duplex include the Rome Formation, Shady Dolomite, and Chilhowee Group. Chilhowee Group rocks are not exposed at the surface within the Bullet Mountain thrust sheet, but are interpreted to underlie the Shady Dolomite within the duplex. Klippes of Chilhowee Group rocks, probably related to the Great Smoky fault, are however, exposed above the Bullet Mountain thrust sheet throughout southeast Tennessee (Rodgers, 1953; Hardeman, 1966). It is suggested in this study that these klippes of Chilhowee Group rocks may possibly be derived from Chilhowee Group rocks in the Bullet Mountain thrust sheet (Plates III, IIIa). Based on cross-section analysis, and because of the occurrence of Shady Dolomite and Chilhowee Group rocks in the Bullet Mountain thrust sheet, a minimum displacement of 25 km (15.5 mi) on the Bullet Mountain fault is estimated (Plates III, IIIa).

Great Smoky fault

In the southern Appalachians, the frontal Blue Ridge fault system separates the rocks of the western Blue Ridge province from the rocks of the Valley and Ridge province. The Great Smoky fault is the frontal Blue Ridge fault in southeastern Tennessee and extends approximately 116 km (78 mi) from Chilhowee Mountain to Bean Mountain (Rodgers, 1953; Hardeman, 1966) (Fig. I-1). The Great Smoky fault thrust very low-grade metasedimentary (anchizone) rocks of the Sandsuck Formation and Chilhowee Group over unmetamorphosed rocks of the Shady Dolomite, Rome Formation, Conasauga Group, Knox Group, and Athens Shale (Rodgers, 1953; McKinney, 1964; Hardeman, 1966; Carter, 1994).

In the study area, the trace of the Great Smoky fault is located 0.6 km (2,000 ft) north of Webb Branch at the Mecca and Tellico Plains 7.5-minute quadrangle boundary, and extends northeastward along the northwest slope of Pine and Mocking Crow Mountains through the city of Tellico Plains (Fig. II-2; Plate I). The fault juxtaposes rocks of the Sandsuck Formation over rocks of the Shady Dolomite and Rome Formation. Throughout much of its length, the Great Smoky fault is mapped by the distribution of residuum because exposures of the fault are poor to nonexistent. The trace of the fault is easily mapped, however, because the lithologic contrasts between the maroon siltstones of the Rome Formation and the carbonate of the Shady Dolomite in the footwall are easily distinguished from the coarser-grained sandstones and weathered tan shales of the Sandsuck Formation in the hanging wall. The Great Smoky fault is a low-angle fault with an undulating surface with an average dip of approximately 15° southeast (McKinney, 1964; this study). Carter (1994) estimated the dip of the fault to range from 10°- 25° southeast.

The Great Smoky fault is not well exposed in the study area. McKinney (1964) observed a gouge zone about two feet wide along a road off Tennessee State Highway 68, 0.6 km (2,000 ft) southwest of the Tellico Plains city limits, and in an old iron pit 0.5 km (1,500 ft) northeast of Coppenger Cemetery. A good exposure of footwall Rome Formation just beneath the Great Smoky fault is exposed in a creek along the northwest slope of an unnamed mountain 0.6 km (2,000 ft) southwest of Conasauga Creek. Residual soils and colluvium cover the fault surface here, but offer good control of the fault trace with shales and sandstones of the Sandsuck formation exposed close by.

The Great Smoky fault is interpreted as a thin-skinned, postmetamorphic, brittle structure (Hamilton, 1961; Hadley and Goldsmith, 1963; King, 1964; Neuman and Nelson, 1965; Carter, 1994; this study). Several lines of evidence support these conclusions, including: (1) the low-angle nature of the fault, as indicated by the coves region in the Great Smoky Mountains National Park, the trace of the fault along the base of Starr Mountain, and seismic reflection data (Cook and others, 1983) along the Tellico River; (2) no basement rocks are exposed in the frontal Great Smoky thrust sheet; (3) metamorphic grade of rocks within the Great Smoky thrust sheet increases southeastward, and are thrust onto unmetamorphosed rocks in the footwall, indicating that faulting and transport of the Great Smoky thrust sheet occurred after the regional metamorphic event; and (4) only brittle deformation is present along the exposed fault trace.

The Great Smoky fault is interpreted in this study as the fault surface that emplaced the quartzite on Groundhog Mountain. Outcrop patterns of the Great Smoky fault in the study area and to the southwest along Starr Mountain provide evidence for the low-angle nature of the fault (Fig. I-2; Plates I, III, IIIa). McKinney interpreted the emplacement of the Chilhowee Group quartzite to be related to an intermediate fault slice beneath the main Great Smoky fault surface. This interpretation is abandoned because of the lack of evidence supporting an intermediate fault beneath the Great Smoky fault in the study area, and because of the low angle of the Great Smoky fault.

The Great Smoky fault may have used the shale beds in the Sandsuck Formation as flats, and ramped across stronger sandstone units as it propagated out of the Ocoee basin onto the carbonate platform on the continental margin (King, 1964; Hatcher and others, 1989a). Hatcher (1978, 1989), Hatcher and others (1989a), and Hatcher and Goldberg (1991) interpreted the Great Smoky fault to have a displacement of approximately 250 km (150 mi). In the Great Smoky Mountains region, a minimum displacement on the Great Smoky fault is estimated to be 10 km (6 mi) based on the distance from the back edge of the windows to the outcrop trace of the fault to the northwest (Hamilton, 1961; King, 1964; Neuman and Nelson, 1965). Southwest of the study area, Carter (1994) estimated the amount of throw to be at least 5.4 km (3.4 mi). In the study area, the minimum displacement on the Great Smoky fault is estimated to be approximately 35 km (22 mi) based on cross section analysis (Plate III).

Structure beneath the Great Smoky thrust sheet

Structures beneath the Great Smoky thrust sheet are interpreted from cross-section construction, retrodeformation, and analysis (Plates III, IIIa; Appendix D). These structures include; the Foothills duplex, an unnamed duplex, a blind thrust fault, the Chestuee fault, and the Saltville fault (Plates III, IIIa). Evidence for these structures are made from geologic observations and interpretations in the study area, and from the down-plunge projection of structures northeast and southwest of the study area. COCORP seismic reflection data (Cook and others, 1983) reprocessed by Prof. J. K. Costain and Cahit Coruh at Virginia Polytechnic Institute and State University (VPI), and unpublished Arco Exploration Company seismic reflection data constrain some of the resolvable structures in the cross section(s).

Three cross-section lines extend from the Valley and Ridge Middle Ordovician syncline near Mount Vernon, TN, through the Foothills belt of southeastern Tennessee and southwestern North Carolina (Plates I, III, IIIa). These cross sections extend approximately 24 km (15 mi) normal to regional strike, and are spaced approximately 10.5 km (6.5 mi) apart. The depth to basement is interpreted to be approximately 5 km (16,500 ft) as determined by seismic reflection data (Cook and others, 1983). The cross sections can be divided into strata above and below the Blue Ridge-Piedmont megathrust sheet. The hanging-wall structures of this megathrust sheet are discussed throughout this chapter. Footwall structures and evidence for the existence of these structures are discussed below as they occur from the southeast to the northwest in the cross section(s) (Plate III, IIIa).

The Foothills duplex is the southeasternmost footwall structure in the cross section(s), and formed subsequent to the emplacement of the Great Smoky thrust sheet. Evidence for the formation of the Foothills duplex is interpreted from windows exposed in the Great Smoky Mountains region (King, 1964; Neuman and Nelson, 1965, Hatcher and others, 1989b), seismic reflection data along the Tellico River (Cook and others, 1983), and deflection and deformation of previously formed structures in the western Blue Ridge foothills of southeastern Tennessee (Carter, 1994; Geddes, 1995; this study). Moderately strong southeast-dipping reflectors extend from the top of the seismic section (sea level) to basement, and are interpreted to represent strata of the Foothills duplex. The Foothills duplex in the cross section(s) is located along strike with the windows in the Great Smoky Mountains region, and with the Foothills duplex in the cross sections of Carter (1994) and Geddes (1995). Lithologically, the Foothills duplex includes the Rome Formation, Conasauga Group, and Knox Group. The Chickamauga Group is interpreted to not be involved in the duplexing beneath the Great Smoky thrust sheet in the study area, because it is not exposed in the southernmost windows (Cades Cove and Calderwood). This indicates the Great Smoky fault has cut down section to the southwest (Geddes, 1995; this study). Exposures of Knox and Chickamauga Group rocks occur in the northern windows in the Great Smoky Mountains region, suggesting the Great Smoky thrust sheet was arched upward during imbrication and duplexing of footwall units.

Northwest of the Foothills duplex is an unnamed duplex that also folds the Great Smoky thrust sheet. This unnamed duplex, like the Foothills duplex, contains rocks of the Rome Formation, Conasauga Group, and Knox Group. The floor thrust to this duplex juxtaposes early Paleozoic Valley and Ridge units, and has a small displacement that decreases to the southwest due to room (space) problems in cross section construction (Plate III, IIIa). It is tentatively hypothesized that the floor thrust of this unnamed duplex may be related to the Pulaski fault in northeastern Tennessee, which thrusts Knox Group and older strata onto Knox and Chickamauga Group rocks.

A thrust fault exposed at the surface northwest of Starr Mountain (Rodgers, 1953; Hardeman, 1966) is interpreted to be a blind thrust in the study area. At the surface, this thrust fault juxtaposes rocks of the Knox and Conasauga Groups against rocks of the Chickamauga and Knox Groups. Seismic reflection data (Cook and others, 1983) reveal weak southeast dipping reflectors in this area, possibly representing units related to the hanging wall of this blind thrust. This blind thrust and structures related to this fault are transected by the Great Smoky fault (Plates III, IIIa). It is interpreted that the blind thrust and associated hanging-wall anticline were decapitated as the Great Smoky thrust sheet was emplaced. This structure may have also acted as an abutment to impede continued movement of the Great Smoky thrust sheet.

The Chestuee fault is not exposed in the study area, but rocks of this thrust sheet are exposed in the northwesternmost portions of the study area. The Chestuee fault is interpreted as a flat in the cross section, and its location within the cross section is dependent on the amount of Chickamauga Group strata exposed in the Middle Ordovician syncline along the northwestern portions of the cross section (Plates III, IIIa). Assuming the Chickamauga Group in conformably underlain by the Knox Group, Conasauga Group, and the Rome Formation, the Chestuee fault is placed at the base of the Rome Formation (Plates III, IIIa). Unpublished seismic reflection data by Arco Exploration Company across the Valley and Ridge in Monroe County in southeastern Tennessee reveal reflectors, interpreted as the Chestuee fault, at about the same elevation as the Chestuee fault in the cross sections. Location of the ramp between the Chestuee and Saltville faults is difficult to distinguish from seismic data. The positioning of this ramp is partially constrained by an assumed ramp angle of 20 degrees, which is determined form southeast-dipping reflectors from seismic data. Also constraining the position of the ramp is the location of structures above this ramp, such as the Foothills duplex.

The Saltville fault is the lowest structure in the cross sections, and separates Valley and Ridge strata from basement. The location of this fault is well constrained by seismic data (Cook and others, 1983). Formations in this thrust sheet are interpreted to include the Rome Formation, Conasauga Group, Knox Group, and parts of the Chickamauga Group. The thickness of the Chickamauga Group changes between cross sections because the Chestuee fault cuts down section to the northeast. This interpretation permits increased thickness of the Chickamauga Group in the Chestuee thrust sheet as the Middle Ordovician syncline that exposes the Chickamauga Group plunges to the northeast.

Interpretations from cross-section construction, retrodeformation, and analysis results in two possible hypotheses concerning the thrusting sequence beneath the Great Smoky thrust sheet: (1) the sequence of deformation is toward the foreland with emplacement of the blind thrust subsequent to duplexing of Valley and Ridge footwall strata, and before the final emplacement of the Blue Ridge thrust sheet; or (2) emplacement of the blind thrust was the first structure to form in the footwall strata and formed out-of-sequence. These interpretations are based on the crosscutting relationships between the blind thrust and the Great Smoky fault interpreted from geologic maps by Rodgers (1953) and Hardeman (1966) (Plates III, IIIa).

The first interpretation concerning the sequence of thrusting results in foreland-directed (northwest) thrusting. The first structure to be emplaced is the Blue Ridge thrust sheet. Duplexing of Valley and Ridge footwall strata beneath the Great Smoky fault results in the formation of the Foothills duplex and the unnamed duplex, respectively. As the Great Smoky fault was folded by duplexing of the Valley and Ridge footwall units, movement along the Great Smoky fault continues, although it must be partially locked. The next structure to form was the blind thrust. Emplacement of the blind thrust resulted in the formation of a hanging-wall anticline, which was then decapitated during the final emplacement of the Blue Ridge thrust sheet. Emplacement of the Chestuee thrust sheet follows in the sequence with the Saltville thrust sheet being the last footwall structure to form in the cross sections.

The second interpretation concerning the sequence of thrusting involves emplacement of the blind thrust and formation of the hanging-wall anticline followed by the emplacement of the Blue Ridge thrust sheet, which decapitates the hanging-wall anticline. The Blue Ridge thrust sheet is then folded due to the formation of the Foothills duplex and unnamed duplex beneath this thrust sheet. The emplacement of the Chestuee and Saltville faults, respectively, follow in the thrusting sequence. Problems with this interpretation requires the blind thrust to be out-of-sequence, which may be kinematically unfeasible.

Maggies Mill fault

The Maggies Mill fault was mapped southwest of the study area by Carter (1994), who interpreted the fault as a brittle structure that juxtaposed rocks of the lower and middle members of the Sandsuck Formation. Previously, the Maggies Mill fault had been mapped as the Sylco Creek fault (Rodgers, 1953), and the Miller Cove fault (Wiener and Merschat, 1992), but Carter (1994) recognized that the Miller Cove fault is southeast of this structure. Carter (1994) observed two important lithologic and structural characteristics of the Maggies Mill fault: (1) lithologic similarities between footwall and hanging wall strata; and (2) a lack of structural or metamorphic discontinuities across the fault. The trace of the fault is mapped on the basis of different footwall and hanging-wall stratigraphy. Carter (1994) estimated the dip of the Maggies Mill fault to range from 25° to 40° southeast.

The Maggies Mill fault is traceable from the southwest into the Tellico Plains 7.5-minute quadrangle along Webb Branch. The fault is traceable northeastward crossing Conasauga Creek at Conasauga Mill, and continuing along the northwest slope of Mocking Crow Mountain before being cut off by the Great Smoky fault near Kirkland Hollow (Fig. II-2; Plate I). Because the trace of the Maggies Mill fault in the study area is only 3.6 km, criterion used by Carter (1994) for mapping the fault was used in this study. Exposure of the fault in the study area is poor, but the fault was mapped based on the following evidence: (1) the abrupt juxtaposition of different stratigraphic sections of the Sandsuck Formation; and (2) geomorphic expression of the contact as the fault is traced along Webb Branch. The fault trace is characterized mostly by coarse-grained quartz sandstone and conglomerate in the hanging wall, and predominantly siltstone and shale in the footwall. The contact between these lithologies is abrupt, unlike the majority of contacts between different lithologies in the Sandsuck, which are dominantly gradational. Through much of its trace, the Maggies Mill fault parallels northeast-trending drainages, and may be the cause of topographic breaks (benches) along some slopes The outcrop pattern of the Maggies Mill fault suggests the fault dips approximately 30° to 40° southeast.

Carter (1994) considered three possible interpretations for the formation of the

Maggies Mill fault and the amount of displacement associated with it: (1) The Maggies Mill fault may be an imbricate of the Miller Cove fault, (2) a slice of the Miller Cove fault, or (3) an imbricate of the Great Smoky fault. For the Maggies Mill fault to be an imbricate of the Miller Cove fault, lithologic similarities should exist between footwall and hanging-wall strata without much displacement (Carter, 1994). No similarities exist between the lithologies bounding the Miller Cove fault, because the hanging wall units are lithologically different, intensely cleaved, and more metamorphosed than the footwall units. If the Maggies Mill fault is a slice of the Miller Cove fault, the lithologies in the footwall would be laterally equivalent to the lithologies in the hanging wall, with horizontal displacement possibly as large as the displacement of the Miller Cove fault (Carter, 1994). Carter (1994) favored the Maggies Mill fault being an imbricate of the Great Smoky fault, because of similarities between lithology, cleavage morphology, cleavage intensity, and metamorphism between hanging wall and footwall strata.

Based on the limited exposure and extent of Maggies Mill fault in the study area, the Maggies Mill fault is interpreted to be an imbricate of the Great Smoky fault because of lithologic similarities between hanging wall and footwall strata (Plates III, IIIa). The hanging-wall strata of the Maggies Mill fault consist of a sequence of quartz sandstone gradationally overlain by shale that locally contains carbonate bodies, while footwall strata consist of a lithologically similar quartz sandstone and shale sequence. Carter (1994) recognized similar lithologic sequences in the hanging wall strata to the southwest. The quartz sandstone/shale sequence in both the footwall and hanging wall of the Maggies Mill fault suggest rocks in the footwall are lithologically similar to rocks in the hanging wall. Additionally, rocks in the hanging wall of the Maggies Mill fault have similar metamorphic grade (anchizone), cleavage morphology, and cleavage intensity with rocks in the footwall. Therefore, based on the evidence presented above and by Carter (1994), the Maggies Mill fault is interpreted to be an imbricate of the Great Smoky fault with an estimated displacement of 1 km (.6 mi) (Plates III, IIIa). Displacement on the fault increases to the southwest into the area mapped by Carter (1994), where the hanging-wall strata of the Maggies Mill fault are interpreted to be thrust onto higher units of the Sandsuck Formation in the footwall.

Miller Cove fault

The Miller Cove fault is a major structure in the western Blue Ridge that thrusts penetratively cleaved chlorite and higher-grade metamorphic rocks of the Wilhite Formation onto less cleaved and less metamorphosed (anchizone) rocks of the Sandsuck Formation (King, 1964; Neuman and Nelson, 1965; Carter, 1994). Because the Miller Cove fault juxtaposes structures that developed during different orogenic events, it is interpreted as a basement fault (Hatcher and others, 1989a), which decapitates regional synmetamorphic folds in cross section (Plates III, IIIa). The Miller Cove fault family extends discontinuously approximately 250 km (167 mi) from northwest of English Mountain to the Cartersville District in northwestern Georgia (Costello, 1984; Hatcher and others, 1989a) (Fig. I-1). In the vicinity of the study area, the Miller Cove fault was mapped as the northern continuation of Salisbury's (1961) Alaculsy Valley fault by Wiener and Merschat (1992).

From the southwest, the Miller Cove fault is exposed in the study area along the base of a prominent line of ridges along Steer Creek. The Miller Cove fault is traceable northeastward along Steer Creek, beneath Tennessee State Highway 68 to Tellico Lake, where the fault trace is located along Quarry Creek to the Tellico River. The fault then is located along a northeast-trending drainage of the Tellico River to Puncheon Hollow in the northeasternmost portion of the study area. The Miller Cove fault is easily mapped because of the distinct lithologic and structural differences between hanging wall and footwall strata, and the geomorphic expression of the fault in the topography. Rocks in the hanging wall of the Miller Cove fault are metamorphosed to chlorite grade, and have a dominant S-surface (foliation) that is characterized by continuous (slaty) cleavage (S_1) in fine-grained lithologies. Locally, these cleaved, fine-grained rocks were later deformed by pressure solution (S_{1a}) and crenulations (S_2). Footwall rocks are metamorphosed to anchizone, and the dominant S-surface (foliation) is a weakly developed slaty cleavage (S_3) in fine-grained rocks. The topographic expression of the fault trace indicates the Miller Cove fault dips approximately 20° to 30° southeast.

The formation of the Miller Cove fault has been interpreted to be a major brittle structure related to the Great Smoky fault, because metamorphic discontinuities across the Miller Cove fault indicate that it is younger than premetamorphic faults, such as the Dunn Creek and Greenbrier faults, and older than the Great Smoky fault (King, 1964; Neuman and Nelson, 1965). Wiener and Merschat (1978) suggested the Alaculsy Valley fault in southeastern Tennessee and northwestern Georgia is a premetamorphic fault related to the Dunn Creek and Line Springs faults in the Great Smoky Mountains region that juxtaposes Snowbird Group, which has now been shown by Costello and Hatcher (1991) to be Walden Creek Group, rocks onto Walden Creek Group rocks. Woodward and others (1991) interpreted the formation of axial-planar cleavage, folds, and minor ductile thrust faults as developing during early emplacement of the Miller Cove thrust sheet in the Great Smoky Mountains region, and related to ductile deformation associated with a moving thrust sheet (after Mitra and Eliott, 1980). They inferred that this early Miller Cove fault was reactivated or truncated by a later brittle Alleghanian structure. Thus, Woodward and others (1991) concluded that the Miller Cove thrust sheet is multiphase structure with both a ductile pre- to synmetamorphic and brittle post-metamorphic history of movement.

Southwest of the study area in the Mecca and McFarland 7.5-minute quadrangles, Carter (1994) interpreted the Miller Cove fault as a brittle structure because of structural and metamorphic discontinuities across the fault, gouge zones, and discrete crenulations. Imbricates of the Miller Cove fault transect preexisting continuos (slaty) cleavage and contain slickenlines. Microstructurally, highly strained and partially recrystallized quartz occur within folded quartz veins and discrete and zonal crenulations are axial planar to the microfolds in the Miller Cove imbricate zone (Carter, 1994). Crosscutting relationships suggest that slaty cleavage developed prior to veining, microfolding, and development of axial-planar crenulations. Gouge zones crosscut all preexisting structures (Carter, 1994).

Evidence for the Miller Cove fault being a postmetamorphic brittle structure in the study area includes many of the structural and metamorphic features observed to the southwest by Carter (1994). Imbricates of the Miller Cove fault were observed west of Tellico Lake and along County Highway 2342 (Rafter Rd.), Tellico Plains 7.5-minute quadrangle (Plate I). These imbricates and related structures, such as fault gouge, crenulations, and slickenlines, transect the preexisting continuous (slaty) cleavage. The juxtaposition of penetratively cleaved rocks onto less cleaved rocks, and brittle fault fabrics associated with imbricates of the Miller Cove fault provide evidence for Alleghanian thrusting of the Miller Cove fault in my study area.

The amount of throw and horizontal displacement on the Miller Cove fault cannot be determined because of the lack of correlative lithologic markers across the fault. Because the Miller Cove fault juxtaposes slaty cleaved chlorite grade rocks onto less cleaved anchizone rocks, Carter (1994) suggested the vertical displacement to be at least 5 km and the horizontal displacement to be at least 10 km to account for the differences in metamorphic grade across the fault (Plates III, IIIa).

Rabbit Creek fault

The Rabbit Creek fault was originally mapped in the Great Smoky Mountains

National Park, and it thrust Great Smoky Group onto Walden Creek Group rocks (Neuman and Nelson, 1965). The Rabbit Creek fault is traceable for approximately 56 km (35 mi) from the vicinity of Cades Cove to the vicinity of Tellico Plains in southeastern Tennessee. The fault was mapped southwestward from the Little Tennessee River to the northeast boundary of this study area by Wiener (unpub.) and Geddes (1995). Criteria used for mapping this fault include a major lithologic contrast across the contact, fault fabrics observed at several locations along the contact, and many distinct topographic lineaments (Neuman and Nelson, 1965; Geddes, 1995).

In the study area, the Rabbit Creek fault is traced from the northeast along the northwest slope of Henson Mountain, and along Big Branch to the Tellico River. Along this portion of the fault trace, sulfidic and graphitic black slate of the Dean Formation have been thrust over green-banded ankeritic metasiltstone of the Wilhite Formation. From the Tellico River southward, the fault trace is located near the top of Grave Mountain, and trends 0.6 km (2,000 ft) southwest of Tennessee State Highway 68 where it is cut off by the Oconaluftee fault. The hanging wall of the fault contains coarse-grained orthoquartzite, graywacke, granule conglomerate, and black slate of the Dean Formation, while rocks in the footwall consist of mostly overturned medium-grained arkosic sandstones of the Wilhite Formation in the footwall (Fig. III-2). The criteria used for mapping the Rabbit Creek fault northeast of the study area (Neuman and Nelson, 1965; Geddes, 1995) are used in this study. The strongest evidence for recognition of the Rabbit Creek fault in the study area is the prominent lithologic changes across the contact. Throughout its trace in the study area, the hanging-wall strata of the Rabbit Creek fault consist of lithologies typical of similar Great Smoky Group lithologies observed in the southeasternmost portions of this study area. The footwall strata contain green-banded metasiltstone and ankeritic metasiltstone, along with arkosic sandstone and conglomerate typical of the Walden Creek Group. The channel conglomerate in the

Figure III-2. Overturned Wilhite sandstone in the footwall of the Rabbit Creek fault along Tennessee State Highway 68 at Grave Mountain, Tellico Plains 7.5-minute quadrangle.

footwall is polymictic, and consists of quartz pebbles and slate chips that are lithologically similar to the underlying Great Smoky Group. Good exposures of footwall and hanging-wall strata of the Rabbit Creek fault in the study area are along Tennessee State Highway 68 at Grave Mountain (Tellico Plains 7.5-minute quadrangle). Here the main fault trace is covered and located in a drainage between the hanging wall and footwall exposures (Figs. II-2, III-1; Plate I). Small brittle faults and slickenlines were recognized in hanging-wall strata near the main trace of the fault. Topographic lineaments were also used to assist mapping the Rabbit Creek fault. The dip of the Rabbit Creek fault ranges from 30 to 60° southeast in the Great Smoky Mountains National Park (Neuman and Nelson, 1965), and from 30° southeast to almost vertical southwest of the park and northeast of the study area (Geddes, 1995). The dip of the Rabbit Creek fault in the study area is estimated from outcrop patterns to be dip 30 to 40° southeast.

Neuman and Nelson (1965) interpreted the Rabbit Creek fault as a predominantly premetamorphic structure that has been reactivated because the fault cuts or is cut by younger faults. Neuman and Nelson (1965) mapped the coarse-grained rocks in the hanging wall as Cades Sandstone unclassified (Great Smoky Group), and the fine-grained rocks in the footwall as Wilhite Formation (Walden Creek Group) and Metcalf Phyllite (Snowbird Group). In the Great Smoky Mountains region, the Cades Sandstone is isolated from the main body of the Great Smoky Group by the Oconaluftee fault. Rocks similar to Cades Sandstone occur in the hanging wall of the Oconaluftee fault, which cuts across footwall strata (Neuman and Nelson, 1965). If the Rabbit Creek fault is related to the Oconaluftee fault, Neuman and Nelson (1965) suggested rocks in the hanging wall would be equivalent to or younger than rocks in the footwall.

Geddes (1995) mapped the Rabbit Creek fault northeast of my study area, from the Tellico River northeastward to Citico Creek, in southeastern Tennessee (Fig. I-2).

Geddes (1995) interpreted the Rabbit Creek fault as a reactivated premetamorphic fault because of the presence of cataclasite, brittle deformation of slaty cleavage, and an increase in metamorphic grade from anchizone and lower chlorite grade to chlorite grade when crossing the structure from northwest to southeast. Geddes (1995) recognized the same lithologic similarities as Neuman and Nelson (1965) between Great Smoky Group rocks in the Rabbit Creek and Oconaluftee thrust sheets. Because of compositional and textural similarities to the Dean Formation in the Oconaluftee thrust sheet, Geddes (1995) correlated the rocks in the Rabbit Creek thrust sheet with the Dean, Ammons, Wehutty, and Copperhill Formations of the Great Smoky Group, and suggested abandoning the name "Cades Sandstone."

I also chose to interpret the Rabbit Creek fault in my study area as a reactivated postmetamorphic brittle fault, because the Rabbit Creek fault cuts earlier-formed structures, and the fault zone contains brittle fault fabrics. Compositional and textural similarities also exist between rocks in the Rabbit Creek thrust sheet and rocks in the hanging wall of the Oconaluftee fault in the study area, thus providing evidence to support the interpretations of Neuman and Nelson (1965) and Geddes (1995) concerning the equivalence of rocks in the Rabbit Creek thrust sheet with those in the hanging wall of the Oconaluftee fault. Footwall and hanging-wall strata of the Rabbit Creek fault are exposed on Tennessee Highway 68 at Graves Mountain (Figs. III-1, III-2). Here the footwall strata consist of folded sandstone of the Wilhite Formation. The Rabbit Creek fault may have propagated through fine-grained metasiltstone and slate separating the two exposures, and is located in a drainage between them. The hanging-wall strata consist of a locally sulfidic orthoquartzite and slate, and is interpreted as belonging to the Great Smoky Group. Minor faults were observed in the hanging-wall strata, and are interpreted as splays of the Rabbit Creek fault. Most of the intense deformation from the Rabbit Creek fault in this area is localized in the folding of the footwall strata. Possible fault breccia was observed in Big Branch, approximately 1250 m (4,000 ft) upstream from its confluence with the Tellico River, providing evidence for brittle deformation.

Displacement on the Rabbit Creek thrust sheet is interpreted to decrease to the southwest (Plates I, III, IIIa). Based on cross section analysis, the Rabbit Creek fault is estimated to have a displacement of approximately 2.3 km (1.4 mi) along cross section line A-A', and a estimated displacement of approximately 1.9 km (1.2 mi) along cross section line B-B'.

Oconaluftee fault

The Greenbrier fault is a major structure in the Great Smoky Mountains region that was first recognized by King and others (1958) and separates the Ocoee Supergroup into two major stratigraphic sequences (King, 1964). King and others (1958) originally interpreted the hanging-wall strata as consisting of Great Smoky Group rocks conformably overlying Snowbird Group, while footwall units consist of Snowbird Group conformably (?) overlain by unclassified Ocoee Supergroup formations and Walden Creek Group. Recent unpublished geologic mapping by C. Montes (pers. comm.) in the Dellwood 7.5-minute quadrangle (North Carolina) suggests the contact between the Snowbird and Great Smoky Groups, originally mapped as conformable by Hadley and Goldsmith (1963), is the continuation of the premetamorphic Greenbrier fault with reactivation and brittle deformation during the Alleghanian orogeny along portions of the fault. In the Great Smoky Mountains National Park, the Greenbrier fault thrust Great Smoky Group over Walden Creek Group, Snowbird Group, rocks of the Rabbit Creek thrust sheet, and Grenville crystalline basement rocks (King and others, 1958; Hadley and Goldsmith, 1963; King, 1964; Neuman and Nelson, 1965) (Fig. I-1). The Greenbrier fault is interpreted as a premetamorphic ductile structure associated with the Taconic orogeny because ductile fault fabrics are present, regional metamorphic isograds transect the fault boundary, and the fault does not deform regional cleavage (Hadley and Goldsmith, 1963; King, 1964; Milton, 1983; Connelly and Dallmeyer, 1990; Woodward and others, 1991; Connelly and Woodward, 1992).

The Oconaluftee fault is both a high-angle dextral fault and a thrust fault in the central and western Great Smoky Mountains (King, 1964; Neuman and Nelson, 1965). At its northern end, the Oconaluftee fault is a dextral strike-slip fault that obliquely cuts the Greenbrier fault (Fig. I-1). The trace of the Oconaluftee fault becomes parallel to the Greenbrier fault south of Wear and Tukaleechee Coves, and was interpreted by Neuman and Nelson (1965) as a low-angle thrust that truncates, overrides, or reactivates the preexisting Greenbrier fault plane. They named this segment of the fault the Oconaluftee-Greenbrier fault. In the southwestern portion of the Great Smoky Mountains National Park, Neuman and Nelson (1965) mapped the lowest formation of Great Smoky Group (Elkmont Sandstone) in the hanging wall of the Oconaluftee, and "Cades Sandstone" (Great Smoky Group) and Metcalf Phyllite (Snowbird Group) in the footwall.

Geddes (1995) mapped the Oconaluftee fault northeast of the study area, and used as evidence the emplacement of Wilhite and Great Smoky Group units over rocks in the Rabbit Creek thrust sheet to map the Oconaluftee fault. Geddes (1995) presented evidence the Oconaluftee fault is a brittle Alleghanian fault because of the truncation of rock units in the Rabbit Creek fault, and the truncation of 1st- and 2nd-order folds. Geddes (1995) suggested the hanging wall of the Oconaluftee fault in the Great Smoky Mountains National Park is composed of the two lowest Great Smoky Group formations (Elkmont and Thunderhead Sandstones), while to the southwest, between the Tellico River and Citico Creek, the two uppermost Great Smoky Group formations (Dean and Ammons) are also exposed in the hanging wall. This change is explained by regional structures. In the Great Smoky Mountains region, 1st-order anticlines bring up older

Great Smoky Group units, but between the Little Tennessee River and Tellico River, the southwest-plunging 1st-order Epperson synclinorium brings down younger Great Smoky Group units, as well as the overlying Wilhite Formation (Carter and others, 1995b). This also is evidence of the small displacement along the Oconaluftee and Rabbit Creek faults.

The Oconaluftee fault is traceable approximately 72 km (45 mi) from near Elkmont, Tennessee, in the Great Smoky Mountains to near Tellico Plains, southeastern Tennessee (Fig. I-1). In my study area, the Oconaluftee fault is located along the northwest slopes of Henson, Tellico, Grave, and Queens Mountains (Tellico Plains 7.5-minute quadrangle). This fault cuts the Rabbit Creek fault along the northwest slope of Grave Mountain, and is cut off by the Miller Cove fault along the northwest base of Queens Mountain (Fig. II-2; Plate I). Rocks in the hanging wall of the Oconaluftee fault consist of coarse-grained conglomerate and graywacke along with slate lenses correlated with the Dean Formation (Great Smoky Group). Conformably overlying these Great Smoky Group lithologies are the metasiltstones of the Walden Creek Group. Footwall lithologies consist mostly of fine-grained graphitic and sulfidic slate, with lenses of orthoquartzite and graywacke, and are interpreted to be correlative with the Dean Formation. The dip of the Oconaluftee fault in the study area ranges from approximately 30° southeast in the northeastern portion of the study area near the Tellico River to approximately 45° southeast southwestward along Tellico, Grave, and Queens Mountains.

In the study area, the Oconaluftee fault is exposed on Tennessee State Highway 165 along the Tellico River (Fig. III-3A), and on Tennessee State Highway 68 at Grave Mountain (Plate I). The main trace of the Oconaluftee fault is 180 m (600 ft) northwest of the bridge crossing the Tellico River on Tennessee State Highway 165 at the Tellico Plains-Bald River Falls 7.5-minute quadrangle boundary (Figs. II-2, III-1; Plate I). From this locale northward to the main fault, numerous thrust faults deform hanging-wall strata. These faults are characterized by brittle fault fabrics, such as fault gouge and

Figure III-3. The Oconaluftee fault zone. (A) Sketch of the Oconaluftee fault zone along the Tellico River, Tennessee State Highway 165, Tellico Plains 7.5-minute quadrangle. (B) The Oconaluftee fault. Location of photograph is indicated by the boxed area in (A).

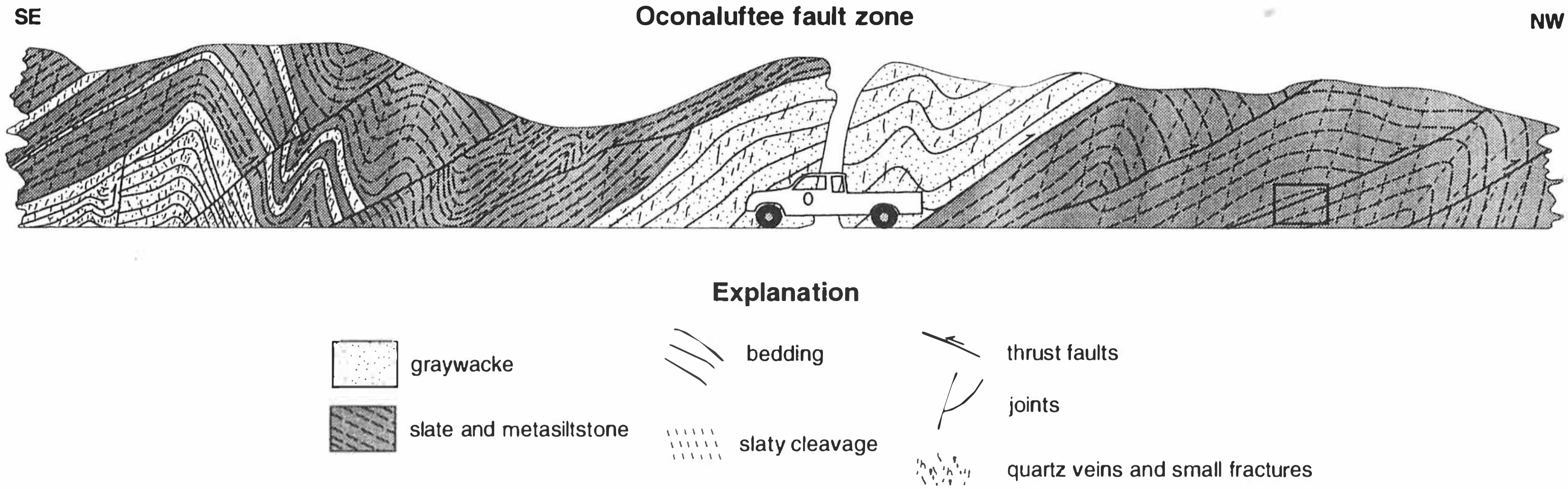
SE
Oconaluftee fault zone
NW
Explanation
graywacke
slate and metasiltstone
bedding
slaty cleavage
thrust faults
joints
quartz veins and small fractures
(A)

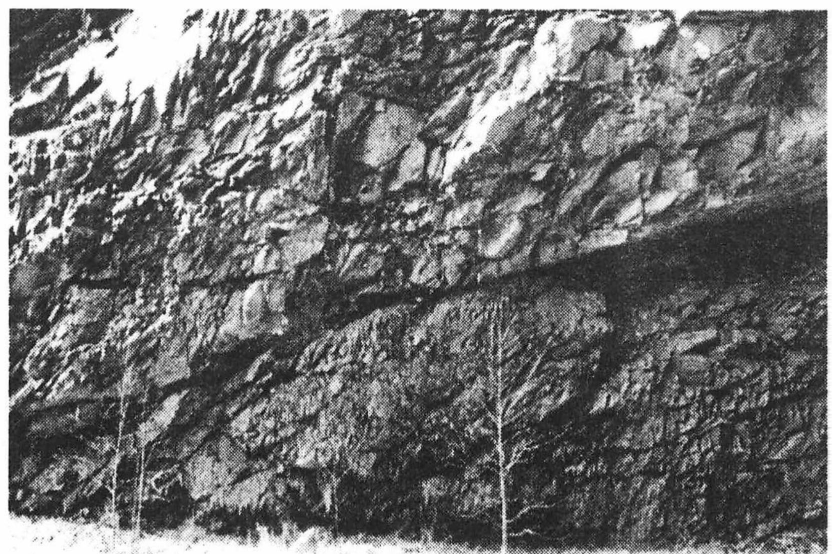
(B)

slickenlines (Fig. III-3B). These faults also decapitate folds and transect the continuous (slaty) cleavage. Similar structural and lithologic relationships are present along the Oconaluftee fault on Tennessee State Highway 68 at Grave Mountain. Here, the hanging-wall strata are deformed by splays from the main Oconaluftee fault. A high-angle strike-slip fault also deforms hanging-wall strata. Dextral strike-slip faulting related to the Oconaluftee fault has been reported northeast of the study area in the Great Smoky Mountains region (Neuman and Nelson, 1965). Similar brittle structures related to the Oconaluftee fault observed along the Tellico River are also present along Tennessee State Highway 68. These structures include gouge, slickenlines, decapitation of folds, and transection of continuous (slaty) cleavage. Based on the evidence presented above, I interpret the Oconaluftee fault as a postmetamorphic structure that transects rocks of the Rabbit Creek thrust sheet (Plate I). Based on cross-section interpretations, a minimum displacement on the Oconaluftee fault is estimated to be approximately 1.4 km (0.9 mi) (Plates III, IIIa).

Minor faults

Minor map-scale faults that deform rocks within the study area include: the Hunt Branch fault, Tellico Mountain fault, a small thrust fault on Payne Ridge, and a normal fault near Coker Creek (Fig. II-2; Plate I). These faults appear to have small displacements, and are not traceable very far along strike. The significance of these faults in this study is that they are mappable structures that displace contacts.

Hunt Branch fault

The Hunt Branch fault was mapped by McKinney (1964), and is exposed on the eastern limb of an anticline in the northern portion of study area (Figs. II-2, III-1; Plate I). McKinney (1964) postulated this fault cut an adjacent syncline and thrust Shady

Dolomite over Rome Formation. The Hunt Branch fault probably dies out southward in the Kirkland Hollow anticlinorium, and apparently merges with the Bullet Mountain fault to the north (McKinney, 1964). McKinney (1964) interpreted the fault to dip 30° east.

Tellico Mountain fault

The Tellico Mountain fault, originally recognized by Poppelreiter (1980), is exposed atop Tellico Mountain on Tennessee State Highway 68 (Figs. III-4A, III-4B). Here, hanging-wall lithologies consist of very coarse-grained granule to cobble conglomerate, and graywacke that is overlain to the southeast by green-banded ankeritic metasiltstone. Footwall units are similar to those in the hanging wall, and consist of coarse-grained granule conglomerate and graywacke overlain by banded metasiltstone. Cobble-size clasts are absent in the exposed footwall sequence. Approximately 90 m (300 ft) northwest of the Tellico Mountain fault the coarse-grained conglomerate and graywacke conformably overlie dark gray to black metasiltstone and slate. The trace of the Tellico Mountain fault extends approximately 3 km (2 mi) along the crest of Tellico Mountain, and dips approximately 35° southeast. In this study, the trace of the Tellico Mountain fault is based on the relationships observed on Tennessee State Highway 68. The fault is interpreted to terminate in an anticline to the southwest 1.7 km (1.1 mi) from the exposure on Tennessee State Highway 68 (Plate I). To the northeast, the fault is difficult to trace because the relationships observed on Tennessee State Highway 68 are not traceable. Therefore, the Tellico Mountain fault is extrapolated northeastward along the crest of Tellico Mountain. Beyond here, evidence for the Tellico Mountain fault diminishes. The stratigraphic throw of the Tellico Mountain fault is approximately 15 m (50 ft), with an estimated horizontal displacement of 25 to 30 m (75 to 100 ft).

Poppelreiter (1980) interpreted this fault as a late Paleozoic fault that thrust coarse-grained units of the Walden Creek Group over fine-grained units of the Walden

Figure III-4. Tellico Mountain fault zone. (A) Sketch of the Tellico Mountain fault zone along Tennessee State Highway 68 at Tellico Mountain, Tellico Plains 7.5-minute quadrangle. (B) The Tellico Mountain fault. Location of photograph is indicated by the outlined area in (A).

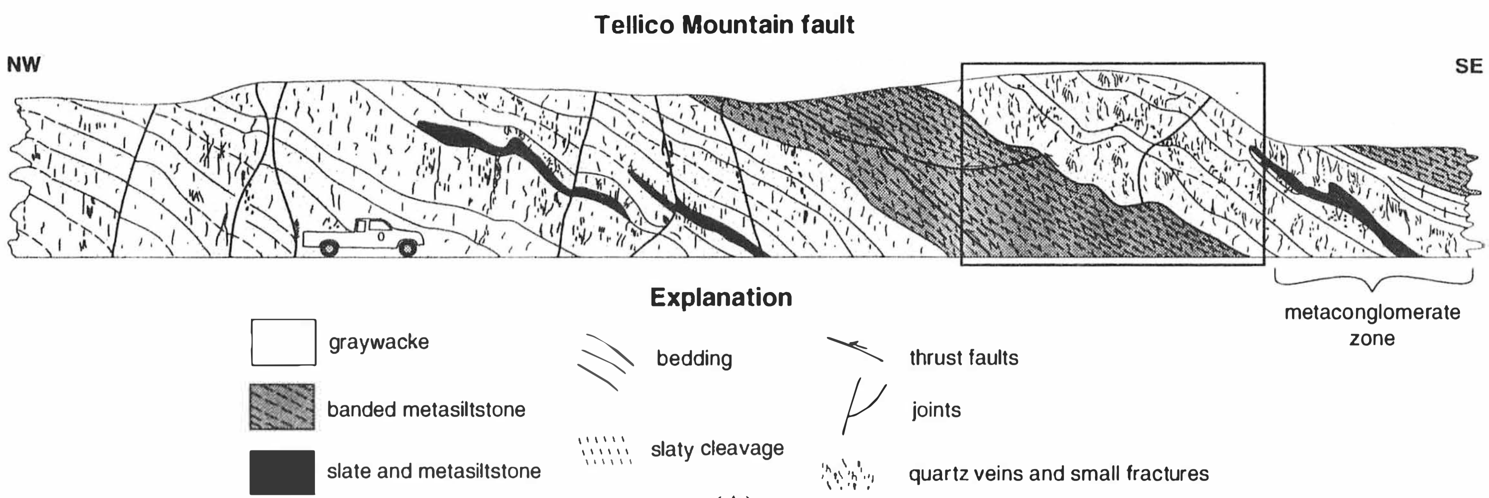
Tellico Mountain fault
NW
SE
metaconglomerate zone
Explanation
graywacke
banded metasiltstone
slate and metasiltstone
bedding
slaty cleavage
thrust faults
joints
quartz veins and small fractures
(A)

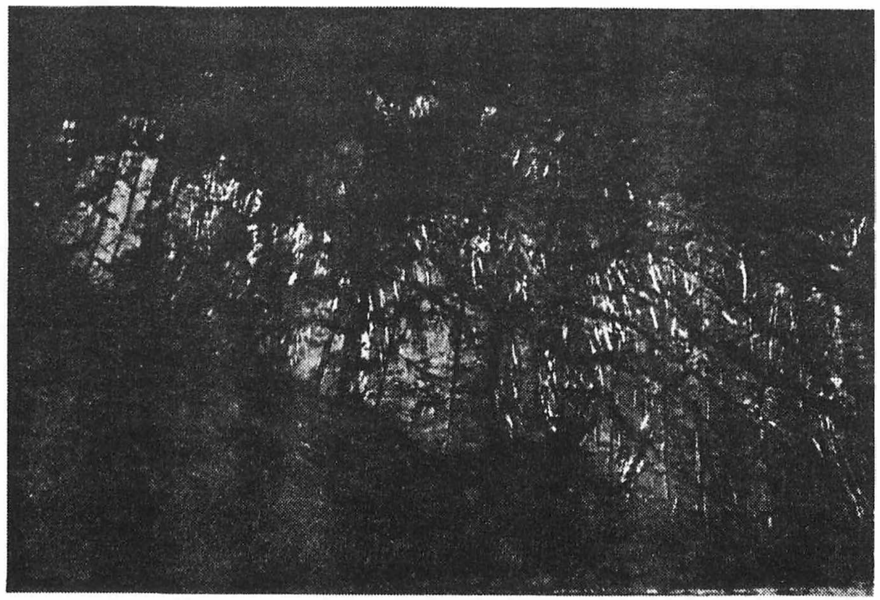
(B)

Creek Group. This thrust is interpreted to have originated in the basal décollement of the Great Smoky fault because of moderately low-angle thrusting on bedding planes and early low-angle extension prependicular to bedding (Poppelreiter, 1980). Poppelreiter (1980) also suggested intense shear strain concentrated along the bounding zones of competent layers was responsible for the thickening and thinning of the interbedded slate and metasiltstone. These layers differentially flow into the overlying strata during compression and upward transport.

In this study, the Tellico Mountain fault is interpreted to repeat a sequence of Dean Formation conglomerate and graywacke overlain by Wilhite Formation metasiltstone. The coarse-grained conglomerate and graywacke in both hanging-wall and footwall sequences are correlated with the Dean Formation of the Great Smoky Group because of similar graywacke and conglomerate composition with other Great Smoky Group units in southeastern Tennessee (Fig. II-5). The metasiltstone in both hanging-wall and footwall sequences is correlated with the Wilhite Formation of the Walden Creek Group because of ankerite-bearing metasiltstones approximately 60 m (200 ft) southeast of the fault. Additionally, the hanging-wall and footwall metasiltstones are lithologically similar. Ankeritic metasiltstones are present just above the Great Smoky Group/Walden Creek Group contact in the southeastern portion of this study area. Thus, the Tellico Mountain fault is interpreted to repeat the Great Smoky Group/Walden Creek Group contact in this portion of the study area.

The Tellico Mountain fault is interpreted as a brittle fault that formed as a result of continued tightening of the Tellico Plains anticlinorium during Alleghanian deformation. Evidence for the brittle nature of this fault include gouge, slickenlines, and truncation of bedding (Fig. III-4B). Some bedding planes of the conglomerate and graywacke in both the hanging wall and footwall contain lenses of slate and metasiltstone that are tectonically thickened in the hinges of folds. Many bedding plane surfaces also contain slickenlines, providing evidence for both flexural flow and flexural slip folding. Additionally, quartz veins are truncated abruptly at the slate contacts and feather out in the finer portions of the graded graywacke beds, representing an early period of west-northwest extension during folding (Poppelreiter, 1980; Carter and others, 1995a).

Other faults

Two small faults were originally mapped within the Wilhite Formation in the study area by Hale (1974). Hale (1974) inferred a thrust fault on Payne Ridge and a normal fault in the Coker Creek area because of the offset of outcrop patterns of sandstone units, bedding orientations, and repetition of sandstone units. Geologic mapping for this study confirms the outcrop patterns of the Wilhite sandstone units as mapped by Hale (1974).

A small thrust fault deformed Wilhite Formation sandstone on Payne Ridge. This fault is located between Payne Ridge and an unnamed ridge to the southeast and is inferred to extend to Sixmile Creek to the northeast. The extent of the fault is uncertain because of the difficulty tracing faults in this area where there are no lithologic contrasts on either side of the contact. Evidence for faulting of this sandstone unit include the offset of the outcrop pattern in the sandstone units, the intensely folded zones of metasiltstone north of the sandstone unit near the fault zone (Hale, 1974), and the narrow linear drainage between Payne Ridge and the unnamed ridge (Plate I). The fault is not exposed, but there are no confirming structures present to account for the abrupt termination of the sandstone. The origin of this fault is possibly related to continued folding of the Payne Ridge anticlinorium during Alleghanian deformation.

In the southern portion of the study area, mostly in the Farner 7.5-minute quadrangle, Hale (1974) mapped a normal fault between Wilhite sandstone units. This normal fault is interpreted to have developed along a small fold on the east limb of a small syncline (Hale, 1974). The trace of this fault extends from southeast of Cataska School northeastward to the Farner/Tellico Plains 7.5-minute quadrangle boundary, while the northeastward extent of the fault into the Tellico Plains 7.5-minute quadrangle is unconfirmed. The northeastern portion of the Farner 7.5-minute quadrangle is included to provide continuity with previously mapped areas within and surrounding the study area. Geologic mapping for this portion of the study area primarily included field checking Hale's (1974) data. The outcrop patterns of the Wilhite sandstone mapped by Hale (1974) were confirmed here. Along the fault, bedding is locally overturned in the footwall where sandstone beds are repeated, but are upright to the northeast where they form the east limb of a small anticline (Hale, 1974). The fault is not exposed. Map patterns, however, along with bedding orientation provide evidence for the fault, and include: (1) sandstone units exposed in the upthrown block contain mappable metasiltstone between sandstone units that are not exposed in the sandstone of down-thrown block; (2) repetition of sandstone units across the fault; and (3) intense folding in this area. This normal fault probably formed during folding of the sandstone. Instead of a normal fault here, the sandstone units could alternately be repeated by intense folding. This requires upright southeast-dipping beds northwest of the beds that are overturned to the southeast. Instead of upright and dipping to the southeast, these beds dip northwest, so I believe that mapping a fault here is the best solution to this outcrop pattern.

Folds

Soft-sediment folds (F_0) and evidence for four tectonic folding events (F_{1-4}) are present in the study area. Tectonic folds in the study area are divisible into 1st- order to 6th-order structures, while syndepositional folds are only 5th- to 6th-order structures (Table III-1). The chronology of the folding events is determined from the relationship between folds to the regional axial-planar slaty cleavage, and to later faulting events. F_0

Table III-1. Size order of folds.

	Order	Amplitude range	Wavelength range	examples
Regional structures	1 st	> 500 m	> 5 km	Murphy synclinorium (F_1) Ducktown anticlinorium (F_1) Epperson synclinorium (F_1)
Map scale (quadrangle) structures	2 nd	500 m - 50 m	5 km - 1 km	Payne Ridge anticlinorium (F_1) Grindstone Ridge anticlinorium (F_1) Tellico Mountain anticlinorium (F_1) Tellico Plains synclinorium (F_3) Kirkland Hollow anticlinorium (F_3)
	3 rd	50 m - 15 m	1 km - 50 m	"Whaleback" anticlines (F_1)
Mesoscale structures	4 th	15 m - 1 m	50 m - 1 m	
	5 th	1 m - 10 cm	1 m - 10 cm	
	6 th	< 10 cm	< 10 cm	

folds are present throughout the study area and occur within bedding, indicating their syndepositional formation. F_1 folds are 1st- and higher-order structures characterized by penetrative axial-planar slaty cleavage, implying a synmetamorphic origin for the formation of these folds. Deformation of slaty cleavage by 5th- and higher-order folds in the Miller Cove thrust sheet defines the F_2 folds. Second- and higher-order F_3 folds occur in the Bullet Mountain, Great Smoky, and Maggies Mill thrust sheets. These folds are interpreted to have formed during post-metamorphic faulting, because fold hinges are oriented subparallel to regional post-metamorphic faults. F_4 folds appear as 2nd-order structures that deform the entire Blue Ridge thrust sheet, and are evident by the occurrence of windows in the Great Smoky Mountains National Park region.

F_0 folds

Soft-sediment F_0 folds are preserved in the study area in the fine-grained rocks of the Sandsuck, Wilhite, and Dean Formations (Fig. III-5). These F_0 folds are 5th- and higher-order open to isoclinal structures, and have fold hinges that generally plunge gently to the northeast and southwest with axial surfaces moderately inclined to nearly recumbent. F_0 folds are recognized by the transection by regional slaty cleavage and intralayer geometry, wherein soft-sediment folds are bounded above and below by bedding surfaces. Most soft-sediment folds have been modified by later folding and faulting events. F_0 folds probably formed by downslope movement of water-saturated sand, silt, and clay in response to gravitational and overburden forces.

F_1 folds

The Miller Cove thrust sheet is dominated by F_1 folds. These folds occur at all scales, from the 1st-order Epperson synclinorium (Laajoki, 1993) and the 2nd-order Payne Ridge anitclinorium to 4th- and higher-order parasitic folds to these regional

Figure III-5. F_0 folds in fine-grained rocks of the Wilhite Formation. 6th-order soft-sediment fold from the Farner 7.5-minute quadrangle. Centimeter scale. Sample courtesy of Mark Carter.

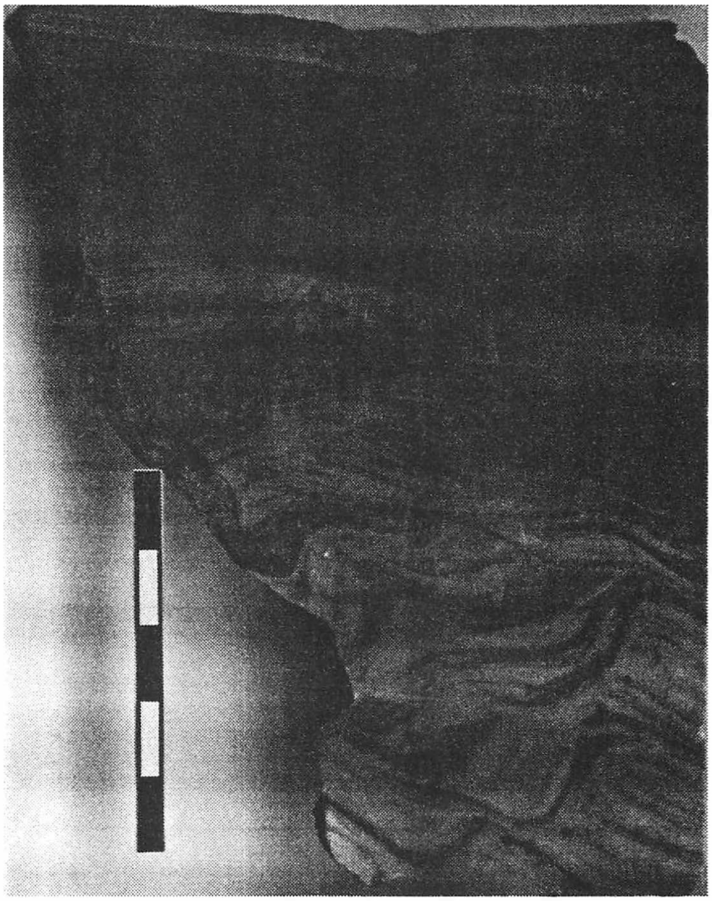

structures (Table III-1). F_1 folds are recognized and distinguished from other fold generations by the axial-planar relationship of these folds to regional slaty cleavage (S_1) (Fig. III-6A).

F_1 fold geometry is scale dependent. Most 1st- and 2nd-order F_1 folds (anticlines) are open to closed structures that are doubly plunging gently to northeast and southwest, and have axial surfaces that are moderately inclined to the southeast. Most 3rd- and higher-order F_1 folds (anticlines) generally are overturned, or steeply inclined to the northwest, with axial surfaces dipping gently to steeply northwest, and hinges doubly plunging gently to the northeast and southwest (Figs. III-6A, III-6B). These folds have a great circle orientation of 139 81° W, and a corresponding β pole of 49 09°. All F_1 folds verge toward the northwest. Slaty cleavage (S_1) in the Miller Cove thrust sheet is axial-planar to F_1 folds (compare Figs. III-6B, III-10B), and the intersection lineation (L_{1x0}) between bedding(S_0) and slaty cleavage (S_1) is subparallel to F_1 fold hinge (Figs. III-6C, III-6D), indicating this folding event and regional metamorphism were coeval.

F_1 folds in the study area are predominantly similar folds. These folds exhibit flexural slip and flexural flow folding that, according to Donath and Parker (1964), depend on the rheology of the layering and on the metamorphic temperatures and pressures to produce variations in ductility between layers. Observed F_1 folds that deform predominantly coarse-grained lithologies produce constant bedding-thickness folds with slickenlines on bedding surfaces. Interbedded coarse- and fine-grained lithologies, however, contain a ductility contrast between layers, and yield by thickening of hinges and thinning of the limbs of the less competent fine-grained lithologies in response to folding. These changes of thickness in the hinges and limbs provide evidence that flexural flow is also present as a folding mechanism in the study area.

Figure III-6. Characteristics of F_1 folds in the Miller Cove thrust sheet. (A) 5th-order F_1 fold near Barnum Creek, station TP-1107, Tellico Plains 7.5-minute quadrangle. Rock hammer (approximately 32 cm long) is located in the hinge of the fold, and is inclined to the southeast parallel to the axial surface. (B) Lower-hemisphere equal-area projection of 66 F_1 poles to axial surfaces. (C) Lower-hemisphere equal-area projection of 66 F_1 fold hinges. (D) Lower-hemisphere equal-area projection of 23 bedding (S_0)-slaty cleavage (S_1) intersection lineations. Note relationship between the intersection lineation (L_{1x0}) between bedding (S_0) and slaty cleavage (S_1), and F_1 fold axes. Also note the relationship between poles to F_1 axial surface measurements and poles to S_1 cleavage (see Fig. III-10B).

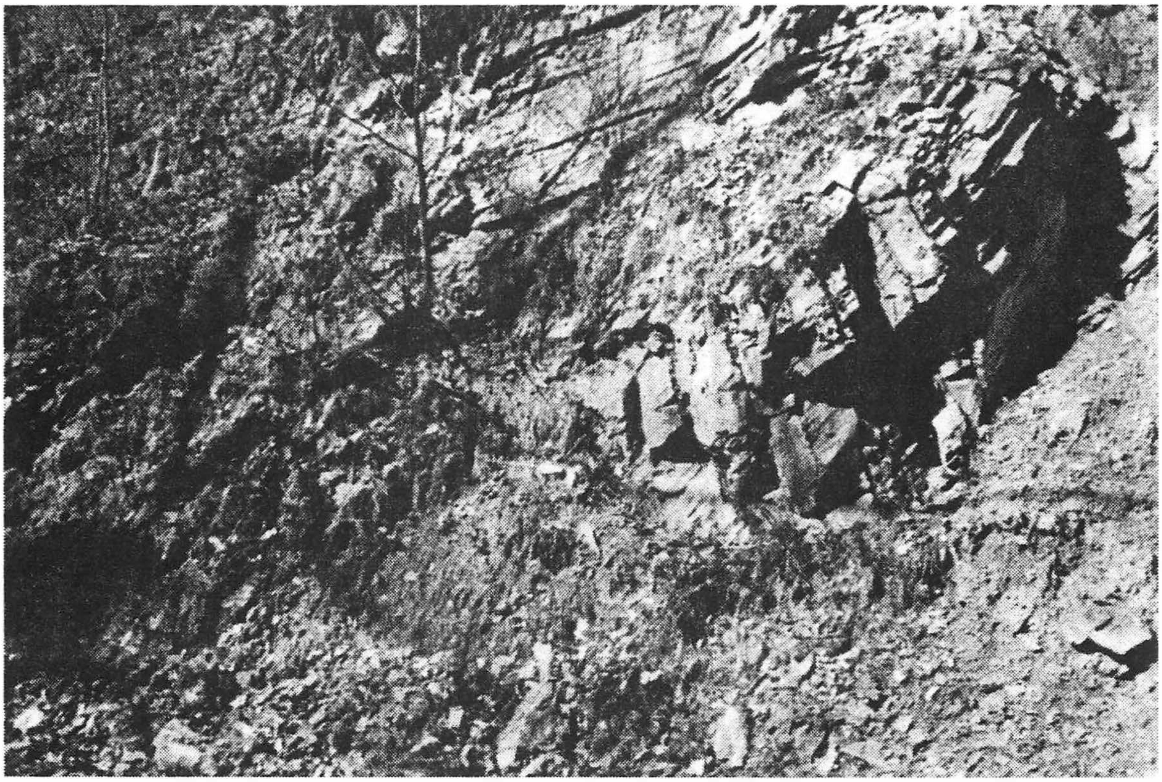

(A)

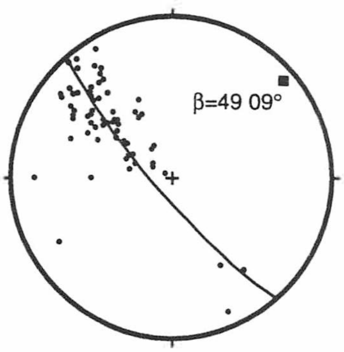

(B)

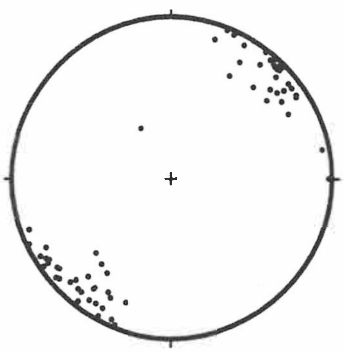

(C)

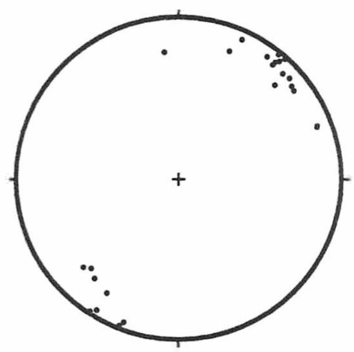

(D)

F_2 folds

Locally slaty cleavage (S_1) within the Miller Cove thrust sheet is deformed by open 5th- and higher-order F_2 folds (Fig. III-7A). These folds plunge gently to the northeast and southwest, with axial surfaces that dip moderately to steeply to the northwest and moderately to the southeast (Figs. III-7B, III-7C). These F_2 folds are classified as kink or chevron folds. F_2 folds are oriented subparallel to hinges of crenulation cleavage (S_2) observed locally in fine-grained rocks within the Miller Cove thrust sheet (compare Figs. III-7C and III-13C). The relationship between these F_2 folds and crenulation cleavage (S_2) is uncertain. The similarities between the orientation of axial surfaces of F_2 folds and crenulation cleavage (S_2), however, suggest they may be related.

Carter (1994) recognized a close spatial relationship between folds similar to these F_2 folds and brittle faults. Discrete zones of chevron-like kink folds occur along the Tellico River road (Tennessee State Highway 165) near the boundary between the Tellico Plains and Bald River Falls 7.5-minute quadrangle (Fig. III-7A). These zones are in close proximity to the Oconaluftee fault and related hanging-wall splays, suggesting these folds maybe related to late Paleozoic faulting.

F_3 folds

F_3 folds are 3rd- and higher-order folds west of the Miller Cove thrust sheet in the Great Smoky and Bullet Mountain thrust sheets. Other F_3 folds include 4th- and higher-order parasitic folds to these structures. F_3 folds in the Great Smoky thrust sheet are gentle to open with tight folds present locally. These folds plunge gently to the northeast and southwest, and have axial surfaces that dip moderately to the southeast (Figs. III-8A, III-8B). F_3 axial surfaces are oriented subparallel to the poorly developed slaty cleavage (S_3) in the Great Smoky thrust sheet, and probably formed coevally (compare Figs. III-

Figure III-7. Characteristics of F_2 folds in the Miller Cove thrust sheet. (A) Near-similar F_2 chevron folds in the Wilhite Formation along the Tellico River, near station BRF-840, Bald River Falls 7.5-minute quadrangle. (B) Lower hemisphere equal-area projection of poles to 15 F_2 axial surfaces. (C) Lower hemisphere equal-area projection of 15 F_2 fold hinges.

(A)

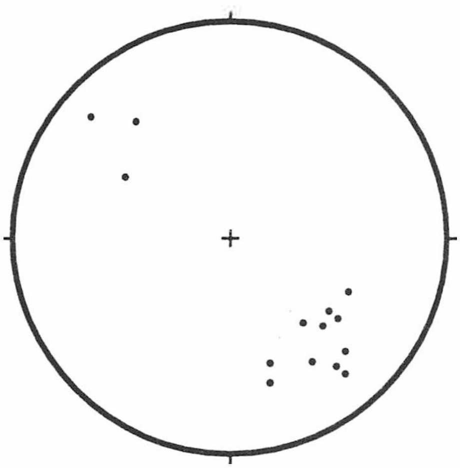

(B)

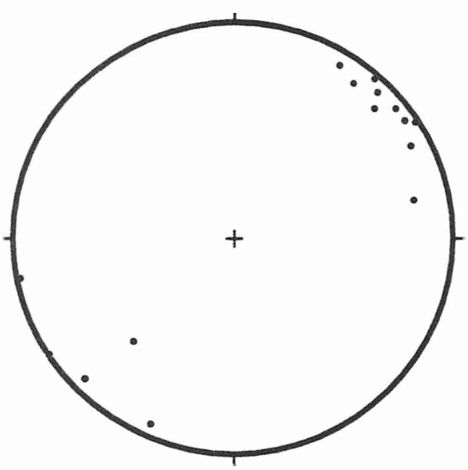

(C)

Figure III-8. Characteristics of F_3 folds in the Great Smoky thrust sheet. (A) Lower-hemisphere equal-area projection of poles to 5 F_3 axial surfaces. (B) Lower-hemisphere equal-area projection of 5 F_3 fold hinges.

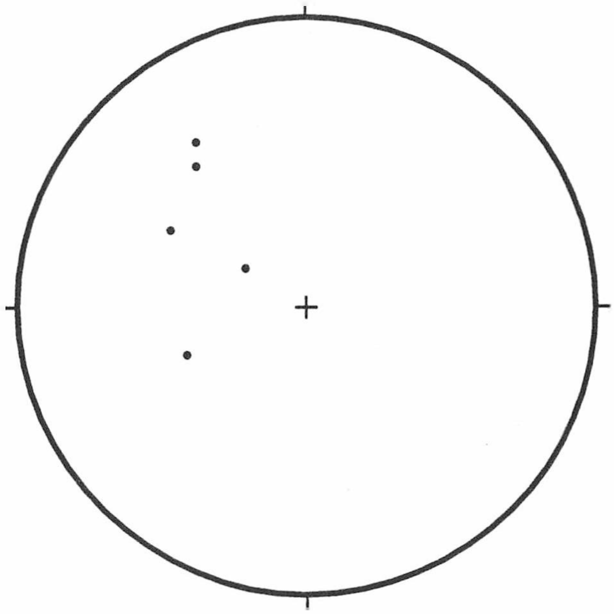
(A)

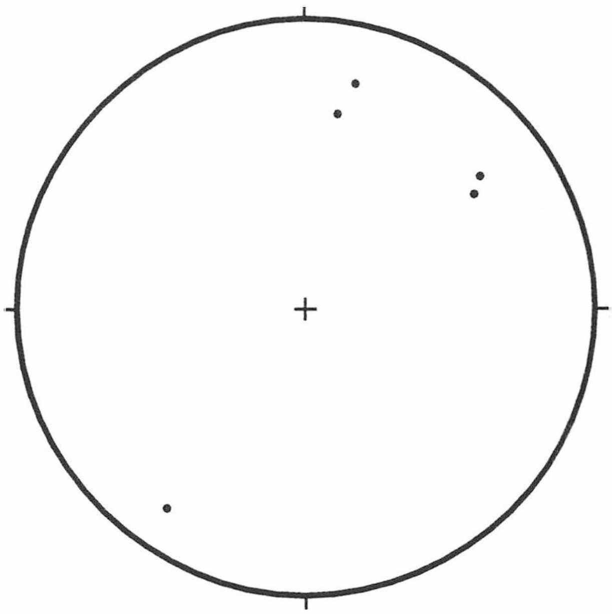
(B)

8A and III-14). F_3 folds are predominantly parallel folds with bedding-parallel slickenlines on fold limbs suggesting flexural slip folding. Detailed mapping southwest of the study area (Carter, 1994) and within the study area by myself revealed locally overturned footwall synclines in the footwall of the Miller Cove and Maggies Mill faults (Plate I). Formation of these folds beneath these faults suggests that folds in the Maggies Mill and Great Smoky thrust sheets may be related to faulting (Carter, 1994; this study).

Fourth- and higher-order F_3 folds also occur in the Bullet Mountain thrust sheet, and include the Kirkland Hollow anticlinorium and the Tellico Plains synclinorium. These folds and parasitic folds to these structures have fold axes oriented parallel to the Bullet Mountain fault (McKinney, 1964). Because the folds in the Great Smoky and Bullet Mountain thrust sheet appear to be related to postmetamorphic faulting rather than synmetamorphic S_1 cleavage development, they are interpreted as F_3 folds.

F_4 folds

F_4 folds in the Blue Ridge thrust sheet have been described to the southwest (Carter, 1994) and northeast (Geddes, 1995) of the study area, and are interpreted to have formed during ramping and duplexing of Paleozoic Valley and Ridge footwall strata (Plates III, IIIa). Footwall deformation has been documented beneath the frontal western Blue Ridge thrust sheets north of the study in the vicinity of the Great Smoky Mountains National Park (Neuman, 1951; King, 1964; Neuman and Nelson, 1965; Hatcher and others, 1989a, 1989b). Here windows expose anticlinal imbricated footwall rocks that provide evidence that duplexing of the footwall arched the Blue Ridge thrust sheet after emplacement.

F_4 folds are interpreted as 3rd- and 2nd-order folds by Carter (1994) and Geddes (1995) to the southwest and northeast of the study area, respectively. Although they did not observe mesoscale folds associated with this folding event, Carter (1994) and Geddes

(1995) provided evidence for this event based on map-scale structures. Carter (1994) suggested these folds deformed the Maggies Mill fault, along with map-scale folds in the hanging wall of the Maggies Mill and Miller Cove faults. Geddes (1995) interpreted that footwall duplexing of early Paleozoic strata produced F_4 folds in the hanging wall of the Blue Ridge thrust sheet. Geddes (1995) provided evidence of this interpretation from observations of the surface geology, which included deflection of the biotite isograd, fold-interference patterns, deflection of bedding and cleavage, and topographic expressions. Geddes (1995) suggested that the Foothills duplex is generally a doubly plunging antiform with doubly plunging culminations at various locations on its surface. The overall dip of the roof of the Foothills duplex has been calculated, using structure contour maps drawn on the base of the Great Smoky thrust sheet, to be 0.6° to the southwest within and between each of the windows in the Great Smoky Mountains National Park region (King, 1964; Neuman and Nelson, 1965; Hatcher and others, 1989b).

Mesoscopic F_4 folds, or foliations related to the F_4 folding event, were not recognized in this study. However, possible surface evidence for this folding event is interpreted from map patterns of earlier formed structures. Structures, such as the Tellico Mountain anticlinorium and Payne Ridge anticlinorium are interpreted to have continued to have tightened as the Great Smoky thrust sheet was folded by duplexing of the Valley and Ridge footwall strata. The retrodeformation of Alleghanian deformation of western Blue Ridge hanging-wall strata shows the opening of some previously formed folds (Plate III; Appendix D). It is also suggested that the thrust fault on Payne Ridge and the normal fault in Coker Creek may have formed due to this folding event. Although surface evidence for the F_4 folding event is inconclusive in the study area, evidence for folding of the Great Smoky thrust sheet is best observed in the windows near the Great Smoky Mountains region. For this reason, the Great Smoky thrust sheet is interpreted to be folded by duplexing of Valley and Ridge footwall strata representing the F_4 folding event.

S-surfaces (foliations)

One depositional S-surface and four tectonic foliations were recognized in the study area. These foliations include bedding (S_0), continuous (slaty) cleavage (S_1), pressure-solution cleavage (S_{1a}), crenulation cleavage (S_2), and discontinuous (slaty) cleavage (S_3). Bedding (S_0) is present throughout the study area and, depending on lithology, influences the development of other S-surfaces. Continuous (slaty) cleavage (S_1) is the most pervasive tectonic S-surface in the Miller Cove thrust sheet and is best developed in fine-grained metasiltstones and slates. Pressure-solution cleavage (S_{1a}) and crenulation cleavage (S_2) are locally developed in fine-grained lithologies within the Miller Cove thrust sheet. A weakly developed discontinuous (slaty) cleavage (S_3) is locally present in fine-grained rocks in the Great Smoky thrust sheet.

S_0 (bedding)

Bedding in the Bullet Mountain thrust sheet, compiled from McKinney (1964), is deformed by the 3nd-order Kirkland Hollow anticlinorium and Tellico Plains synclinorium, higher-order parasitic folds, and the Hunt Branch fault. Bedding in the Bullet Mountain thrust sheet dips both gently to moderately southeast, and moderately northwest (Fig. III-9A). Poles to bedding in the Bullet Mountain thrust sheet defines a great circle with orientation 137 89° W, and β pole with orientation 47 01°. In the Great Smoky thrust sheet, bedding dips moderately to the southeast, with poles to bedding defining a great circle with orientation 312 86° N, and β pole orientation of 222 04° (Fig. III-9B).

In the Miller Cove thrust sheet, bedding is deformed by the Rabbit Creek and Oconaluftee faults, the Epperson synclinorium, the Payne Ridge, Grindstone Ridge, and Tellico Mountain anticlinoriums, higher-order parasitic folds, and many meso- and

Figure III-9. Lower-hemisphere equal-area projections of S_0 (bedding) data in the Bullet Mountain, Great Smoky, and Miller Cove thrust sheets. Stereoplots include scatter, contoured at 2% per 1% area, and Kamb contoured with a 3.0 σ base value using a 2.0 σ contour interval. (A) 123 poles to bedding in Bullet Mountain thrust sheet. Using Kamb contour, area counted equals 6.8%. (B) 118 poles to bedding in the Great Smoky thrust sheet. Using Kamb contour, area counted equals 7.1%. (C) 1934 poles to bedding in the Miller Cove thrust sheet. Using Kamb contour, area counted equals 0.5%.

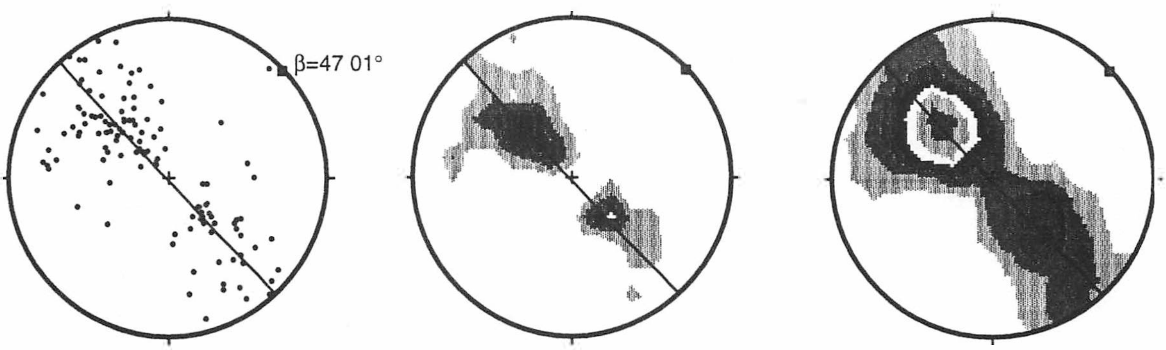

(A)

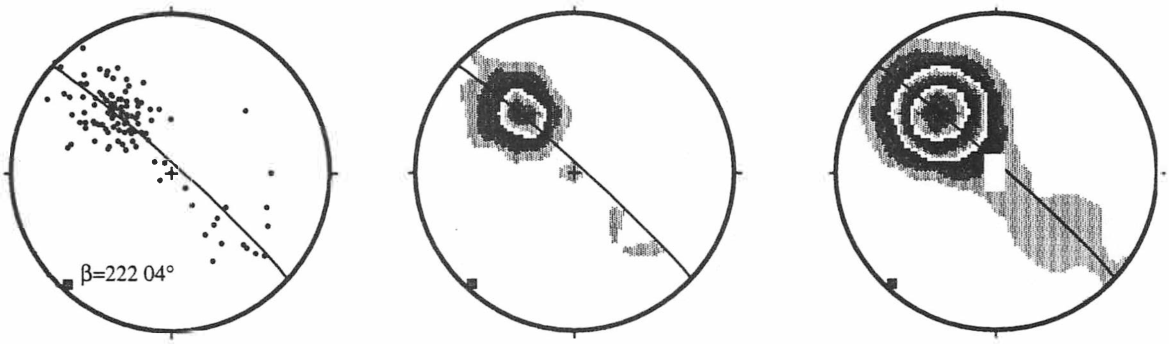

(B)

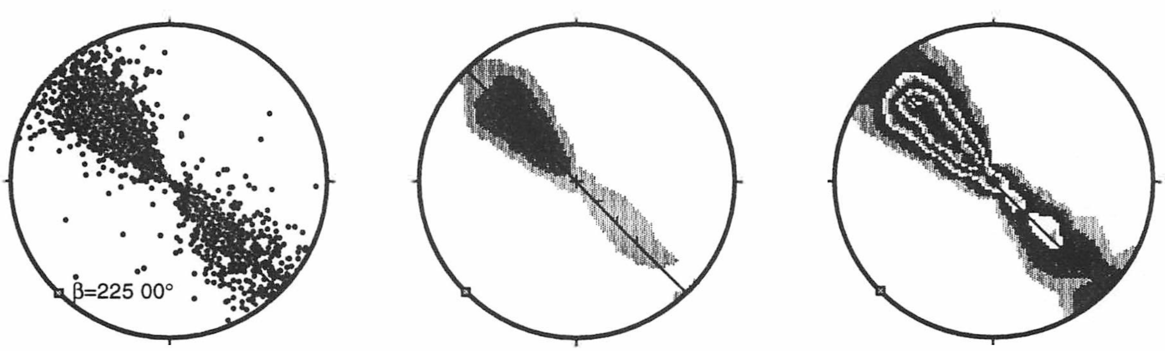

(C)

smaller-scale faults. Generally, bedding in the Miller Cove thrust sheet dips moderately to the southeast, but gentle and steeply southeast- and northwest-dipping beds frequently occur. Poles to bedding in the Miller Cove thrust sheet define a great circle orientation of 315 90° N, and β pole orientation of 225 00° (Fig. III-9C). Comparison of the stereoplots in the Bullet Mountain, Great Smoky, and Miller Cove thrust sheets reveal similar great circles and corresponding β poles.

S_1 (slaty cleavage)

S_1 is the dominant tectonic foliation in the Miller Cove thrust sheet, and is best developed in banded metasiltstone and slate (Fig. III-10A). S_1 is axial-planar to F_1 folds, and dips predominantly to the southeast (Fig. III-10B). Poles to S_1 (slaty cleavage) in the Miller Cove thrust sheet show a great circle with an orientation of 132 89°S, and β pole orientation of 42 1° (Fig. III-10B). Refraction of slaty cleavage across layers of different grain size occurs throughout the study area. Upon weathering, cleaved rocks tend to part preferentially along cleavage (S_1) planes rather than bedding (S_0) planes, as well as along the intersection between cleavage and bedding (Fig. III-10A).

S_1 is more intensely developed from northwest to southeast across the study area in the direction of increasing metamorphic grade. S_1 is characterized by smooth disjunctive (Powell, 1979) moderately to closely spaced slaty cleavage in fine-grained rocks, and anastomosing to rough disjunctive widely spaced cleavage in coarse-grained rocks. In the northwestern portion of the Miller Cove thrust sheet, S_1 formed both by pressure-solution and the alignment of clay minerals recrystallized to chlorite and muscovite (sericite) (Fig. III-11A) . Cleavage selvages generally range from 0.05 mm- to 0.5 mm-thick, and separate poorly- to moderately-developed microlithons that are 0.02 mm- to 0.3 mm-thick (Fig. III-11A).

In the southeastern portion of the Miller Cove thrust sheet, cleavage intensity

Figure III-10. Characteristics of S_1 (slaty cleavage) in the Miller Cove thrust sheet. (A) Slaty cleavage (S_1) in banded metasiltstone of the Wilhite Formation. Bedding (S_0) dips gently to the southeast, while slaty cleavage dips steeply to the southeast (see Fig III-6D for L_{0x1} orientations). Bee hive (scale) is attached to a bedding surface. Near station BRF-850, Tellico River, Bald River Falls 7.5-minute quadrangle. (B) Lower-hemisphere equal-area projections of 1273 poles to S_1 (slaty cleavage) in the Miller Cove thrust sheet. Stereoplots include scatter, contoured at 2% per 1% area, and Kamb contoured with a 3.0 σ base value using a 2.0 σ contour interval and 0.7% of the area counted.

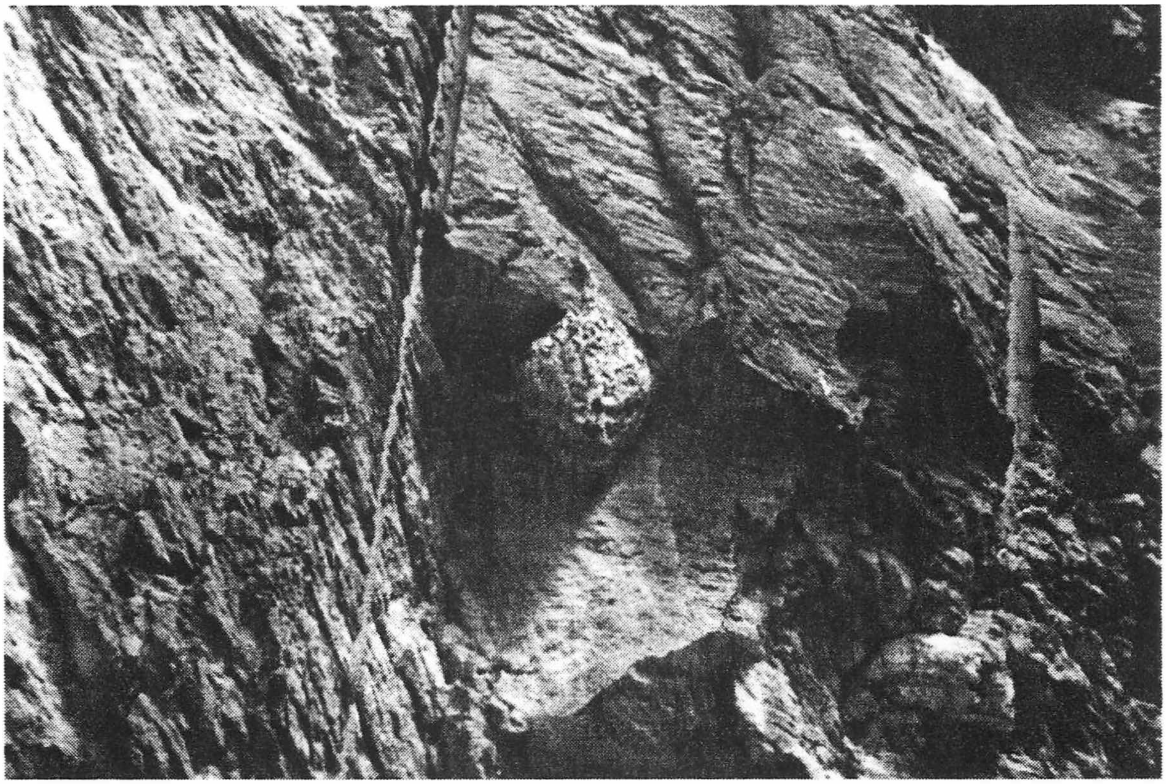

(A)

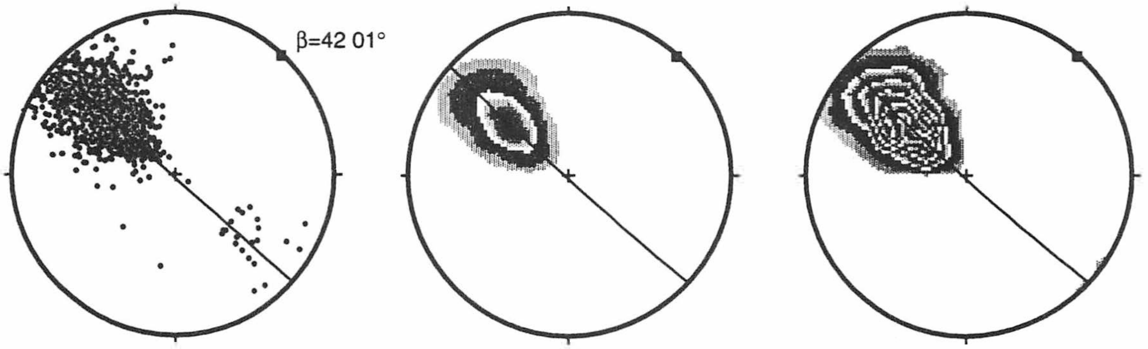

(B)

Figure III-11. Increased development of slaty cleavage (S_1) from northwest to southeast across the study area. (A) Enlarged negative image (from thin section) of bedding, pressure-solution, and slaty cleavage relationship in banded metasiltstone in the northwestern portion of Miller Cove thrust sheet. Station TP-146, approximately 600 m (2,000 ft) north of Epperson Church, Tellico Plains 7.5-minute quadrangle. Field of view is approximately 2 cm. (B) Enlarged negative image (from thin section) of bedding and slaty cleavage relationship in the banded metasiltstone of the Wilhite Formation in the southeastern portion of Miller Cove thrust sheet. Station BRF-259, Tellico River, Bald River Falls 7.5-minute quadrangle. Field of view is approximately 2 cm.

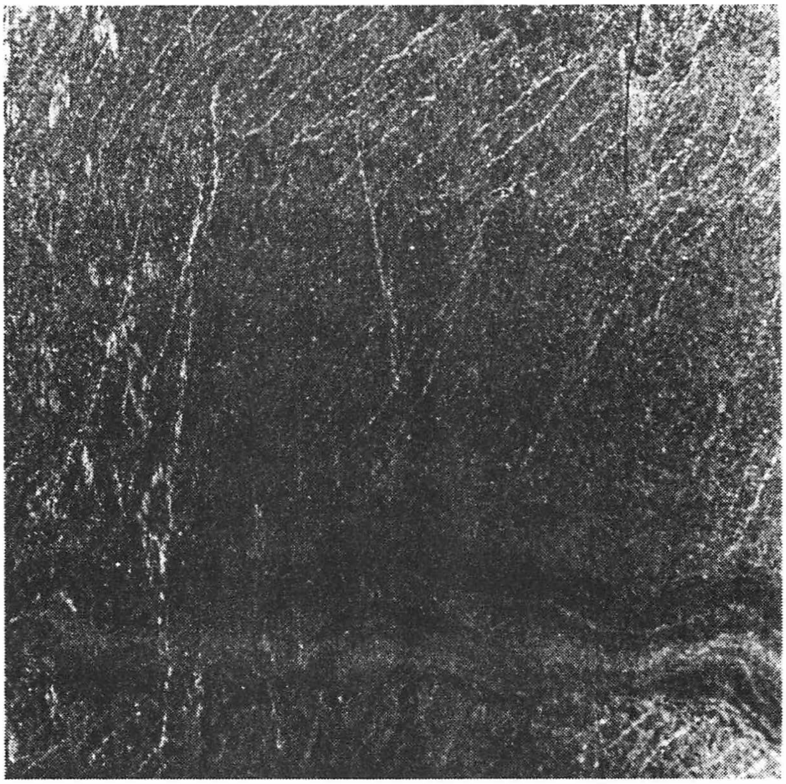

(A)

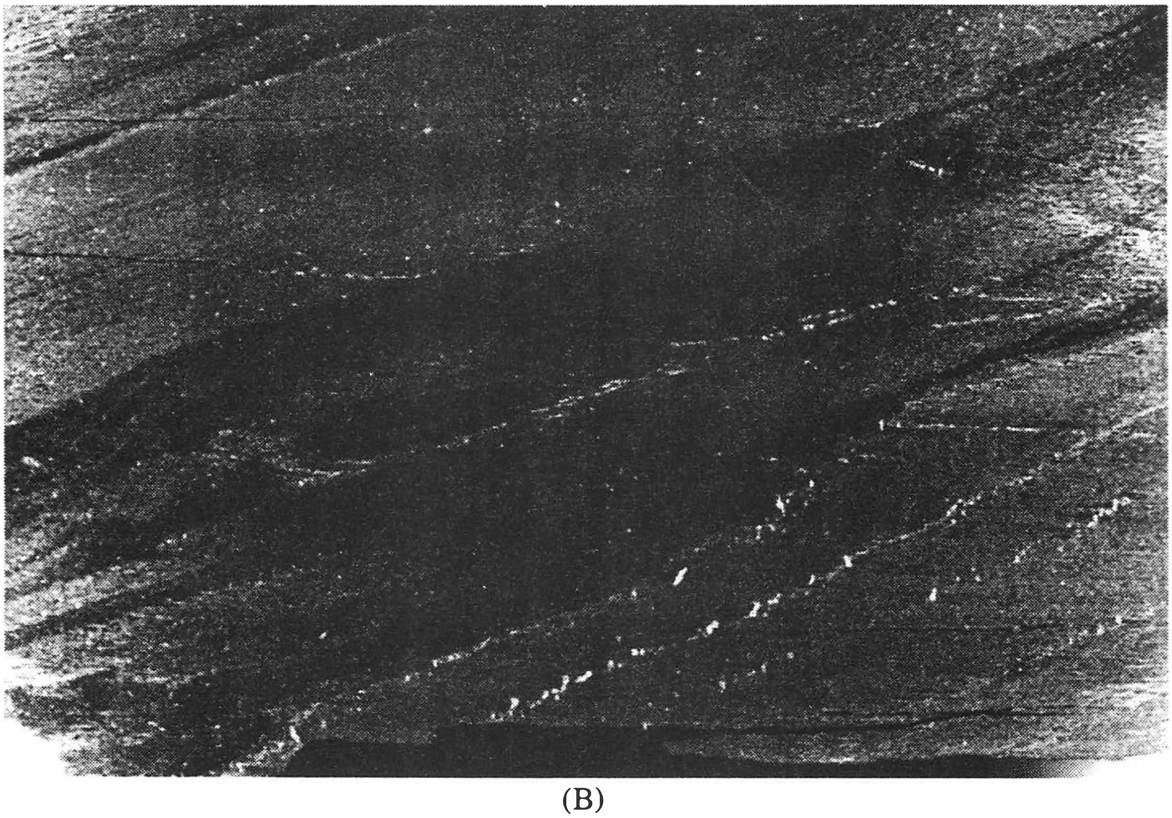

(B)

increases and becomes nearly continuous. Cleavage selvages range from 0.02 mm to 0.5 mm thick, and consist of strongly aligned chlorite, biotite, and muscovite with evidence of pressure solution along these selvages (Fig. III-11B). The recrystallized clays are so strongly oriented that microlithon boundaries are usually obliterated. It appears the importance of pressure-solution diminishes as a cleavage-forming mechanism in this region of the study area.

Coarse-grained rocks in the Miller Cove thrust sheet locally exhibit an anastomosing to rough disjunctive narrowly-to broad-spaced cleavage (Powell, 1979), probably related to S_1. This cleavage is better developed in clay-rich sandstone and conglomerate, and appears as thin clay-rich seams that anastomose around large quartz and feldspar grains. In the easternmost portion of the study area, quartz pebbles have been flattened and rotated toward the plane of cleavage. The common orientation of S_1 in both fine- and coarse-grained lithologies, along with the refraction of S_1 between the different lithologies, indicate the spaced cleavage in coarse-grained rocks in the Miller Cove thrust sheet is related to S_1 that has developed in finer-grained lithologies.

S_{1a} (pressure-solution cleavage)

Fine-grained rocks in the Miller Cove thrust sheet locally exhibit a secondary stylolitic disjunctive spaced cleavage (S_{1a}) (Powell, 1979) formed by pressure solution. This S_{1a} cleavage appears as thin dark bands (< 0.5 mm) that are spaced 0.1 cm to 1.0 cm apart (Fig. III-12A), and was recognized nearby to the southwest by Carter (1994). This pressure-solution cleavage is best observed microscopically. When observed mesoscopically, these surfaces generally dip moderately to the northwest (Fig. III-12B). To the southwest and northeast of the study area, Carter (1994) and Geddes (1995) observed pressure-solution cleavage dipping moderately to steeply to the northwest and southeast. This pressure-solution cleavage (S_{1a}) is moderately coherent, and rocks

Figure III-12. Characteristics of S_{1a} (pressure solution) cleavage in the Miller Cove thrust sheet. (A) Enlarged negative image (from thin section) of pressure-solution (S_{1a}) cleavage in banded metasiltstone in the Miller Cove thrust sheet. Pressure-solution (S_{1a}) cleavage is defined by the white lines suborthogonal to bedding (S_0) and at acute angles to slaty (S_1) cleavage. Station BRF-590, Tobe Creek, Bald River Falls 7.5-minute quadrangle. Field of view is approximately 7 cm. (B) Lower-hemisphere equal-area projection of 7 poles to S_{1a} (pressure solution) cleavage.

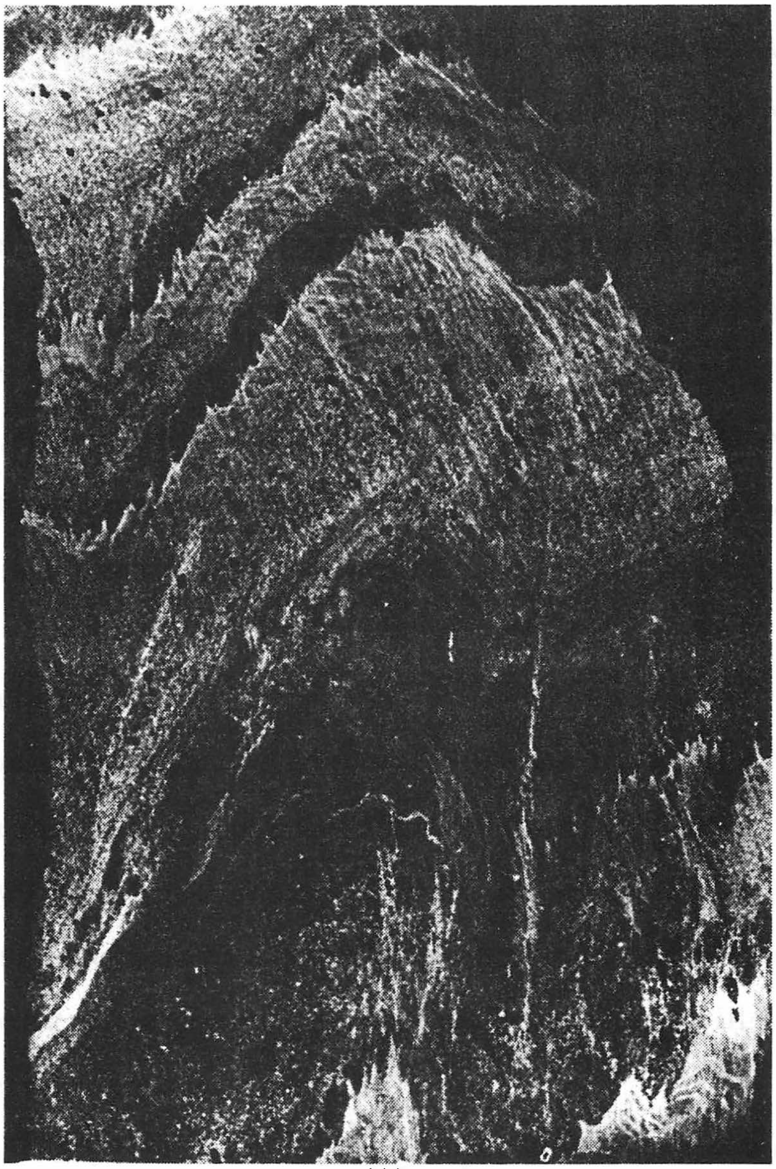
(A)

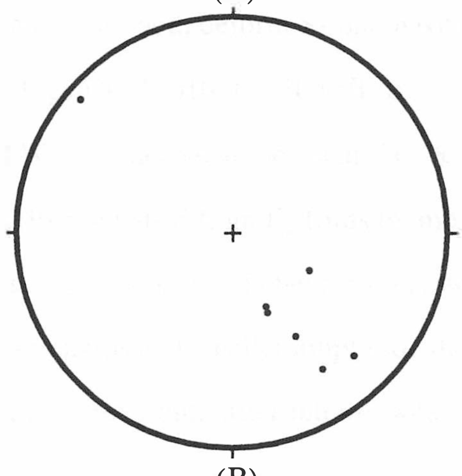
(B)

usually do not part along this surface. Opaque and other insoluble minerals accumulated along these S_{1a} surfaces, suggesting that S_{1a} cleavage formed by a pressure-solution mechanism. This pressure-solution cleavage is distinguished from bedding, and cleavage-parallel pressure-solution selvages by cross-cutting relationships (Fig. III-12A). S_{1a} is predominantly oriented suborthogonal to S_0 in fold hinges, and usually overprints S_1. The relationship between S_{1a} and S_1 is not totally clear. Normally, S_{1a} overprints and deforms S_1, but occasionally S_1 deforms S_{1a}. Carter (1994) observed reorientation of recrystallized clay minerals into parallelism with S_{1a}, suggesting that the S_{1a} formed coevally with S_1 and possibly continued afterwards.

S_2 (crenulation cleavage)

S_2 is a zonal crenulation cleavage (Powell, 1979) that deforms S_1 and is developed in the fine-grained rocks of the Miller Cove thrust sheet. This cleavage is characterized by 0.1 to 1.0 cm-thick bands that deform S_1 surfaces (Fig. III-13A). The axial surfaces of these crenulations dip both to the southeast and northwest (Fig. III-13B), and have hinges that plunge gently to the northeast and southwest (Fig. III-13C). These crenulations are interpreted to have formed by buckling.

The relationship between crenulation cleavage (S_2) and F_2 is not clear. They are interpreted to be related because they both deform S_1 and have similar axial plane and hinge orientations (compare Figs III-7B, III-7C, III-13B, III-13C). S_2 and F_2 also occur near each other in deformed Wilhite metasiltstones near the Oconaluftee fault. Crenulation cleavage (S_2) is distinguished from F_2 folds by morphology (compare Figs. III-7A, III-13A). F_2 folds are more kinked and chevron-like, whereas S_2 surfaces are more subtle, with longer wavelengths and smaller amplitude than F_2 folds. Cohesion across the crenulated surfaces is strong until after intense weathering, when the rocks preferentially part along these surfaces. Since S_2 cleavage is interpreted to be related to

Figure III-13. Characteristics of S_2 (crenulation) cleavage in the Miller Cove thrust sheet. (A) Crenulation (S_2) cleavage in banded metasiltstone of the Wilhite Formation near the Oconaluftee fault. Station BRF-840, Tellico River, Bald River Falls 7.5-minute quadrangle. (B) Lower-hemisphere equal-area projection of 13 S_2 poles to axial surfaces. (C) Lower-hemisphere equal-area projection of 13 S_2 axes.

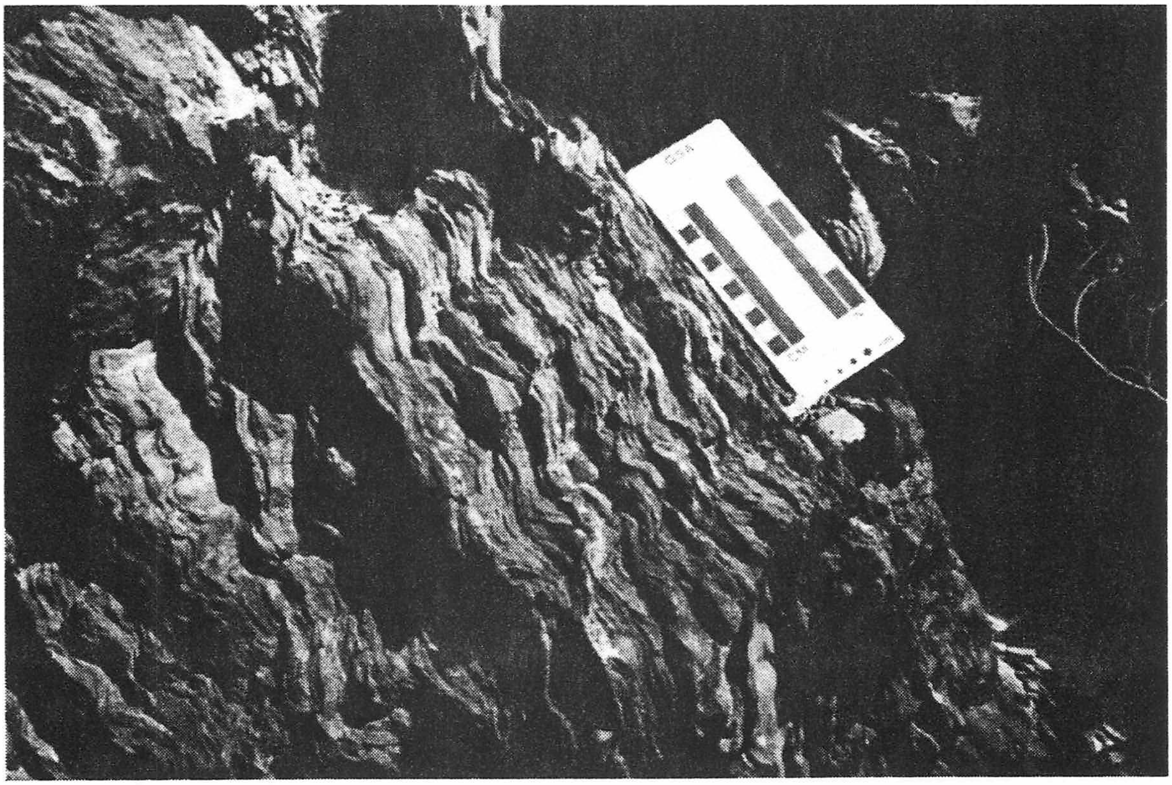

(A)

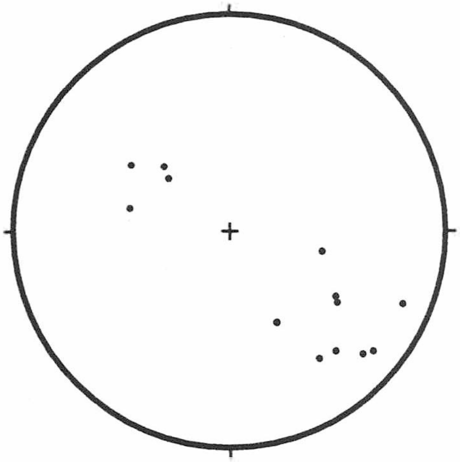

(B)

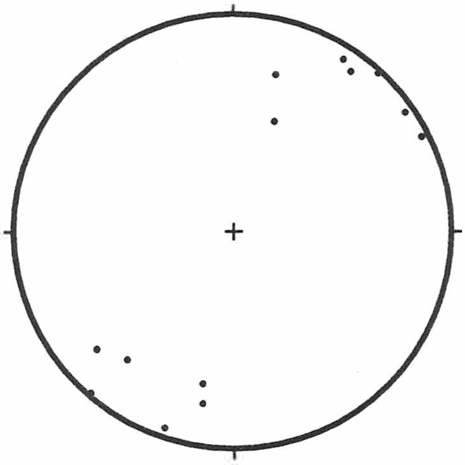

(C)

F_2 folds, by analogy it is inferred that S_2 postdates S_{1a}.

S_3 (slaty cleavage)

A S_3 cleavage is locally developed in the Great Smoky thrust sheet. This cleavage formed in fine-grained siltstone and shale of the Sandsuck Formation, and generally dips moderately to the southeast with a great circle orientation of 314 87°N and corresponding β pole with an orientation of 224 3°(Fig. III-14). S_3 cleavage is axial-planar to F_3 folds in the Great Smoky thrust sheet. A moderate to strong spaced cleavage is also locally developed in the fine-grained rocks of the Great Smoky thrust sheet. To the southwest of this study area, Carter (1994) observed pencil structures related to a spaced cleavage higher in the stratigrapic sections of the Sandsuck Formation. These pencil structures were not observed in the lower stratigraphic sections of the Sandsuck Formation in this study.

Slaty cleavage (S_3) in the Great Smoky thrust sheet is similar to slaty cleavage (S_1) in the Miller Cove thrust sheet. S_3 in the Great Smoky thrust sheet has similar orientation (compare Figs. III-10B and III-14), weathering characteristics, and cleavage-forming mechanisms. Cohesion is weak along weathered S_3 surfaces resulting in flat chips of siltstone and shale similar to those in the Miller Cove thrust sheet. Spaced pressure-solution selvages occur along S_3 and contain iron oxide residues and weakly aligned clay minerals. The primary mechanism of cleavage formation appears to be related to pressure solution (Carter, 1994; this study).

Joints and veins

Joints and veins occur throughout the study area. These structures transect bedding and all other structures except for late-stage brittle faults, which deform veins in many instances. Joints and veins are prominent in the fine-grained metasiltstone and slate

Figure III-14. Lower-hemisphere equal-area projection of 18 poles to S_3 (slaty cleavage) in Great Smoky thrust sheet.

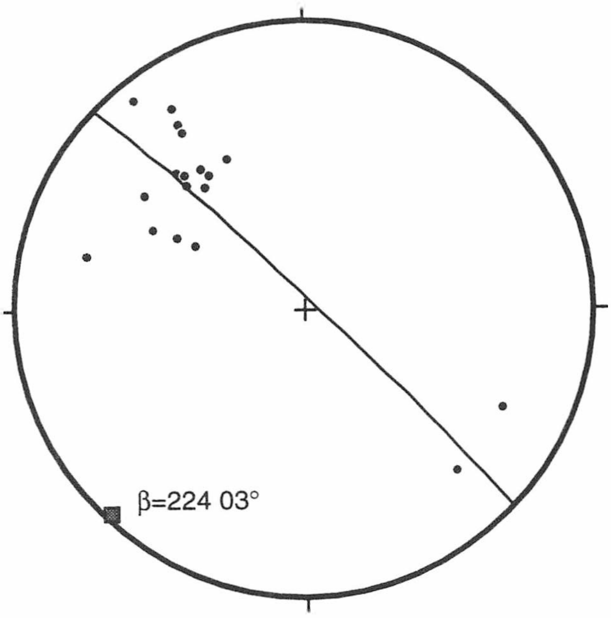
β=224 03°

lithologies, and are very common in the coarse-grained sandstone and conglomerate (see Chapter IV, joint section, for discussion of joint orientation). Drainage is frequently joint controlled. Portions of a strongly incised drainage can flow tens of meters along a single joint surface. Spacing between joints and veins are variable. On the average, spacing between joint and vein sets range from 0.5 to 1.5 m. The aperture of joints and thickness of vein sets are also variable. Spacing ranges from less than 1.0 mm for most joints, and averages approximately 0.5 m for veins. Veins are mostly filled with quartz and minor amounts of carbonate. Gold-bearing quartz veins occur in the metasiltstone in the southeastern portion of study area near Coker Creek (Hale, 1974).

Structural chronology of the western Blue Ridge in southeastern Tennessee

Rocks of the Ocoee Supergroup that were deposited along the Laurentian margin were initially deformed by the Ordovician Taconic orogeny (Fig. III-15). Early in this event, the rocks of the western Blue Ridge were deformed by the Rabbit Creek, Line Springs, Dunn Creek, and Greenbrier faults, and by folds related to the emplacement of these structures. During the metamorphic event accompanying this orogeny, western Blue Ridge rocks were synchronously metamorphosed and regionally folded. The resulting Barrovian metamorphism increases from chlorite-grade in the western Blue Ridge to sillimanite-grade to the east in the central Blue Ridge. In the western Blue Ridge Foothills belt in southeastern Tennessee, the Taconic metamorphic event (up to biotite grade) initiated the development of open to closed 1st- and higher-order F_1 folds, axial-planar slaty cleavage (S_1), and pressure-solution cleavage (S_{1a}) (Fig III-15). The pressure-solution cleavage (S_{1a}) may have developed coevally with the formation of F_1 folds and slaty cleavage (S_1) during the waning stages of this event. Taconian metamorphism and related structures account for most of the deformation preserved in the rocks of the western Blue Ridge Foothills in southeastern Tennessee.

Figure III-15. Chronology of orogenic events and related structures of the western Blue Ridge in southeastern Tennessee (modified from Carter, 1994).

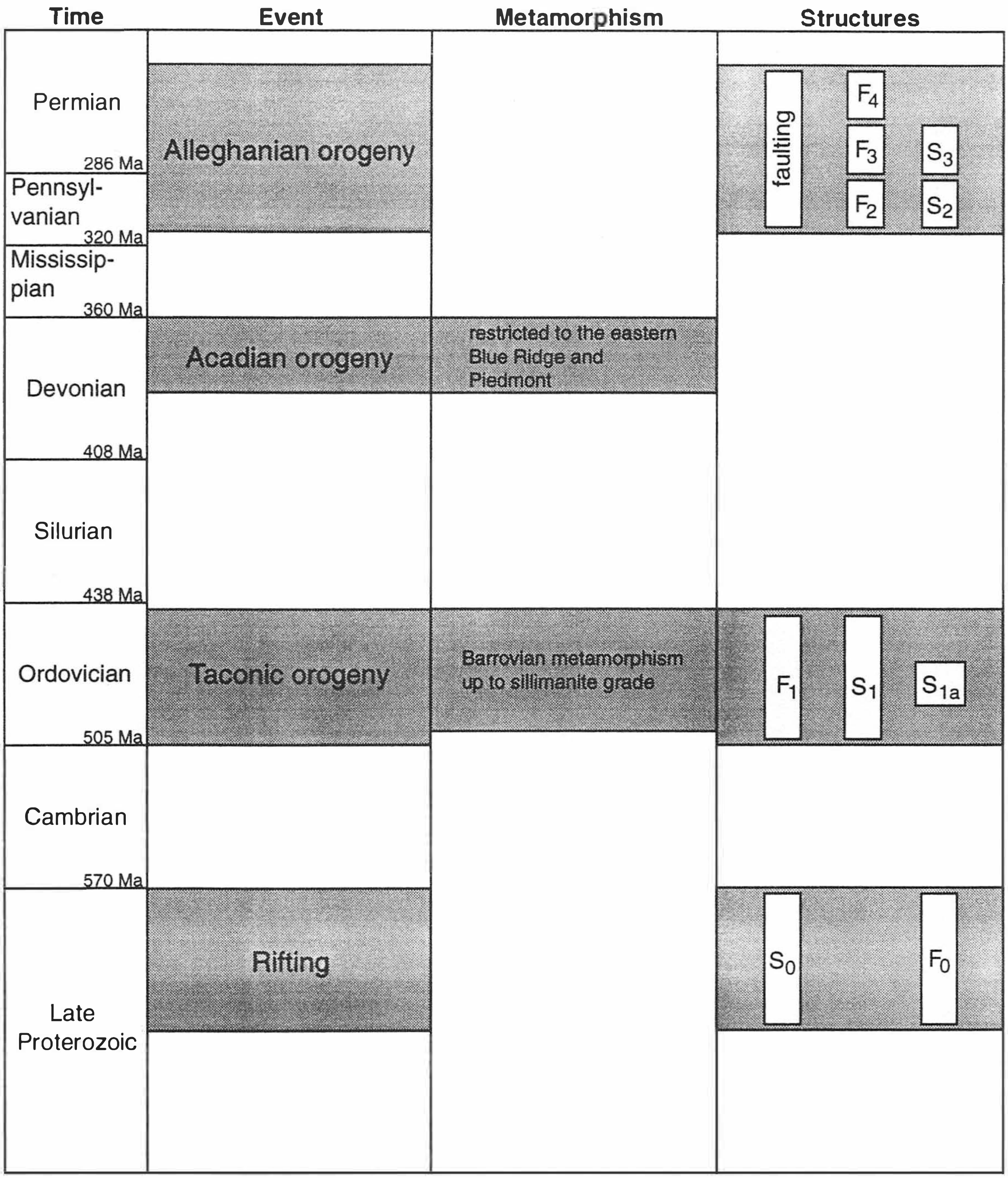
Time
Event
Metamorphism
Structures
Permian
286 Ma
Pennsyl-
vanian
320 Ma
Mississip-
pian
360 Ma
Devonian
408 Ma
Silurian
438 Ma
Ordovician
505 Ma
Cambrian
570 Ma
Late
Proterozoic
Alleghanian orogeny
Acadian orogeny
Taconic orogeny
Rifting
restricted to the eastern
Blue Ridge and
Piedmont
Barrovian metamorphism
up to sillimanite grade
faulting
F_4
F_3
F_2
S_3
S_2
F_1
S_1
S_{1a}
S_0
F_0

The second orogenic event to deform the rocks of the western Blue Ridge was the late Paleozoic Alleghanian orogeny. Structures related to this orogeny exhibit brittle deformation attributed to the emplacement of the Blue Ridge megathrust sheet, which accounts for the extensive foreland fold-thrust belt in the central and southern Appalachians. Evidence for this orogeny includes development of the Blue Ridge fault system along the entire length of the Laurentian margin, westward movement of the Blue Ridge-Piedmont megathrust sheet onto the Laurentian platform, and faulted Mississippian rocks in the footwall of the Great Smoky fault. In southeastern Tennessee, emplacement of these brittle faults initiated the development of F_2 kink folds and a local crenulation cleavage (S_2). These structures are interpreted to be Alleghanian because they deform regional slaty cleavage (S_1) (Fig. III-15). Alleghanian brittle faults include the Rabbit Creek (reactivated premetamorphic fault), Oconaluftee, Miller Cove, Maggies Mill, and Great Smoky faults. These structures clearly transect and deform the older pervasive Taconian structures. The emplacement of the Maggies Mill and Great Smoky faults is interpreted to have resulted in the formation of F_3 folds and a local slaty cleavage (S_3) that is axial planar to these folds. Alternatively, it is possible F_3 folds and related axial planar slaty cleavage (S_3) formed during the Taconian orogeny, because of the similar orientations between F_1 folds and S_1 (slaty) cleavage in the Miller Cove thrust sheet and F_3 folds and S_3 (slaty) cleavage in the Great Smoky thrust sheet (compare Figs. III-6, III-8, III-10, III-14). Additionally, finite-strain measurements in sandstones near these brittle structures record relatively high strains. During the final emplacement of the frontal Blue Ridge thrust sheets, Valley and Ridge footwall strata beneath the Blue Ridge megathrust sheet were thrust into duplexes, and western Blue Ridge hanging wall rocks were gently folded into F_4 folds.

Strain analysis

Recent studies that have attempted to quantify western Blue Ridge strain in eastern Tennessee were conducted by Lewis (1988) and Walters (1988), using the R_f/ϕ method (Ramsay, 1967; Dunnet, 1969; Dunnet and Siddans, 1971; Lisle, 1977; Lisle, 1985). Lewis (1988) used quartz grains as strain markers from 17 samples of the Thunderhead Sandstone (Great Smoky Group) in the Greenbrier thrust sheet near Wear Cove (Table III-2). He reported R_{xy}, R_{xz}, and R_{yz} values between 1.11 and 3.44 with means and standard deviations of 1.62 ± 0.34, 2.32 ± 0.54, and 1.44 ± 0.26, respectively. Lewis (1988), using quartz grains as strain markers, recognized that some strain ellipsoids associated with these strain values were oriented subparallel to the Greenbrier fault, and concluded these are related to the emplacement of the Greenbrier fault. Other ellipsoids are possibly related to later thrusting and deformation of the Greenbrier fault. Lewis (1988) concluded that the ellipsoids recorded superimposed strain from the initial emplacement and later deformation of the Greenbrier fault. Walters (1988) studied the relationships between the Greenbrier, Rabbit Creek, and Great Smoky faults near Cades Cove. He used quartz grains as strain markers, and analyzed eight samples of "Cades" and Elkmont Sandstones (Great Smoky Group). Walters (1988) reported R_{xz} and R_{yz} values between 1.20 and 4.60 with means and standard deviations of 2.56 ± 1.09 and 2.24 ± 0.82, respectively (Table III-2). A R_{xy} value of 1.05 was obtained from one sample. Walters (1988) reported comparatively low strains in the Elkmont Sandstone (R_{xz} of 1.57 ± 0.13) relative to the "Cades" Sandstone (R_{xz} of 2.94 ± 1.16), and concluded that the Elkmont Sandstone is the upright anticlinal backlimb of a fold nappe that exposes "Cades Sandstone" on the overturned forelimb. Walters (1988) interpreted that an overturned nappe developed in the hanging wall of the Rabbit Creek fault after the emplacement of the Greenbrier fault. Walters (1988) also concluded that the measured finite strains are the final product of superimposed incremental strains associated with the complex

Table III-2. Western Blue Ridge strain analysis.

Rock unit	Thrust sheet	R_{xy}	R_{xz}	R_{yz}	Method	Reference
Thunderhead Sandstone	Greenbrier	1.62	2.32	1.44	R_f/ϕ	Lewis, 1988
Elkmont Sandstone "Cades" Sandstone	Greenbrier Rabbit Creek	1.05	2.56	2.24	R_f/ϕ	Walters, 1988
Thunderhead Sandstone and rocks of Webb Mountain Roaring Fork Sandstone Shields, Wilhite, and Sandsuck Formations	Greenbrier Dunn Creek Miller Cove	1.14 1.25	1.33 1.53	1.17 1.23	R_f/ϕ normalized Fry	Connelly, 1993
Sandsuck Formation Wilhite and Dean Formations	Great Smoky and Maggies Mill Miller Cove	1.12 1.23	1.22 1.24	1.37 1.52	R_f/ϕ normalized Fry	Carter, 1994
Sandsuck Formation Wilhite and Dean Formations Dean Formation	Great Smoky Miller Cove Rabbit Creek	1.33 1.61	1.71 2.27	1.30 1.43	R_f/ϕ normalized Fry	This study

structural history of the Cades Cove region.

In the Great Smoky Mountains National Park region, Connelly (1993) analyzed 69 sandstone samples from various Ocoee Supergroup units within three premetamorphic thrust sheets south of English Mountain. He employed both R_f/ϕ and normalized Fry methods (Fry, 1979; Erslev, 1988). Using the R_f/ϕ method, Connelly (1993) recorded R_{xy}, R_{xz}, and R_{yz} values between 1.01 and 1.79 with means and standard deviations of 1.14 ± 0.11, 1.33 ± 0.16, and 1.17 ± 0.08, respectively (Table III-2). The normalized Fry method yielded R_{xy}, R_{xz}, and R_{yz} values between 1.03 and 3.24 with means and standard deviations of 1.25 ± 0.24, 1.53 ± 0.28, and 1.23 ± 0.11, respectively (Table III-2). Both methods reveal an increase in strain values toward the southeast into the hinterland, with strain values for the Fry method typically 5 to 20 percent greater than those determined by the R_f/ϕ method. The large strain values of the normalized Fry method suggest at least some strain was inhomogeneously concentrated in the matrix (Connelly, 1993), or samples were collected near faults. Using a strain factorization technique (Ramsay and Huber, 1983; Kligfield and others, 1984) that has been proven as a viable modeling technique in the Appalachian foreland (Couzens and others, 1993), Connelly (1993) attempted to model kinematically the deformation along the hanging wall flat-and-ramp portions of the thrust sheets. Unfortunately, the strain factorization technique failed to predict consistently the observed finite strains in these western Blue Ridge thrust sheets.

Southwest of the study area, Carter (1994) analyzed nine coarse-grained sandstone and granule conglomerate samples from the Great Smoky, Maggies Mill, and Miller Cove thrust sheets, using both R_f/ϕ and normalized Fry methods (Dunnet, 1969; Fry, 1979; Peach and Lisle, 1979; Erslev, 1988). Carter (1994) also measured the long, intermediate, and short axes of pebbles from an exposure, and plotted them on a Flinn diagram (Flinn, 1962). R_{xy}, R_{xz}, and R_{yz} values from the R_f/ϕ method range between 1.05 and 1.63 with means and standard deviations of 1.12 ± 0.05, 1.22 ± 0.14, and $1.37 \pm$

0.18, respectively (Carter, 1994) (Table III-2). Using the normalized Fry method, Carter (1994) reported R_{xy}, R_{xz}, and R_{yz} values between 1.03 and 1.78, with means and standard deviations of 1.23 ± 0.13, 1.24 ± 0.12, and 1.52 ± 0.17, respectively (Table III-2). Measured quartz pebbles from conglomerates yielded R_{xy}, R_{xz}, and R_{yz} values of 1.57 ± 0.31, 1.75 ± 0.45, and 2.71 ± 0.8, respectively. Strain values from the R_f/ϕ and normalized Fry methods and measured pebbles fall within the field of apparent flattening on the Flinn diagram (Carter, 1994). Carter's (1994) data and conclusions are consistent with strain measurements from previous studies north of the Little Tennessee River (Lewis, 1988; Walters, 1988; Connelly, 1993). Carter (1994) concluded that strain increases towards the southeast with no correspondence of the X/Y plane to regional slaty cleavage, because of non-coaxial incremental strains produced during the F_2 event, or from a strain event that developed prior to regional F_2 deformation. Carter (1994) suggested that, because strain magnitudes and orientations are similar to those in the Great Smoky Mountains, the strain history may be the result of one period of pre- to synmetamorphic deformation rather than a superposition of polyphase strain events.

The purpose of this strain analysis study is to determine the amount of internal strain in coarse-grained sandstone and conglomerate of the Walden Creek and Great Smoky Groups in southeastern Tennessee using both the R_f/ϕ (Dunnet, 1969; Peach and Lisle, 1979) and normalized Fry (Fry, 1979; Erslev, 1988) methods. The importance of this study is the contribution of strain data to the existing set of strain data for the western Blue Ridge in southeastern and eastern Tennessee. The results of this study are compared with strain studies to the northeast in the Great Smoky Mountains where major premetamorphic faults are abundant, and to the southwest where predominantly synmetamorphic folds are exposed. Additional strain analysis of samples within reactivated premetamorphic structures, such as the Rabbit Creek thrust sheet, may provide insight into the polyphase deformational history of the western Blue Ridge.

Methodology

Ten oriented samples of coarse-grained Wilhite sandstone and Dean graywacke from the Great Smoky and Miller Cove thrust sheets were collected for strain analysis (Fig. III-16). These samples were oriented in the field with respect to bedding with three mutually perpendicular thin sections (parallel to bedding, perpendicular to bedding, and perpendicular to strike) cut from each sample. Modal analyses were performed to estimate the amount of quartz, feldspar, and matrix in the samples (Appendix B). Thin sections placed in a Beseler 45MX enlarger produced large negative photographs for measurements. Approximately 200 quartz grain boundaries in these photographs were digitized using a Kurta Model 12X17 digitizing tablet and associated Penworks software for the Apple Macintosh computer, and input into strain software developed by Adolph Yonkee (Weber State) for the Macintosh computer. R_f/ϕ plots using methods developed by Dunnet (1969) and Peach and Lisle (1979), and normalized Fry plots using methods developed by Fry (1979) and Erslev (1988) were also generated with Yonkee's programs. The orientation and magnitude of the strain ellipse for each thin section (three per sample) were determined for both the R_f/ϕ and normalized Fry data sets. For each method, the three ellipses for each sample were used to calculate the orientation and magnitude of the strain ellipsoid for each sample using a method described by Owens (1984).

Additionally, 75 quartz pebbles from an exposure of Dean Formation conglomerate along Forest Service Trail 126A to Basin Gap (station BRF-575, Bald River Falls 7.5-minute quadrangle) were collected and measured for plotting on a Flinn diagram. These pebbles were oriented with their long and intermediate axes rotated from the bedding plane toward the cleavage plane, suggesting that the observed shapes of the pebbles were the result of tectonic strain modifying original depositional shape. The

Figure III-16. Location of samples used for strain analysis.

Geologic abbreviations: BMF-Bullet Mountain fault; ES-Epperson synclinorium; GRA-Grindstone Ridge anticlinorium; GSF-Great Smoky fault; HBF-Hunt Branch fault; KHA-Kirkland Hollow anticlinorium; MMF-Maggies Mill fault; MCF-Miller Cove fault; OF-Oconaluftee fault; PRA-Payne Ridge anticlinorium; RCF-Rabbit Creek fault; TMA-Tellico Mountain anticlinorium; TMF-Tellico Mountain fault; TPS-Tellico Plains synclinorium; U-upthown fault block; D-downthrown fault block.

Geographic abbreviation: TP-Tellico Plains.

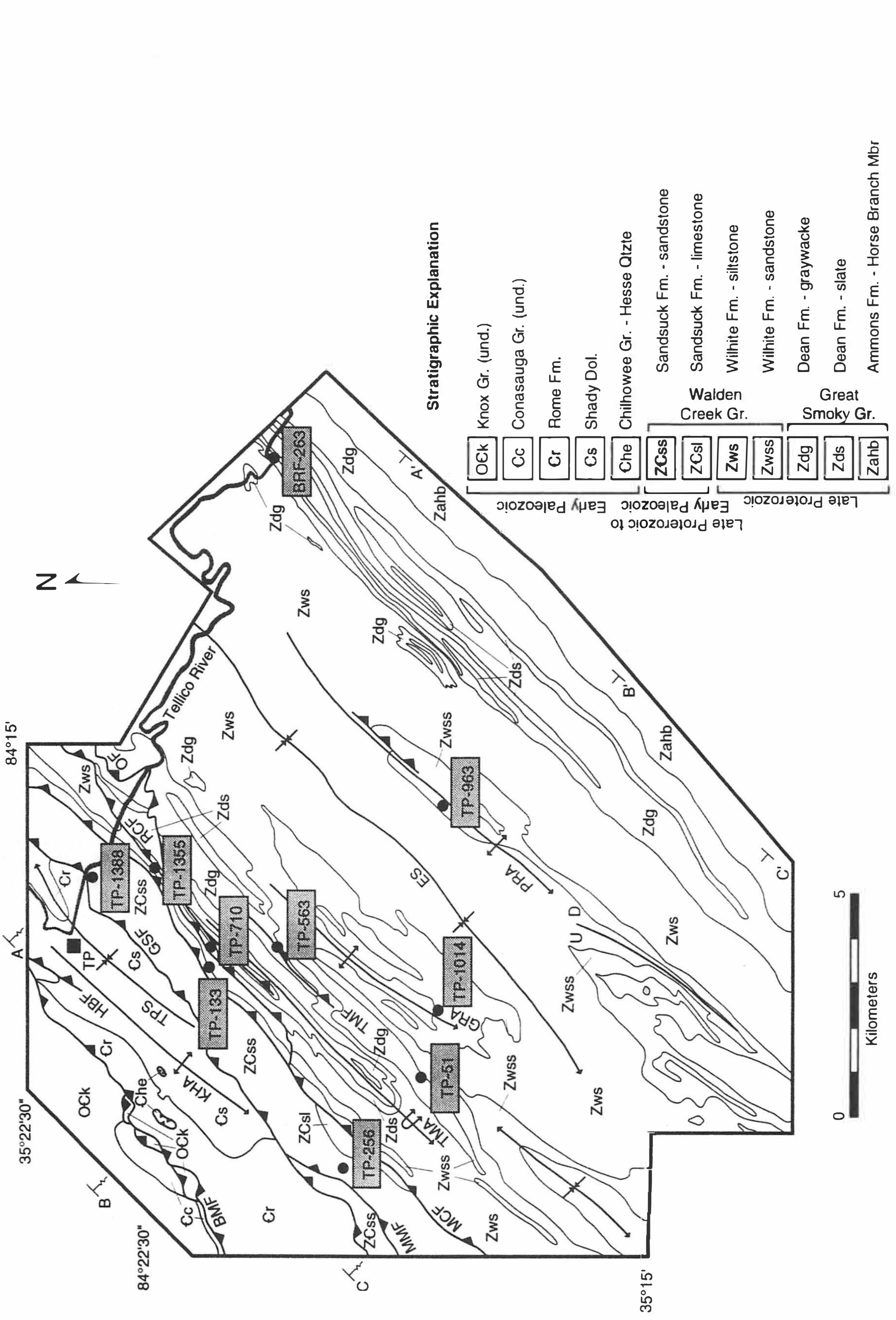
Stratigraphic Explanation
OCk Knox Gr. (und.)
Cc Conasauga Gr. (und.)
Cr Rome Fm.
Cs Shady Dol.
Che Chilhowee Gr. - Hesse Qtzte
Early Paleozoic
ZCss Sandsuck Fm. - sandstone
ZCsl Sandsuck Fm. - limestone
Walden Creek Gr.
Late Proterozoic to Early Paleozoic
Zws Wilhite Fm. - siltstone
Zwss Wilhite Fm. - sandstone
Zdg Dean Fm. - graywacke
Zds Dean Fm. - slate
Zahb Ammons Fm. - Horse Branch Mbr
Great Smoky Gr.
Late Proterozoic
N
Tellico River
84°15'
84°22'30"
35°22'30"
35°15'
TP-1388
TP-1355
TP-710
TP-563
TP-133
TP-1014
TP-963
TP-51
TP-256
BRF-263
HBF
TPS
GSF
RCF
KHA
TMF
GRA
ES
PRA
TMA
MCF
MMF
BMF
0 5
Kilometers

three principal axes of each pebble were measured, and the ratios of the principal axes were calculated to determine Flinn's (1962) *k*. These ratios were then plotted on a Flinn diagram for graphical analysis.

Results of study

The strain analysis of coarse-grained rocks in the study area is consistent with previous strain analyses of coarse-grained lithologies in the Ocoee Supergroup northeast and southwest of the study area. R_f/ϕ method results in R_{xy}, R_{xz}, R_{yz} ratios ($X>Y>Z$) between 1.05 and 2.30 with means and standard deviations of 1.33 ± 0.19, 1.71 ± 0.26, and 1.30 ± 0.16, respectively (Table III-2; Appendix C). R_f/ϕ values generally increase in magnitude to the southeast in the direction of increasing metamorphic grade, and near postmetamorphic brittle faults (Fig. III-17; Plate III). The orientations of the principal strain axes are variable, but general trends are recognized: X axes generally parallel strike, Y axes are normal to strike and parallel to transport direction, and Z axes generally plunge moderately northwest (Fig. III-18A). The orientation of the Y axes is highly variable. Seven of the ten R/ϕ values fall within the field of apparent constriction on a Flinn diagram (Fig. III-19A). Half of the R_f/ϕ values reveal minimal constriction and flattening.

Strain ratios (R_{xy}, R_{xz}, R_{yz}) determined by the normalized Fry method range between 1.11 and 3.20 with means and standard deviations of 1.61 ± 0.26, 2.27 ± 0.35, and 1.43 ± 0.08, respectively (Table III-2; Appendix C). Because of the amount of matrix material and the lack of consistent packing of quartz grains, only seven of the ten samples were analyzed. Strain ratios from the normalized Fry method also increase to the southeast and near fault zones (Fig. III-20). Orientation of the principal axes from the normalized Fry method, although variable, is similar to the orientations obtained from the R_f/ϕ method. The X and Z axes are generally parallel and normal to regional strike,

Figure III-17. X/Y axial ratios as determined by the R_f/ϕ method. Trend of the X axis is indicated for each ellipse. Interpretive Flinn diagram shows progressive deformation to the southeast.

Geologic abbreviations: BMF-Bullet Mountain fault; ES-Epperson synclinorium; GRA-Grindstone Ridge anticlinorium; GSF-Great Smoky fault; HBF-Hunt Branch fault; KHA-Kirkland Hollow anticlinorium; MMF-Maggies Mill fault; MCF-Miller Cove fault; OF-Oconaluftee fault; PRA-Payne Ridge anticlinorium; RCF-Rabbit Creek fault; TMA-Tellico Mountain anticlinorium; TMF-Tellico Mountain fault; TPS-Tellico Plains synclinorium; U-upthown fault block; D-downthrown fault block.

Geographic abbreviation: TP-Tellico Plains.

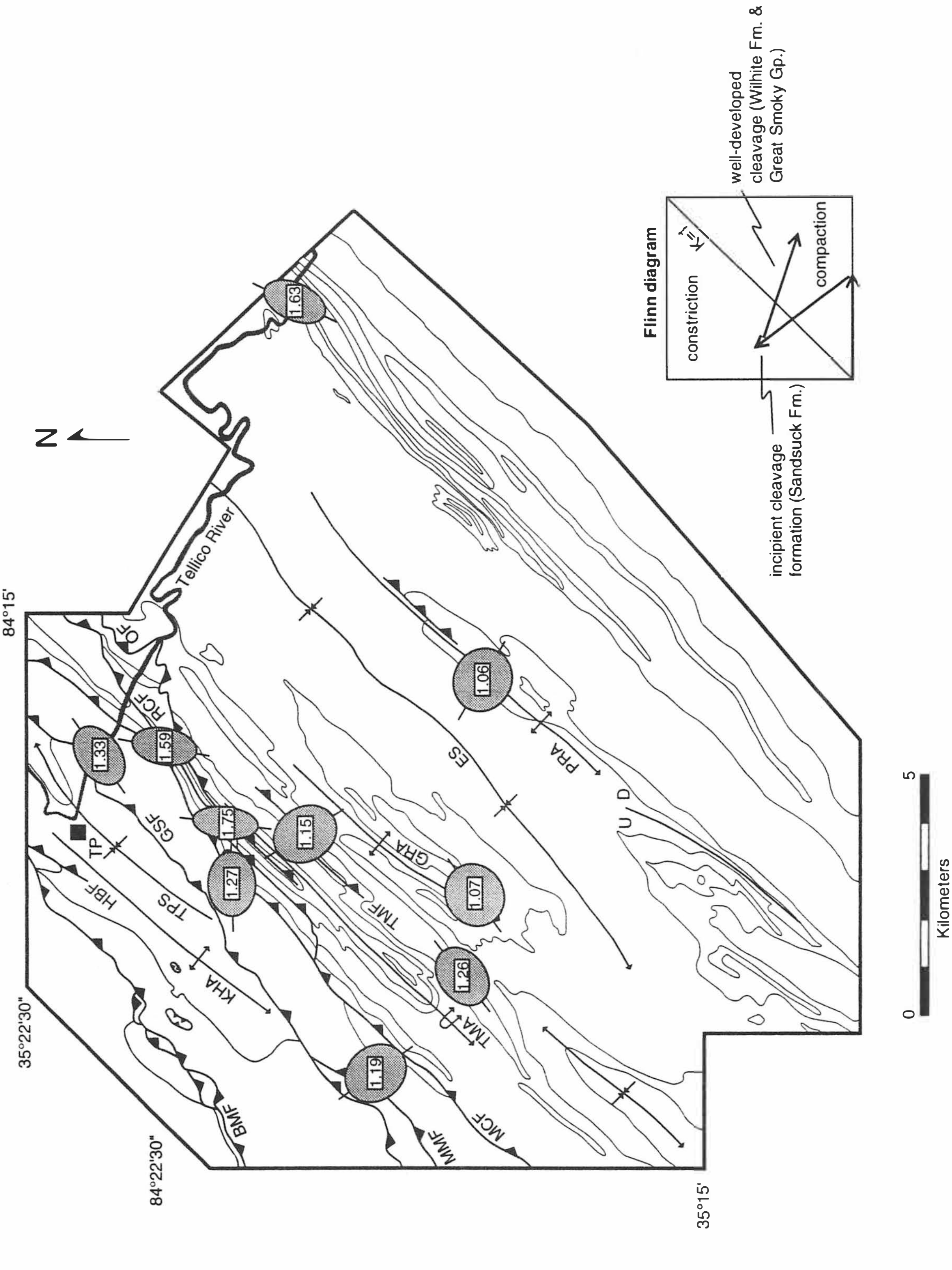
84°22'30"
35°22'30"
84°15'
35°15'
N
Tellico River
OF
RCF
GSF
TP
TPS
HBF
KHA
BMF
MMF
MCF
TMF
TMA
GRA
ES
PRA
U
D
1.33
1.59
1.75
1.15
1.27
1.07
1.26
1.19
1.06
1.63
0
5
Kilometers
Flinn diagram
constriction
compaction
k=1
incipient cleavage
formation (Sandsuck Fm.)
well-developed
cleavage (Wilhite Fm. &
Great Smoky Gp.)

Figure III-18. Lower-hemisphere equal-area projections of strain ellipsoid axes. See Appendix C for axes data. (A) R_f/ϕ method. (B) normalized Fry method.

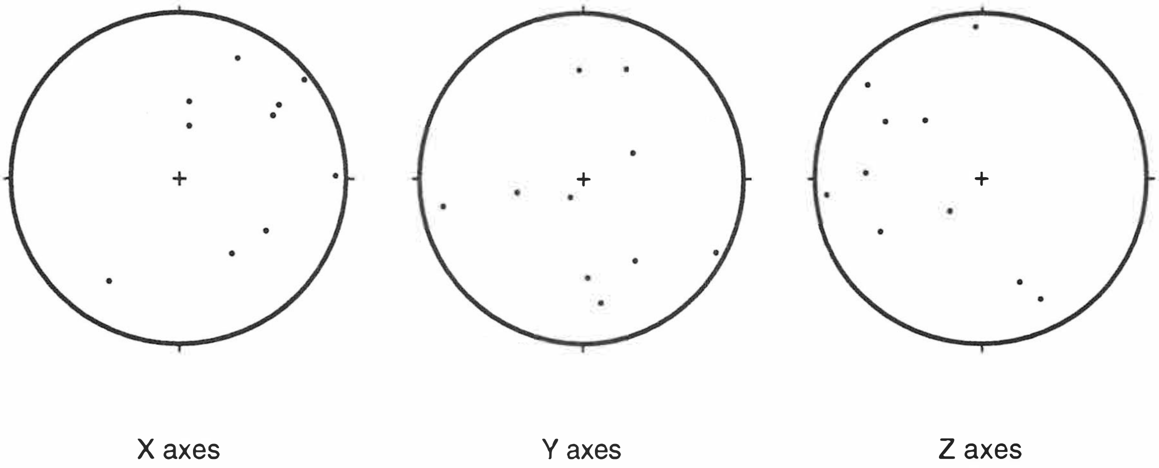

(A)

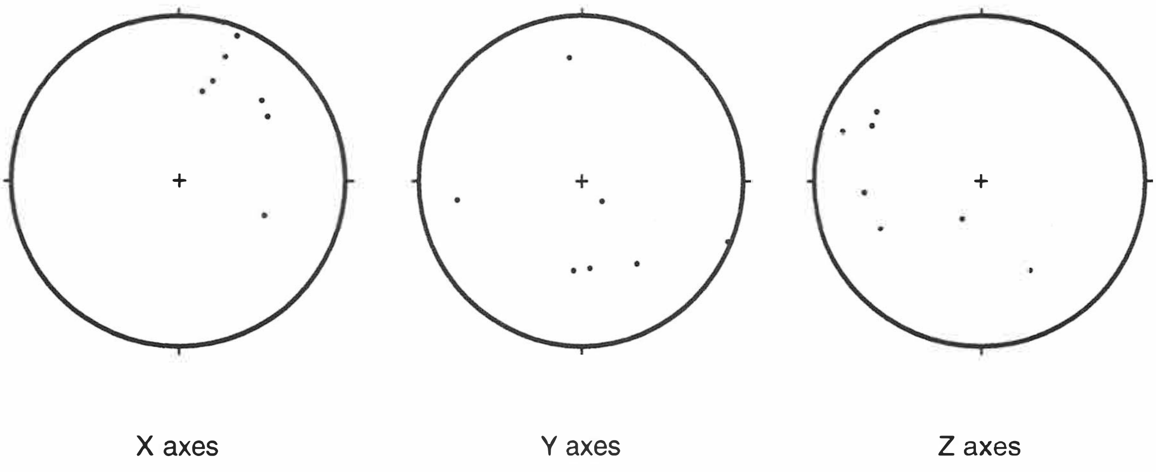

(B)

Figure III-19. Flinn diagram of R_f/ϕ and normalized Fry strain values in each thrust sheet. (A) R_f/ϕ values. (B) normalized Fry values.

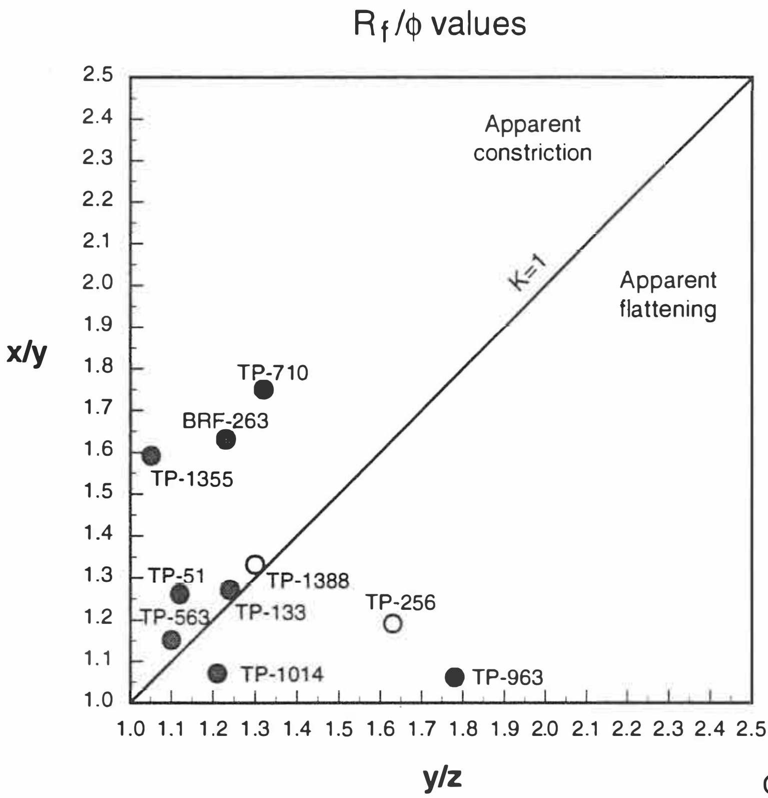

Rf/ϕ values
x/y
y/z
Apparent constriction
Apparent flattening
K=1
TP-710
BRF-263
TP-1355
TP-51
TP-1388
TP-133
TP-563
TP-256
TP-1014
TP-963

(A)

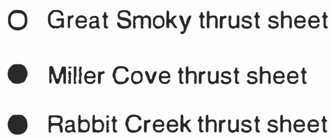

Great Smoky thrust sheet
Miller Cove thrust sheet
Rabbit Creek thrust sheet

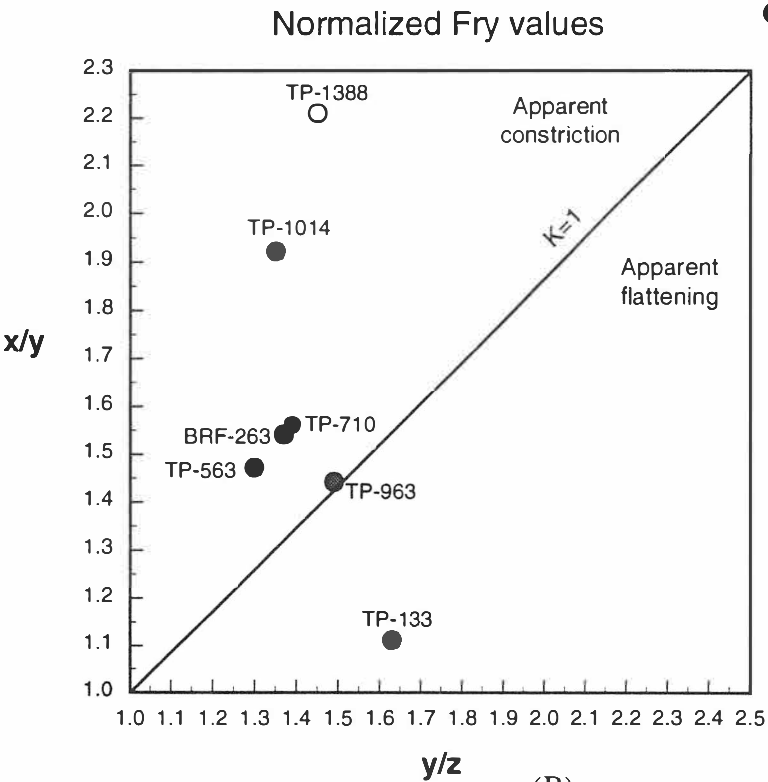

Normalized Fry values
x/y
y/z
Apparent constriction
Apparent flattening
K=1
TP-1388
TP-1014
BRF-263
TP-710
TP-563
TP-963
TP-133

(B)

Figure III-20. X/Y axial ratios as determined by the normalized Fry method. Trend of the X axis is indicated for each ellipse. Interpretive Flinn diagram shows progressive deformation to the southeast.

Geologic abbreviations: BMF-Bullet Mountain fault; ES-Epperson synclinorium; GRA-Grindstone Ridge anticlinorium; GSF-Great Smoky fault; HBF-Hunt Branch fault; KHA-Kirkland Hollow anticlinorium; MMF-Maggies Mill fault; MCF-Miller Cove fault; OF-Oconaluftee fault; PRA-Payne Ridge anticlinorium; RCF-Rabbit Creek fault; TMA-Tellico Mountain anticlinorium; TMF-Tellico Mountain fault; TPS-Tellico Plains synclinorium; U-upthown fault block; D-downthrown fault block.

Geographic abbreviation: TP-Tellico Plains.

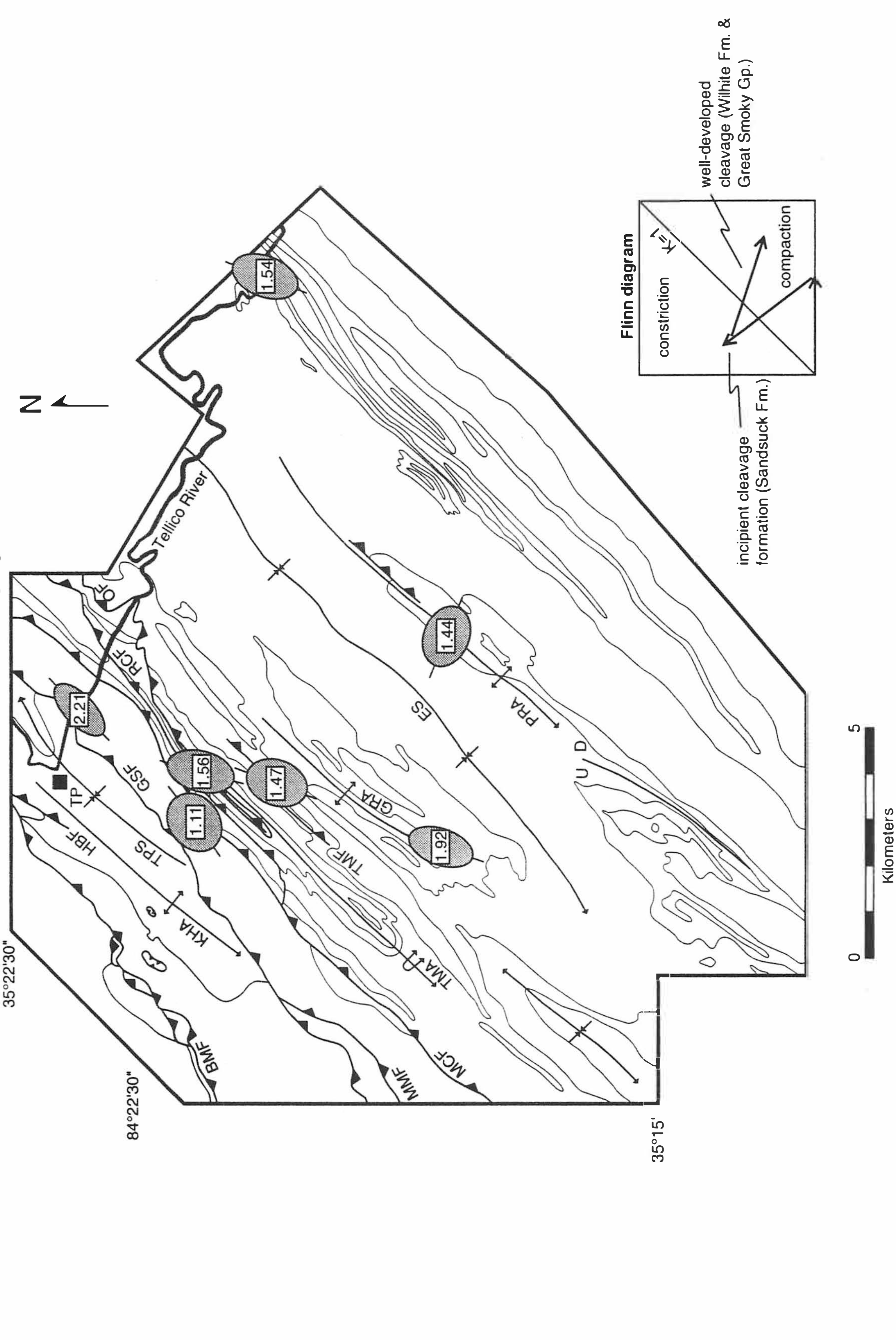

N
84°15'
35°22'30"
84°22'30"
35°15'
Tellico River
BMF
MMF
MCF
HBF
TPS
TP
GSF
RCF
OF
KHA
TMA
TMF
GRA
ES
PRA
U
D
2.21
1.56
1.11
1.47
1.92
1.44
1.54
0
5
Kilometers
Flinn diagram
constriction
k=1
compaction
well-developed cleavage (Wilhite Fm. & Great Smoky Gp.)
incipient cleavage formation (Sandsuck Fm.)

respectively. Orientation of the Y axes is generally parallel to transport direction (Fig. III-18B). Six of the seven normalized Fry values fall in the field of apparent flattening on a Flinn diagram with one of those values revealing minimal constriction (Fig. III-19B).

Two assumptions are required for the measurement of pebbles to yield simple finite strain ratios. These assumptions include: original sphericity of the pebble before deformation, and minimal loss of the pebble volume due to pressure solution. Nearly spherical pebbles are rare but have been observed in Wilhite sandstone. Additionally, the majority of quartz pebbles observed were rotated from the bedding plane and toward the plane of cleavage. The effects of pressure solution on most pebbles are negligible.

The principal axes of 75 quartz pebbles oriented parallel to regional slaty cleavage record mean R_{xy}, R_{xz}, and R_{yz} (X>Z>Y) values of 1.32 ± 0.18, 2.22 ± 0.39, and 1.70 ± 0.29, respectively (Appendix C). When plotted on a Flinn diagram, 88 percent of quartz pebbles fall within the field of apparent flattening (Fig. III-21).

Discussion of results

Two values of strain for (seven out of ten samples) each sample(s) were generated from the R_f/ϕ and normalized Fry methods. The R_f/ϕ method describes strain based on axial ratios and orientation of grains (grain shape), while the normalized Fry method creates a graphical estimate of strain based on the distribution of grain centers. The normalized Fry method was used for only seven of the ten samples, because of the large amount of matrix material and subsequent lack of closely packed quartz grains in the three unused samples. To determine which method yielded the best results, fabric elements and microstructures of each sample in each thrust sheet were analyzed (Table III-3). Fabrics observed in the samples include a depositional fabric, a tectonic fabric, or a combination of both. Other important considerations for determining the fabric of the sample was the packing of quartz grains, and amount of matrix material present in the

Figure III-21. Flinn diagram of 75 flattened quartz pebbles from Basin Gap, station BRF-575, Bald River Falls 7.5-minute quadrangle.

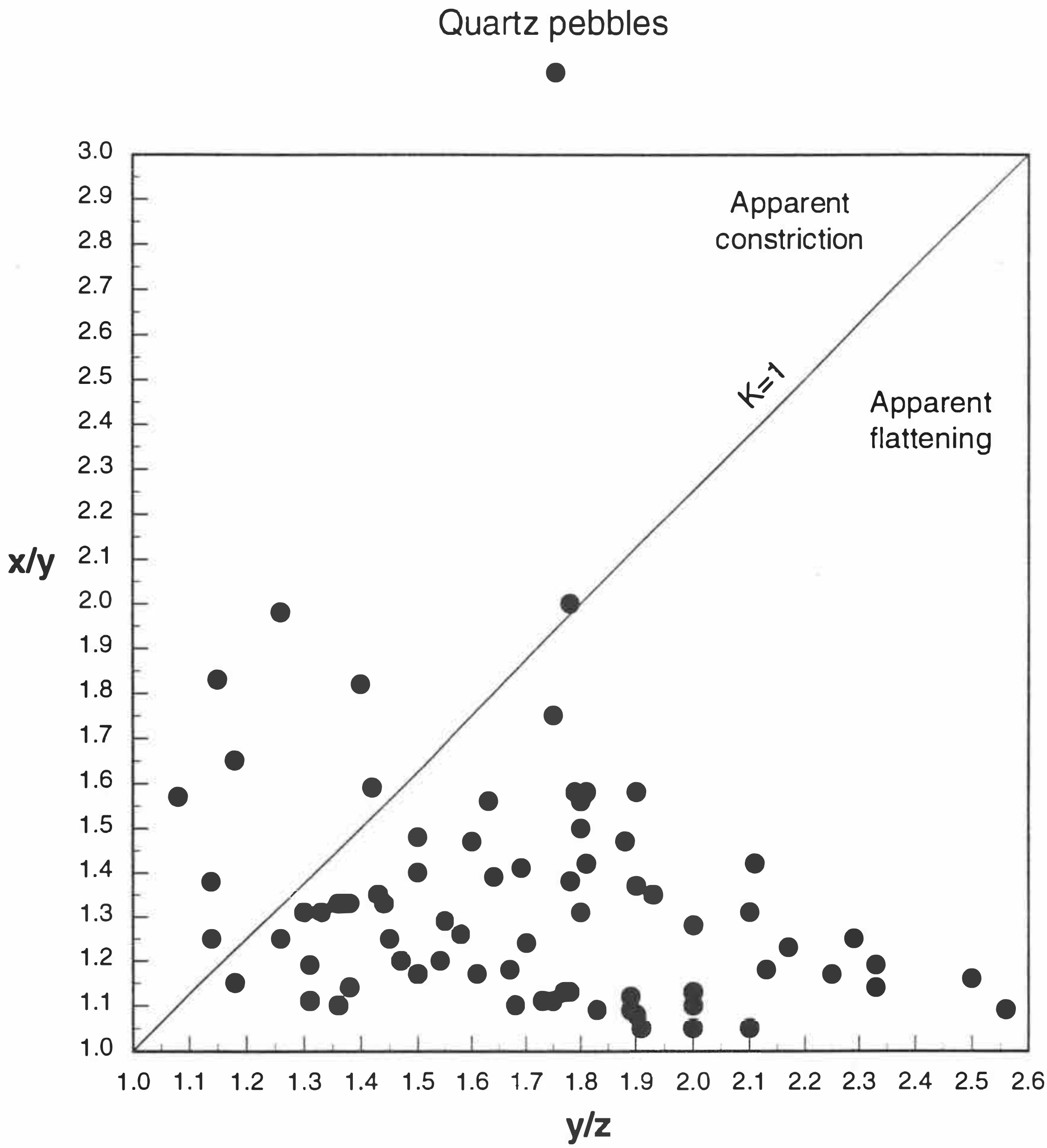

Quartz pebbles
3.0
2.9
2.8
2.7
2.6
2.5
2.4
2.3
2.2
2.1
2.0
1.9
1.8
1.7
1.6
1.5
1.4
1.3
1.2
1.1
1.0
x/y
Apparent
constriction
K=1
Apparent
flattening
1.0 1.1 1.2 1.3 1.4 1.5 1.6 1.7 1.8 1.9 2.0 2.1 2.2 2.3 2.4 2.5 2.6
y/z

Table III-3. Microstructural anaylsis of strain samples.

thrust sheet	statigraphic unit	sample	fabrics	microstructures	comments*
Great Smoky	Sandsuck fm.	TP-256	Matrix supported with a predominant depositional fabric.	Undulatory extinction, fluid inclusion planes, and sutured grain boundaries.	R_f/ϕ method only. Ellipses not consistent with ellipsoid.
	Sandsuck fm.	TP-1388	Tectonic and depositional fabrics with closely packed quartz grains.	Undulatory extinction, fluid inclusion planes, and sutured grain boundaries.	R_f/ϕ and normalized Fry methods. Fry ellipses not consistent with ellipsoid.
Miller Cove	Wilhite fm.	TP-51	Matrix supported with a predominant depositional fabric.	Undulatory extinction, sutured grain boundaries, and pressure solution.	R_f/ϕ method only. Deformation focused in the matrix.
	Wilhite fm.	TP-133	Prominent tectonic fabric with closely packed quartz grains.	Undulatory extinction, sutured grain boundaries, deformation laminae, and pressure solution.	R_f/ϕ and normalized Fry methods.
	Wilhite fm.	TP-963	Tectonic and depositional fabrics with moderately packed quartz grains.	Undulatory extinction, sutured grain boundaries, and pressure solution.	R_f/ϕ and normalized Fry methods. R_f/ϕ ellipses not consistent with ellipsoid.
	Wilhite fm.	TP-1014	Tectonic and depositional fabrics with moderately packed quartz grains.	Undulatory extinction, sutured grain boundaries, and pressure solution.	R_f/ϕ and normalized Fry methods. Fry ellipses not consistent with ellipsoid.
	Wilhite fm.	TP-1355	Matrix supported with a predominant depositional fabric.	Undulatory extinction, sutured grain boundaries, and pressure solution.	R_f/ϕ method only. Ellipses not consistent with ellipsoid.
	Dean fm.	TP-563	Matrix supported with a predominant depositional fabric and minor tectonic fabric.	Undulatory extinction, sutured grain boundaries, and pressure solution.	R_f/ϕ and normalized Fry methods.
	Dean fm.	BRF-263	Tectonic and depositional fabrics with moderately packed quartz grains.	Undulatory extinction, sutured grain boundaries, and pressure solution.	R_f/ϕ and normalized Fry methods.
Rabbit Creek	Dean fm.	TP-710	Prominent tectonic fabric with closely packed quartz grains.	Undulatory extinction, sutured grain boundaries, deformation laminae, and pressure solution.	R_f/ϕ and normalized Fry methods. Fry ellipses not consistent with ellipsoid.

* The lack of consistency between ellipses and ellipsoid occurs when Owen's (1984) method for calculating the ellipsoid fails to achieve similarity of results between the six calculation attempts.

samples. If the sample was grain supported, it was considered to have closely packed quartz grains, where grain boundaries were in contact with each other. The determination of whether deformation was partitioned in the matrix or in the quartz grains was also an important factor in determining which strain method was more reliable. If deformation was concentrated in the quartz grains, the sample was considered to have a prominent tectonic fabric. These samples contained deformed quartz grains. Matrix-supported samples with relatively unstrained quartz grains were interpreted as lacking a tectonic fabric. These samples were considered to have a predominantly depositional fabric. Tectonic microstructures observed in quartz in coarse-grained lithologies included sweeping and patchy undulatory extinction, fluid inclusion planes, deformation lamellae, sutured and serrated grain boundaries, intragranular fractures, and transgranular stylolites. These microstructures are characteristic of low-grade metamorphic rocks (Groshong, 1988; Knipe, 1989; Lloyd and Knipe, 1992; Onasch and Dunne, 1993), and were produced by deformation mechanisms including dislocation glide, dislocation creep, pressure-solution, and microfracturing. The strain ratios of the three ellipses generated by the R_f/ϕ and normalized Fry method for each sample may not be consistent with the strain ratios of the principal axes of the strain ellipsoid as calculated using Owens (1984) method. The lack of consistency between ellipses and ellipsoid occurs when Owen's (1984) method for calculating the ellipsoid fails to achieve similarity of results between the six calculation attempts. In these situations the strain ratios of the three ellipses are important because of their consistency with the fabrics present in the thin-section photographs from which the ellipses were calculated. Samples that have strain ellipse values inconsistent with the principal axes of the strain ellipsoid are denoted in Appendix C by an asterisk.

R_f/ϕ and normalized Fry strain values are relatively low in the Great Smoky thrust sheet. The two samples (TP-256 and TP-1388) analyzed from this thrust sheet exhibit both depositional and tectonic fabric components. Sample TP-1388 is located in the quartz-rich coarse-grained lithologies in the lower portions of the Sandsuck Formation, and in close proximity to the Great Smoky fault. Sample TP-256 is located higher in the stratigraphic sequence where lithologies are finer grained and often interbedded with shale. Sample TP-256 exhibits a better depositional fabric than TP-1388; TP-1388, however, contains a more pronounced tectonic fabric and has closely packed quartz grains (Table III-3). Because of the amount of matrix material and the predominantly depositional fabric in TP-256, the normalized Fry method was not used for this strain analysis. In both samples, the R_f/ϕ method provides the most reliable results because of this method's dependency on grain shape. Microstructures observed in both samples include sweeping undulatory extinction, sutured grain boundaries, fluid-inclusion planes, and intragranular fractures (Fig. III-22A, III-22B). Of the two samples analyzed in this thrust sheet, only one set of ellipses (TP-1388; R_f/ϕ) show any consistency with the strain ellipsoid. This sample (TP-1388) has a pronounced tectonic fabric and closely packed quartz grains. Sample TP-1388 has higher strain values than sample TP-256, and is probably due to sample TP-1388's closer proximity to the Great Smoky fault (Fig III-16, Appendix C). Much of the strain in sample TP-256 is probably concentrated in the matrix. The parallel orientation of the X axes to regional strike may also suggest a component of diagenetic compaction (Fig. III-18; Appendix C).

Strain values in the Miller Cove thrust sheet were obtained from seven samples collected on the upright backlimb of anticlines throughout this thrust sheet (Fig. III-16). Five of these samples were collected from the Wilhite Formation (Walden Creek Group) and two from the Dean Formation (Great Smoky Group). Fabrics present in the Wilhite Formation generally exhibit a prominent depositional fabric along with a locally prominent tectonic fabric. Generally, these samples are matrix supported and lack closely packed grains, making them unsuitable for normalized Fry analysis (Table III-3).

Figure III-22. Microstructures in the Great Smoky thrust sheet. (A) Enlarged inverted negative image (from thin section) of microstructures from sample TP-256, Conasauga Creek, Tellico Plains 7.5-minute quadrangle. Field of view is approximately 2 cm. (B) Enlarged inverted negative image (from thin section) of microstructures from sample TP-1388, Tellico River, Tellico River 7.5-minute quadrangle. Field of view is approximately 2 cm.

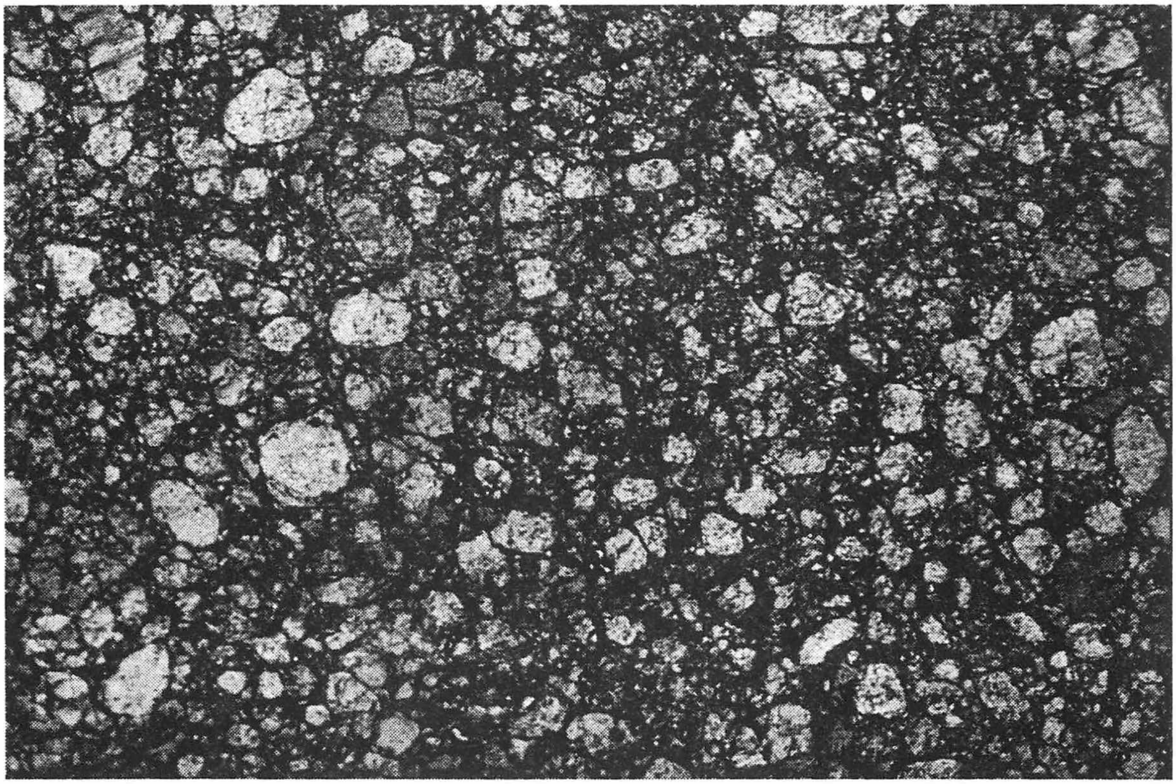

(A)

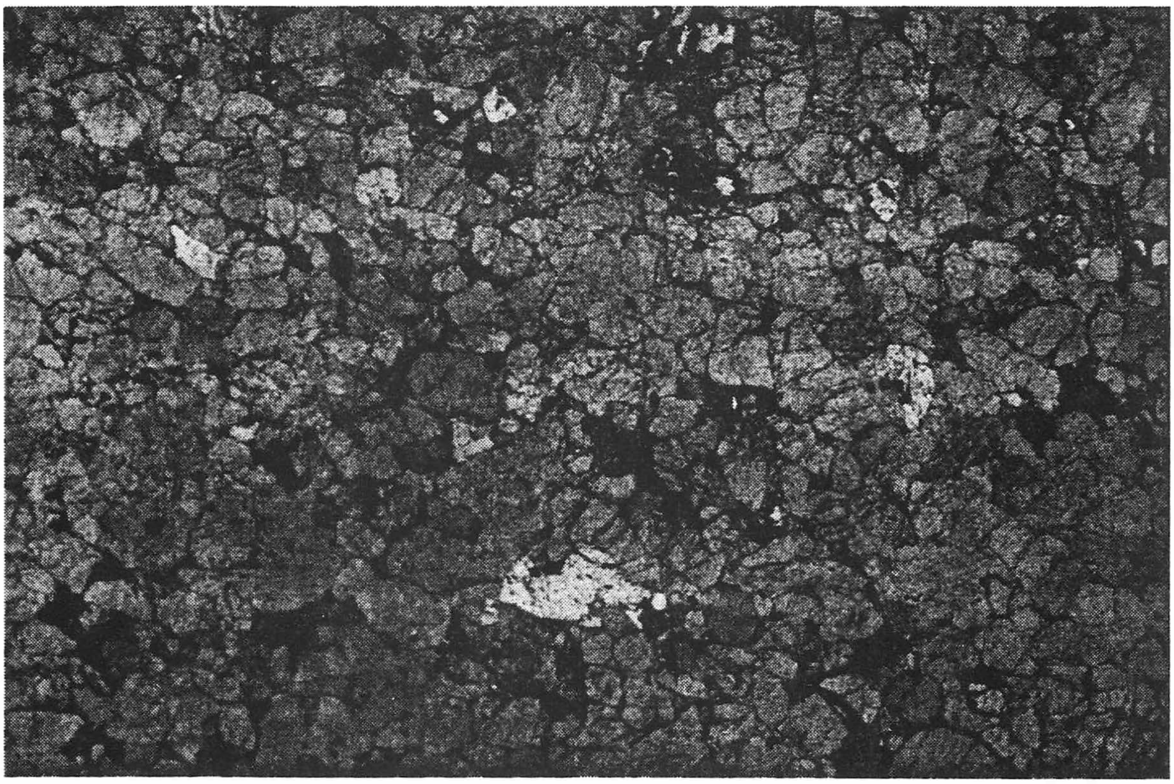

(B)

Samples from the Dean Formation also reveal a depositional and local tectonic fabric, but are more poorly sorted and packed than the Wilhite samples (Fig. III-23A, III-23B). Microstructures in the Miller Cove thrust sheet include patchy and sweeping undulatory extinction, sutured and serrated grain boundaries, subgrains, deformation laminae, intragranular fractures, and pressure solution (Fig. III-23A, III-23B). Here, as in the Great Smoky thrust sheet, normalized Fry analysis yields strain values higher than values obtained from the R_f/ϕ method. Both R_f/ϕ and normalized Fry analyses result in strain values that increase to the southeast, with some relatively large strains near faults (Figs. III-17, III-20; Appendix C; Plate III). The R_f/ϕ method is interpreted to be a more reliable method for determining strain in this thrust sheet, because strain values generated from this method better reflect grain shape and apparent strains observed in the thin section photos. The large strain values associated with the normalized Fry method may be related to deformation partitioned in the matrix. Because of the high amount of matrix material and the lack of packed grains, two samples (TP-51 and TP-1355) were not analyzed by the normalized Fry method. Of the samples analyzed in the Miller Cove thrust sheet, the ellipses of samples TP-963, TP-1355 (R_f/ϕ), and TP-1014 (normalized Fry) are not consistent with the strain ellipsoid. For these samples, the ellipses generated from the R_f/ϕ and normalized Fry method should be also considered along with the strain ellipsoid, because the strain ellipses more closely resemble the apparent strain observed in the thin-section photographs.

Strain values from the Rabbit Creek thrust sheet are analyzed from one sample from the Dean Formation. (Fig. III-16). This sample exhibits a pronounced tectonic fabric and closely packed quartz grains. Microstructures include sweeping undulatory extinction, sutured grain boundaries, and deformation laminae (Fig. III-24). Strain values for both the R_f/ϕ and normalized Fry methods are high (Figs. III-17, III-20; Appendix C). The high strain values for this sample are probably the result of the emplacement of the

Figure III-23. Microstructures in the Miller Cove thrust sheet. (A) Enlarged inverted negative image (from thin section) of microstructures from sample TP-133, Tennessee State Highway 68, Tellico Plains 7.5-minute quadrangle. Field of view is approximately 2 cm. (B) Enlarged inverted negative image (from thin section) of microstructures from sample TP-563, Tennessee State Highway 68, Tellico Plains 7.5-minute quadrangle. Field of view is approximately 2 cm.

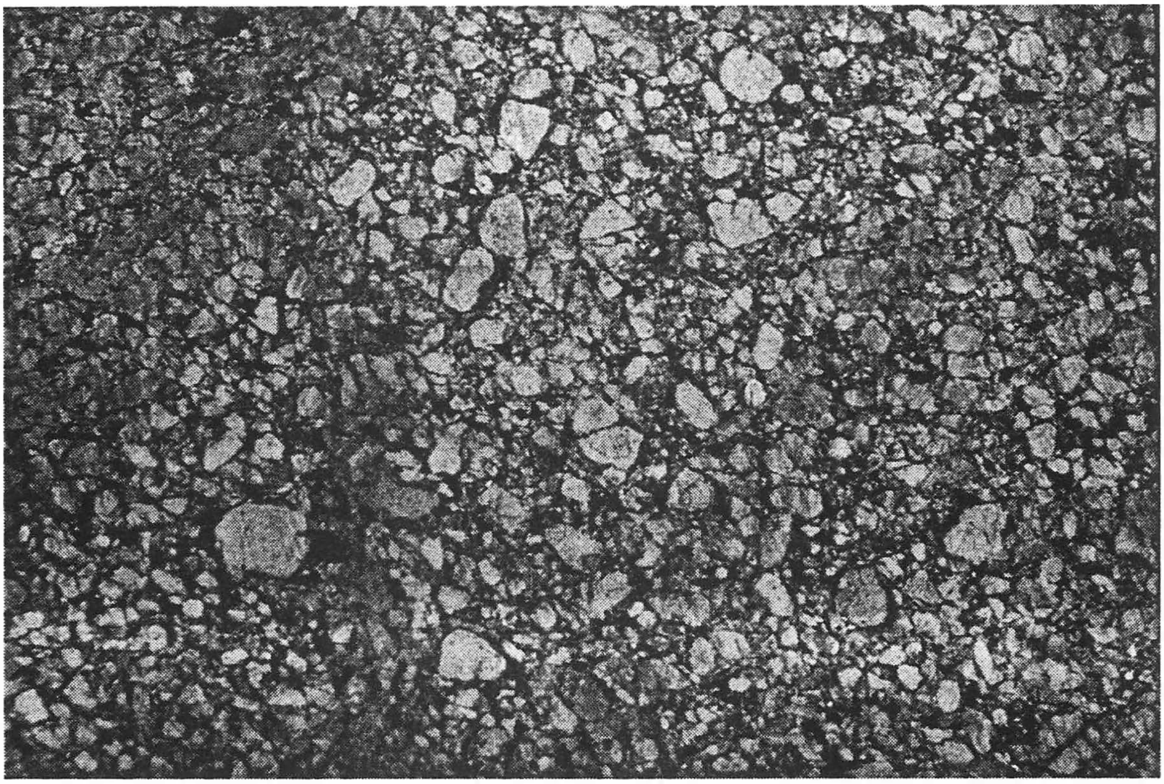

(A)

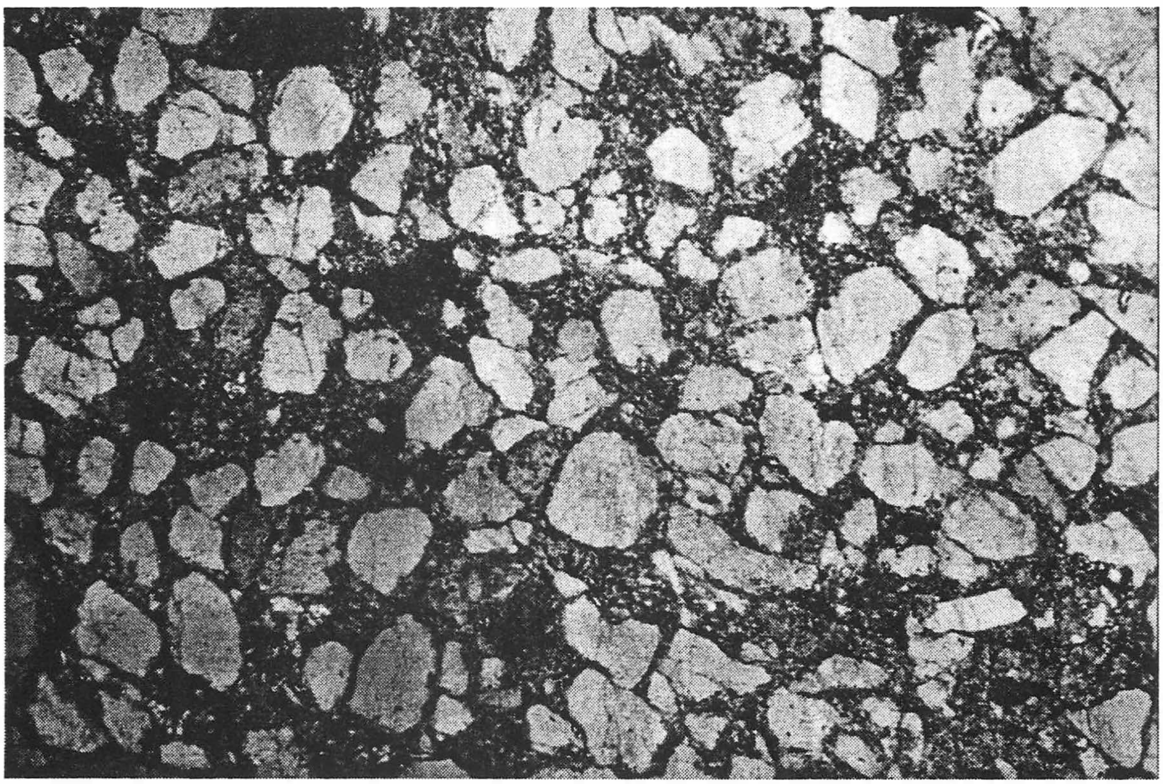

(B)

Figure III-24. Microstructures in the Rabbit Creek thrust sheet. Enlarged inverted negative image (from thin section) of microstructures from sample TP-710, Tennessee State Highway 68, Tellico Plains 7.5-minute quadrangle. Field of view is approximately 2 cm.

Rabbit Creek and Oconaluftee faults. Strain ellipses generated by the R_f/ϕ method are more consistent with the strain ellipsoid than the strain ellipses generated by the normalized Fry method. For this reason, the R_f/ϕ method is interpreted to be a more reliable measure of the finite strain in this sample.

Strain analysis conclusions

1) Mean strain ratios determined by the R_f/ϕ method are 1.33, 1.71, and 1.30, respectively. Strain ratios determined by the normalized Fry method are 10 to 25 percent higher. These ratios are consistent with previous studies in the Great Smoky Mountains National Park region, and in the western Blue Ridge foothills to the southwest of the study area.

2) Strain increases to the southeast in the direction of increasing metamorphic grade, and near late Paleozoic brittle faults. Observed microstructures such as undulatory extinction, deformation lamellae, sutured grain boundaries, stylolites, intragranular fractures, and fluid-inclusion planes are indicative of low-grade metamorphic deformation mechanisms such as dislocation creep, pressure solution, and brittle fracturing.

3) The principal strain axes of the strain ellipsoid are oriented so that X axes are strike parallel, Y axes are parallel to transport direction, and Z axes plunge moderately to the northwest. The R_f/ϕ method yields more reliable results because of the consistent orientations of the strain ellipsoid, and consistent fits of the strain ellipses with the three-dimensional strain ellipsoid.

4) Strain analysis (R_f/ϕ and normalized Fry) suggest that rocks of the western Blue Ridge Foothills in the study area were deformed by at least one strain event.

Chapter IV

Environmental Assessment of the Sixmile Creek and Rocky Branch Watersheds, Northwest Slope of Waucheesi Mountain

Introduction

The purpose of this chapter is to apply some of the geologic data and information gathered during this study from two watersheds to a hypothetical site environmental assessment for possible residential development (Fig. IV-1; Plate IV). This assessment uses geologic information to distinguish among possible alternative locations for residential development. Geologic variables such as mechanical discontinuities in bedrock, lithologic type, geomorphic features (surficial deposits, slopes, soils), and ground and surface water are considered in this assessment. This area was assessed according to these geologic factors and the potential impact on the local environment related to residential development, such as increased runoff, degradation of water quality, and habitat destruction. Residential development of this area would include the construction of residences, roads, and public utilities (electricity, sewer, water). Several small tracts within the assessment watershed have already been developed, and are located in the northwestern portion of the watersheds.

Methodology

A 5.2 km^2 (2.1 mi^2) tract of land was selected along the northwest slope of Waucheesi Mountain between Sixmile Creek and Rocky Branch drainages for evaluation for potential residential development in this portion of southeastern Tennessee (Fig. IV-1; Plate IV). This area was chosen because it is typical in terms of land being developed in this area for both second homes and permanent residences. The geologic mapping portion of this study included description and measurement of lithologic and structural

Figure IV-1. Physiographic units of study area showing location of environmental assessment area. Assessment area is outlined in the southeastern portion of the map. Refer to Figs. II-2, III-1, and Plate I for stratigraphic and structural explanations.

Geologic abbreviations: BMF-Bullet Mountain fault; ES-Epperson synclinorium; GRA-Grindstone Ridge anticlinorium; GSF-Great Smoky fault; HBF-Hunt Branch fault; KHA-Kirkland Hollow anticlinorium; MCF-Miller Cove fault; MMF-Maggies Mill fault; OF-Oconaluftee fault; PRA-Payne Ridge anticlinorium; RCF-Rabbit Creek fault; TMA-Tellico Mountain anticlinorium; TPS-Tellico Plains synclinorium; U-upthrown fault block; D-downthrown fault block; K-klippe.

Geographic abbreviation: TP-Tellico Plains.

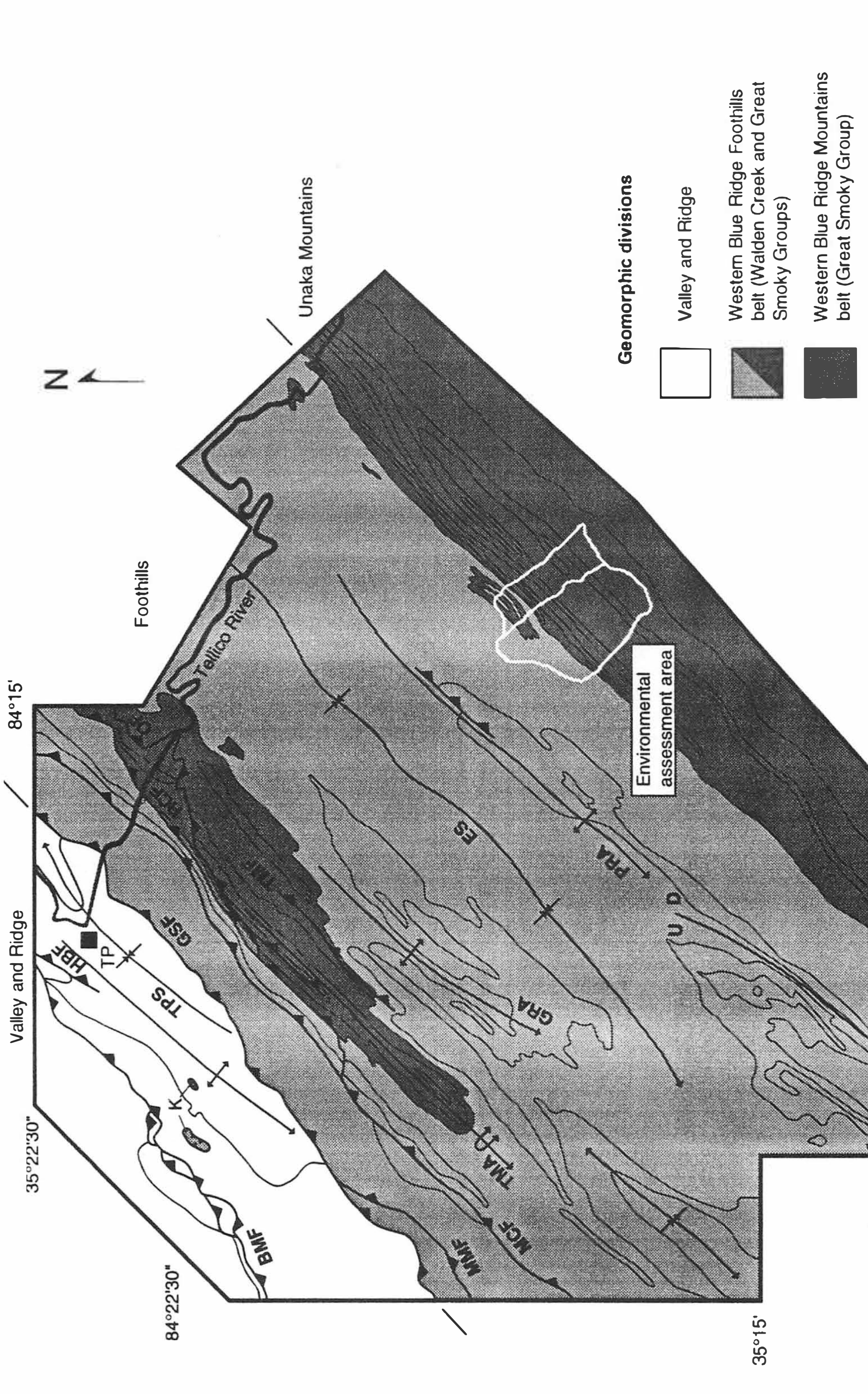
Valley and Ridge
Foothills
Unaka Mountains
35°22'30"
84°22'30"
84°15'
35°15'
N
Tellico River
Environmental assessment area
HBF
TP
TPS
GSF
BCF
TMF
ES
PRA
GRA
TMA
MCF
MMF
BMF
K
U
D
0
5
Kilometers
Geomorphic divisions
Valley and Ridge
Western Blue Ridge Foothills belt (Walden Creek and Great Smoky Groups)
Western Blue Ridge Mountains belt (Great Smoky Group)

discontinuities (bedding, contacts, cleavage, joints, and faults) between the Sixmile Creek and Rocky Branch drainages (Fig. IV-1; Plate I). The aerial extent of surficial deposits and sulfide-bearing map units are also identified. Slope gradients and stream density are geomorphic factors considered in this assessment.

Bedrock Geology

The environmental assessment site is located in the southeastern portion of the study area along the northwest slope of Waucheesi Mountain (Fig. IV-1; Plate IV). Here the rocks consist of the Great Smoky and Walden Creek Groups, as described in Chapters II and III (Fig. IV-1; Plate I). Lithologic units within the assessment area include graywacke and slate of the Dean Formation (Great Smoky Group), conformably overlain by the metasiltstone of the Wilhite Formation (Walden Creek Group) (Fig. IV-1; Plate I). Approximately 75 percent of the area consists of a graded sequence of granule- to pebble-size conglomerate, graywacke, and slate of the Dean Formation. Numerous mappable slate lenses within the Dean Formation are also exposed in the watersheds. The remaining portions of the assessment area are underlain by Wilhite Formation metasiltstone located in the northwestern portion of the tract.

The regional structure in this portion of southeastern Tennessee is a southeast-dipping, southwest-plunging, overturned forelimb related to the first-order Ducktown anticlinorium. Parasitic folds to this larger structure were also indicated by the presence of upright northwest- and southeast-dipping beds. All contacts within this area are interpreted as conformable. Map-scale faults were not observed, and minor faults are difficult or impossible to observe without excavation. Bedding (S_0) is easily recognized in the graded, coarse-grained lithologies of the Dean Formation. Bedding in the mappable slate lenses is difficult to recognize because of the pervasive slaty cleavage, but is very prominent in the banded metasiltstones of the Wilhite Formation. All of the units are deformed by regional slaty cleavage (S_1)–best developed in the fine-grained lithologies–but also is present in the coarse-grained lithologies. Joints are common in both fine- and coarse-grained lithologies in the assessment area. These joints are either unfilled, or filled with quartz and calcite.

The fine-grained rocks of the Dean Formation, especially the mappable slate lenses, are the most sulfidic lithologies in the assessment area. The coarse-grained graywacke of the Dean Formation contains considerably lesser amounts of pyrite. The Wilhite Formation metasiltstone and slate also contain small to moderate amounts of locally abundant pyrite.

Rock discontinuities

Discontinuities are any planar structure or surface in a rock mass along which the rock mass may break or separate. Discontinuities are also the primary controlling factor of mass strength and deformability in a rock mass (Johnson and DeGraff, 1988). Bedding planes, lithologic contacts, cleavage, joints, and faults are discontinuities present in the assessment area. Discontinuities can be characterized by orientation, spacing, continuity, separation of discontinuity surface, and thickness and, if present, nature of joint fillings (Johnson and DeGraff, 1988). Strengths of rock masses imparted to a large degree by shear strengths of discontinuity surfaces typically depend on one or more of these characteristics, and are summarized by Bieniawski (1973) and Cording and others (1975) (Johnson and DeGraff, 1988).

The influence of discontinuity orientation on rock mass strength is evident in the slope failures along one or more discontinuities (Johnson and DeGraff, 1988). Hazardous mass-wasting processes may occur as a result of discontinuity or intersection of discontinuities providing a glide plane for the rock mass to move. Spacing of discontinuities also affects the overall rocks mass strength (Johnson and DeGraff, 1988).

Close spacing and extent of discontinuities reduce total strength of the rock mass (Johnson and DeGraff, 1988). The spacing and orientation of discontinuities may also cause wedge failures. Surface characteristics of discontinuities involve three factors: (1) waviness or undulation of the surface, which results in variations in orientation or attitude along a given discontinuity; (2) asperities on the surface of the discontinuity; and (3) physical properties of the material that may fill the space between two bounding surfaces of a discontinuity (Johnson and DeGraff, 1988; Pollard and Aydin, 1988). All these factors contribute to the strength of the rock mass. Where slope stability is involved, the undulatory nature of the surface has a greater influence on a rock mass strength than the asperities on a discontinuity, because asperities are sheared off by movement, resulting in a smoother surface (Johnson and DeGraff, 1988). The amount of separation between joint surfaces and the presence of filling material also have a profound influence on the strength of a jointed rock mass (Johnson and DeGraff, 1988).

The influence of these mechanical discontinuities, combined with topography, vegetation, and climate, is important when considering landslide potential (Varnes, 1984). Landslides are classified as either falls, topples, slides, lateral spreads, or flows (Varnes, 1978). Falls, slides, and flows are the most common landslides. Landslides tilt, shear, and pull apart rock and soil, resulting in destruction of man-made structures, economic losses, and sometimes human casualties. Landslides are caused either by the decreased ability of a slope to resist gravitational forces, an increased effectiveness of gravity acting on a slope, or a combination of these two factors (Varnes, 1958). These causes are important factors in determining slope stability, which represents the balance between driving forces (shear stress) and resisting forces (shear strength). This relationship is expressed as a ratio where slope stability equals shear strength divided by shear stress. Ratios greater than 1 denote slope stability. Ratios of 1 or less theoretically exceed geomorphic thresholds, and slope failures occur (Ritter and others, 1995). Factors that increase shear stress include: removal of lateral support, addition of mass, earthquakes, regional tilting, removal of underlying support, and lateral pressure. Factors that decrease shear stress include weathering, pore water, and structural features (discontinuities) (Varnes, 1958).

Lithologic discontinuities

In this environmental site assessment, lithologic discontinuities include bedding planes and lithologic contacts. Bedding in Wilhite metasiltstone is recognizable and generally does not form a mechanical discontinuity, even in weathered rock. Bedding in Dean Formation graywacke and slate is coherent where fresh, but where weathered, forms mechanical discontinuities. Lithologic contacts between different rock types also form mechanical discontinuities. These discontinuity may influence the shear strength of the rock mass to a greater extent than some bedding planes, because of the different physical properties associated with the different rock types.

Bedding

Bedding orientations are consistent in the assessment area and dip gently to steeply southeast and northwest with a great circle orientation of 134 87° S and corresponding β of 44 03° (Fig. IV-2A; also see Fig. III-9). In the fine-grained lithologies of the Wilhite Formation, bedding is generally coherent and the likelihood of slope instability related to bedding is low. In the turbiditic Dean Formation, bedding in the coarse- and fine-grained lithologies more readily forms mechanical discontinuities (bedding-parallel fractures) than the more homogeneous fine-grained rocks of the Wilhite Formation. Additionally, in the coarse-grained units, beds are thick, possibly resulting in slope failures that involve blocks of substantial size. Since bedding dips generally to the southeast and the topographic slope dips northwest, landslides in this area are probably

Figure IV-2. Orientation of mesoscopic structures within the Sixmile Creek and Rocky Branch watersheds. (A) Lower-hemisphere equal-area projection of 87 poles to bedding. (B) Lower-hemisphere equal-area projection of 49 poles to slaty cleavage. (C) Lower-hemisphere equal-area projection of 130 poles to joints. Stereoplots include scatter and contoured at 2% per 1% area.

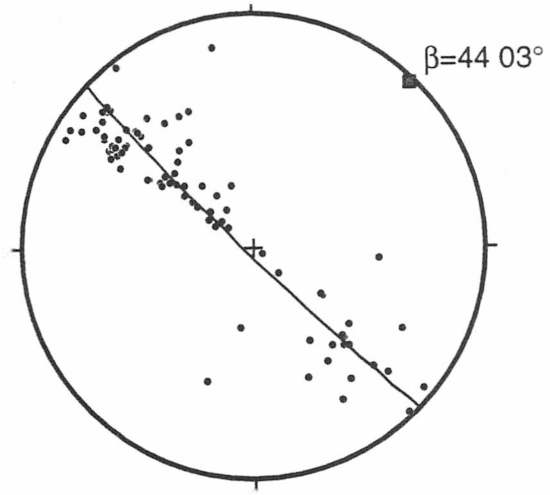

(A)

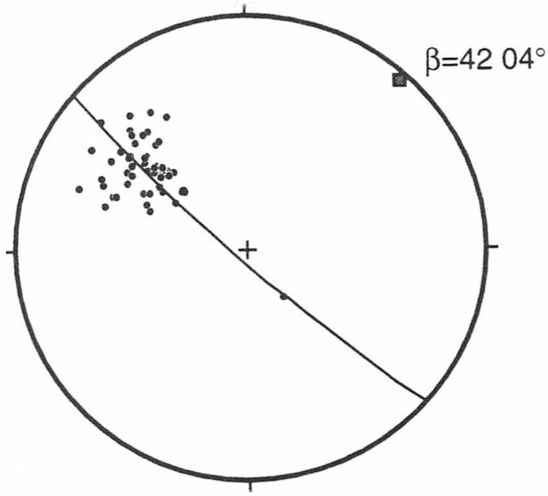

(B)

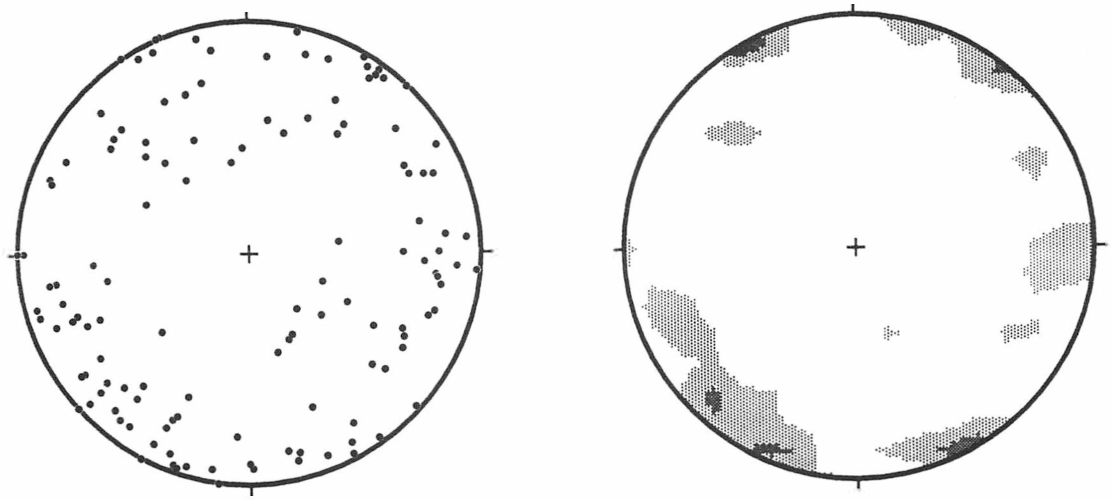

(C)

not directly related to bedding, but more commonly to slope-parallel joints. The intersection and combination of bedding and other discontinuities, such as a northwest-dipping joint set, probably influenced slope failure in the watersheds.

Contacts

Lithologic contacts in the watershed are oriented parallel to bedding and are not very coherent when weathered (Fig. IV-1; Plate I). The major lithologic contact in the area is the contact between the overlying Wilhite Formation metasiltstone and the underlying Dean Formation conglomerate and graywacke. Other lithologic contacts in this area are between the conglomerate and graywacke units, and the mappable slate lenses in the Dean Formation. Lithologic changes are frequent in the watersheds, and the different physical properties associated with each rock type vary across the contact. Weathering of these heterogeneous materials may potentially cause slope instability, especially in combination with slope steepness and heavy rainfall.

Tectonic discontinuities

Structural discontinuities observed in the watershed include cleavage, joints, and faults. The dominant discontinuity in the fine-grained lithologies is slaty cleavage (S_1). Joints are common in all lithologies, but are more prevalent in the fine-grained rocks. No major faults were observed in the assessment area.

Cleavage

Slaty cleavage (S_1) is a major discontinuity in the watershed, and is best developed in the fine-grained lithologies. This discontinuity is consistent in orientation with moderate dip to the southeast with a great circle orientation of 132 86° S and a corresponding β of 42 04° (Fig. IV-2B). Cleavage surfaces weather readily to form excellent release surfaces, and are involved in both planar and wedge instabilities.

Joints

Joints are common discontinuities in the watersheds in both the metasiltstone lithologies of the Wilhite Formation, and the Dean Formation granule- to pebble-size conglomerate and graywacke. Some of the joints are filled with quartz that welds the walls of fractures together making them very coherent. Gold-bearing quartz veins have been reported in the metasiltstone units, while similar quartz veins (Unaka veins) in the conglomerate and graywacke lack gold (Rove, 1929; Hale, 1974). The quartz veins in the coarse-grained Great Smoky Group lithologies along the northwest slope of the Unicoi Mountains are referred to as the Unaka veins, and were once thought to be gold-bearing (Ashley, 1911).

The most prominent set of joints and quartz veins strike northwest and dip steeply to the northeast and southwest (Fig. IV-2C; Appendix A). Less prominent joint sets and quartz veins are also recognized. One set strikes northeast (parallel to regional strike) and dips steeply to the southeast and northwest, while another set strikes almost east-west and dips steeply to the north and south (Fig. IV-2C; Appendix A). The orientation of joint sets varies, but are generally suborthogonal and subparallel to larger F_1 fold axes (compare Figs. IV-2C and III-6C). This suborthogonal and subparallel relationship between joints and veins and fold axes indicates the formation of these structures probably occurred coevally. Similar relationships between joints, veins, and axial surfaces were observed to the northeast of the study area by Geddes (1995). The intersection of the different joint and vein sets, combined with the orientation of bedding and cleavage, provide potential surfaces for possible wedge failures and landslides. Additionally, the steepness of topography increases slope instability along these discontinuities.

Faults

No major faults were observed in the assessment area. Small-scale faults and associated fractures may be revealed upon excavation, but should not cause slope stability problems. Small-scale faults within the assessment area have small displacements, and are generally characterized by poorly developed discontinuous fault planes.

Sulfidic zones

Varying sulfide mineral concentrations were observed throughout the assessment area (Appendix B). Generally, the greater concentration of visible pyrite is observed in the black slate lenses in the Dean Formation (Fig. IV-1; Plate I). Microscopic analysis of the coarser-grained graywackes reveals that they also contain pyrite, but the concentrations are less and the pyrite crystals are smaller. Disseminated sulfides are also more common in the fine-grained lithologies. This is important because the smaller disseminated crystals have more surface area and are more readily decomposed to produce acid runoff (Reed and others, 1995). Hale (1974) reported sulfide minerals in host rock and in the vein systems at the Sixmile Creek adit in the assessment area. Excavation and exposure of bedrock that contains as little as 0.5 percent sulfide mineral content, such as pyrite, have the potential to acidify surface water runoff and become hazardous to downstream environments (Byerly and Middleton, 1981; Winchester, 1981; Byerly, 1990; Reed and others, 1995). In order for the development of this area to have a low environmental impact during construction, the handling, treatment, and placement of the sulfidic material must be considered.

Geomorphology

This environmental assessment of the Sixmile Creek and Rocky Branch watersheds lies within the Foothill Belt (Chilhowee Mountain-Walden Creek district) and High

Western Blue Ridge (Unaka Mountains district) geomorphic subsection of the Western Blue Ridge section in southeastern Tennessee (Hack, 1982; Carter and others, 1996). Geomorphic subdivisions are identified and mapped based on similarities or differences in geologic structure, lithology, topography, and geologic history (Thornbury, 1965). Approximately 75 percent of the assessment area lies within the Unaka Mountains district and is underlain by the Dean Formation. The remaining portion of the assessment area lies within the Chilhowee Mountain-Walden Creek district and is underlain by the Wilhite Formation. These districts have similar geologic structure and history, but are differentiated from each other by lithology and the influence of the regional structure on topography.

The terrain within the Unaka Mountains district is rugged and very steep, while the terrain in the Walden Creek district is less rugged and not as steep. The assessment area has a relief of about 2,000 ft (650 m) with the lowest elevation of 1,560 ft (480 m) near the confluence of Sixmile Creek and Rocky Branch. The highest elevation is 3,692 ft (1,180 m) on Waucheesi Mountain (Plate V). Natural slopes in this region commonly approach 35 degrees with slope increasing to almost 60 degrees near the top of Waucheesi Mountain. Drainage patterns are dendritic and are interpreted to be partly controlled by the trends of joints, cleavage, and bedding.

Surficial deposits

Surficial deposits are important geomorphic features within the watershed that will directly affect residential development include surficial deposits. Surficial deposits include nontransported residual soils, and transported unconsolidated materials. Transported unconsolidated material include alluvium, colluvium, and landslide deposits. Residual soils are ubiquitous within the watersheds and vary in thickness. Mapping these soils was not included in this assessment. Alluvium, colluvium, and landslide deposits are unconsolidated transported material mapped in the assessment area (Fig. IV-3; Plate IV). Alluvial deposits are more prominent and thicker in the larger drainages in the northwestern portion of the watershed, but are common in smaller drainages throughout the watersheds. Generally, alluvial deposits consist of clay- to cobble-size materials. Colluvial deposits are mostly concentrated at the base of slopes, and consist of clay- to gravel-size material.

Landslide deposits and landslide potential are important features and processes that most characterize the geomorphology within the watersheds. Two large areas within the watersheds consist of transported material by previous landslides, and are located near the headwaters of the Sixmile Creek and Rock Branch drainages. Using the classification of Varnes (1978), the landslides here would be debris slides and debris flows. Debris slides are rapid mass movements initiating along one or more regular to irregular, discrete movement surfaces. They involve primarily soil, vegetation, water, entrapped air, and upper bedrock layers (Varnes, 1978). Debris flows are rapid mass movements with continuous internal deformation (Varnes, 1978). Debris slides and flows have been investigated throughout the southern Blue Ridge and were suggested to be triggered by heavy rains (Clark, 1987). Clark (1987) stated that these slides and flows occur in existing hillslope depressions and move downslope with the common movement interface along the bedrock-soil contact. The slide surface is locally identifiable in the upper portions of the valley here as a northwest-dipping joint surface. Slippage and flowage are also common in deep soils. Neary and Swift (1987) presented evidence for rainfall thresholds of more than 125 mm over 3 days triggering landslides in the southern Appalachians. Neary and Swift (1987) also concluded that heavy rainfall, saturated soils, steep slopes, and shallow soils were major factors influencing debris avalanches in western North Carolina. The dangers and consequences of rapid debris slides and flows within the watersheds would create serious hazards to residential development of this area. The

Figure IV-3. Geologic map of the Sixmile Creek and Rocky Branch watersheds. Boundaries of the watersheds and assessment area are indicated by heavy black line. Quaternary deposits are shaded. Contour interval equals 200 feet. See Fig. II-2 and Plate I for stratigraphic explanation.

Geologic abbreviations: Qac-alluvium and colluvium undifferentiated; Qal-alluvium; Qc-colluvium; Zws-Wilhite Formation metasiltstone; Zdg-Dean Formation graywacke and conglomerate; Zds-Dean Formation slate.

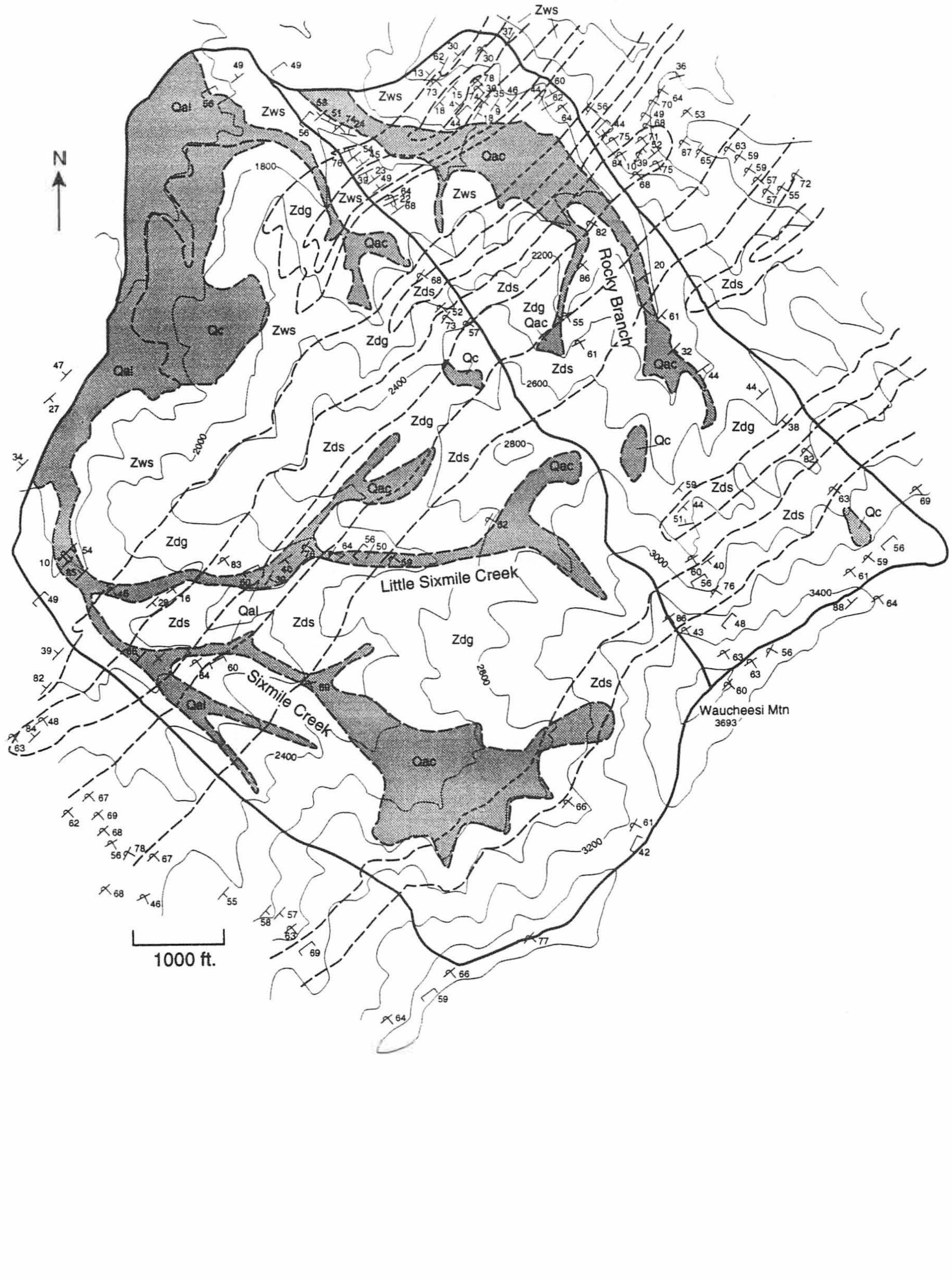
N
1000 ft.
Zws
Zds
Zdg
Qal
Qac
Qc
Rocky Branch
Little Sixmile Creek
Sixmile Creek
Waucheesi Mtn
3693
1800
2000
2200
2400
2600
2800
3000
3200
3400

possible cause of landsliding within the watersheds is multivariant; steep slopes, combined with orientation of discontinuities, shallow soils, and heavy rainfall events are important factors that influence landsliding in this area.

Conclusions and recommendations

Mechanical discontinuities present in bedrock within the Sixmile Creek and Rocky Branch watersheds include joints, cleavage, bedding, lithologic contacts, and small-scale faults. The intersection of the most prominent discontinuities (joints, cleavage, and bedding) provide potential surfaces for wedge failures and landslides. These mechanical discontinuities decrease the shear strength of the rock mass, which directly affects slope stability. Other factors influencing slope stability include topography, vegetation, and extremely high precipitation events. Evidence for at least two mass movement events are located within the watersheds. Potential for future landslides exist in the same areas as the previous landslides. Steep slopes near the headwaters of Sixmile Creek and Rocky Branch drainages probably represent the areas that may be susceptible to future landslides. The landslides within the watersheds are classified as debris slides and debris flows. Previous investigations in the southern Appalachians suggest that landslides are triggered by constant high rainfall events (Clark, 1987; Neary and Swift, 1987).

From a geological perspective, residential development within the watersheds should be restricted to the lower elevations, but not in hollows or on debris fans. These areas should be underlain by the relatively homogenous Wilhite metasiltstone. Residences should be constructed on the spurs of ridges, and not in hollows or sides of ridges. Additionally, water and sewer lines should not be located in alluvial or landslide debris. During heavy rainfall events, flash floods are common, and landslide potential increases. Inevitably, any roads constructed in these watersheds will be damaged due to flooding and/or mass movement of unconsolidated materials. Therefore, repeated repairs of these roads becomes a long-term economic issue. Residential development within the watersheds will also inevitably negatively impact the water quality due to possible acidic drainage and sedimentation.

Chapter V
Conclusions

1) Sedimentary and metasedimentary rocks exposed in the study area belong to the Great Smoky and Walden Creek Groups of the Upper Proterozoic Ocoee Supergroup in southeastern Tennessee. Great Smoky Group lithologies are correlated with the Horse Branch Member (oldest) of the Ammons Formation and the Dean Formation, whereas the overlying Walden Creek Group lithologies are correlated with the Wilhite Formation and the Sandsuck Formation (youngest). In addition to these units, unmetamorphosed Paleozoic rocks of the Valley and Ridge are exposed beneath the western Blue Ridge thrust sheet in the study area.

2) The contact between the predominantly coarser-grained Great Smoky Group (Dean Formation) and the predominantly finer-grained Walden Creek Group (Wilhite Formation) is conformable. This contact had been interpreted to be the southern continuation of the Greenbrier fault south of the Great Smoky Mountains National Park. Great Smoky Group lithologies consist of granule- to pebble-conglomerate, graywacke, sandstone, and slate, whereas Walden Creek Group lithologies consist of metasiltstone, sandstone, and carbonate.

3) Six major brittle thrust faults, four generations of folds, and four S-surfaces deform the rocks in the study area. The faults include the Bullet Mountain, Great Smoky, Maggies Mill, Miller Cove, Rabbit Creek, and Oconaluftee faults, and divide the area into four thrust sheets. The Bullet Mountain fault represents the floor thrust of a duplex containing Paleozoic rocks beneath the western Blue Ridge thrust sheet. The Great Smoky fault is the roof thrust that transported metamorphosed western Blue Ridge rocks

onto unmetamorphosed rocks of the Valley and Ridge, and emplaced Hesse Quartzite (Chilhowee Group) on Groundhog Mountain. The Miller Cove fault thrust chlorite-grade, cleaved rocks of the Wilhite Formation onto lower-grade, less-cleaved rocks of the Sandsuck Formation. The Rabbit Creek fault is a reactivated syn- to premetamorphic fault that thrust Great Smoky Group rocks onto Walden Creek Group rocks. The Oconaluftee fault also is a reactivated syn- to premetamorphic fault that juxtaposes rocks of the Dean Formation. The Maggies Mill and Oconaluftee faults are major structures in the Great Smoky and Miller Cove thrust sheets, respectively, and may be out-of-sequence.

4) Rocks in the Miller Cove and Rabbit Creek thrust sheets are deformed by axial-planar F1 folds, chevron-like (kink) F_2 folds, slaty cleavage (S_1), pressure-solution cleavage (S_{1a}), and a crenulation cleavage (S_2). Axial-planar F_1 folds along with slaty cleavage (S_1) and pressure-solution cleavage (S_{1a}) developed as a result of the metamorphic event during the Taconic orogeny, while chevron-like (kink) F_2 folds and crenulation cleavage (S_2) developed as a result of faulting during the Alleghanian orogeny. Rocks in the Great Smoky thrust sheet were deformed by F_3 folds and by slaty cleavage (S_3), which formed during the Alleghanian orogeny. Alternatively, F_3 folds and S_3 (slaty) cleavage may have formed during the Taconian orogeny because of similarity in orientation with F_1 folds and S_1 (slaty) cleavage in the Miller Cove thrust sheet. The F_4 folding event represents gentle folding of the Blue Ridge thrust sheet due to duplexing of Valley and Ridge footwall units.

5) Cross-section construction and line- and area-balanced retrodeformation reveals the following sequence of deformational events for the western Blue Ridge Foothills in southeastern Tennessee: (1) emplacement of the Blue Ridge thrust sheet; (2) formation of

the Foothills dupex; (3) formation of the unnamed duplex; (4) emplacement of the blind thrust; (5) continued displacement along the Great Smoky fault due to duplexing, which resulted in the decapitation of the hanging-wall anticline related to the blind thrust; and (6) emplacement of the Chestuee and Saltville faults, respectively.

6) Strain analysis (R_f/ϕ and normalized Fry methods) suggests that rocks of the western Blue Ridge in the study area were deformed by at least one strain event during the Taconic orogeny. Strain values throughout the study area are relatively low, increasing toward the southeast in the direction of increasing deformation and metamorphic grade, and near late Paleozoic brittle faults.

7) Application of geologic data to an environmental assessment for a hypothetical residential development suggest that slope instabilities exist within the Sixmile Creek and Rocky Branch watersheds. Evidence for slope instabilities includes the recognition of previous landslides, combined with mechanical discontinuity characteristics, topography, vegetation, and climate. Previous landslides are classified as debris slides and debris flows. Development within these watersheds should be concentrated on ridge spurs in the relatively homogenous Wilhite Formation metasiltstones.

References cited

References cited

Ashley, G. H., 1911, The gold fields of Coker Creek, Monroe County, Tennessee: Tennessee Geological Survey, Resources of Tennessee, v. 1, p. 78-107.

Ausburn, M. P., 1983, Stratigraphy, structure, and petrology of the northern half of the Topton quadrangle, North Carolina [M. S. thesis]: Tallahassee, Florida State University, 174 p.

Bieniawski, Z. T., 1973, Engineering classification of jointed rock masses: Transactions South African Institute of Civil Engineering, v. 15, p. 335-343.

Broadhead, T. W., Hatcher, R. D., Jr., and Costello, J. O., 1991, Tectonic and stratigraphic implications of mid-Paleozoic (?) fossils from the Late Proterozoic (?) Walden Creek Group rocks in the Foothills belt, eastern Tennessee, *in* Kish, S. A., ed., Studies of Precambrian and Paleozoic stratigraphy in the western Blue Ridge: Carolina Geological Society Guidebook, p. 39-44.

Butler, J. R., 1972, Age of regional metamorphism in the Carolinas, Georgia and Tennessee southern Appalachians: American Journal of Science, v. 272, p. 319-333.

Byerly, D. W., 1990, Guidelines for handling excavated acid-producing materials: Federal Highway Administration Special Document D. O. T. FHWA–DF-89-0011, 81 p.

Byerly, D. W., and Middleton, W. M., 1981, Evaluation of the acidic drainage potential of certain Precambrian rocks in the Blue Ridge province: Proceedings of the 32nd Annual Highway Geology Symposium, p. 174-185.

Campbell, M. R., 1899, Description of the Bristol quadrangle (Virginia-Tennessee): U. S. Geological Survey Geologic Atlas, Folio 59, 6 p.

Carter, M. W., 1994, Stratigraphy and structure of a portion of the western Blue Ridge foothills, Polk and Monroe counties, southeast Tennessee [M. S. thesis]: Knoxville, University of Tennessee, 233 p.

Carter, M. W., Martin, S. L., Geddes, D. J., Hatcher, R. D., Jr., Lombardi, C. E., and Costello, J. O., 1993a, Western Blue Ridge tectonics of southeastern Tennessee, northern Georgia, and southwestern North Carolina-Preliminary results, Part I: Structure: Geological Society of America Abstracts with Programs, v. 25, p. A-484.

Carter, M. W., Martin, S. L., Geddes, D. J., Broadhead, T. W., Hatcher, R. D., Jr., and Costello, J. O., 1993b, Western Blue Ridge tectonics of southeastern Tennessee, northern Georgia, and southwestern North Carolina-Preliminary results, Part II: Stratigraphy: Geological Society of America Abstracts with Programs, v. 25, p. A-484.

Carter, M. W., Geddes, D. J., Hatcher, R. D., Jr., and Martin, S. L., 1995a, Stratigraphic and structural relationships in the western Blue Ridge of southeastern Tennessee, *in* Driese, S. G., ed., Guidebook for field trip excursions, Southeast Section, Geological Society of America: University of Tennessee Department of Geological Sciences, Studies in Geology 24, p. 91-128.

Carter, M. W., Geddes, D. J., Hatcher, R. D. Jr., and Martin, S. L., 1995b, Stratigraphic and structural relationships of the Walden Creek group (Ocoee Supergroup), western Blue Ridge foothills, Tennessee and North Carolina: Southeast Section, Geological Society of America Abstracts with Programs, v. 27, no. 2, p. 42.

Carter, M. W., Hatcher, R. D., Jr., Geddes, D. J., Martin, S. L., and Montes, C., 1995c, New lithotectonic framework in the western Blue Ridge, southern Appalachians: Building on earlier USGS work: Geological Society of America Abstracts with Programs, v. 27, p. A-223.

Carter, M. W., Clark, G. M., and Lietzke, D. A., 1996, Bedrock geology, Quaternary geology, geomorphology, and pedology of part of the Western Blue Ridge geomorphic section, southern Blue Ridge subprovince, between Gatlinburg, Tennessee, and Hot Springs, North Carolina, *in* Foss, J. E., Clark, G. M., Lee, S. Y., and Leitzke, D. A., eds., Clays in and for the environment--Clay Mineral Society 1996, Great Smoky Mountains, Tennessee: The Clay Minerals Society field trip guidebook, Special Publication 96-02, v. 38, p. 1-25.

Clark, G. M., 1987, Debris slide and debris flow historical events in the Appalachians south of the glacial border: Geological Society of America Reviews in Engineering Geology, v. 7, p. 125-138.

Connelly, J. B., 1993, Structural development, strain history, and timing of deformation in the eastern Great Smoky Mountains [Ph. D. dissertation]: Knoxville, University of Tennessee, 178 p.

Connelly, J. B., and Dallmeyer, R. D., 1990, Ordovician (?) or Silurian (?) metamorphism in the western Blue Ridge, Tennessee: Evidence form $^{40}Ar/^{39}Ar$ whole-rock phyllite ages: Geological Society of America Abstracts with Programs, v. 22, p. 231.

Connelly, J. B., and Dallmeyer, R. D., 1991, Polymetamorphic evolution of the western Blue Ridge, Tennessee and North Carolina; Evidence from $^{40}Ar/^{39}Ar$ ages: Geological Society of America Abstracts with Programs, v. 23, p. 18.

Connelly, J. B., and Woodward, N. B., 1992, Taconian foreland-style thrust system in the Great Smoky Mountains, Tennessee: Geology, v. 20, p. 177-180.

Cook, F. A., Brown, L. D., Kaufman, S., and Oliver, J. E., 1983, The COCORP seismic reflection traverse across the southern Appalachians: American Association of Petroleum Geologists Studies in Geology no. 14, 61 p.

Cording, E. J., Hendron, A. J., Jr., MacPherson, H. H., Hansmire, W. H., Jones, R. A., Mahar, J. W., and O'Rouke, T. D., 1975, Methods for geotechnical observations and instrumentation in tunneling: Department of Civil Engineering, University of Illinois at Urbana-Champaign, Report number UILU-ENG 75 2022, v. 1 and 2, 566 p.

Costello, J. O., 1978, Shear zones in the Corbin gneiss of Georgia, *in* Short contributions to the geology of Georgia: Georgia Geological Survey Bulletin 93, p. 32-37.

Costello, J. O., 1984, Relationships between the Cartersville fault and Great Smoky fault in the southern Appalachians: A reinterpretation [M. S. thesis]: Columbia, University of South Carolina, 75 p.

Costello, J. O., 1986, Corbin gneiss complex: Southernmost exposures of Grenville basement in the Appalachian Blue Ridge: Geological Society of America Centennial Field Guide, Southeastern Section, p. 277-280.

Costello, J. O., 1993, Studies in Appalachian foreland-to-hinterland transition zone geology, Georgia and Tennessee [Ph.D. dissertation]: Columbia, University of South Carolina, 144 p.

Costello, J. O., and Hatcher, R. D., Jr., 1986, Contact relationships between the Walden Creek Group and Great Smoky Group in Ocoee Gorge, Tennessee: Implications for the regional extent of the Greenbrier fault: Geological Society of America Abstracts with Programs, v. 18, p. 216.

Costello, J. O., and Hatcher, R. D., Jr., 1991, Problems of stratigraphic correlation between Great Smoky, Snowbird, and Walden Creek Groups between the Great Smoky National Park, central east Tennessee, and Ocoee Gorge, southeastern Tennessee, *in* Kish, S. A., ed., Studies of Precambrian and Paleozoic stratigraphy in the western Blue Ridge: Carolina Geological Society Guidebook, p. 13-25.

Couzens, B. A., Dunne, W. M., Onasch, C. M., and Glass, R., 1993, Strain variations and three-dimensional strain factorization at the transition from the southern to the central Appalachians: Journal of Structural Geology, v. 15, p.451-464.

Dallmeyer, R. D., 1975, Incremental $^{40}Ar/^{39}Ar$ ages of biotite and hornblende from retrograde basement gneisses of the southern Blue Ridge: Their bearing on the age of Paleozoic metamorphism: American Journal of Science, v. 275, p. 444-460.

DeWindt, J. T., 1975, Geology of the Great Smoky Mountains, Tennessee and North Carolina, with road log for field excursion, Knoxville-Clingmans Dome-Maryville: Compass, v. 52, p. 73-129.

Donath, F. A., and Parker, R. B., 1964, Folds and folding: Geological Society of America Bulletin, v. 75, p. 45-62.

Dunnet, D., 1969, A technique of finite strain analysis using elliptical particles: Tectonophysics, v. 2, p. 117-136.

Dunnet, D., and Siddans, A. W. B., 1971, Non-random sedimentary fabrics and their modification by strain: Tectonophysics, v. 12, p. 307-325.

Erslev, E. A., 1988, Normalized center-to-center strain analysis of packed aggregates: Journal of Structural Geology, v. 10, p. 201-209.

Fairly, W. M., 1965, The Murphy syncline in the Tate quadrangle, Georgia: Georgia Geological Survey Bulletin 75, 71 p.

Flinn, D., 1962, On folding during three-dimensional progressive deformation: Geological Society of London Quarterly Journal, v. 118, p. 385-433.

Fry, N., 1979, Random point distributions and strain measurements in rocks: Tectonophysics, v. 60, p. 89-105.

Geddes, D. J., 1995, Stratigraphy, structure, and environmental site assessment of a portion of the western Blue Ridge, Monroe County, Tennessee [M. S. thesis]: Knoxville, University of Tennessee, 195 p.

Groshong, R. H., Jr., 1988, Low-temperature deformation mechanisms and their interpretation: Geological Society of America Bulletin, v. 100, p. 1329-1360.

Hack, J. T., 1982, Physiographic divisions and differential uplift in the Piedmont and Blue Ridge: U. S. Geological Survey Professional Paper 1265, 49 p.

Hadley, J. B., 1970, The Ocoee Series and its possible correlatives, *in* Fisher, G. W., Pettijohn, F. J., Reed, J. C., and Weaver, K. N., eds., Studies in Appalachian geology: Central and southern: New York, Wiley Interscience, p. 247-260.

Hadley, J. B., and Goldsmith, R., 1963, Geology of the eastern Great Smoky Mountains, North Carolina and Tennessee: U. S. Geological Survey Professional Paper 349-B, 118 p.

Hadley, J. B., and Nelson, W. H., 1971, Geologic map of the Knoxville quadrangle, North Carolina, Tennessee, and South Carolina: U. S. Geological Survey Miscellaneous Investigations Map I-654, scale 1:250,000.

Hale, R. C., 1974, Gold deposits of the Coker Creek district, Monroe County, Tennessee: Tennessee Division of Geology Bulletin 72, 93 p.

Hamilton, W. B., 1961, Geology of the Richardson Cove and Jones Cove quadrangles, Tennessee: U. S. Geological Survey Professional Paper 349-A, 55 p.

Hardeman, W. D., 1966, Geologic map of Tennessee: Tennessee Division of Geology, scale 1:250,000.

Hatcher, R. D., Jr., 1972, Developmental model for the southern Appalachians: Geological Society of America Bulletin, v. 83, p. 2735-2760.

Hatcher, R. D., Jr., 1978, Tectonics of the western Piedmont and Blue Ridge, southern Appalachians: Review and speculation: American Journal of Science, v. 278, p. 276-304.

Hatcher, R. D., Jr., 1989, Tectonic synthesis of the U. S. Appalachians, Chapter 14, *in* Hatcher, R. D., Jr., Thomas, W. A., and Viele, G. W., eds., The Appalachian - Ouachita Orogen in the United States: Boulder, Geological Society of America, The Geology of North America, v. F-2, p. 7-100.

Hatcher, R. D., Jr., Thomas, W. A., Geiser, P. A., Snoke, A. W., Mosher, S., and Wiltschko, D. V., 1989a, Alleghanian orogen, Chapter 5, *in* Hatcher, R. D., Jr., Thomas, W. A., and Viele, G. W., eds., The Appalachian-Ouachita orogen in the United States: Boulder, Geological Society of America, The Geology of North America, v. F-2, p. 233-318.

Hatcher, R. D., Jr., Larson, K. W., and Neuman, R. B., 1989b, Western Great Smoky Mountains windows: The foothills duplex, *in* Hatcher, R. D., Jr., and Thomas, W. A., eds., Southern Appalachian windows: Comparison of styles, scales, geometry, and detachment levels of thrust faults in the foreland and internides of a thrust-dominated orogen: 27th International Geological Congress Field Trip Guidebook T167, p. 49-60.

Hatcher, R. D., Jr., and Goldberg, S. A., 1991, The Blue Ridge province, *in* Horton, J. W., Jr., and Zullo, V. A., eds., The Geology of the Carolinas - Carolina Geological Society 50th Anniversary Volume: Knoxville, The University of Tennessee, p. 11-35.

Hatcher, R. D., Jr., Costello, J. O., and Broadhead, T. W., 1991, Carbonate in Walden Creek Group-Sandsuck Formation, *in* Kish, S. A., ed., Studies of Precambrian and Paleozoic stratigraphy in the western Blue Ridge: Carolina Geological Society Guidebook, p. 79-86.

Hayes, C. W., 1891, The overthrust faults of the southern Appalachians: Geological Society of America Bulletin, v. 2, p. 141-154.

Hayes, C. W., 1895, Description of the Cleveland sheet (Tennessee): U. S. Geological Survey Geologic atlas, Folio 20, 12 p.

Hayes, C. W., 1900, Geological relations of the iron-ores in the Cartersville District, Georgia: American Institute of Mining Engineers Transactions, v. 30, p. 403-419.

Hernon, R. M., 1968, Geology of the Ducktown, Isabella, and Persimmon Creek quadrangles, Tennessee and North Carolina: U. S. Geological Survey Open-File Report, 71 p.

Hopson, J. L., Hatcher, R. D., Jr., and Stieve, A. L., 1989, Geology of the eastern Blue Ridge, northeastern Georgia and the adjacent Carolinas, *in* Fritz, W. J., Hatcher. R. D., Jr., and Hopson, J. L., eds., Geology of the eastern Blue Ridge of northeastern Georgia and the adjacent Carolinas: Georgia Geological Society Guidebook, v. 9, p. 1-40.

Hurst, V. J., 1955, Stratigraphy, structure, and mineral resources of the Mineral Bluff quadrangle, Georgia: Georgia Geological Survey Bulletin 63, 137 p.

Hurst, V. J., and Schlee, J. S., 1962, Ocoee metasediments, north-central Georgia, southeast Tennessee: Southeastern Section, Geological Society of America Guidebook 3, Georgia Department of Mines, Mining, and Geology, 28 p.

Johnson, R. B., and DeGraff, J. V., 1988, Principles of engineering geology: New York, Wiley, 497 p.

Keith, A., 1895, Description of the Knoxville sheet (Tennessee-North Carolina): U. S. Geological Survey Geologic Atlas, Folio 16, 6 p.

Keith, A., 1903, Description of the Cranberry quadrangle (North Carolina-Tennessee): U. S. Geological Survey Geologic Atlas, Folio 90, 9 p.

Keith, A., 1904, Description of the Asheville quadrangle (Tennessee-North Carolina): U. S. Geological Survey Geologic Atlas, Folio 116, 10 p.

Keith, A., 1907a, Description of the Nantahala quadrangle (North Carolina-Tennessee): U. S. Geological Survey Geologic Atlas, Folio 143, 11 p.

Keith, A., 1907b, Description of the Roan Mountain quadrangle (Tennessee-North Carolina): U. S. Geological Survey Geologic Atlas, Folio 151, 12 p.

Keller, F. B., 1980, Late Precambrian stratigraphy, depositional history, and structural chronology of part of the Tennessee Blue Ridge [Ph. D. dissertation]: New Haven, Yale University, 353 p.

King, P. B., 1949, The base of the Cambrian in the southern Appalachians: American Journal of Science, v. 247, p. 513-530, 622-645.

King, P. B., 1964, Geology of the central Great Smoky Mountains, Tennessee: U. S. Geological Survey Professional Paper 349-C, 148 p.

King, P. B., Furguson, H. W., Craig, L. C., and Rodgers, J., 1944, Geology and manganese deposits of northeastern Tennessee: Tennessee Division of Geology Bulletin 52.

King, P. B., Hadley, J. B., Neuman, R. B., and Hamilton, W. B., 1958, Stratigraphy of the Ocoee Series, Great Smoky Mountains, Tennessee, and North Carolina: Geological Society of America Bulletin, v. 69, p. 947-966.

King, P. B., and Furguson, H. W., 1960, Geology of northeasternmost Tennessee: U. S. Geological Survey Professional Paper 311, 136 p.

Kish, S. A., 1989, Igneous and metamorphic history of the eastern Blue Ridge, southwestern North Carolina: K-Ar and Rb-Sr studies, *in* Fritz, W. J., Hatcher, R. D., Jr., and Hopson, J. L., eds., Geology of the eastern Blue Ridge of northeast Georgia and the adjacent Carolinas: Georgia Geological Society Guidebook, v. 9, p. 41-55.

Kish, S. A., 1991, Potassium-argon dating in the western Blue Ridge of North Carolina and Tennessee, *in* Kish, S. A., ed., Studies of Precambrian and Paleozoic stratigraphy in the western Blue Ridge: Carolina Geological Society Guidebook. p. 69-77.

Kligfield, R., Crespi, J., Naruk, S., and Davis, G. H., 1984, Displacement and strain patterns of extensional orogens: Tectonics, v. 3, p. 577-609.

Knipe, R. J., 1989, Deformation mechanisms-recognition from natural tectonites: Journal of Structural Geology, v. 11, p. 127-146.

Knoll, A. H., and Keller, F. B., 1979, Late Precambrian microfossils from the Walden Creek Group, Ocoee Supergroup, Tennessee: Geological Society of America Abstracts with Programs, v. 11, p. 185.

Laajoki, K., 1993, Revision of the lithostratigraphy of the Walden Creek Group in southeastern Tennessee and its implications to the basin models of the Ocoee Supergroup: Southeastern Section, Geological Society of America Abstracts with Programs, v. 5, p. 28.

Laurence, R. A., and Palmer, A. R., 1963, Age of Murray Shale and Hesse Quartzite on Chilhowee Mountain, Blount County, Tennessee: U. S. Geological Survey Professional Paper 475-C, p. C53-C54.

Lewis, J. C., 1988, Structural geology and finite strain analysis of the Precambrian Thunderhead Sandstone along the Greenbrier fault and Roundtop klippe [M. S. thesis]: Knoxville, University of Tennessee, 186 p.

Lisle, R. J., 1977, Clastic grain shape and orientation in relation to cleavage from the Aberystwyth Grits, Wales: Tectonophysics, v. 39, p. 381-395.

Lisle, R. J., 1985, Geological strain analysis: A manual for the R_f/ϕ method: New York, Pergamon Press, 99 p.

Lloyd, G. E., and Knipe, R. J., 1992, Deformation mechanisms accomodating faulting of quartzite under upper crustal conditions: Journal of Structural Geology, v. 14, p. 127-143.

McConnell, K. I., and Costello, J. O., 1980, Guide to geology along a traverse through the Blue Ridge and Piedmont provinces of north Georgia, *in* Frey, R. W., ed., Excursions in southeastern geology: American Geological Institute, v. 1, p. 241-258.

McConnell, K. I., and Costello, J. O., 1982, Relationship between Talladega belt rocks and Ocoee Supergroup rocks near Cartersville, Georgia, *in* Bearce, D. N., Black, W. W., Kish, S. A., and Tull, J. F., eds., Tectonic studies in the Talladega and Carolina slate belts, southern Appalachian orogen: Geological Society of America Special Paper 191, p. 19-30.

McConnell, K. I., and Costello, J. O., 1984, Basement-cover rock relationships along the western edge of the Blue Ridge thrust sheet in Georgia: Geological Society of America Special Paper 194, p. 263-280.

McKinney, T. F., 1964, Geology along the Great Smoky fault, Groundhog Mountain area, Tellico Plains, Tennessee [M. S. thesis]: Knoxville, University of Tennessee, 49 p.

Merschat, C. E., and Hale, R. C., 1983, Geologic map and mineral resources summary of the Farner quadrangle, Tennessee and North Carolina: North Carolina Geological Survey Geologic Map GM 133-NE, scale 1:24,000.

Merschat, C. E., and Wiener, L. S., 1973, Provisional geologic map of the Ocoee Supergroup, southwestern North Carolina and southeastern Tennessee: Geological Society of America Abstracts with Programs, v. 5, p. 420.

Michél-Levy, A., 1877, De lemploi du microscope polarisant a lumière parallèle: Annuel Mines, v. 12, p. 392-471.

Milton, D. J., 1983, Garnet-biotite geothermometry confirms the premetamorphic age of the Greenbrier fault, Great Smoky Mountains, North Carolina: Geological Society of America Abstracts with Programs, v. 15, p. 90.

Mitra, G., and Elliott, D., 1980, Deformation of the basement in the Blue Ridge and the development of the South Mountain cleavage, *in* Wones, D. R., ed., Proceedings, the Caledonides in the USA: Virginia Tech Department of Geological Sciences, Memoir 2, p. 307-311.

Mohr, D. W., 1975, Stratigraphy and structure of part of the Great Smoky and Murphy belt groups, western North Carolina: American Journal of Science, v. 273-A, p. 41-71.

Neary, D. G., and Swift, L. W., Jr., 1987, Rainfall thresholds for triggering a debris avalanching event in the southern Appalachian Mountains: Geological Society of America Reviews in Engineering Geology, v. 7, p. 81-92.

Neuman, R. B., 1951, The Great Smoky fault: American Journal of Science, v. 249, p. 740-754.

Neuman, R. B., and Nelson, W. H., 1965, Geology of the western part of the GreatSmoky Mountains, Tennessee: U. S. Geological Survey Professional Paper 349-D, 81 p.

Odom, A. L., Kish, S. A., and Leggo, P. J., 1973, Extension of "Grenville basement" to the southern extremity of the Appalachians: U-Pb ages of zircons: Geological Society of America Abstracts with Programs, v. 5, p. 425.

Onasch, C. M., and Dunne, W. M., 1993, Variation in quartz arenite deformation mechanisms between a roof sequence and duplexes: Journal of Structural Geology, v. 15, p. 465-475.

Owens, W. H., 1984, The calculation of a best-fit ellipsoid from elliptical sections on arbitrarily oriented planes: Journal of Structural Geology, v. 6, p. 571-578.

Peach, C. L., and Lisle, R. J., 1979, A Fortran IV program for the analysis of tectonic strain using deformed elliptical markers: Computers and Geosciences, v. 5, p. 325-334.

Pettijohn, F. J., 1949, Sedimentary rocks, 1st ed., New York, Harper, 526 p.

Phillips, H. E., 1952, The geology of the Starr Mountain area, southeast Tennessee [M. S. thesis]: Knoxville, University of Tennessee, 61 p.

Pollard, D. D., and Aydin, A., 1988, Progress in understanding jointing over the past century: Geological Society of America Bulletin, v. 100, p. 1181-1204.

Poppelreiter, B. S., 1980, A structural analysis of metasedimentary rocks of the Ocoee Supergroup above the Great Smoky overthrust in southeast Tennessee [M. S. thesis]: Knoxville, University of Tennessee, 115 p.

Powell, C. McA., 1979, A morphological classification of rock cleavage: Tectonophysics, v. 58, p. 21-34.

Rackley, R. I., 1951, Geology of the Bean Mountain area [M. S. thesis]: Knoxville, University of Tennessee, 76 p.

Ramsay, J. G., 1967, Folding and fracturing of rocks: New York, McGraw-Hill, 568 p.

Ramsay, J. G., and Huber, M. I., 1983, The techniques of modern structural geology, volume 1: Strain analysis: London, Academic Press, 307 p.

Rankin, D. W., 1975, The continental margin of eastern North America in the southern

Appalachians: The opening and closing of the Proto-Atlantic ocean: American Journal of Science, v. 275-A, p. 298-336.

Rankin, D. W., Drake, A. A., Jr., Glover, L., III, Goldsmith, R., Hall, L. M., Murray, D. P., Ratcliff, N. M., Read, J. F., Secor, D. T., and Stanley, R. S., 1989, Pre-orogenic terranes *in* Hatcher, R. D., Jr., Thomas, W. A., and Viele, G. W., eds., The Appalachian-Ouachita orogen in the United States: Boulder, Geological Society of America, The Geology of North America, v. F-2, p. 7-100.

Rast, N., and Kohles, K. M., 1986, The origin of the Ocoee Supergroup: American Journal of Science, v. 286, p. 593-616.

Reed, B. C., McConnell, W. T., and Mullen, D. M., 1995, Potential for slope instability and acidic runoff along a section of the U. S. 19 corridor; Cherokee, Graham, and Swain Counties, North Carolina: Proceedings of the 46th Annual Highway Geology Symposium, p. 14-24.

Ritter, D. F., Kochel, R. C., and Miller, J. R., 1995, Process geomorphology, 3rd ed., Dubuque, Brown, 546 p.

Rodgers, J., 1953, Geologic map of east Tennessee with explanatory text: Tennessee Division of Geology Bulletin 58, Part II, 168 p.

Rodgers, J., 1991, Evolution of ideas about the Ocoee conglomerates and slates, *in* Kish, S. A., ed., Studies of Precambrian and Paleozoic stratigraphy in the western Blue Ridge: Carolina Geological Society Guidebook, p. 1-12.

Rove, O. N., 1926, Reconnaissance of the gold deposits of eastern Tennessee; University of Wisconsin [unpub. M. S. thesis], 92 p.

Safford, J. M., 1856, A geological reconnaissance of the state of Tennessee: Nashville, 1st Biennial Report of the State Geologist, 164 p.

Safford, J. M., 1869, Geology of Tennessee: Nashville, Mercer, 550 p.

Salisbury, J. W., 1961, Geology and mineral resources of the northwest quarter of the Cohutta Mountain quadrangle: Georgia Geological Survey Bulletin 71, 61 p.

Stose, G. W., and Stose, A. J., 1949, Ocoee Series of the southern Appalachians: Geological Society of America Bulletin, v. 60, p. 267-320.

Sutton, T. C., 1971, Relationship between metamorphism and geologic structure along the Great Smoky fault system, Parksville quadrangle, Polk and Bradley Counties, Tennessee [Ph.D. dissertation]: Knoxville, University of Tennessee, 148 p.

Thompson, T. W., and Tull, J. F., 1991, Stratigraphy of the Mineral Bluff Group, southwestern North Carolina, *in* Kish, S. A., ed., Studies of Precambrian and Paleozoic stratigraphy in the western Blue Ridge: Carolina Geological Society Guidebook, p. 97-110.

Thornbury, W. D., 1965, Regional geomorphology of the United States: New York, Wiley, 609 p.

Tull, J. F., and Groszos, M. S., 1988, Murphy belt: Stratigraphic complexities and regional correlations, *in* Fritz, W. J., and LaTour, T. E., eds., Geology of the Murphy belt and related rocks, Georgia and North Carolina: Georgia Geological Society Guidebook, v. 8, no. 1, p. 35-74.

Tull, J. F., and Groszos, M. S., 1990, Nested Paleozoic "successor" basins in the southern Appalachian Blue Ridge: Geology, v. 18, p. 1046-1049.

Tull, J. F., Thompson, T. W., Groszos, M. S., Aylor, J. G., Jr., and Kish, S. A., 1991, Murphy belt stratigraphic nomenclature, *in* Kish, S. A., ed., Studies of Precambrian and Paleozoic stratigraphy in the western Blue Ridge: Carolina Geological Society Guidebook, p. 79-86.

Tull, J. F., Ausich, W. I., Groszos, M. S., and Thompson, T. W., 1993, Appalachian Blue Ridge cover sequence ranges at least into the Ordovician: Geology, v. 21, p. 215-218.

Unrug, R., and Unrug, S., 1990, Paleontological evidence of Paleozoic age for the Walden Creek Group, Ocoee Supergroup, Tennessee: Geology, v. 18, p. 1041-1045.

Unrug, R., Unrug, S., and Palmes, S. L., 1991, Carbonate rocks of the Walden Creek Group in the Little Tennessee River valley: Modes of occurrence, age, and significance for the basin evolution of the Ocoee Supergroup, *in* Kish, S. A., ed., Studies of Precambrian and Paleozoic stratigraphy in the western Blue Ridge: Carolina Geological Society Guidebook, p. 27-36.

Varnes, D. J., 1958, Landslide types and processes, *in* Eckel, E., ed., Landslides and engineering practice: Highway Research Board, Special Report 29, p. 20-47.

Varnes, D. J., 1978, Slope movement types and processes, *in* Schuster, R. L., and Krizek, R. J., eds., Landslides–Analysis and controls: National Research Council, Highway Research Board Special Report 176, p. 11-33.

Walcott, C. D., 1890, The fauna of the lower Cambrian or *Olenellus* zone: U. S. Geological Survey, 10th Annual Report, pt. 1, p. 509-760.

Walker, J. D., and Driese, S. G., 1991, Constraints on the position of the Precambrian-Cambrian boundary in the southern Appalachians: American Journal of Science, v. 291, p. 258-283.

Walters, R. R., 1988, Structural geometries, fabrics, and stratigraphic relationships in the Cades Cove region, Great Smoky Mountains National Park [M. S. thesis]: Knoxville, University of Tennessee, 155 p.

Walters, R. R., and Woodward, N. B., 1987, Structural relationships in the Cades Cove area, Great Smoky Mountains National Park, Tennessee: Geological Society of America Abstracts with Programs, v. 19, p. 880.

Wiener, L. S., unpub., Geologic map of the Citico-Tellico area, Monroe and Blount Counties, Tennessee: unpublished Ph. D. dissertation map, scale 1:24,000.

Wiener, L. S., and Merschat, C. E., 1978, Summary of geology between the Great Smoky fault at Parksville, Tennessee and basement rocks of the Blue Ridge at Glade Gap, North Carolina, *in* Milici, R. C., ed., Field trips in the southern Appalachians, Tennessee Division of Geology Report of Investigation No. 37, p. 2-29.

Wiener, L. S., and Merschat, C. E., 1981, Provisional geologic map of southwest North Carolina, southeast Tennessee, and north Georgia: North Carolina Geological Survey Open-File Map, scale 1:250,000.

Wiener, L. S., and Merschat, C. E., 1992, Geologic map of southwestern North Carolina, including adjoining southeastern Tennessee and north Georgia: North Carolina Geological Survey, scale 1:250,000.

Winchester, P. W., Jr., 1981, Some geotechnical aspects of early planning along corridor K, Appalachian Development Highway; Section between Andrews and Almond, North Carolina: Proceedings of the 32nd Annual Highway Geology Symposium, p. 186-202.

Woodward, N. B., Connelly, J. B., Walters, R. R., and Lewis, J. C., 1991, Tectonic evolution of the Great Smoky Mountains, *in* Kish, S. A., ed., Studies in Precambrian and Paleozoic stratigraphy in the western Blue Ridge: Carolina Geological Society Guidebook, p. 57-68.

Appendices

Appendix A

Structural data

APPENDIX A — Structural Data

*Sta#	Bedding	Cleavage: S_1	Cleavage: S_2	Cleavage: S_2 Axial Surface	Fracture	Fold: Hinge	Fold: Axial Surface	S_0xS_1 Intersection Lineation
TP 1	N42E, 68SE	N30E, 88SE						
2	N25E, 50SE				N27E, 63NW			
					N63W, 81NE			
					N32E, 67NW			
					N73W, 78SW			
3	N35E, 73SE	N35E, 73SE						
4	N54E, 21SE				N52W, 80SE			
					N68E, 61NW			
					N23W, 76SW			
5	N54E, 84SE	N31E, 65SE						
6	N42E, 40SE							
7	N53E, 67SE	N44E, 79SE						
8		N50E, 85SE						
9	N40E, 38NW	N40E, 52SE						
10	N43E, 22NW	N47E, 56SE			N09W, 73NE			
					N21E, 81SE			
					N04W, 83SW			
					N49E, 26NW			
					N41E, 34NW			
11	N06E, 54SE	N50E, 62SE			N24W, 72SW			
					N65E, 35NW			
					N53W, 54SW			
12	N73E, 40SE	N34E, 60SE						
13		N35E, 70SE			N77E, 81NW			
					N63E, 87NW			
					N43E, 61NW			
					N11W, 52NE			
					N24W, 66NE			
					N76E, 78NW			

*Sta#	Bedding	Cleavage: S_1	Cleavage: S_2	Cleavage: S_2 Axial Surface	Fracture	Fold: Hinge	Fold: Axial Surface	S_0xS_1 Intersection Lineation
TP 14	N30E, 55SE	N65E, 40SE			N69E, 63SE			
					N27E, 77SE			
					N67W, 57NE			
15	N50E, 75SE							
16						223, 14	N49E, 79SE	
						209, 19	N34E, 51SE	
						219, 31	N32E, 62SE	
17	N38E, 45SE							
18	N60E, 80SE	N50E, 34SE						
19	N60E, 64SE							
20	N59E, 55SE							
21	N46E, 36SE							
22		N30E, 42SE						
23	N43E, 26SE							
24	N31E, 85SE							
25	N43E, 62SE							
26	N38E, 62SE							
27		N38E, 79SE						
28	N31E, 65SE							
29	N40E, 68SE				N49W, 78NE			
30	N55E, 17SE	N37E, 81SE						
31		N44E, 64SE						
32	N46E, 33SE	N50E, 60SE			N36W, 77NE			
33		N46E, 70SE						
34	N30E, 35SE	N30E, 77SE						
35	N34E, 18SE	N18E, 41SE			N80E, 78SE			
36	N39E, 19SE	N36E, 60SE			N43W, 77NE			

*Station numbers correspond to stations on Plate II.
Stations with a TP prefix are located on the Tellico Plains 7.5-minute quadrangle.
Stations with a BRF prefix are located on the Bald River Falls 7.5-minute quadrangle.
Stations with an F prefix are located on the Farner 7.5-minute quadrangle.
Stations TP-1420 to TP-1575 compiled from McKinney (1964).
Stations F-75 to F-169 compiled from Hale (1974).
Fracture measurements followed by (f) denote fractures that are filled.
Stations are listed in the order in which they were visited along successive traverses.

*Sta#	Bedding	Cleavage S_1	Cleavage $S_{1'}$	Cleavage S_1 Axial Surface	Fracture	Fold Hinge	Fold Axial Surface	S_0xS_1 Intersection Lineation
TP 37	N55E, 33SE	N29E, 88SE			N21W, 78NE			
38	N34E, 49SE	N43E, 52SE						
39		N42E, 26SE			N70W, 86NE			
40		N42E, 83SE						
41	N43E, 36NW	N35E, 66SE						
42	N34E, 44SE	N34E, 60SE			N75E, 65SE			
43		N25E, 52SE						
44	N50E, 27SE	N26E, 63SE			N59E, 75NW			
45		N29E, 51SE						
46	N20E, 07SE	N20E, 70SE						
47	N41E, 27SE	N40E, 46SE			N61E, 86SE			
48	N33E, 60SE							
49		N1 6E, 54SE						
50	N70E, 54SE							
51	N49E, 29SE							
52	N25E, 52SE				N86W, 68NE			
53	N55E, 75SE	N40E, 82SE						
54	N50E, 75SE	N43E, 85SE						
55	N53E, 42SE							
56	N56E, 38NW				N54W, 87SW			
57	N43E, 60NW	N38E, 58SE						
58	N40E, 11SE	N21E, 64SE			N68W, 82NE			
					N31E, 52NW			
					N22E, 28NW			
					N44E, 77SE(f)			
59	N46E, 20SE							
60	N44E, 51SE							
61	N34E, 47SE							
62	N39E, 22SE	N21E, 75SE						
63		N42E, 66SE						
64	N47E, 43SE				N10W, 64SW			
65	N34E, 29SE	N34E, 71SE						
66	N41E, 45SE	N31E, 72SE			N20W, 68NE			
67	N35E, 29SE							
68	N34E, 67SE							
69		N34E, 83SE						
70	N45E, 59SE	N45E, 75SE						
71		N35E, 76SE						
72		N43E, 78SE						
73	N35E, 30SE	N20E, 74SE						
74		N40E, 74SE						
75	N41E, 17SE	N32E, 75SE						
76		N42E, 75SE			N05W, 74SW			
77		N30E, 55SE						

*Sta#	Bedding	Cleavage S_1	Cleavage $S_{1'}$	Cleavage S_1 Axial Surface	Fracture	Fold Hinge	Fold Axial Surface	S_0xS_1 Intersection Lineation
TP 78	N50E, 53NW	N54E, 76SE						
79						40, 4	N36E, 04SE	
80		N38E, 73SE						
81		N52E, 69SE						
82	N41E, 36SE	N69E, 63SE						
83	N60E, 55SE	N60E, 71SE						
84	N64E, 58SE	N64E, 58SE						
85	N40E, 77SE	N35E, 64SE						
86	N42E, 30SE	N80E, 35SE						
87		N36E, 63SE						
88		N34E, 60SE						
89	N46E, 51SE							
90	N47E, 33SE				N80E, 33SE			
91	N35E, 62SE							
92	N35E, 42SE							
93	N35E, 55SE	N20E, 55SE						
94	N30E, 52SE				N77W, 87SW			
95	N40E, 52SE	N34E, 67SE						
96		N53E, 75SE						
97	N30E, 43SE	N44E, 46SE						
98	N35E, 41SE							
99	N30E, 44SE							
100	N35E, 41SE	N31E, 66SE						
101	N43E, 20SE							
102		N38E, 53SE						
103		N65E, 28SE						
104	N48E, 23NW	N48E, 74SE						
105		N56E, 68SE						
106	N30E, 16SE	N30E, 66SE			N07E, 70NW			
					N67W, 80SW			
107		N29E, 74SE						
108	N41E, 55SE	N30E, 62SE						
109		N25E, 74SE						
110		N42E, 57SE						
111	N37E, 50SE	N40E, 85SE						
112	N37E, 53SE	N37E, 63SE						
113	N43E, 66NW	N24E, 83SE						
114	N42E, 73SE							
115	N31E, 50SE							
116	N21W, 59NE							
117		N40E, 63SE						
118		N41E, 61SE						
119		N40E, 65SE						
120		N30E, 81SE						

*Sta#	Bedding	Cleavage S_1	Cleavage S_{1a}	Cleavage S_2 Axial Surface	Fracture	Fold Hinge	Fold Axial Surface	S_0xS_1 Intersection Lineation
TP 121		N40E, 61SE						
122		N34E, 76SE						
123		N33E, 71SE						
124	N45E, 33SE	N45E, 73SE			N08E, 71NW			
125	N47E, 46SE	N47E, 69SE						
126	N46E, 46SE	N46E, 75SE						
127	N50E, 25SE	N30E, 68SE						
128	N45E, 31SE	N45E, 76SE						
129	N39E, 50SE				N65E, 45SE			
130	N44E, 46SE	N44E, 65SE						
131	N45E, 20SE	N45E, 55SE			N40W, 72SW			
132	N35E, 30SE							
133	N55E, 45SE				N10E, 73NW			
					N30W, 83SW			
134	N35E, 35SE							
135	N35E, 39SE	N35E, 66SE						
136		N43E, 78SE						
137		N31E, 71NW			N03E, 65NW			
138	N40E, 35NW	N56E, 77NW						
139	N44E, 70SE	N48E, 44SE						
140		N45E, 52SE						
141		N40E, 48SE						
142	N43E, 39NW	N38E, 46SE						
143		N36E, 42SE			N07W, 32SW			
144	N30E, 32SE	N34E, 53SE						
145		N33E, 49SE						
146	N35E, 46SE							
147		N40E, 37SE						
148	N34E, 55NW	N38E, 57SE						
149		N33E, 41SE						
150	N10E, 45NW	N10E, 17SE						
151	N21E, 25NW	N34E, 44SE			N59W, 88SW			
152	N55E, 85NW	N34E, 17SE						
153						214, 29	N34E, 63SE	
154	N62E, 60NW	N30E, 42SE						
155		N45E, 64SE						
156						236, 9	N56E, 18SE	
157	N20E, 50NW	N39E, 70SE						
158		N42E, 58SE						
159	N36E, 14SE	N34E, 57SE						
160	N38E, 27SE	N35E, 53SE	N26E, 33NW					
161	N39E, 47SE							
162		N68E, 45SE						
163	N62E, 22SE	N46E, 49SE						

*Sta#	Bedding	Cleavage S_1	Cleavage S_{1a}	Cleavage S_2 Axial Surface	Fracture	Fold Hinge	Fold Axial Surface	S_0xS_1 Intersection Lineation
TP 164	N70E, 21SE							
165	N65E, 30SE							
166	N53E, 30SE	N56E, 63SE						
167	N42E, 45NW							
168	N36E, 41SE		N66E, 33NW					
169	N51E, 22SE							
170	N42E, 29SE							
171	N51E, 39SE							
172	N36E, 27SE							
173	N35E, 66SE							
174		N19E, 26SE		N43E, 72NW				
				15, 26				
175	N43E, 27SE							
176	N35E, 43SE							
177		N35E, 36SE						
178	N24E, 28SE							
179	N41E, 60SE							
180	N57E, 28NW							
181		N35E, 64SE						
182	N21E, 29SE				N62E, 82NW(f)			
183	N43E, 30SE							
184	N30E, 44SE		N41E, 82SE					
185		N31E, 58SE						
186		N49E, 64SE						
187	N37E, 14NW	N36E, 74SE						
188	N37E, 22NW							
189	N80E, 32NW	N45E, 62SE						
190	N48E, 32NW							
191	N51E, 20SE							
192	N44E, 40SE							
193		N58E, 36SE						
194	N52E, 25SE			N34E, 45SE				
				20, 45				
195	N47E, 19SE	N56E, 48SE						
196	N49E, 34SE							
197	N34E, 27SE							
198	N14E, 16NW							
199	N70E, 51SE							
200		N41E, 38SE						
201	N38E, 57SE							
202	N27E, 40SE							
203	N36E, 49NW	N31E, 53SE						
204		N29E, 08NW						
205		N30E, 56SE						

*Sta#	Bedding	Cleavage S_1	Cleavage S_{1a}	Cleavage S_2 Axial Surface	Fracture	Fold Hinge	Fold Axial Surface	$S_0 x S_1$ Intersection Lineation
TP 206		N16E, 24SE						
207	N49E, 41SE							
208		N39E, 34SE						
209		N51E, 35SE						
210	N36E, 25SE							
211	N35E, 26SE							
212	N35E, 72SE							
213		N41E, 34SE						
214	N40E, 35SE							
215	N54E, 32SE							
216	N49E, 90							
217	N40E, 63NW							
218		N49E, 33SE						
219						329, 60	N30W, 70NE	
220	N38E, 28SE	N31E, 70SE						
221	N34E, 42SE							
222		N55E, 44SE						
223	N50E, 30SE	N39E, 38SE						
224		N40E, 38SE						
225	N51E, 45SE							
226	N19E, 56SE							
227	N51E, 52SE							
228	N30E, 48SE							
229	N31E, 48SE							
230	N36E, 40SE							
231		N34E, 31SE						
232	N49E, 52SE							
233		N27E, 42SE						
234	N29E, 90							
235	N35E, 38NW	N54E, 55SE						
236		N40E, 33SE						
237		N29E, 35SE						
238	N31E, 10NW							
239	N26E, 82SE	N35E, 30SE						
240	N21E, 76SE							
241	N45E, 80SE							
242	N32E, 63SE							
243	N51E, 42SE							
244	N65E, 35SE				N43W, 84NE			
245	N50E, 28SE	N49E, 48SE						
246	N59E, 35SE	N42E, 76SE		N49E, 63NW				
				229, 19				
247	N54E, 34SE	N51E, 52SE						
248	N57E, 27SE							

*Sta#	Bedding	Cleavage S_1	Cleavage S_{1a}	Cleavage S_2 Axial Surface	Fracture	Fold Hinge	Fold Axial Surface	$S_0 x S_1$ Intersection Lineation
TP 249	N53E, 46SE							
250		N30E, 42SE						
251	N29E, 55SE	N14E, 66SE						
252	N41E, 62SE							
253		N54E, 50SE						
254	N40E, 26SE							
255	N34W, 07NE							
256	N55E, 47SE							
257	N40W, 90							
258	N67E, 40SE							
259	N55E, 85SE							
260	N44E, 85SE							
261	N73E, 50SE							
262						10, 32	N29E, 45SE	
263	N49E, 57SE							
264	N65E, 55SE							
265	N40E, 35SE							
266		N45E, 66SE						
267	N55E, 84NW	N62E, 60SE						
268	N53E, 66SE							
269						53, 7	N55E, 64SE	219, 21
270	N35E, 85SE	N43E, 62SE						
271		N55E, 67SE						
272	HORIZONTAL	N09E, 65SE						
273	N17E, 55NW	N44E, 41SE						
274	N03W, 40SW							
275	N55E, 83NW							
276		N49E, 56SE						
277		N61E, 67SE						
278		N36E, 39SE						
279	N32E, 33NW							
280	N24E, 05NW							
281	N59E, 69SE							
282	N41E, 69SE	N30E, 40SE						
283	N90E, 28S							
284	N30E, 30NW	N35E, 64NW						
285	N34W, 66SW	N46W, 38NE						
286	N49E, 29NW	N53E, 38SE						
287	N45E, 24NW	N33E, 52NW				51, 7	N52E, 62NW	
288	N46E, 12SE	N54E, 64SE						
289	N40E, 19SE							
290	N42E, 45SE							
291	N46E, 19SE	N46E, 27SE						
292	N58E, 39SE				N80W, 87NE			

*Sta#	Bedding	Cleavage S_1	Cleavage $S_{1'}$	Cleavage S_2 Axial Surface	Fracture	Fold Hinge	Fold Axial Surface	S_0xS_1 Intersection Lineation
TP 293	N39E, 25SE							
294	N34E, 26SE							
295	N57E, 51SE							
296	N53E, 45SE							
297	N40E, 45SE							
298		N49E, 53SE						
299		N47E, 59SE						
300	N50E, 15SE	N52E, 27SE						
301		N32E, 52SE						
302	N33E, 41SE							
303		N54E, 65SE						
304		N34E, 78SE						
305	N51E, 45NW							
306	N50E, 53SE							
307	N51E, 26SE							
308	N51E, 71NW							
309	N51E, 50NW							
310	N53E, 64SE							
311		N63E, 49SE						
312		N25E, 66SE						
313	N47E, 35SE	N45E, 25SE						
314	N55E, 20SE							
315		N61E, 60SE						
316		N60E, 65SE						
317	N58E, 90							
318	N44E, 68SE							
319	N53E, 62SE	N65E, 62SE						
320		N43E, 56SE						
321	N49E, 37NW	N57E, 61SE						
322	N40E, 16NW	N25E, 50SE						
323		N27E, 80SE						
324	N36E, 66NW	N46E, 64SE						
325	N37E, 55SE							
326	N05E, 55NW							
327		N34E, 76SE						
328	N68E, 38SE	N68E, 30SE						
329		N31E, 51SE						
330	N24E, 38SE							
331		N58E, 37SE						
332						235, 7	N55E, 74SE	
333	N58E, 08SE	N51E, 57SE						
334	N63E, 34SE							
335		N53E, 47SE						
336	N28E, 68SE							
TP 337	N47E, 21SE	N51E, 85NW						
338	N49E, 68SE	N49E, 80SE						
339	N42E, 47SE	N53E, 58SE						
340	N42E, 33SE	N36E, 74SE				224, 10	N36E, 74SE	
341		N21E, 77SE						
342	N35E, 28SE	N46E, 57SE						
343		N37E, 79SE						
344		N30E, 71SE						
345		N25E, 84NW						
346	N35E, 16SE	N35E, 66SE				215, 17	N35E, 66SE	
347		N30E, 85SE						
348	N45E, 10SE	N47E, 80SE						
349	N36E, 55SE							
350	N28E, 61SE							
351	N35E, 35SE							
352	N31E, 56SE							
353	N50E, 36SE							
354	N36E, 68SE							
355	N46E, 61NW							
356	N23E, 62SE							
357	N42E, 66SE							
358	N33E, 79NW							
359	N27E, 54SE	N39E, 56SE						
360	N22E, 62NW							
361	N27E, 62SE							
362	N13E, 78SE							
363	N33E, 27NW	N27E, 62SE						21, 16
364	N17E, 48SE							
365	N40E, 30SE							
366	N32E, 73SE							
367	N35E, 90							
368	N31E, 48SE	N36E, 58SE						
369	N27E, 44SE							
370	N41E, 43SE							
371		N36E, 47SE						
372	N32E, 57SE							
373	N59E, 26SE	N59E, 89SE						
374	N42E, 61SE							
375	N47E, 42SE							
376	N57E, 68SE							
377	N32E, 90							
378	N55E, 66SE	N46E, 70SE						
379		N61E, 48SE						
380		N35E, 82SE						

*Sta#	Bedding	Fabric Element: Cleavage S_1	Cleavage S_{1a}	Cleavage S_2 Axial Surface	Fracture	Fold Hinge	Fold Axial Surface	S_0xS_1 Intersection Lineation
TP 381	N49E, 28SE							
382	N46E, 58SE							
383	N47E, 59SE							
384	N40E, 16SE	N38E, 75SE						
385		N34E, 54SE						
386		N43E, 60SE						
387	N58E, 48SE	N58E, 60SE						
388	N45E, 45SE							
389	N35E, 20NW	N37E, 59SE						
390	HORIZONTAL	N41E, 55SE						
391	N57E, 50SE	N34E, 52SE						
392	N36E, 52SE							
393	N45E, 41SE							
394	N37E, 61SE							
395		N20E, 71SE						
396	N44E, 55SE							
397	N49E, 39SE							
398	N41E, 80SE							
399		N43E, 79SE						
400		N43E, 60SE						
401	N49E, 21SE	N30E, 67SE						
402	N37E, 25SE	N36E, 76NW						
403	N55E, 25SE							
404	N44E, 51SE							
405	N51E, 31SE							
406	N53E, 18SE							
407		N35E, 86SE						
408	N35E, 70SE							
409	N45E, 37SE							
410	N42E, 67SE							
411	N45E, 46SE							
412	N31E, 27SE	N31E, 83SE						
413	N51E, 69SE							
414		N44E, 58SE						
415		N49E, 39SE						
416		N49E, 36SE						
417		N47E, 48SE						
418	N44E, 24SE							
419	N49E, 40SE							
420	N55E, 44SE							
421		N48E, 49SE						
422		N41E, 54SE						
423	N45E, 43SE							
424	N48E, 39SE							

*Sta#	Bedding	Fabric Element: Cleavage S_1	Cleavage S_{1a}	Cleavage S_2 Axial Surface	Fracture	Fold Hinge	Fold Axial Surface	S_0xS_1 Intersection Lineation
IP 425	N43E, 44SE							
426	N35E, 40SE	N34E, 69SE						
427	N53E, 48SE	N53E, 72SE						
428	N54E, 38SE							
429		N48E, 76SE						
430	N43E, 19NW							
431	N40E, 35SE							
432	N35E, 35SE	N35E, 73SE						
433		N40E, 71SE						
434		N45E, 86SE						
435	N37E, 36SE							
436	N58E, 33SE							
437	N66E, 39SE							
438	N63E, 40SE							
439	N65E, 19NW	N65E, 74SE						
440		N52E, 77SE						
441	N35E, 12NW	N35E, 59SE						
442	N46E, 08SE	N46E, 88SE						
443	N55E, 41SE							
444	N66E, 33SE							
445		N51E, 38SE						
446	N56E, 36SE							
447	N48E, 16SE	N56E, 60SE		N40E, 75NW				
				219, 25				
448		N39E, 62SE						
449						211, 9	N47E, 57SE	
450	N41E, 27NW	N41E, 64SE						
451	N27E, 86NW	N41E, 64SE						
452		N35E, 81SE						
453	N45E, 17SE	N47E, 44SE						
454	N31E, 27SE	N65E, 57SE						211, 5
455	N35E, 47NW	N33E, 39SE						
456	N31E, 29NW	N21E, 60SE			N60W, 65SW			
457		N28E, 70SE						
458	N47E, 27NW	N40E, 58SE						
459		N41E, 71SE						
460						30, 27	N45E, 61SE	
461	N33E, 43NW	N31E, 69SE						
462	N39E, 09NW	N41E, 65SE						
463	N47E, 16NW	N45E, 69SE						226, 21
464		N49E, 85SE						
465	N59E, 38SE							
466	N41E, 46NW							
467	N23E, 39SE							

*Sta#	Bedding	Cleavage: S_1	Cleavage: $S_{1'}$	Cleavage: S_2 Axial Surface	Fracture	Fold: Hinge	Fold: Axial Surface	S_0xS_1 Intersection Lineation
TP 468	N46E, 46SE							
469	N35E, 35NW							
470	N35E, 40SE							
471	N23E, 31SE							
472	N30E, 42SE							
473	N31E, 39SE							
474		N07W, 13NE						
475		N49E, 47SE						
476		N24E, 50SE						
477	N35E, 44NW	N29E, 55SE						
478	N35E, 08NW	N35E, 39SE						
479	N35E, 77SE							
480	N34E, 33SE							
481	N50E, 24SE							
482	N53E, 29SE							
483		N30E, 76SE						
484	N17E, 43SE							
485	N36E, 40SE							
486	N42E, 31SE							
487	N37E, 42SE	N62E, 71NW						
488	N33E, 32SE							
489	N18E, 36SE							
490		N15E, 51SE						
491		N33E, 46SE						
492		N28E, 48SE						
493	N46E, 50SE							
494	N45E, 56SE							
495		N46E, 46SE						
496		N51E, 34SE						
497	N54E, 25NW	N65E, 61SE						
498		N54E, 76SE						
499	N46E, 42SE							
500	N51E, 44SE							
501		N49E, 52SE						
502	N49E, 39SE							
503		N56E, 66SE						
504	N49E, 35SE							
505		N56E, 63SE						
506	N45E, 68SE							
507		N37E, 68SE						
508		N37E, 71SE						
509		N22E, 82SE						
510	N31E, 68SE							
511	N43E, 68SE	N13E, 33SE						

*Sta#	Bedding	Cleavage: S_1	Cleavage: $S_{1'}$	Cleavage: S_2 Axial Surface	Fracture	Fold: Hinge	Fold: Axial Surface	S_0xS_1 Intersection Lineation
TP 512		N25E, 76SE						
513	N43E, 77SE	N35E, 68SE						
514	N48E, 47SE	N40E, 70SE				215, 16	N40E, 70SE	
515		N34E, 34SE						
516		N49E, 25SE						
517		N25E, 38SE						
518		N35E, 59SE						
519		N40E, 25SE						
520	N39E, 79NW	N39E, 19SE						39, 8
521	N46W, 74NE	N59E, 16NW						
522	N41E, 24NW	N44E, 60SE						
523	N45E, 59NW	N39E, 26SE						
524	N24E, 69SE	N24E, 21SE						
525	N56E, 54SE							223, 24
526	N65E, 71SE							
527	N64E, 80SE							
528		N46E, 52SE						
529	N26E, 72SE							
530	N21E, 84SE							
531	N50E, 39SE							
532	N34E, 64SE							
533	N19E, 36NW	N39E, 50SE						211, 18
534	N21E, 35SE							
535	N37E, 68SE							
536	N56E, 06SE							
537						232, 29	N52E, 52SE	
538	N57E, 34SE							
539	N58E, 44SE							
540	N49E, 52SE							
541	N55E, 36SE							
542	N47E, 45SE							
543	N28E, 51SE							
544	N64E, 51SE							
545	N47E, 66SE							
546	N51E, 41SE							
547	N65E, 42SE							
548	N37E, 58SE							
549	N45E, 55SE							
550	N42E, 32SE	N34E, 72SE						200, 5
551		N42E, 54SE						
552	N66E, 52SE	N61E, 71SE						
553	HORIZONTAL							
554						60, 23		
555						241, 11	N67E, 80NW	

*Sta#	Bedding	Cleavage S_1	Cleavage $S_{1'}$	Cleavage S_2 Axial Surface	Fracture	Fold Hinge	Fold Axial Surface	S_1xS_1 Intersection Lineation
TP 556		N46E, 69SE						
557	N27E, 29SE	N38E, 59SE						
558	N64E, 55NW	N37E, 48SE						
559	N67E, 33NW	N35E, 58SE						
560	N47E, 35NW							
BRF 1	N52E, 39NW	N40E, 37SE						45, 19
2		N34E, 64SE						
3		N15E, 41SE						
4	N35E, 03SE	N24E, 34SE						
5		N33E, 39SE						
6		N63E, 47SE						
7	N47E, 66SE							
8	N62E, 53SE							
9	N55E, 57SE							
10	N60E, 55SE							
11	N58E, 73SE	N65E, 54SE						
12	N56E, 46SE							
13	N63E, 48SE							
14	N50E, 53SE							
15		N25E, 38SE						
16		N71E, 44SE						
17	N42E, 52SE							
18		N43E, 52SE						
19	N55E, 36SE							
20	N64E, 63NW							
21		N53E, 44SE		N13E, 39SE				
				191, 29				
22		N64E, 46SE						
23		N45E, 54SE						
24		N50E, 69SE						
25	N45E, 55SE							
26	N42E, 53SE							
27	N62E, 08SE	N45E, 38SE		N45E, 35SE				
				42, 2				
28	N23E, 37NW	N21E, 37SE		N23E, 76NW				
				199, 5				
29		N20E, 22SE						
30	N27E, 82NW	N15E, 41SE						
31	N37E, 39NW	N37E, 39SE						
32	N29E, 17SE	N62E, 40SE						
33	N38E, 24SE	N37E, 54SE						
34		N42E, 41SE						
35		N11E, 51SE						
36	N54E, 18NW	N54E, 59SE						

*Sta#	Bedding	Cleavage S_1	Cleavage $S_{1'}$	Cleavage S_2 Axial Surface	Fracture	Fold Hinge	Fold Axial Surface	S_1xS_1 Intersection Lineation
BRF 37	N51E, 37NW	N51E, 54SE						
38		N38E, 56SE						
39	N39E, 48NW	N09W, 40SW						
40	N55E, 55SE							
41	N39E, 60NW							
42	N43E, 45NW	N43E, 44SE						
43		N34E, 31SE						
44	N24E, 09NW	N26E, 34SE						
TP 561	N51E, 47SE							
562	N58E, 64SE							
563	N51E, 36SE							
564	N34E, 08SE	N34E, 80SE						
565	N41E, 44SE							
566	N23E, 46SE							
567	N29E, 41SE							
568	N49E, 37SE							
569	N73E, 51SE							
570	N36E, 44SE							
571	N49E, 40SE							
572		N43E, 54SE			N79E, 76NW			
573	N54E, 26SE	N45E, 74SE						
574		N51E, 78SE						
575	N39E, 45SE							
BRF 53	N39E, 59SE	N39E, 84SE						
54	N43E, 64SE	N39E, 54SE						
55	N52E, 69NW	N43E, 40SE						
56	N41E, 22NW	N38E, 48SE						
57	N53E, 75NW	N45E, 48SE						
58	N81E, 37NW	N38E, 48SE			N46W, 89SW			
					N44E, 51SE			
59	N11E, 29NW	N19E, 51SE						
60						51, 7	N27E, 43SE	
61	N39E, 71NW	N32E, 33SE						
62	N46E, 80SE	N36E, 49SE			N27E, 39NW			
					N43E, 88NW			
63	N46E, 54SE							
64	N33E, 84SE	N47E, 47SE						
65		N46E, 39SE						
66	N43E, 05SE	N41E, 37SE				57, 8	N41E, 37SE	
67		N51E, 37SE						
68	N52E, 38SE							
69	N41E, 50SE							
70	N48E, 41SE							
71	N38E, 69SE	N47E, 42SE						

		Fabric Element						
		Cleavage				Fold		S_0xS_1
*Sta#	Bedding	S_1	S_{1a}	S_2 Axial Surface	Fracture	Hinge	Axial Surface	Intersection Lineation
BRF 72	N49E, 52SE							
73	N41E, 74SE							
74	N49E, 54SE							
75	N30E, 55SE	N39E, 42SE						
76	N47E, 50SE							
77	N53E, 48SE							
78	N45E, 49SE							
79		N47E, 52SE						
80	N44E, 54SE							
81	N49E, 60SE							
82	N24E, 24SE							
83	N29E, 56SE							
84	N49E, 64SE							
85	N51E, 85SE							
86	N57E, 75SE	N57E, 51SE						
87	N48E, 51NW	N48E, 27SE						
88	N51E, 55NW	N51E, 29SE						
89	N44E, 85NW	N44E, 30SE						
90	N36E, 52NW	N43E, 30SE						
91		N42E, 29SE						
92	N42E, 59NW	N42E, 13SE						
93	N39E, 71NW	N39E, 34SE						
94	N37E, 63NW	N37E, 26SE						
95		N39E, 27SE						
96	N55E, 18NW	N55E, 30SE						
97		N51E, 49SE						
98		N35E, 27SE						
99	N44E, 42NW	N44E, 29SE						
100		N36E, 20SE						
101	N35E, 37NW	N35E, 30SE						
102		N44E, 38SE						
103		N39E, 46SE						
104		N52E, 36SE						
105	N41E, 90	N41E, 25SE						
106	N45E, 61SE	N45E, 42SE						
107	N40E, 87SE	N40E, 36SE						
108	N23E, 90	N23E, 90SE						
109	N47E, 62NW	N30E, 44SE						
110	N44E, 62SE	N44E, 24SE						
TP 576	N31E, 79SE							
577	N79E, 34SE							
BRF 111	N43E, 47NW	N27E, 31SE						
112	N37E, 34SE							
113	N48E, 57SE							

		Fabric Element						
		Cleavage				Fold		S_0xS_1
*Sta#	Bedding	S_1	S_{1a}	S_2 Axial Surface	Fracture	Hinge	Axial Surface	Intersection Lineation
BRF 114	N33E, 47SE	N07E, 46SE						
115	N57E, 47SE							
116	N50E, 55SE							
117	N41E, 51SE							
118		N36E, 73SE						
119	N49E, 73SE							
120	N57E, 56SE							
121	N45E, 55SE							
122	N56E, 57SE	N49E, 69SE						
123	N57E, 52SE	N38E, 57SE						
133	N23E, 19SE	N33E, 49SE						
134	N25E, 11SE	N42E, 49SE						
135	N37E, 70NW	N35E, 35SE						
136	N49E, 69SE	N45E, 34SE						
137	N54E, 56NW	N34E, 28SE		N55E, 61NW				
				55, 5				
138						24, 3	N39E, 12SE	
139	N06E, 32NW	N0E, 21E						
140	N70W, 06NE	N02E, 51SE						
141	N05E, 15SE	N40E, 51SE						24, 6
142	N44E, 26SE	N26E, 51SE						
143	N0E, 15E	N23E, 45SE						
144	N24W, 10NE	N28E, 47SE						
145	HORIZONTAL	N03E, 40SE						
146	N39E, 43NW	N27E, 25SE						
147	N50E, 15NW	N55E, 46SE						
148	N33E, 71NW	N35E, 42SE						
149	N35E, 08SE	N25E, 46SE						211, 2
150	N20E, 24SE	N36E, 29SE						
151	N35E, 11NW	N17E, 43SE						41, 2
152						90, 2	N31E, 23SE	
153	N35E, 22NW	N35E, 38SE						
154	N37E, 22NW					31, 0	N27E, 25SE	
155	N36E, 33NW	N33E, 34SE		N34E, 50NW				
				36, 10				
156	N37E, 32SE	N56E, 65SE						
157	HORIZONTAL	N39E, 30SE						
158	N36E, 39NW	N49E, 38SE						
159	N27E, 21SE	N23E, 65SE						
160	N40E, 21NW	N22E, 43SE						
161	N32E, 06SE	N34E, 52SE						
162	N34E, 50NW	N22E, 26SE						
163	N27E, 82SE	N37E, 29SE						
164	N31E, 90	N31E, 29SE						

	Fabric Element							
		Cleavage				Fold		S_0xS_1
*Sta#	Bedding	S_1	S_{1a}	S_2 Axial Surface	Fracture	Hinge	Axial Surface	Intersection Lineation
BRF165	N21E, 30NW							
166	N37E, 90	N37E, 33SE						
167	N39E, 90	N32E, 30SE						
168	N19E, 19NW	N20E, 29SE						
169						200, 18	N31E, 11SE	
170		N32E, 24SE						
171		N31E, 41SE						
172	N57E, 43NW	N45E, 19SE						
173		N46E, 28SE						
174		N32E, 36SE						
175		N30E, 31SE						
176	N49E, 78NW	N15E, 43SE						
177	N38E,64NW	N44E, 38SE						
178	N49E, 54NW	N29E, 43SE						
179	N44E, 34NW	N44E, 38SE						
180	N42E, 82SE	N42E, 40SE						
181	N70E, 39NW	N70E, 39SE						
182	N55E, 25NW	N45E, 35SE						
196		N40E, 34SE						
197	N55E, 60NW	N19E, 40SE						
198	N47E, 86NW	N35E, 40SE						
199	N45E, 40NW	N44E, 30SE						
200	N42E, 40NW	N42E, 35SE						
201	N46E, 74SE	N40E, 34SE						
202	N41E, 37NW	N37E, 36SE						
203	N46E, 58SE	N31E, 27SE						
204	N65E, 51SE	N43E, 28SE						
205	N46E, 65SE	N46E, 22SE						
206	N30E, 78SE	N27E, 20SE						
207		N41E, 21SE						
208	N55E, 80SE	N25E, 47SE						
209	N47E, 69SE	N30E, 42SE						
210	N34E, 72SE	N32E, 32SE						
211	N32E, 64SE	N32E, 26SE						
212	N51E, 74SE	N51E, 26SE						
213	N47E, 51SE	N47E, 34SE						
214	N55E, 90	N45E, 37SE						
215	N44E, 88NW	N45E, 39SE						
216	N47E, 31NW	N41E, 35SE						
217	N49E, 86NW	N49E, 34SE						
218	N41E, 82NW	N33E, 42SE						
219	N49E, 54SE	N49E, 21SE						
220	N54E, 44NW	N54E, 36SE						
221						201, 2	N21E, 20SE	

	Fabric Element							
		Cleavage				Fold		S_0xS_1
*Sta#	Bedding	S_1	S_{1a}	S_2 Axial Surface	Fracture	Hinge	Axial Surface	Intersection Lineation
BRF 222	N37E, 37NW	N47E, 37SE						
223	N45E, 11SE	N45E, 37SE						
224		N43E, 49SE						
225	N42E, 59SE							
226		N46E, 41SE						
227		N31E, 35SE						
228		N45E, 39SE						
229	N49E, 69SE	N49E, 44SE						
230		N44E, 56SE						
231	N39E, 59SE							
232	N51E, 61SE							
233	N47E, 64SE							
234	N47E, 88NW							
235	N31E, 56SE							
236	N43E, 63SE							
237	N34E, 60SE							
249	N49E, 65SE							
250	N45E, 59SE	N39E, 31SE						
251	N38E, 85NW							
252	N54E, 24SE							
253	N43E, 10SE							
254	N41E, 06NW	N37E, 46SE						
255	N41E, 11SE	N36E, 40SE						
256	N33E, 20SE							
257	N06E, 33NW							
258	N68E, 16SE	N49E, 56SE						
259	N56E, 11SE							
260						231, 11	N51E, 42SE	
261	N26E, 86NW	N46E, 52SE						
262	N19E, 56SE							
263	N24W, 54NW	N29E, 18SE						
270		N10W, 18NE						
271	N65E, 88SE	N65E, 80SE						
272	N64E, 80SE	N64E, 45SE						
273	N47E, 56SE	N47E, 28SE						
274	N40E, 50SE							
275	N49E, 74SE	N49E, 28SE						
276	N47E, 90							
277	N44E, 90							
278	N34E, 90							
279	N38E, 67SE							
280	N31E, 58SE							
281	N41E, 55SE							
282	N42E, 90							

*Sta#	Bedding	Cleavage: S_1	Cleavage: S_{1a}	Cleavage: S_2 Axial Surface	Fracture	Fold: Hinge	Fold: Axial Surface	S_xS_1 Intersection Lineation
BRF 283	N58E, 60SE							
284	N42E, 78SE	N42E, 36SE						
285	N36E, 55SE	N14E, 34SE						
286	N37E, 68SE							
287	N32E, 60SE							
288	N33E, 80NW							
300	N40E, 67SE	N40E, 41SE						40, 5
301	N39E, 68SE	N39E, 12SE						39, 10
302	N50E, 80SE	N30E, 39SE						
303	N38E, 86NW	N38E, 20SE						
304	N45E, 40NW	N35E, 39SE						
305	N39E, 86NW	N53E, 29SE						
306	N41E, 79NW	N34E, 46SE						
307	N35E, 54SE	N35E, 26SE						
308	N49E, 65SE	N42E, 14SE						
309	N45E, 52SE	N40E, 34SE						
310	N48E, 51SE	N48E, 20SE						
311	N40E, 38SE	N40E, 10SE						
312	N49E, 76SE	N56E, 28SE						52,12
313	N47E, 88NW	N47E, 38SE						
314	N50E, 79NW	N50E, 22SE						
315	N46E, 60NW	N46E, 42SE						
316	N46E, 56NW	N46E, 32SE						
317	N48E, 62NW	N42E, 34SE						
318	N36E, 60NW	N36E, 32SE						
319	N41E, 85NW	N41E, 28SE						
320	N60E, 65NW	N47E, 38SE						
321	N65E, 54SE	N53E, 21NW		N63E, 39NW				
				63, 4				
322		N43E, 44SE						
323	N35E, 18SE	N55E, 61SE						
324	N32E, 04NW	N33E, 51SE						
325	N38E, 09SE	N41E, 44SE			N70E, 71SE			
					N62E, 62SE			
326		N43E, 49SE						
327		N45E, 49SE						
328	N50E, 53NW	N52E, 39SE						
329	N50E, 64NW	N40E, 39SE						
330	N49E, 78SE	N48E, 35SE						
331	N45E, 62SE	N46E, 25SE						
332	N52E, 74SE	N52E, 36SE						
333	N50E, 62SE	N39E, 25SE						
334	N34E, 51SE	N42E, 28SE						
335	N41E, 77SE	N43E, 35NW						

*Sta#	Bedding	Cleavage: S_1	Cleavage: S_{1a}	Cleavage: S_2 Axial Surface	Fracture	Fold: Hinge	Fold: Axial Surface	S_xS_1 Intersection Lineation
BRF 336	N45E, 53NW	N45E, 26SE						
337		N45E, 70SE						
338	N43E, 77NW	N32E, 41SE						
339	N49E, 54SE							
340	N55E, 52SE	N55E, 25SE						
341	N48E, 82NW	N60E, 43SE						
342		N45E, 38SE						
343	N61E, 46SE	N30E, 40SE						
344	N51E, 83SE	N30E, 38SE						
345	N52E, 31NW	N45E, 44SE						
346	N62E, 22NW	N35E, 35SE						
347	N49E, 86NW	N27E, 34SE						
348	N56E, 71NW	N49E, 29SE						
349	N46E, 49NW	N29E, 30SE						35, 8
350	N67E, 22NW	N36E, 24SE						
351	N37E, 41NW	N41E, 28SE						
352	N20E, 36NW	N28E, 28SE						
353	N36E, 40NW	N37E, 28SE						
354	N46E, 17NW	N56E, 28SE						
355						41, 3	N36E, 35SE	
356	HORIZONTAL	N35E, 28SE						
357	N52E, 21SE	N38E, 46SE						
358	N54E, 34NW	N36E, 27SE						
359	N66E, 44NW	N45E, 18SE						
360	N55E, 11SE	N25E, 47SE						
361	N72E, 13SE	N34E, 40SE						
362	N69E, 79SE	N47E, 30SE						
363	N29E, 83NW	N39E, 23SE		N32E, 48NW				
				32, 7				
364	N55E, 67NW	N35E, 17SE						
365	N49E, 82NW	N49E, 29SE						
366	N26W, 16SW	N22E, 28SE						
367	N60E, 56NW	N34E, 22SE				44, 2	N47E, 41SE	
368	N45E, 24NW	N29E, 29SE						
369	N37E, 63SE	N21E, 23SE						
370						45, 3	N12E, 22SE	
371	N51E, 29NW	N48E, 25SE						
372	N11E, 11NW	N37E, 22SE						
373	N03E, 42NW	N13E, 16SE						
374	N11E, 26NW	N42E, 38SE						
375	N40E, 73SE	N48E, 32SE						
376	N41E, 20NW	N16E, 21SE						
377		N49E, 15SE						
378	N55E, 38NW	N39E, 36SE						

*Sta#	Bedding	Cleavage: S_1	Cleavage: $S_{1\cdot}$	S_2 Axial Surface	Fracture	Fold: Hinge	Fold: Axial Surface	S_0xS_1 Intersection Lineation
BRF 379	N49E, 68SE	N47E, 41SE				42, 5	N40E, 44SE	
380	N57E, 56SE	N42E, 34SE				56, 7	N48E, 46SE	
381	N59E, 54SE	N63E, 12SE						
382	N53E, 55SE	N29E, 37SE						
383	N49E, 55SE	N43E, 22SE						
384	N39E, 58SE	N51E, 21SE						
385	N50E, 57SE	N26E, 36SE						
386	N49E, 61SE	N26E, 37SE						
387	N54E, 67SE	N53E, 24SE						
388	N55E, 57SE							
389	N62E, 53SE							
390	N52E, 63SE	N52E, 31SE						
391	N60E, 62SE							
392	N65E, 68SE	N46E, 42SE						
393	N54E, 50SE							
394	N72E, 69SE	N44E, 53SE						
395	N62E, 76SE	N62E, 58SE						
396	N57E, 60SE	N57E, 52SE						
397	N55E, 64SE	N55E, 51SE						
398	N60E, 64SE	N32E, 50SE						
399	N53E, 54SE	N48E, 42SE						
400	N52E, 61SE	N57E, 33SE						
401	N52E, 69SE	N40E, 53SE						
402	N45E, 69SE	N45E, 16SE						
403	N58E, 58SE							
404	N61E, 62SE							
405	N56E, 68SE	N56E, 46SE						
406	N64E, 74NW	N44E, 42SE						
407	N62E, 57NW	N32E, 44SE						
408	N61E, 60SE	N37E, 46SE						
409	N47E, 76SE							
410	N65E, 74NW							
411	N61E, 82SE	N20E, 50SE						
412	N82E, 30NW	N56E, 41SE						
413	N75E, 68SE	N50E, 34SE						
414	N62E, 53SE	N20E, 40SE						
415	N62E, 54SE	N39E, 39SE						
416		N67E, 50SE						
417	N72E, 58SE							
418	N39E, 52SE	N48E, 61SE				208, 9	N28E, 50SE	
419	N42E, 60SE	N14E, 45SE						
420	N45E, 57SE	N39E, 30SE						
421	N38E, 82SE	N32E, 35SE						
422	N53E, 80SE	N32E, 33SE						

*Sta#	Bedding	Cleavage: S_1	Cleavage: $S_{1\cdot}$	S_2 Axial Surface	Fracture	Fold: Hinge	Fold: Axial Surface	S_0xS_1 Intersection Lineation
BRF 423	N45E, 67SE	N41E, 40SE						
424						79, 5	N38E, 29SE	
425	N41E, 67SE	N31E, 54SE						
426	N43E, 71SE	N39E, 43SE						
427	N55E, 42SE	N41E, 21SE						
428	N51E, 59SE	N25E, 21SE						
429	N35E, 64SE	N10E, 53SE						
430	N30E, 38SE	N11E, 36SE		N13E, 36NW 190, 21				
431	N52E, 49SE	N31E, 23SE			N09W, 76NE			
432	N34E, 73NW	N15E, 40SE						
433	N22E, 49NW	N22E, 43SE						
434	N40E, 46NW	N35E, 62SE						
435	N53E, 84SE	N47E, 34SE						
436	N54E, 76NW	N42E, 42SE						
437	N41E, 30NW	[illegible]						
438	N49E, 57SE	N28E, 39SE						
439	N61E, 60SE	N34E, 39SE						
440	N53E, 59SE							
441	N50E, 58SE							
442	N30E, 72SE							
443	N54E, 53SE							
444	N52E, 52SE							
445		N42E, 42SE						
446	N31E, 39NW	N40E, 35SE						
447	N12E, 32NW	N37E, 42SE						
448		N44E, 43SE						
449		N26E, 44SE						
450	N45E, 26NW	N44E, 41SE						
451	N51E, 41SE							
452						37, 2	N45E, 42SE	
453		N37E, 42SE						
454	N37E, 63SE							
455	N30E, 71SE							
456	N50E, 51SE							
460		N65E, 60SE						
463		N47E, 56SE						
465		N27E, 41SE						
466	N26E, 48NW	N43E, 56SE			N55E, 87NW			
467	N40E, 74NW	N40E, 12SE						
468	N43E, 40NW	N43E, 45SE						
469	N44E, 59SE	N44E, 49SE						
470	N39E, 67SE	N39E, 33SE						
471	N40E, 71NW	N40E, 26SE						

*Sta#	Bedding	Cleavage: S_1	Cleavage: $S_{1'}$	Cleavage: S_2 Axial Surface	Fracture	Fold: Hinge	Fold: Axial Surface	S_0xS_1 Intersection Lineation
BRF 472	N49E, 30NW	N62E, 72SE						
473	N55E, 38NW	N40E, 49SE						
474		N41E, 69SE						
475	N30E, 38NW	N27E, 42SE						
476	N45E, 33NW	N25E, 38SE						
477		N55E, 46SE						
478				N41E, 30SE				
				221, 2				
479	N62E, 42NW	N34E, 48SE						50, 11
480	N44E, 90	N51E, 42SE						
481	N31E, 57SE							
482	N43E, 51NW	N51E, 67SE						
483	N50E, 62NW	N51E, 68SE						
484	N38E, 09SE	N25E, 28SE						
485	N47E, 16SE	N45E, 44SE						
486	N36E, 04SE	N60E, 34SE						
487	N31E, 37SE							
488	N28E, 25SE							
489	N24E, 42SE	N42E, 57SE						
490	N45E, 70NW	N43E, 32SE						
491	N59E, 85NW	N74E, 36SE						
492	N55E, 75SE	N65E, 27SE						
493	N41E, 36NW	N37E, 37SE						
494	N45E, 37NW	N45E, 51SE						
495	N57E, 45NW	N59E, 52SE						
496	N43E, 49NW	N24E, 40SE						
497	N62E, 63NW	N24E, 43SE						
498	N31E, 71NW	N22E, 27SE						
499	N55E, 50SE	N25E, 22SE						
500	N79E, 62NW	N20E, 35SE						
501	N55E, 78SE	N33E, 15SE						
502	N36E, 56SE	N30E, 29SE						
503	N41E, 66SE	N51E, 47SE						
504	N63E, 80NW	N63E, 52SE						
505	N42E, 60SE	N53E, 42SE						
506	N50E, 90	N56E, 48SE						
507	N39E, 69SE	N32E, 42SE						
508	N52E, 81NW	N49E, 56SE						
509	N61E, 26SE	N21E, 50SE						
510	N40E, 59SE	N21E, 27SE						
511						214, 9	N33E, 48SE	
512	N37E, 46NW	N37E, 55SE						
513	N28E, 20SE	N30E, 44SE						
514	N30E, 44SE							

*Sta#	Bedding	Cleavage: S_1	Cleavage: $S_{1'}$	Cleavage: S_2 Axial Surface	Fracture	Fold: Hinge	Fold: Axial Surface	S_0xS_1 Intersection Lineation
BRF 515	N40E, 35SE	N40E, 58SE						
516	N22E, 35SE	N31E, 58SE						
517	N39E, 40NW							
518	N36E, 34NW	N44E, 46SE						
519	N05E, 25SE	N31E, 44SE						
520	N52E, 49NW	N49E, 45SE						
521	N39E, 39NW	N39E, 54SE						
522	N36E, 42NW	N36E, 49SE						
523	N49E, 43NW	N32E, 56SE						
524	N22E, 25SE	N07E, 47SE						
525	N49E, 52NW	N18E, 33SE						
526	N24E, 68SE	N24E, 46SE						
527	N41E, 85SE	N69E, 53SE						
528	N34E, 90	N43E, 53SE						
529		N42E, 42SE						
530	N43E, 55SE							
531	N66E, 60NW	N60E, 21SE						
532	N52E, 85SE	N53E, 36SE						
533	N45E, 70SE	N45E, 33SE						
534	N43E, 75SE	N43E, 33SE						
536	N51E, 56SE							
537	N40E, 60SE	N40E, 38SE						
538	N47E, 58SE							
539	N48E, 62SE							
540	N32E, 48SE	N32E, 32SE						
541	N33E, 54SE	N33E, 25SE						
542	N31E, 52SE	N31E, 28SE						
543	N30E, 62SE	N42E, 44SE						
544	N39E, 55SE							
545	N37E, 62SE	N37E, 48SE						
546	N31E, 45SE							
547	N45E, 64SE							
548	N45E, 42NW	N45E, 57SE						
549	N53E, 17NW	N42E, 41SE						
550	HORIZONTAL							
551	N25E, 64NW							
552	N31E, 69NW	N39E, 77SE						
553	N30E, 88SE	N30E, 42SE						
554	N36E, 62SE							
555	N33E, 65SE	N33E, 35SE						
556	N42E, 57SE	N42E, 30SE						
557	N52E, 58SE	N52E, 40SE						
558	N49E, 59SE							
559	N45E, 54SE							

*Sta#	Bedding	Cleavage S_1	Cleavage S_2	S_2 Axial Surface	Fracture	Fold Hinge	Fold Axial Surface	S_1xS_2 Intersection Lineation
BRF 560	N39E, 59SE	N39E, 39SE						
561	N44E, 57SE							
562	N46E, 24SE							
563	N44E, 20SE							
564	N36E, 58NW							
565	N41E, 85SE	N41E, 70SE						
566	N48E, 64SE							
567	N38E, 60SE							
568	N39E, 59SE							
569	N37E, 76SE							
570	N40E, 59SE							
571	N29E, 64SE							
572	N27E, 59SE							
573	N31E, 69SE							
574	N31E, 68SE							
575	N31E, 57SE	N31E, 39SE						
576	N30E, 55SE							
577	N35E, 57SE	N35E, 44SE						
578	N41E, 57SE	N41E, 30SE						
579	N44E, 59SE							
580	N32E, 59SE	N32E, 38SE						
581	N31E, 63SE	N31E, 44SE						
582	N27E, 65SE	N27E, 27SE						
583	N29E, 87SE							
584	N43E, 53SE							
585	N23E, 67SE	N23E, 18SE						
586	N25E, 62SE	N25E, 30SE						
587	N23E, 63SE	N23E, 43SE						
588	N51E, 56SE							
589		N31E, 37SE						
590	N40E, 52NW	N47E, 49SE						
591						220, 10	N61E, 39SE	
592	N41E, 71SE	N41E, 51SE						
593	N40E, 49SE							
594	N35E, 68SE	N35E, 24SE						
595	N36E, 70SE	N36E, 20SE						
596	N36E, 64SE							
597	N60E, 36NW	N44E, 44SE						
598	N57E, 68SE	N59E, 39SE						
599	N65E, 84SE	N65E, 38SE						
600	N53E, 75SE	N53E, 21SE						
601	N55E, 90	N65E, 57SE						
602		N39E, 44SE						
603	N34E, 64SE	N34E, 30SE						

*Sta#	Bedding	Cleavage S_1	Cleavage S_2	S_2 Axial Surface	Fracture	Fold Hinge	Fold Axial Surface	S_1xS_2 Intersection Lineation
BRF 604	N45E, 62NW	N45E, 40SE						
605	N54E, 60NW	N44E, 40SE						
606	N39E, 44NW	N39E, 45SE						
607	N38E, 30SE							
608	N40E, 35SE	N41E, 72SE						
609	N35E, 18SE	N22E, 52SE						
610	N45E, 46NW	N43E, 41SE						
611	N43E, 74SE				N63W, 70SW			
612	N34E, 78SE							
613	N30E, 15SE	N20E, 66SE						
614	N37E, 73SE							
615	N45E, 13NW							
616	N29E, 62NW	N29E, 38SE						
617	N35E, 30NW	N35E, 36SE						
618	N38E, 30SE	N38E, 58SE			N61E, 68SE			
619	N38E, 37SE	N43E, 30SE						
620		N41E, 52SE						
621	N57E, 34SE	N48E, 55SE						
623		N47E, 46SE						
624	N45E, 16SE	N55E, 42SE						
625	N30E, 44SE	N22E, 67SE				51, 24	N51E, 84SE	
626	N51E, 61NW	N16E, 46SE						
627	N56E, 71NW	N30E, 33SE						
628	N64E, 38NW	N29E, 33SE						
629	N75E, 52SE	N75E, 52SE						
630						245, 2	N67E, 44SE	
631	N35E, 44NW	N67E, 32SE						
632	N40E, 17NW	N39E, 12SE						
633	N51E, 85SE	N78E, 29SE						
634	N58E, 55NW	N63E, 27SE						
635						51, 16	N65E, 36SE	
636		N30E, 29SE						
637	N44E, 42NW	N37E, 42SE						
638	N34E, 62SE	N50E, 35SE						
639	N67E, 86NW	N52E, 32SE						
640	N31E, 37NW	N55E, 38SE						
641	N45E, 59NW	N30E, 27SE						
642		N47E, 44SE						
643	N44E, 66NW	N33E, 28SE						
644	N57E, 64NW	N38E, 12SE						
645		N49E, 65SE						
646	N47E, 48NW	N39E, 54SE						
647	N71W, 51NE	N24E, 52SE			N52E, 88NW			
648	N44E, 74SE	N17E, 54SE						

*Sta#	Bedding	Cleavage: S_1	Cleavage: S_{1a}	Cleavage: S_2 Axial Surface	Fracture	Fold: Hinge	Fold: Axial Surface	$S_o x S_1$ Intersection Lineation
BRF 649	N81W, 29NE	N22E, 37SE						
650	N79E, 76SE							
651	N61E, 54SE							
652	N51E, 45NW	N49E, 50SE						
653	N71E, 23SE							
654	N59E, 39NW	N29E, 42SE			N87E, 38SE			
655	N46E, 49NW	N24E, 39SE			N87E, 38SE			
656						217, 4	N37E, 45SE	
657	N39E, 59NW	N39E, 38SE						
658						207, 17	N36E, 55SE	
659	N48E, 82NW	N46E, 53SE						
660	N51E, 39NW	N48E, 59SE						
661	N52E, 36NW	N39E, 34SE						
662	N55E, 57NW	N45E, 39SE						
663		N35E, 46SE						
664	N39E, 57NW	N39E, 46SE						
665	N41E, 62NW	N41E, 34SE						
666	N57E, 64SE	N35E, 38SE						
667	N60E, 90	N57E, 41SE						
668	N43E, 51SE							
669	N39E, 69SE	N43E, 27SE						
670	N39E, 80NW	N42E, 56SE						
671	N43E, 82SE	N73E, 51SE						
672	N48E, 62SE							
673	N42E, 58SE							
674	N51E, 48SE							
675	N47E, 62SE							
676	N36E, 40SE	N36E, 40SE						
677	N32E, 40SE	N81W, 49SW			N81W, 49SW			
678	N36E, 55SE	N32E, 29SE						
679	N33E, 45SE							
680	N43E, 43SE	N43E, 32SE						
681	N41E, 58SE							
682	N58E, 81SE	N48E, 49SE						
683	N47E, 69SE							
684	N49E, 37NW							
685	N37E, 42NW	N34E, 62SE						
694	N56E, 42NW	N35E, 59SE						
695	N59E, 64SE	N48E, 39SE						
696	N57E, 90	N41E, 38SE						
697	N65E, 77SE	N45E, 29SE						69, 10
698	N56E, 59SE	N41E, 19SE						
699	N54E, 90	N50E, 37SE						
700	N57E, 49NW	N36E, 51SE						

*Sta#	Bedding	Cleavage: S_1	Cleavage: S_{1a}	Cleavage: S_2 Axial Surface	Fracture	Fold: Hinge	Fold: Axial Surface	$S_o x S_1$ Intersection Lineation
BRF 701		N59E, 56SE						
702	N48E, 47NW	N48E, 48SE						
703	N57E, 27SE							
704	N49E, 34NW	N29E, 43SE						
705	N41E, 35NW	N37E, 62SE						
TP 578	N35E, 89NW							
579	N59E, 51SE							
580		N22E, 28SE						
581	N39E, 43NW	N33E, 49SE						
582	N51E, 89NW	N43E, 44SE						
583	N41E, 88NW	N47E, 45SE						
584	N56E, 59NW	N41E, 61SE						
585	N55E, 24NW	N55E, 52SE						
586	N30E, 33SE	N30E, 33SE						
587	N35E, 39NW	N30E, 62SE						
588		N35E, 41SE						
589	N51E, 48NW							
590	N37E, 65NW	N37E, 42SE						
591	N47E, 68NW	N45E, 50SE						
592	N46E, 38NW	N55E, 50SE						
593	N49E, 48SE							
BRF 706	N43E, 68NW	N40E, 43SE						
707	N56E, 22SE	N44E, 38SE						
708	N56E, 64SE	N30E, 40SE						
709	N36E, 68SE							
710	N44E, 52SE				N07W, 64NE			
711	N40E, 73SE	N29E, 49SE						
712	N45E, 57SE							
713	N38E, 59SE				N75E, 63SE			
					N64W, 71NE			
714	N33E, 44SE	N33E, 68SE						
715	N67E, 51NW	N42E, 44SE			N69E, 78SE			
716	N45E, 60SE				N74E, 70NW			
717	N49E, 40SE							
718		N50E, 56SE						
719	N44E, 76SE							
721	N35E, 63SE							
722		N52E, 49SE						
723	N47E, 39NW	N47E, 53SE						
724	N55E, 82NW	N55E, 55SE						
725	N51E, 48SE	N51E, 22SE						
726	N51E, 84NW							
727	N55E, 63SE	N55E, 17SE						
728	N51E, 40NW	N49E, 43SE						

	Fabric Element							
		Cleavage				Fold		S_0xS_1
*Sta#	Bedding	S_1	$S_{1'}$	S_2 Axial Surface	Fracture	Hinge	Axial Surface	Intersection Lineation
BRF 729	N42E, 52NW	N49E, 53SE						
730	N58E, 47SE				N51W, 62NE(f)			
731	N53E, 48SE							
732	N43E, 69SE	N43E, 35SE						
733	N44E, 69SE	N44E, 32SE						
734	N51E, 54SE	N51E, 38SE			N62E, 33NW			
735	N52E, 62SE	N52E, 27SE						
736	N53E, 67SE	N53E, 24SE						
737	N48E, 69SE	N48E, 55SE						
738	N40E, 68SE							
739	N63E, 56SE	N63E, 39SE						
740	N25E, 78SE	N25E, 46SE						
741	N45E, 57SE							
742	N56E, 46SE							
743	N40E, 68SE							
744	N49E, 71SE	N49E, 46SE						
745	N63E, 30SE	N63E, 18SE						
746					N72W, 62SW	218, 10	N38E, 54SE	
747	N40E, 85NW	N22E, 51SE						
748	N33E, 45SE				N663, 81SE			
					N54E, 69SE			
					N49W, 78SW			
					N662, 84SE			
749	N51E, 28SE	N44E, 42SE						
750	N55E, 16SE	N46E, 61SE						
751	N33E, 83SE	N33E, 49SE			N70E, 77SE			
752		N51E, 50SE						
753	N34E, 39SE							
754	N39E, 40SE							
755	N42E, 76SE	N42E, 49SE						
756	N36E, 64SE	N36E, 38SE						
757		N48E, 56SE						
758	N45E, 59SE	N45E, 59SE						
759	N39E, 59SE				N67E, 77SE			
					N61E, 80SE			
760	N36E, 62SE							
761	N52E, 64SE				N48E, 55SE			
762	N56E, 75NW				N66W, 54SW			
763	N52E, 59SE	N52E, 38SE						
764	N54E, 68SE							
765	N51E, 54SE							
766	N56E, 54SE							
767	N56E, 43SE	N56E, 22SE						
768	N59E, 48SE				N05E, 88NW			

	Fabric Element							
		Cleavage				Fold		S_0xS_1
*Sta#	Bedding	S_1	$S_{1'}$	S_2 Axial Surface	Fracture	Hinge	Axial Surface	Intersection Lineation
BRF 769	N57E, 50SE				N15W, 84NE			
770	N57E, 60SE							
771	N55E, 56SE							
772	N30E, 54SE							
773		N57E, 56SE						
774	N76E, 36SE	N61E, 60SE						
775		N55E, 38SE						
776	N67E, 72SE							
777	N52E, 67SE	N60E, 59SE						
778	N46E, 60SE	N46E, 46SE						
779	N69E, 72SE							
TP 594	N32E, 18NW	N32E, 48SE						
595	N47E, 36SE	N57E, 72SE						
596	N35E, 24SE	N33E, 47SE						
597	N31E, 32SE				N89E, 82NW			
598	N36E, 25SE							
599	N28E, 20SE							
600						203, 5	N23E, 25SE	
601	N22E, 62NW							
602	N39E, 44SE	N35E, 69SE						
603	N37E, 52SE							
604	N42E, 70NW	N42E, 51SE						
605	N37E, 45SE							
606	N61E, 60SE							
607		N34E, 49SE						
608	HORIZONTAL							
609	N32E, 54SE							
610	N46E, 41SE							
611	N54E, 47SE	N37E, 47NW			N47W, 68NE			
612	N18E, 27SE	N39E, 54SE						
613	N42E, 26NW	N25E, 44SE						
614	N32E, 69NW	N37E, 70SE						
615	N31E, 85NW							
616	N35E, 80SE							
617	N27E, 68NW	N10E, 60SE						
618		N26E, 64SE						
619	N20E, 74NW				N90E, 80N			
620	N48E, 56SE							
621	N54E, 22SE							
622	N53E, 35SE							
623	N55E, 27SE	N36E, 57SE			N65W, 68NE			
624	N41E, 32SE	N31E, 81SE						
625		N31E, 47SE						
626		N31E, 71SE						

*Sta#	Bedding	Cleavage: S_1	Cleavage: S_2	Cleavage: S_2 Axial Surface	Fracture	Fold: Hinge	Fold: Axial Surface	S_0xS_1 Intersection Lineation
TP 627	N57E, 46SE				N45E, 66SE(f)			
628	N33E, 73SE							
629	N49E, 42SE							
630	N48E, 22SE							
631	N33E, 45SE							
632	N43E, 45SE							
633	N39E, 43SE	N39E, 62SE						
634	N39E, 34SE							
635	N35E, 39SE							
636	N32E, 17NW	N23E, 30SE						
637		N33E, 37SE						
638	N36E, 48NW	N36E, 25SE						
639	N37E, 12NW	N37E, 37SE						
640	N23E, 25SE	N34E, 29SE						
641	HORIZONTAL	HORIZONTAL						
642	N47E, 34SE	N47E, 36SE						
643	HORIZONTAL							
644	N59E, 19NW							
645	N39E, 64SE	N39E, 24SE						
646	N66E, 69SE	N42E, 19SE						
647	N39E, 29SE	N39E, 56SE						
648	N33E, 52NW	N28E, 39SE						
649	N41E, 49NW							
650	N27E, 28NW	N29E, 43SE						
651	N30E, 43NW							
652	N45E, 29SE							
653	N69E, 29SE							
654	N53E, 51SE							
655	N44E, 45SE							
656	N31E, 32SE							
657	N59E, 34SE							
658						53, 25	N22W, 17NE	
659	N33E, 48SE							
660	N23E, 43SE							
661	N34E, 47SE							
662	N47E, 35SE							
663	N39E, 38SE				N35W, 68NE			
664	N16E, 55SE							
665	N71E, 59SE							
666		N41E, 65SE						
667	N81E, 41SE							
668	N58E, 59SE							
669	N58E, 31SE							
670	N52E, 44SE							

*Sta#	Bedding	Cleavage: S_1	Cleavage: S_2	Cleavage: S_2 Axial Surface	Fracture	Fold: Hinge	Fold: Axial Surface	S_0xS_1 Intersection Lineation
TP 671	N47E, 51SE							
672	N43E, 11SE	N43E, 50SE						
673	N31E, 09NW	N31E, 87SE						
674	N21E, 90	N31E, 54SE						
675	N21E, 80NW							
676	N31E, 64NW							
677		N39E, 68SE						
678						31, 17	N31E, 23SE	
679	N41E, 48SE							
680	N43E, 36SE							
681	N54E, 50SE							
BRF 780	N47E, 59SE							
781		N39E, 32SE						
782	N49E, 45SE							
783	N42E, 52SE							
784	N34E, 26NW							
785	N65E, 46NW							
786		N40E, 64SE						
787		N49E, 55SE						
788		N56E, 49SE						
789		N47E, 51SE						
790	N37E, 54SE							
791	N54E, 57SE							
TP 682	N63E, 11NW	N63E, 36SE						
683		N37E, 29SE						
684	HORIZONTAL	N47E, 33SE						
685	N25E, 11SE	N25E, 50SE						
686	HORIZONTAL	N64E, 32SE						
687	N58E, 05SE	N64E, 45SE						
688	N56E, 24SE	N56E, 39SE						
689		N71E, 25SE						
690		N51E, 12SE						
691		N45E, 36SE						
692	N49E, 17SE	N50E, 75SE						
693	N27E, 13SE	N27E, 46SE						
694		N35E, 59SE						
695		N31E, 39SE						
696	N35E, 30SE							
697	N45E, 48NW	N45E, 56SE						
BRF 792	N53E, 11NW	N45E, 27SE						
793	N34E, 07NW	N34E, 18SE						
TP 698	N41E, 70NW							
699	N39E, 30NW	N39E, 43SE						
700	N49E, 26NW	N49E, 36SE						

*Sta#	Bedding	Fabric Element: Cleavage S_1	Cleavage S_{1a}	Cleavage S_2 Axial Surface	Fracture	Fold Hinge	Fold Axial Surface	S_0xS_1 Intersection Lineation
TP 701	N50E, 20SE							
702	N61E, 31SE	N61E, 59SE						
703		N41E, 50SE						
704	N65E, 38SE				N41E, 65SE(f)			
705	N48E, 46SE							
706	N40E, 41SE	N40E, 58SE						
707	N41E, 45SE							
708	N30E, 30SE							
709	N50E, 58SE							
710	N54E, 31SE				N65E, 85SE			
711	N66E, 32SE							
712	N53E, 11SE				N71W, 87NE			
713	N32E, 17NW	N33E, 30SE						
714	N49E, 22NW							
715	N39E, 38SE							
716	N61E, 52SE							
717		N40E, 27SE						
BRF 794	N64E, 68SE	N34E, 22SE						
795	N44E, 72NW	N44E, 32SE						
796	N63E, 45NW	N51E, 41SE						
797	N68E, 41NW	N52E, 40SE						
798	N55E, 59NW	N35E, 52SE						
799	N64E, 50NW							
800	N58E, 63SE	N49E, 39SE						
801	N37E, 37NW	N26E, 55SE						
802	N49E, 49SE							
803	N41E, 29SE							
804	N36E, 56SE							
805	N37E, 64SE							
806	N55E, 11NW	N52E, 43SE						
807	N62E, 48NW	N48E, 50SE						
808						229, 5	N40E, 46SE	
809	N44E, 24NW	N44E, 45SE						
810	N51E, 68SE	N51E, 44SE						
811	N61E, 64SE	N61E, 64SE						
812	N53E, 46SE				N49W, 78NE			
813	N51E, 36SE							
814	N54E, 36SE							
815	N40E, 51SE							
816	N55E, 49SE							
817	N61E, 63SE							
818	N65E, 52SE							
819	N61E, 62SE							
820	N66E, 50SE							

*Sta#	Bedding	Fabric Element: Cleavage S_1	Cleavage S_{1a}	Cleavage S_2 Axial Surface	Fracture	Fold Hinge	Fold Axial Surface	S_0xS_1 Intersection Lineation
BRF 821	N44E, 53SE				N53W, 59SW			
822	N66E, 69SE	N58E, 19SE						
823	N59E, 58SE	N57E, 31SE						
824	N47E, 79SE							
825	N41E, 73SE	N41E, 37SE						
826	N53E, 68SE							
827	N59E, 74SE							
828	N27E, 46SE							
829	N38E, 58SE							
830	N44E, 58SE							
TP 718	N59E, 58NW	N25E, 36SE						
719	N27E, 31SE							
720		N25E, 43SE						
721	N34E, 29NW	N34E, 69SE						
722						45, 5	N45E, 19SE	
723	N61E, 12NW							
724	N40E, 27SE	N35E, 80SE						
725	HORIZONTAL	N36E, 50SE						
726	N37E, 57NW	N25E, 47SE						
727	N40E, 69NW	N31E, 39SE						
728	N54E, 31NW	N44E, 21SE						
729	HORIZONTAL	N30E, 21SE						
730	N30E, 11NW	N30E, 29SE						
731	N44E, 31NW	N42E, 32SE						
732	N68E, 34NW	N30E, 43SE						
733	N49E, 64SE	N49E, 34SE						
734	N57E, 88SE	N57E, 41SE						
735	N52E, 39NW	N52E, 25SE						
736	N53E, 47NW	N44E, 46SE						
737	N69E, 53NW	N54E, 26SE						
738	N50E, 39NW	N50E, 35SE			N54W, 84SW			
739	N60E, 51NW	N45E, 35SE						
740	N41E, 68NW	N41E, 37SE						
741	N57E, 12NW	N37E, 48SE						
742	N51E, 11NW	N49E, 55SE						
743	N25E, 43SE	N29E, 63SE						
744	N61E, 42NW	N39E, 52SE						
745		N40E, 71SE						
746	N47E, 38SE	N33E, 72SE						
747	N63E, 45SE				N73W, 45NW			
748	N32E, 29NW	N42E, 68SE						
749	N47E, 45SE							
750	N41E, 44SE							
751		N33E, 19SE						

*Sta#	Bedding	S_1	S_{1a}	S_2 Axial Surface	Fracture	Fold: Hinge	Fold: Axial Surface	$S_0 x S_1$ Intersection Lineation
IP 752	N12W, 32NE	N12W, 32NE						
753	N45E, 22NW	N29E, 48SE						
754	N33E, 22NW	N33E, 47SE						
755	N39E, 21NW	N24E, 44SE						
756	N69E, 58NW	N24E, 29SE						
757	N51E, 90							
758	N49E, 58NW	N49E, 38SE						
759	N43E, 59NW							
760	N29E, 17NW	N29E, 50SE						
761	N59E, 69NW							
762		N19E, 48SE						
763		N55E, 62SE						
764		N59E, 53SE						
765		N31E, 34SE						
766		N59E, 56SE						
767	N44E, 58SE							
768	N51E, 59SE	N51E, 63SE						
769	N57E, 61SE							
770	N41E, 36SE							
771	N46E, 31SE							
772	N59E, 59SE							
773	N64E, 39SE							
774		N37E, 54SE						
775	N23E, 46SE							
776	N38E, 41SE	N22E, 74SE						
777	N58E, 45SE							
778						239, 5	N59E, 82SE	
						237, 7	N57E, 70SE	
						235, 3	N55E, 68SE	
779	N55E, 49SE							
780	N39E, 45SE	N39E, 52SE						
781						232, 10	N52E, 64SE	
782	N51E, 43SE	N51E, 76SE						
783						41, 3	N41E, 74SE	
784	N41E, 42NW	N41E, 66SE						
785	N48E, 70NW					42, 24	N42E, 68SE	
786	N53E, 58NW							
787	N34E, 47NW							
788	N28E, 50NW							
789	N53E, 33SE							
790		N64E, 60SE						
791	N34E, 45SE							
792	N60E, 30SE							
793	N63E, 33SE							

*Sta#	Bedding	S_1	S_{1a}	S_2 Axial Surface	Fracture	Fold: Hinge	Fold: Axial Surface	$S_0 x S_1$ Intersection Lineation
IP 794	N74W, 48NE							
795	N49E, 62SE	N49E, 62SE						
796	N65E, 44SE							
797	N44E, 46SE							
798	N45E, 53SE							
799	N49E, 82NW							
800	N21E, 57NW							
801		N27E, 44SE						
802	N60E, 44SE							
803	N40E, 50SE							
804	N58E, 35SE							
805	N75W, 35SW							
806	N65E, 32SE							
807	N88E, 71SE							
808	N83E, 34SE				N20E, 79SE			
809	N60E, 30SE							
810	N33E, 72NW							
811	N28E, 7NW							
812	N41E, 41SE							
813						43, 6	N43E, 42SE	
814	N38E, 05SE							
815	N32E, 19NW	N32E, 74SE						
816		N33E, 56SE						
817		N33E, 56SE						
818		N37E, 73SE						
819	N48E, 31NW	N48E, 72SE						
820		N47E, 49SE						
821		N57E, 82SE						
822	N75W, 25SW	N47E, 57SE						
823		N45E, 50SE						
824	N30E, 30SE	N30E, 65SE						
825		N88E, 60SE						
826	N65E, 46SE							
827	N48E, 30SE	N48E, 30SE						
828	N37E, 24SE							
829	N71E, 55SE							
830	N59E, 44SE	N59E, 44SE						
831	N33E, 39SE							
832	HORIZONTAL							
833	N20E, 54NW							
834	N72E, 35SE							
835	N39E, 33NW	N50E, 68SE						
836						48, 18	N48E, 65SE	
837	N46E, 39SE	N39E, 86SE						

*Sta#	Bedding	Cleavage S_1	Cleavage S_{1a}	Cleavage S_2 Axial Surface	Fracture	Fold Hinge	Fold Axial Surface	S_0xS_1 Intersection Lineation
TP 838	N74E, 39SE	N76E, 54SE						
839	N64E, 48SE							
840	N53E, 35SE	N63E, 82SE						
841	N57E, 47SE	N57E, 47SE	N65E, 31NW					
842	N53E, 38SE	N53E, 64SE						
843	N49E, 51SE	N49E, 68SE						
844	N48E, 41SE	N45E, 72SE						
845	N37E, 70NW	N46E, 46SE						
846	N85E, 38NW	N52E, 48SE						
847	N74E, 31SE							
848		N65E, 41SE						
849	N55E, 72SE	N55E, 72SE						
850	N35E, 84NW	N35E, 48SE						
851	N39E, 37SE							
852	N36E, 31SE	N36E, 79SE						
853	N05E, 45NW							
854	N35E, 29NW							
855	N37E, 69SE							
F 12								47, 9
17	N43E, 44NW	N53E, 43SE						
TP 856	N37E, 26SE				N77E, 84SE(f)			
857	N36E, 24SE							
858	N40E, 19SE	N40E, 40SE						
859	N32E, 18SE	N26E, 59SE						
860	N39E, 11SE							
861	N39E, 14SE							
862	N33E, 48SE							
863	N52E, 72SE							
864	N39E, 54SE	N39E, 54SE						
865	N37E, 58SE	N37E, 58SE						
866	N43E, 47SE							
867	N53E, 40NW	N45E, 48SE						
868	N43E, 20NW	N20E, 24SE						
869						61, 18	N61E, 19SE	
870	N55E, 22SE							
871	N51E, 37SE							
872	N49E, 37SE							
873	N39E, 64SE							
874	N46E, 29SE	N46E, 51SE						
875	N33E, 72SE	N33E, 72SE						
876	N43E, 58SE	N43E, 81SE						
877		N33E, 82SE						
879	N64E, 51NW	N67E, 25SE						
880	N51E, 57NW	N47E, 27SE						

*Sta#	Bedding	Cleavage S_1	Cleavage S_{1a}	Cleavage S_2 Axial Surface	Fracture	Fold Hinge	Fold Axial Surface	S_0xS_1 Intersection Lineation
TP 881	N64E, 43SE							
882	N62E, 31NW							
883	N47E, 17NW	N47E, 84SE						
884		N76E, 57SE						
885	N52E, 37SE							
886	N41E, 61SE	N41E, 61SE						
887	N49E, 41SE	N49E, 41SE			N74E, 37NW			
888	HORIZONTAL							
889	N37E, 40SE							
890		N37E, 17SE						
891	N45E, 57SE							
892	N32E, 57NW	N62E, 57SE						
893	N59E, 37SE							
894	N46E, 63SE	N46E, 63SE						
F 18	N41E, 23SE				N52W, 85SW			
19	N49E, 82SE	N49E, 52SE						
20	N39E, 68SE							
21	N39E, 65SE	N25E, 33SE			N17W, 84NE			
22	N22E, 32SE							
23	N51E, 82NW	N51E, 43SE						
24	N63E, 88SE	N68E, 33SE						
25	N50E, 84SE	N63E, 33SE						
26	N31E, 28NW							
27	N39E, 51SE							
28	N54E, 68SE	N54E, 55SE						
29	N41E, 63SE							
30	N49E, 23NW							
31	N36E, 59SE							
32	N38E, 64SE							
33	N52E, 53SE							
34	N63E, 66SE							
35	N59E, 66SE							
36	N46E, 68SE							
37	N61E, 60SE							
38	N58E, 74SE							
39	N33E, 64SE							
40	N47E, 64SE							
41	N42E, 53SE							
42	N41E, 51NW	N48E, 71SE						
43	N35E, 44NW	N45E, 56SE						
44	N43E, 55NW							
45	N36E, 90							
46	N44E, 90							
47	N51E, 47NW							

		Fabric Element						
		Cleavage				Fold		S_0xS_1
*Sta#	Bedding	S_1	$S_{1'}$	S_2 Axial Surface	Fracture	Hinge	Axial Surface	Intersection Lineation
F 48	N45E, 17NW	N42E, 67SE						
49	N49E, 31NW	N49E, 53SE						
50		N40E, 54SE						
51	N45E, 82NW							
52	N45E, 36NW							
53	N39E, 48NW							
54						21, 2	N21E, 57SE	
55	N35E, 12SE							
56	N41E, 24NW							
57	N34E, 17SE							
58	N43E, 17NW	N36E, 28SE						
59	N57E, 15NW							
TP 895	N35E, 23NW							
896	N33E, 17NW	N31E, 41SE						
897	N19E, 16NW	N19E, 31SE						
F 60	N37E, 15SE	N37E, 63SE						
61	N37E, 32SE	N30E, 74SE						
62	N42E, 23SE							
63	N41E, 19SE							
64	N29E, 51SE							
TP 898	N50E, 46SE							
899	N37E, 23SE							
900	N72E, 90							
901	N56E, 31SE							
902	N45E, 56SE							
903	N14E, 56SE							
904	N49E, 51SE							
905	N44E, 90							
906	N29E, 59NW							
907					N0E, 56W			
908	N40W, 52SW							
909	N45E, 55NW							
910	N34E, 56SE							
911	N56E, 68SE							
912	N49E, 56SE							
913	N61E, 35SE							
914	N44E, 46SE							
915	N49E, 55SE							
916	N49E, 29SE							
917	N23E, 35SE							
918	N56E, 47SE							
919	N44E, 63NW							
920	N0E, 53W							
921	N53E, 52SE							

		Fabric Element						
		Cleavage				Fold		S_0xS_1
*Sta#	Bedding	S_1	$S_{1'}$	S_2 Axial Surface	Fracture	Hinge	Axial Surface	Intersection Lineation
TP 922	N46E, 31SE							
923	N31E, 29SE							
924	N53E, 43SE							
925	N43E, 48SE							
926	N29E, 18SE	N35E, 72SE						
927	N26E, 61SE	N33E, 42SE						
928	N28E, 24SE							
929	N52E, 32SE							
930	N29E, 56SE							
931	N56E, 63SE							
932	N55E, 21SE	N47E, 49SE						
933						56, 30	N56E, 58SE	
934	N47E, 47SE							
935	N63E, 63SE							
936	N67E, 46SE							
937	N61E, 37NW							
938	N61E, 49SE							
939	N31W, 90							
940	N34E, 45SE							
941	N34E, 49SE							
942	N57E, 24SE							
943	N27E, 26SE							
944		N55E, 47SE						
945	N43E, 38SE							
946	N54E, 26SE							
947	N39E, 43SE	N39E, 48SE	N56E, 65NW		N04E, 79NW			
					N20E, 71NW			
948	N31E, 52SE							
949	N49E, 71SE							
950	HORIZONTAL							
951						13, 21	N33E, 20SE	
952	N65E, 52NW							
953	N31E, 61SE	N31E, 36SE						
954	N45W, 90							
955	N37E, 72SE							
BRF 831	N54E, 30SE	N30E, 44SE						
832	N57E, 31SE	N57E, 54SE			N0E, 87E			
833						22S, 34	N53E, 56SE	
834	N49E, 33SE	N55E, 65SE			N42W, 72NE			
835	N57E, 24SE	N57E, 57SE						
836	N49E, 35SE					46, 10	N37E, 76SE	
837	N59E, 46SE							
838	N59E, 79NW							
839	N50E, 25SE	N46E, 63SE				55, 17	N46E, 63SE	

*Sta#	Bedding	Cleavage S_1	Cleavage $S_{1'}$	S_2 Axial Surface	Fracture	Fold Hinge	Fold Axial Surface	$S_2 \times S_1$ Intersection Lineation
BRF 840						250, 6	N61E, 53NW	
841						18, 10	N07E, 74SE	
842	N41E, 41SE	N41E, 64SE						
844	N42E, 42SE	N71E, 66NW						
845	N43E, 44SE	N76E, 53NW						
846	N44E, 58SE							
847	N40E, 63NW							
848	N53E, 61NW				N0E, 71W(f)			
849	N47E, 48SE							
850	HORIZONTAL	N49E, 61SE						
851	N57E, 68SE	N57E, 68SE						
852	N46E, 41SE							
TP 956	N44E, 73SE							
957						220, 20	N40E, 55SE	
958	N39E, 51NW	N35E, 30SE			N26E, 40SE(f) N73W, 85NE			
959	N41E, 84NW							
960	N11W, 31SW							
961	N22E, 43SE							
962	N36E, 43SE							
963	N54E, 58SE							
964	N38E, 30SE				N18E, 73SW			
965	N35E, 31SE							
966	N42E, 42NW	N39E, 79SE						
967	N36E, 40NW	N32E, 42SE						
968	N43E, 56SE							
969	N61E, 30NW	N55E, 63SE						
BRF 853	N34E, 65NW							
854	N45E, 90	N56E, 40SE						
855	N49E, 64SE							
856		N51E, 60SE			N77E, 84SE			
857	N57E, 69SE							
858	N54E, 66SE				N67E, 71SE			
859	N15E, 61SE				N50E, 34SE			
860		N24E, 42SE						
861	N44E, 77SE							
862	N37E, 66SE		N58E, 47NW					
863		N49E, 59SE						
864	N48E, 64SE							
865		N59E, 69SE						
866	N45E, 63SE							
867	N38E, 57SE							
868	N53E, 58SE							
869	N43E, 55SE							

*Sta#	Bedding	Cleavage S_1	Cleavage $S_{1'}$	S_2 Axial Surface	Fracture	Fold Hinge	Fold Axial Surface	$S_2 \times S_1$ Intersection Lineation
TP 970	N35E, 16NW	N35E, 59SE						
971	N28E, 21SE	N36E, 43SE						38, 2
972	N62E, 18SE	N17E, 69SE						
973	N36E, 82NW	N32E, 35SE						
974	N48E, 60NW	N26E, 41SE						
975	N37E, 62NW				N42W, 42NE			
976	N61E, 74NW	N55E, 55SE						
977	N31E, 71SE	N38E, 39SE						
978		N39E, 32SE						
979	N21E, 22NW							
980	N29E, 26NW	N29E, 31SE						
981	N0E, 09W	N28E, 21SE						
982	N21E, 06NW	N13E, 21SE						
983	N27E, 03NW	N27E, 17SE						
984	N18E, 39NW	N27E, 22SE						
985	N29E, 28NW	N21E, 26SE						
986	HORIZONTAL	N49E, 50SE						
987	N30E, 59NW	N34E, 40SE						
988	N20E, 52NW	N30E, 31SE						
989	N18E, 10NW	N35E, 45SE						
990	N02E, 82NW	N26E, 35SE						
991	N48E, 55NW	N48E, 21SE						
992		N35E, 52SE						
993		N48E, 42SE						
994	N28E, 11SE	N34E, 23SE						
995	N48E, 14SE	N48E, 41SE						
996	N24E, 24SE							
997	N21E, 28SE				N62W, 90			
998	N48E, 17SE				N68E, 90			
999	N44E, 24SE	N44E, 69SE						
1000		N31E, 31SE						
1001		N21E, 24SE						
1002	N64E, 55NW	N66E, 32SE						
1003	N78E, 66NW	N32E, 25SE						
1004	N52E, 18SE	N56E, 46SE						
1005	N58E, 90							
1006	N26E, 59NW	N23E, 56SE						
1007	N57E, 60SE							
1008		N51E, 50SE						
1009	N59E, 45SE							
1010	N49E, 72SE							
1011	N44E, 43NW							
1012	N79E, 61SE							
1013		N44E, 17SE						

*Sta#	Bedding	Cleavage S_1	Cleavage S_{1a}	S_2 Axial Surface	Fracture	Fold Hinge	Fold Axial Surface	$S_{1a}xS_1$ Intersection Lineation
TP 1014	N44E, 40SE				N15W, 72NE			
1015	N37E, 38SE				N57E, 90			
1016	N24E, 64SE							
1017	N44E, 40SE							
1018	N67E, 50SE							
1019	N37E, 62SE							
1020	N36E, 64SE							
1021	N71E, 35NW							
1022	N75E, 51NW	N22E, 47SE						
1023	N22E, 62NW							
1024	N39E, 44SE							
1025	N19E, 79SE							
1026	N29E, 72NW							
1027	N46E, 16SE	N46E, 31SE						
1028	N50E, 03NW	N50E, 77SE						
1029	HORIZONTAL							
1030	N26E, 20SE				N36W, 79NE			
1031	N21E, 13SE							
1032		N32E, 52SE						
1033	N28E, 38NW							
1034	N75E, 28SE							
1035	N32E, 52SE				N69E, 83NW(f)			
					N21W, 71NE			
1036	N27E, 36SE							
1037	N29E, 56NW							
1038	N35E, 48SE	N39E, 39SE						
1039	N55E, 60SE							
1040	N65E, 34SE							
1041	N54E, 34SE							
1042	N53E, 36SE							
1043	N24E, 55NW	N36E, 60SE						
1044	N21E, 70NW							
1045	N57E, 19SE	N35E, 45SE						
1046	N16E, 88SE							
1047	N51E, 74NW							
1048	N75W, 24SW							
1049	N34E, 41NW							
1050	N38E, 40NW							
1051	N63E, 44SE							
BRF 870	N68E, 33SE							
871	N62E, 24SE				N48E, 44SE			
872	N51E, 62NW							
873		N37E, 56SE						
874	N42E, 50SE							

*Sta#	Bedding	Cleavage S_1	Cleavage S_{1a}	S_2 Axial Surface	Fracture	Fold Hinge	Fold Axial Surface	$S_{1a}xS_1$ Intersection Lineation
BRF 875	N59E, 85SE							
876						44, 6	N44E, 58SE	
TP 1052	N54E, 47SE							
1053	N44E, 34SE				N38E, 64SE(f)			
					N42W, 90			
1054	N28E, 65SE							
1055	N40E, 59SE							
1056		N29E, 49SE						
1057	N63E, 64SE	N27E, 24SE						
1058	N35E, 30NW	N32E, 51SE						
1059	N37E, 26NW	N34E, 41SE						
1060	N21E, 12NW	N21E, 52SE						201, 2
1061	N32E, 24SE	N21E, 41SE						
1062	N44E, 21NW	N41E, 34SE						
1063		N24E, 41SE						
1064	N69E, 15NW	N47E, 48SE						
1065	N78E, 24NW	N41E, 38SE						
1066	N72E, 24NW	N59E, 44SE						
1067	N42E, 58NW	N37E, 26SE			N29W, 66SW			
1068	N58E, 36NW	N54E, 40SE						
1069		N45E, 36SE						
1070	N49E, 50NW	N47E, 34SE						
1071	N56E, 04NW	N56E, 56SE						
1072	N41E, 08NW	N31E, 61SE						
1073	N57E, 19NW	N44E, 36SE			N0E, 90			
1074	N41E, 62NW	N41E, 49SE						
1075	N49E, 59NW							
1076	N45E, 24SE	N39E, 49SE						
1077	N41E, 16SE	N35E, 38SE						
1078	N36E, 14SE	N36E, 49SE						
1079	N55E, 14SE	N33E, 48SE						
1080	N47E, 06NW	N40E, 44SE						
1081	N56E, 03NW	N32E, 44SE						
1082	N59E, 26SE							
1083	N60E, 18NW	N43E, 34SE						
1084	N35E, 32NW	N42E, 45SE						
1085	N48E, 15SE							
1086	N24E, 21NW							
1087	N39E, 06SE							
1088		N41E, 46SE						
1089	N53E, 20SE	N55E, 56SE						
1090	N41E, 19SE							
1091	N36E, 90							
1092	N33E, 61SE							

*Sta#	Bedding	Cleavage: S_1	Cleavage: S_{1a}	Cleavage: S_2 Axial Surface	Fracture	Fold: Hinge	Fold: Axial Surface	S_0xS_1 Intersection Lineation
TP 1093	N41E, 06SE	N35E, 061SE	N45E, 69NW					
1094	HORIZONTAL							
1095	N10E, 30SE	N29E, 665E						
1096	HORIZONTAL							
1097	N25E, 495E							
1098	N52E, 395E							
1099	N36E, 425E							
1100	N50E, 665E							
1101	N54E, 345E							
1102	N52E, 80NW							
1103	N53E, 28NW							
1104	N36E, 70NW	N42E, 825E						
1105		N37E, 79NW						
1106	N46E, 46NW							
1107	N58E, 395E							
1108						38, 11	N61E, 355E	
1109	HORIZONTAL							
1110	N46E, 385E							
1111	N66E, 235E							
1112	N39E, 255E							
1113	N37E, 185E							
1114	N33E, 225E	N22E, 825E			N64W, 72NE			
1115	N58E, 145E							
1116	N27E, 46NW							
1117						52, 12	N48E, 865E	
1118	N38E, 365E	N32E, 885E						
1119	N30E, 66NW							
1120	N44E, 175E	N39E, 175E						
1121	N23E, 10SE							
1122	N41E, 61NW							
1123	N49E, 24NW							
1124	N56E, 095E	N33E, 725E			N52W, 68NE			
1125	N62E, 115E							
1126	N44E, 395E							
1127	N55E, 335E							
1128	N33E, 185E							
1129	N47E, 865E							
1130	N40E, 475E	N42E, 84NW						
1131	N22E, 395E	N25E, 865E						
1132	N38E, 865E							
1133	N10E, 105E	N25E, 645E				29, 6	N31E, 615E	
1134	N41E, 245E	N36E, 455E						
1135	N40E, 135E	N42E, 445E						
1136	N50E, 265E	N29E, 495E						

*Sta#	Bedding	Cleavage: S_1	Cleavage: S_{1a}	Cleavage: S_2 Axial Surface	Fracture	Fold: Hinge	Fold: Axial Surface	S_0xS_1 Intersection Lineation
TP 1137	HORIZONTAL	N04E, 20SE						
1138	N10E, 125E							
1139	N74E, 285E	N50E, 41SE						
1140	N52E, 185E	N53E, 47SE			N04W, 57NE			
1141	N68E, 385E	N68E, 54SE						
1142	N38E, 235E							354, 22
1143	HORIZONTAL	N30E, 17SE						44, 10
1144	N58E, 30SE	N40E, 51SE						
1145	N43E, 46NW							
1146	N36E, 725E							
1147	N33E, 265E							
1148	N39E, 165E				N67E, 900			
1149	HORIZONTAL							
1150	N23E, 41SE							
1151	N54E, 16SE				N67E, 90			
1152	N40E, 48SE							
1153	N41E, 38SE							
1154	N67E, 38NW							
1155	N36E, 20SE							
1156	N23E, 39SE							
1157	N37E, 30SE							
1158	N37E, 395E	N27E, 54SE						
1159	N32E, 265E							
1160	N37E, 215E							
1161	N59E, 275E							
1162	N33W, 205W	N37E, 64SE						
1163	N41E, 48SE	N41E, 62SE						
1164	N55E, 24SE	N39E, 55SE						
1165		N35E, 68SE						
1166		N49E, 60SE						
1167	N44E, 26SE							
1168		N41E, 52SE						
1169	N43E, 285E	N23E, 60SE						
1170	N43E, 385E							
1171	N26E, 285E	N26E, 68SE						
1172	N28E, 29SE							
1173						208, 3	N37E, 31SE	
1174	N71E, 44SE	N45E, 60SE						
1175	N81E, 605E	N79E, 85SE						
1176	N30E, 36SE							
1177	N47E, 59SE	N47E, 59SE						
1178	N34E, 185E	N72E, 09NW						
1179	N37E, 175E							
1180	N39E, 15SE	N38E, 38SE						

		Fabric Element						
		Cleavage				Fold		$S_0 x S_1$
*Sta#	Bedding	S_1	S_{1a}	S_2 Axial Surface	Fracture	Hinge	Axial Surface	Intersection Lineation
TP 1181	N38E, 35SE	N56E, 70SE						
1182	N71E, 40SE							
1183	N52E, 63SE	N52E, 46SE						
1184	N47E, 60SE							
1185	N51E, 59SE	N51E, 31SE						
1186	N46E, 62SE							
1187	N55E, 59SE	N48E, 31SE						
1188	N52E, 57SE							
1189	N41E, 55SE							
1190	N54E, 58SE	N54E, 58SE						
1191	N48E, 59SE	N49E, 31SE						
1192	N44E, 56SE							
1193	N47E, 42SE							
1194	N57E, 42SE	N52E, 27SE						
1195	N62E, 40SE							
1196	N41E, 69SE	N46E, 36SE						
1197	N59E, 82SE	N49E, 48SE						
1198	N45E, 20NW	N46E, 58SE						
1199	N45E, 47SE				N55W, 80NE			
1200	N55E, 53SE							
1201	N56E, 50SE							
1202	N49E, 12SE							
1203	N40E, 12SE							
1204		N49E, 60SE						
1205	N41E, 35NW	N37E, 38SE						
1206	N47E, 34NW	N27E, 43SE						
1207	N21E, 56NW	N37E, 18SE						
1208	HORIZONTAL							
1209	N21E, 14NW							
1210	HORIZONTAL							
1211	HORIZONTAL							
1212	N0E, 14E							
1213		N47E, 22SE						
1214	HORIZONTAL	N21E, 36SE						
1215	N21E, 26SE	N21E, 46SE						
1216	N44E, 59SE							
1217	N22E, 39NW	N32E, 14SE						
1218	N20E, 03NW	N11E, 39SE						
1219	HORIZONTAL	HORIZONTAL						
1220	N20E, 16NW	N29E, 35SE						
1221		N35E, 20SE						
1222	N22E, 12NW	N27E, 25SE						
1223	N27E, 16SE	N27E, 30SE						
1224	N33E, 09SE	N26E, 30SE						

		Fabric Element						
		Cleavage				Fold		$S_0 x S_1$
*Sta#	Bedding	S_1	S_{1a}	S_2 Axial Surface	Fracture	Hinge	Axial Surface	Intersection Lineation
TP 1225	N26E, 12SE	N26E, 42SE						
1226	N23E, 16SE	N56E, 48SE						
1227	N61E, 18SE							
BRF 877	N49E, 42SE	N35E, 70SE						
878	N65E, 42SE	N60E, 58SE						
879	N68E, 18NW	N44E, 58SE						
880	N54E, 70SE	N54E, 42SE						
881	N51E, 69SE							
882	N54E, 30SE							
883	N34E, 52SE							
884	N54E, 69SE	N45E, 50SE						
885	N40E, 60SE							
886	N42E, 52SE							
887	N44E, 42SE							
888	N56E, 90	N61E, 40SE						
889	N56E, 45SE							
890	N56E, 28SE							
891	N58E, 72SE							
892	N54E, 56SE							
893	N54E, 56SE							
894	N43E, 89SE							
TP 1228	N35E, 28SE							
1229	N43E, 48SE	N43E, 68SE						
1230	N31E, 12SE							
1231	N50E, 11SE							
1232	N34E, 16NW	N44E, 48SE						
1233	N46E, 11SE	N46E, 52SE						
1234	N30E, 28NW	N30E, 50SE						
1235	N29E, 36NW	N31E, 62SE						
1236	HORIZONTAL	N47E, 35SE						
1237	N39E, 04NW	N39E, 20SE						
1238	N55E, 04SE	N59E, 50SE						
1239	N59E, 39NW	N22E, 24SE						
1240	N04W, 12NE							
1241		N66E, 36SE						
1242		N66E, 32SE						
1243	N39E, 08SE	N59E, 32SE						
1244	HORIZONTAL							
1245	N42E, 04SE							
1246	N39E, 14SE							
1247	N38E, 10SE	N35E, 40SE						
1248	N32E, 11SE	N34E, 50SE						
1249	N31E, 19SE							
1250	HORIZONTAL	N63E, 29SE						

*Sta#	Bedding	Cleavage S_1	Cleavage S_{1a}	Cleavage S_2 Axial Surface	Fracture	Fold Hinge	Fold Axial Surface	$S_0 x S_1$ Intersection Lineation
TP 1251	HORIZONTAL							
1252	N39E, 14SE	N35E, 29SE						
1253	HORIZONTAL	N41E, 26SE						
1254	N42E, 88NW	N49E, 48SE						
1255	N42E, 24NW	N32E, 30SE						
1256	N37E, 19NW	N21E, 24SE						
1257	N48E, 56NW	N44E, 24SE						
1258	N56E, 80SE	N56E, 50SE						
1259	N29E, 38SE	N44E, 71SE						
1260	N46E, 33SE							
1261	N26E, 44NW	N25E, 51SE						
1262	N37E, 18NW	N45E, 46SE						
1263	N30E, 14SE							
1264	N40E, 10NW							
1265	N75E, 12NW	N24E, 10SE						
1266	N41E, 31SE	N10E, 50SE						
1267	N32E, 29SE							
1268		N29E, 40SE						
1269	N32E, 12SE							
1270	HORIZONTAL							
1271	N30E, 26SE	N26E, 70SE						
1272	N59E, 15SE							
1273	N59E, 40SE	N39E, 60SE						
1274	N46E, 18SE							
1275	N56E, 18SE	N56E, 59SE						
1276	N39E, 24SE							
1277	N47E, 38SE							
1278	N51E, 44SE							
1279	N62E, 44SE							
1280	N43E, 28SE							
1281	N53E, 66SE							
1282	N33E, 33SE							
1283	N38E, 29SE							
1284	N37E, 09SE	N28E, 54SE						
1285	N52E, 36SE							
1286	N47E, 11NW	N47E, 66NW			N26W, 66SW			
1287	N41E, 42SE	N41E, 52SE						
1288	N33E, 34NW	N27E, 66NW						
1289	N45E, 57NW	N57E, 72SE						
1290	N42E, 68NW	N51E, 82SE						
1291	N45E, 34NW	N47E, 54SE						
1292	N57E, 20NW	N36E, 57SE						
1293		N51E, 45SE						
1294	N48E, 49SE	N47E, 62SE						

*Sta#	Bedding	Cleavage S_1	Cleavage S_{1a}	Cleavage S_2 Axial Surface	Fracture	Fold Hinge	Fold Axial Surface	$S_0 x S_1$ Intersection Lineation
TP 1295	N63E, 46SE	N61E, 58SE						
1296	N45E, 68SE				N41E, 66SW			
1297	N55E, 42SE	N46E, 68SE						
1298	N55E, 56SE							
1299	N48E, 33SE	N40E, 58SE						
1300	N48E, 36SE	N42E, 72SE						
1301	N49E, 48SE	N49E, 52SE			N82W, 90			
1302	N57E, 26SE							
1303	N53E, 34SE							
1304	N50E, 19SE	N44E, 46SE			N24W, 60NE			
1305	N44E, 12SE							
1306	N42E, 38SE	N52E, 58SE						
1307	N52E, 18SE	N52E, 58SE						
1308	N49E, 41SE	N49E, 64SE						
1309		N57E, 58SE						
1310	N46E, 85SE							
BRF 895	N60E, 16NW	N50E, 38SE						
896	N22E, 11NW	N40E, 54SE						
897	N49E, 20SE	N50E, 54SE						
TP 1311	N47E, 08SE	N44E, 54SE						
1312	N40E, 63SE							
1313	N56E, 33SE							
1314	N36E, 36SE							
1315	N61E, 42SE	N51E, 56SE						
1316	N41E, 31SE	N45E, 65SE						
1317	N54E, 80NW	N50E, 82SE						
1318	N31E, 17NW	N35E, 26SE						
1319	N27E, 82SE							
1320	N57E, 31SE							
1321	N58E, 22SE							
1322	N61E, 36SE	N89E, 68SE						
1323	N24E, 14NW							
1324		N45E, 66SE						
1325	N62E, 29NW							
1326	N40E, 42SE	N40E, 82SE						
1327		N44E, 60SE						
1328	N45E, 32SE							
1329	N45E, 39SE	N45E, 76SE						
1330		N46E, 56SE						
1331	N71E, 43SE	N71E, 68SE						
1332	N34E, 26SE	N46E, 58SE						
1333	N55E, 22NW	N61E, 62SE						
1334	N44E, 21SE	N59E, 44SE						
1335	N43E, 26SE							

		Fabric Element						
		Cleavage				Fold		S_0xS_1
*Sta#	Bedding	S_1	S_2	S_2 Axial Surface	Fracture	Hinge	Axial Surface	Intersection Lineation
TP 1336	N65E, 22NW	N49E, 68SE						
1337	N45E, 50NW				N62E, 64SE(f)			
1338	N39E, 50SE							
1339	N40E, 37SE	N39E, 66SE						
1340	N30E, 35SE							
1341	N56E, 80NW	N51E, 58SE						
1342	N45E, 21NW	N37E, 71SE						
1343		N41E, 58SE						
1344	N54E, 49SE							
1345		N49E, 78SE						
1346						228, 6	N40E, 47SE	
BRF 898	N63E, 67SE	N27E, 31SE						
899	N44E, 46NW							
900	N36E, 25NW	N46E, 40SE						
901	N53E, 06NW							
902	N69E, 13NW	N50E, 37SE						
TP 1347	N39E, 14SE	N33E, 49SE						
1348	N39E, 33SE							
1349		N29E, 82SE						
1350	N34E, 69NW							
1351	N31E, 12SE	N66E, 36SE						
1352		N21E, 45SE						
1353	N65E, 65SE	N55E, 40SE			N29E, 65NW(f)			
1354	N42E, 44NW	N68E, 63SE						
1355	N45E, 38SE							
1356	N39E, 41SE	N31E, 71SE						
1357	N39E, 54SE	N39E, 76SE						
1358	N66E, 66SE							
1359	N67E, 31NW							
1360	N58E, 90							
1361	N45E, 60SE							
1362	N78E, 59SE							
1363	N57E, 55SE	N60E, 30SE						
1364	N67E, 28SE							
1365	N85E, 59SE	N85E, 59SE						
1366	N69E, 70SE							
1367	N59E, 20SE				N84W, 74SW			
1368	N51E, 20SE							
1369	N32E, 31SE	N42E, 82SE						
1370	N32E, 71SE							
1371	N61E, 20NW	N45E, 65SE						
1372		N47E, 64SE						
1373	N22E, 52SE	N39E, 82SE						
1374	N57E, 41NW	N57E, 32SE						

		Fabric Element						
		Cleavage				Fold		S_0xS_1
*Sta#	Bedding	S_1	S_2	S_2 Axial Surface	Fracture	Hinge	Axial Surface	Intersection Lineation
TP 1375	N31E, 19SE	N41E, 64SE						
1376	N37E, 29SE	N47E, 70SE						
1377	N42E, 48SE							
1378	N32E, 30SE	N42E, 76SE						
1379	N58E, 24SE	N58E, 82SE						
1380	N44E, 74SE							
1381	N55E, 20SE	N55E, 70SE						
1382	N34E, 10SE							
1383	N35E, 44SE							
1384	N43E, 42SE							
1385	N57E, 42SE							
1386	N30E, 76SE	N28E, 49SE						
1387	N38E, 76SE							
1388	N75W, 34SW							
1389	N42E, 54SE							
1390	N34E, 41SE							
1391	N49E, 48SE							
1392	N53E, 38SE							
1393	N59E, 24NW							
1394	N52E, 41SE							
1395	N51E, 35NW							
1396	N55E, 46NW							
1397	N57E, 63SE							
1398	N45E, 39SE							
1399	N41E, 32SE							
1400	N53E, 38SE							
1401	N45E, 42SE							
1402	N41E, 27NW							
1403	N47E, 21NW							
BRF 903	N53E, 43SE							
904	N53E, 86SE							
905	N51E, 61SE							
906	N55E, 55SE							
907	N53E, 86SE							
908	N30E, 82SE				N66W, 78NE			
909	N30E, 59NW							
910	N52E, 66SE							
911	N59E, 82SE							
912	N55E, 64SE							
913	N53E, 76SE							
914	N32E, 61SE				N66W, 78NE(f)			
					N57W, 85SW			
915	N42E, 32SE							
916	N59E, 44SE							

		Fabric Element						
		Cleavage				Fold		S_0xS_1 Intersection
*Sta#	Bedding	S_1	S_{1a}	S_2 Axial Surface	Fracture	Hinge	Axial Surface	Lineation
BRF 917	N45E, 44NW							
918	N44E, 38SE				N55W, 81SW			
919	N38E, 82SE				N55W, 81SW			
920	N39E, 63SE							
F 65	N53E, 68SE							
66	N45E, 67SE							
67	N49E, 43NW							
68	N43E, 65SE							
69	N47E, 67NW							
70	N54E, 43SE							
71	N43E, 65NW							
72	N42E, 19NW	N31E, 50SE						
73	N60E, 52NW							
74	N42E, 75NW							
BRF 921	N52E, 67SE							
922	N48E, 64SE							
923	N59E, 79SE							
924	N45E, 60SE							
925	N45E, 42SE							
TP 1404		N41E, 50SE						
1405	N36E, 36SE	N36E, 62SE						
1406	N36E, 26SE	N36E, 79SE						
1407	N53E, 48SE							
1408		N64E, 84SE						
1409	N30E, 22SE	N38E, 72SE						
1410	N39E, 19SE	N39E, 61SE						
1411		N22E, 69SE						
1412	N45E, 12SE	N45E, 64SE						
1413		N38E, 72SE						
1414	N43E, 34SE							
1415	N47E, 45SE							
1416	N67E, 51NW	N61E, 30SE						
1417	N37E, 40SE							
1418	N16E, 38SE							
1419		N20E, 63SE						
1420	N67E, 65SE							
1421	N83E, 15SE							
1422	N55E, 42SE							
1423	N20E, 76SE							
1424	N53E, 30NW							
1425	N38E, 60SE							
1426	N38E, 61SE							
1427	N23E, 34SE							
1428	N39E, 38SE							

		Fabric Element						
		Cleavage				Fold		S_0xS_1 Intersection
*Sta#	Bedding	S_1	S_{1a}	S_2 Axial Surface	Fracture	Hinge	Axial Surface	Lineation
TP 1429	N37E, 56SE							
1430	N59E, 35SE							
1431	N10W, 42SE							
1432	N22E, 15SE							
1433	N79E, 49SE							
1434	N70E, 32SE							
1435	N48E, 63SE							
1436	N51E, 88SE							
1437	N75E, 52NW							
1438	N63E, 86SE							
1439	N52E, 24SE							
1440	N45E, 19SE							
1441	N52E, 37SE							
1442	N85E, 40SE							
1443	N68E, 54SE							
1444	N52E, 37SE							
1445	N62E, 57SE							
1446	N39E, 27NW							
1447	N70E, 38SE							
1448	N43E, 68NW							
1449	N48E, 63SE							
1450	N70E, 65SE							
1451	N76E, 78SE							
1452	N17E, 38SE							
1453	N86E, 52NW							
1454	N80E, 32NW							
1455	N73E, 57NW							
1456	N62E, 35SE							
1457	N38E, 47SE							
1458	N88E, 80NW							
1459	N73E, 22SE							
1460	N73E, 50SE							
1461	N28E, 57SE							
1462	N09E, 60SE							
1463	N55E, 80SE							
1464	N75E, 60SE							
1465	N27E, 52SE							
1466	N52E, 17SE							
1467	N69E, 81SE							
1468	N42E, 44SE							
1469	N34E, 24NW							
1470	N52E, 10SE							
1471	N63E, 65NW							
1472	N43E, 17SE							

*Sta#	Bedding	Fabric Element: Cleavage S_1	Cleavage $S_{1'}$	Cleavage S_2 Axial Surface	Fracture	Fold: Hinge	Fold: Axial Surface	S_0xS_1 Intersection Lineation
TP 1473	N60E, 27SE							
1474	N57E, 80NW							
1475	N67E, 29NW							
1476	N64E, 68NW							
1477	N47E, 25NW							
1478	N50E, 27NW							
1479	N36E, 24NW							
1480	N45E, 81NW							
1481	N47W, 83SW							
1482	N41E, 46SE							
1483	N50E, 52SE							
1484	N64E, 62SE							
1485	N62E, 36NW							
1486	N40E, 24NW							
1487	N55E, 67SE							
1488	N27E, 63SE							
1489	N42E, 33SE							
1490	N66E, 30SE							
1491	N65E, 30SE							
1492	N60E, 45SE							
1493	N22E, 80SE							
1494	N61E, 85SE							
1495	N18E, 47SE							
1496	N45E, 40SE							
1497	N80E, 64NW							
1498	N15E, 68SE							
1499	N31E, 65NW							
1500	N35E, 42NW							
1501	N81E, 25SE							
1502	N86E, 35NW							
1503	N39E, 21SE							
1504	N71E, 22SE							
1505	N32E, 43SE							
1506	N18W, 50NE							
1507	N06E, 65SE							
1508	N50E, 68SE							
1509	N54E, 52SE							
1510	N27E, 66NW							
1511	N27E, 28SE							
1514	N46E, 57SE							
1515	N45E, 33SE							
1516	N45E, 21SE							
1517	N45E, 36SE							
1518	N53E, 27NW							

*Sta#	Bedding	Fabric Element: Cleavage S_1	Cleavage $S_{1'}$	Cleavage S_2 Axial Surface	Fracture	Fold: Hinge	Fold: Axial Surface	S_0xS_1 Intersection Lineation
TP 1519	N25E, 36SE							
1520	N46W, 40SW							
1521	N71E, 59SE							
1522	N47E, 09SE							
1523	N49E, 87NW							
1524	N49E, 71SE							
1525	N59E, 52NW							
1526	N47E, 70SE							
1527	N52E, 36NW							
1528	N56E, 36SE							
1529	N36E, 33SE							
1530	N49E, 61NW							
1531	N39E, 53SE							
1532	N52E, 56NW							
1533	N42E, 28NW							
1534	N13E, 66SE							
1535	N39E, 49NW							
1536	N15E, 35SE							
1537	N40E, 80NW							
1538	N25E, 52SE							
1539	N39E, 60NW							
1540	N09E, 20NW							
1541	N10E, 18NW							
1542	N34E, 84SE							
1543	N57E, 68SE							
1544	N83E, 30NW							
1545	N07E, 68SE							
1546	N25E, 27SE							
1547	N59E, 11SE							
1548	N05W, 30NE							
1549	N04E, 64SE							
1550	N38W, 40NE							
1551	N58E, 32SE							
1552	N36E, 40SE							
1553	N53E, 82SE							
1554	N47E, 28SE							
1555	N40E, 34SE							
1556	N61E, 48SE							
1557	N64E, 40SE							
1558	N42E, 41SE							
1559	N0E, 45W							
1560	N43E, 22NW							
1561	N43E, 30NW							
1562	N51E, 27NW							

	Fabric Element								
			Cleavage				Fold		S_2xS_1
*Sta#	Bedding	S_1	$S_{1'}$	S_2 Axial Surface	Fracture	Hinge	Axial Surface		Intersection Lineation
TP 1563	N40E, 50SE								
1564	N30E, 44NW								
1565	N45E, 34NW								
1566	N47E, 57NW								
1567	N33E, 52SE								
1568	N51E, 56SE								
1569	N32E, 42NW								
1570	N57E, 72NW								
1571	N53E, 60SE								
1572	N75E, 81NW								
1573	N67E, 65SE								
1574	N37E, 45NW								
1575	N45E, 22NW								
F 75	N61E, 90								
76	N56E, 88SE								
77	N60E, 82NW								
78	N50E, 73SE								
79	N51E, 83SE								
80	N47E, 62SE								
81	N45E, 69SE								
82	N34E, 40SE								
83	N50E, 56SE								
84	N57E, 71SE								
85	N46E, 83NW								
86	N31E, 60NW								
87	N46E, 81NW								
88	N17E, 81SE								
89	N63E, 44NW								
90	N53E, 90								
91	N42E, 71NW								
92	N42E, 55SE								
93	N40E, 50SE								
94	N22E, 32SE								
95	N53E, 85SE								
96	N49W, 37NE								
97	N05E, 37SE								
98	N36E, 77NW								
99	N22E, 74SE								
100	N53E, 77NW								
101	N43E, 80NW								
102	N46E, 76NW								
103	N45E, 86SE								
104	N27E, 70SE								
105	N41E, 76NW								

	Fabric Element								
			Cleavage				Fold		S_2xS_1
*Sta#	Bedding	S_1	$S_{1'}$	S_2 Axial Surface	Fracture	Hinge	Axial Surface		Intersection Lineation
F 106	N59E, 46NW								
107	N45E, 88SE								
108	N50E, 46NW								
109	N43E, 43NW								
110	N37E, 59SE								
111	N51E, 20SE								
112	HORIZONTAL								
113	N45E, 45NW								
114	N22E, 35NW								
115	N59E, 52NW								
116	N45E, 28SE								
117	N46E, 23SE								
118	N0E, 0SE								
119	N13W, 115W								
120	N52E, 17SE								
121	N05E, 07SE								
122	HORIZONTAL								
123	N42E, 63NW								
124	N10E, 16NW								
125	N70E, 25SE								
126	N23W, 295W								
127	N25E, 11NW								
128	N57E, 15NW								
129	N08W, 265W								
130	N08W, 115W								
131	HORIZONTAL								
132	N45E, 05SE								
133	N31E, 52NW								
134	N51E, 24NW								
135	N28E, 66NW								
136	HORIZONTAL								
137	N02W, 18NE								
138	N11E, 45SE								
139	N04E, 44SE								
140	N01E, 18SE								
141	N55W, 15NE								
142	N11E, 35SE								
143	N43E, 26SE								
144	N50E, 38SE								
145	N21E, 26SE								
146	N31E, 26SE								
147	N69E, 13SE								
148	N08W, 25NE								
149	N37E, 54SE								

		Fabric Element							
		Cleavage				Fold		S_0xS_1 Intersection Lineation
*Sta#	Bedding	S_1	S_{1a}	S_2 Axial Surface	Fracture	Hinge	Axial Surface	
F 150	N47E, 38SE							
151	N04E, 19SE							
152	N07E, 23SE							
153	N52E, 12NW							
154	N10E, 12SE							
155	N25E, 33SE							
156	N58E, 34NW							
157	HORIZONTAL							
158	N50W, 11SW							
159	N45E, 50SE							
160	N10E, 11SE							
161	N30E, 38NW							
162	N35E, 55SE							
163	N15E, 07SE							
164	N09E, 14SE							
165	N20E, 10NW							
166	N30E, 25SE							
167	N55E, 33NW							
168	N58E, 24NW							
169	N16E, 14SE							

		Fabric Element						
		Cleavage				Fold		S_0xS_1 Intersection Lineation
*Sta#	Bedding	S_1	S_{1a}	S_2 Axial Surface	Fracture	Hinge	Axial Surface	

Appendix B

Modal analysis

Modal analyses of coarse-grained clastic rocks from the study area.

Stratigraphic unit	Hesse Quartzite	Sandsuck Formation	Wilhite Formation					
Sample no.	GH 2	TP-1388v	TP-51v	TP-133	TP-289	TP-722	TP-928	TP-963v
Quartz	91.7	71.6	50.0	60.5	53.8	50.9	58.2	87.3
Plagioclase (comp.)		0.7	14.6 (An_{35})	9.5 (An_{35})	9.5 (An_{36})	17.7 (An_{36})	12.5 (An_{34})	2.8
Microcline		11.6		0.7	1.6	1.0	1.0	
Perthite			1.5	0.7	1.0	1.6	0.3	
Clay/ Sericite		11.8	12.8	10.2	8.1	11.8	9.7	0.9
Chlorite			10.7	7.4	5.3	9.2	7.4	3.9
Muscovite	0.1	0.5	5.2	2.9	3.2	4.7	2.7	0.8
Biotite			Tr	Tr	Tr	0.3	0.1	
Hematite	7.1	2.8	1.4	1.0	6.7	0.6	2.1	3.3
Pyrite						1.1	0.9	
Magnetite/ Illmenite	0.4		0.1	0.2	0.2		1.3	
Carbonate			2.1	5.3	9.1		3.2	
Ankerite								
Tourmaline	0.2	0.3	1.0	0.4	0.7	0.6	0.2	0.5
Zircon		Tr	0.1	0.2		0.2	0.2	
Apatite			Tr					
Lithic fragments	0.5	0.7	0.7	1.0	0.8	0.3	0.2	0.5
Total	100.0	100.0	100.0	100.0	100.0	100.0	100.0	100.0
No. of pts. counted	1000	1000	1000	1000	1000	1000	1000	1000

*Plagioclase compositions determined using the Michel-Lévy (1877) method.

Modal analyses of coarse-grained clastic rocks from the study area (continued).

Stratigraphic unit	Wilhite Formation	Dean Formation						
Sample no.	TP-998	TP-563	TP-710	BRF-391	BRF-459	BRF-481	BRF-846	
Quartz	77.0	53.8	78.1	57.0	65.2	54.7	50.2	
Plagioclase (comp.)	1.5 (An_{36})	12.2 (An_{33})	1.6	9.7 (An_{35})	14.0 (An_{35})	14.0 (An_{34})	9.9 (An_{35})	
Microcline	0.2		0.9	1.4				
Perthite		Tr		1.0	0.3	0.8	0.5	
Clay/ Sericite	1.9	21.5	0.4	4.9	0.6		11.8	
Chlorite	2.6	10.9	12.8	20.6	15.8	22.0	23.3	
Muscovite	0.5	0.3	0.8	1.5	0.4	0.1		
Biotite	Tr			Tr	1.5	6.3		
Hematite	1.1	1.1	2.0	2.1	0.8	2.1	3.8	
Pyrite	0.1		3.0	0.2	0.5			
Magnetite/ Illmenite	0.1			0.5	0.7		0.1	
Carbonate	14.3	Tr						
Ankerite								
Tourmaline	0.2	0.2	0.3	0.9	0.2	Tr	0.4	
Zircon	0.4		0.1	Tr	Tr			
Apatite	0.1			0.2				
Lithic fragments				Tr			Tr	
Total	100.0	100.0	100.0	100.0	100.0	100.0	100.0	
No. of pts. counted	1000	1000	1000	1000	1000	1000	1000	

*Plagioclase compositions determined using the Michel-Lévy (1877) method.

Modal analysis of ankeritic metasiltstone from the study area.

Stratigraphic unit	Wilhite Formation
Sample no.	TP-343
Quartz	28.7
Plagioclase (comp.)	0.2
Microcline	
Perthite	
Clay/ Sericite	3.3
Chlorite	51.0
Muscovite	5.2
Biotite	
Hematite	3.3
Pyrite	
Magnetite/ Illmenite	
Carbonate	
Ankerite	8.1
Tourmaline	0.2
Zircon	Tr
Apatite	
Lithic fragments	
Total	100.0
No. of pts. counted	1000

Modal analysis of carbonate lithology from the study area.

Stratigraphic unit	Sandsuck Formation
Sample no.	TP-534
Micritic calcite	60.3
Sparry calcite	34.0
Intraclasts	
Onkolites	
Quartz	4.6
Plagioclase (comp.)	0.4
Magnetite	0.1
Hematite	0.5
Clay/ Sericite	
Biotite	
Chlorite	0.1
Muscovite	
Total	100.0
No. of pts. counted	1000

Appendix C
Strain data

Three–dimensional finite strain analysis (Rf/ϕ)

INPUT DATA **OWENS' OUTPUT DATA**

Sample	Orientation	Plane	Strike	Dip	Rake	Ratio	Axis	Stretch	Axis Trend	Axis Plunge	x/y	x/z	y/z	Solution
*TP-256	N55E, 47SE	b	055	47 S	62	1.12	z	0.68	272.7	32.2	1.19	1.94	1.63	q33
		p	055	43 N	168	1.12	y	1.11	22.7	28.5				
		v	145	90	44	1.20	x	1.32	144.7	44.4				
TP-1388	N70E, 32SE	b	070	32 S	138	1.06	z	0.76	300.6	33.5	1.33	1.74	1.30	q22
		p	070	58 N	30	1.21	y	0.99	177.4	39.6				
		v	160	90	60	1.22	x	1.32	55.6	32.5				
TP-51	N49E, 29SE	b	049	29 S	4	1.19	z	0.86	315.6	49.6	1.26	1.41	1.12	q11
		p	049	61 N	5	1.35	y	0.96	146.1	39.9				
		v	139	90	47	1.12	x	1.21	51.7	5.2				
TP-133	N79E, 49SE	b	079	49 S	41	1.23	z	0.80	357.7	9.1	1.27	1.58	1.24	q11
		p	079	41 N	1	1.51	y	0.99	213.9	78.8				
		v	169	90	86	1.19	x	1.26	88.8	6.5				
*TP-963	N30E, 39SE	b	030	39 S	79	1.29	z	0.67	241.8	32.5	1.06	1.88	1.78	q22
		p	030	51 N	39	1.47	y	1.19	357.9	34.6				
		v	120	90	67	1.07	x	1.26	121.3	38.6				
TP-1014	N44E, 40SE	b	044	40 S	17	1.29	z	0.86	154.0	19.8	1.07	1.29	1.21	q33
		p	044	50 N	30	1.21	y	1.04	275.7	55.6				
		v	134	90	110	1.19	x	1.11	53.5	26.9				
*TP-1355	N45E, 38SE	b	045	38 S	50	1.06	z	0.83	264.3	7.9	1.59	1.66	1.05	q11
		p	045	52 N	64	1.16	y	0.87	170.7	24.5				
		v	135	90	104	1.46	x	1.38	10.8	64.1				
TP-563	N57E, 28SE	b	057	28 S	136	1.19	z	0.89	310.2	13.1	1.15	1.27	1.10	q11
		p	057	62 N	160	1.18	y	0.98	64.9	60.8				
		v	147	90	75	1.14	x	1.13	213.8	25.6				
BRF-263	N55E, 39SE	b	055	39 S	5	1.38	z	0.74	223.7	67.9	1.63	2.00	1.23	q22
		p	055	51 N	12	1.43	y	0.91	118.3	6.2				
		v	145	90	165	1.28	x	1.48	25.9	21.1				
TP-710	N54E, 31SE	b	054	31 S	8	1.46	z	0.69	159.6	34.4	1.75	2.30	1.32	q11
		p	054	59 N	30	1.36	y	0.91	259.2	13.7				
		v	144	90	125	1.93	x	1.59	7.5	52.3				
									MEAN		1.33	1.71	1.30	
									STD DEV		±0.19	±0.26	±0.16	

* Strain ratio of ellipses not consistent with principal axes of strain ellipsoid.

Three-dimensional finite strain analysis (normalized Fry)

INPUT DATA **OWENS' OUTPUT DATA**

Sample	Orientation	Plane	Strike	Dip	Rake	Ratio	Axis	Stretch	Axis Trend	Axis Plunge	x/y	x/z	y/z	Solution
*TP-1388	N70E, 32SE	b	070	32 S	131	1.26	z	0.60	297.1	27.7	2.21	3.20	1.45	q11
		p	070	58 N	30	1.26	y	0.87	174.4	45.8				
		v	160	90	70	1.24	x	1.92	45.7	31.3				
TP-133	N79E, 49SE	b	079	49 S	45	1.24	z	0.70	304.2	26.4	1.11	1.80	1.63	q33
		p	079	41 N	174	1.40	y	1.14	184.9	44.6				
		v	169	90	84	1.41	x	1.26	53.6	33.8				
TP-963	N30E, 39SE	b	030	39 S	120	1.38	z	0.68	243.9	34.4	1.44	2.13	1.49	q22
		p	030	51 N	39	1.44	y	1.01	353.6	26.2				
		v	120	90	17	1.38	x	1.45	112.2	44.2				
*TP-1014	N44E, 40SE	b	044	40 S	6	1.33	z	0.66	263.6	30.6	1.92	2.59	1.35	q33
		p	044	50 N	45	1.35	y	0.89	144.9	39.1				
		v	134	90	100	1.21	x	1.71	19.0	35.9				
TP-563	N57E, 28SE	b	057	28 S	131	1.60	z	0.74	290.2	14.2	1.47	1.91	1.30	q33
		p	057	62 N	162	1.28	y	0.96	134.3	74.5				
		v	147	90	75	1.21	x	1.41	21.7	6.1				
BRF-263	N55E, 39SE	b	055	39 S	176	1.86	z	0.70	206.0	68.6	1.54	2.11	1.37	q11
		p	055	51 N	3	1.73	y	0.96	111.7	1.7				
		v	145	90	155	1.47	x	1.48	21.1	21.3				
*TP-710	N54E, 31SE	b	054	31 S	1	1.54	z	0.69	151.0	37.7	1.56	2.17	1.39	q11
		p	054	59 N	36	1.30	y	0.96	261.0	23.9				
		v	144	90	126	1.94	x	1.50	15.3	42.9				
									MEAN		1.61	2.27	1.43	
									STD DEV		±0.26	±0.35	±0.08	

Samples TP-256, TP-51, and TP-1355 not used for normalized Fry method.

* Strain ratio of ellipses not consistent with principal axes of strain ellipsoid.

Measurements of quartz pebble principal axes and axial ratios

n	x	y	z	x/y	y/z	x/z	n	x	y	z	x/y	y/z	x/z
1	29.0	25.0	10.0	1.16	2.50	2.90	39	22.0	20.0	10.0	1.10	2.00	2.20
2	42.5	21.5	17.0	1.98	1.26	2.50	40	21.0	18.0	12.0	1.17	1.50	1.75
3	26.5	22.0	15.0	1.20	1.47	1.77	41	21.0	20.0	10.0	1.05	2.00	2.10
4	27.0	17.0	12.0	1.59	1.42	2.25	42	23.5	16.0	10.0	1.47	1.60	2.35
5	16.5	15.0	11.0	1.10	1.36	1.50	43	19.0	17.0	9.0	1.12	1.89	2.11
6	23.5	20.0	12.0	1.18	1.67	1.96	44	20.0	16.0	7.0	1.25	2.29	2.86
7	31.0	21.0	14.0	1.48	1.50	2.21	45	24.0	21.0	9.0	1.14	2.33	2.67
8	36.5	27.0	14.0	1.35	1.93	2.61	46	21.0	11.5	10.0	1.83	1.15	2.10
9	19.5	17.5	10.0	1.11	1.75	1.95	47	27.0	20.0	14.0	1.35	1.43	1.93
10	25.0	21.0	9.0	1.19	2.33	2.78	48	28.0	18.0	10.0	1.56	1.80	2.80
11	22.0	14.0	13.0	1.57	1.08	1.69	49	34.0	21.5	12.0	1.58	1.79	2.83
12	21.0	17.0	10.0	1.24	1.70	2.10	50	24.0	19.0	12.0	1.26	1.58	2.00
13	30.0	19.0	10.5	1.58	1.81	2.86	51	21.0	19.0	14.5	1.11	1.31	1.45
14	21.0	16.0	12.0	1.31	1.33	1.75	52	24.0	18.0	12.5	1.33	1.44	1.92
15	25.0	21.0	16.0	1.19	1.31	1.56	53	20.0	15.5	10.0	1.29	1.55	2.00
16	20.0	15.0	11.0	1.33	1.36	1.82	54	30.5	19.5	12.0	1.56	1.63	2.54
17	27.0	18.0	10.0	1.50	1.80	2.70	55	25.0	23.0	9.0	1.09	2.56	2.78
18	25.0	18.0	11.0	1.39	1.64	2.72	56	18.5	17.0	9.0	1.09	1.89	2.06
19	25.5	14.0	10.0	1.82	1.40	2.55	57	20.0	17.0	8.0	1.18	2.13	2.50
20	27.0	19.0	10.5	1.42	1.81	2.57	58	17.0	14.5	9.0	1.17	1.61	1.89
21	21.0	15.0	10.0	1.40	1.50	2.10	59	21.0	18.0	8.0	1.17	2.25	2.63
22	32.0	16.0	9.0	2.00	1.78	3.56	60	22.0	16.0	9.0	1.38	1.78	2.45
23	22.0	19.5	11.0	1.13	1.77	2.00	61	22.0	21.0	10.0	1.05	2.10	2.20
24	21.0	19.0	11.0	1.11	1.73	1.91	62	15.0	13.0	11.0	1.15	1.18	1.36
25	31.0	22.0	13.0	1.41	1.69	2.38	63	21.0	15.0	10.0	1.40	1.50	2.10
26	27.5	21.0	10.0	1.31	2.10	2.75	64	18.0	16.5	9.0	1.09	1.83	2.00
27	24.0	20.0	13.0	1.20	1.54	1.85	65	22.0	21.0	11.0	1.05	1.91	2.00
28	20.5	19.0	10.0	1.08	1.90	2.05	66	21.5	13.0	11.0	1.65	1.18	1.95
29	30.0	19.0	10.0	1.58	1.90	3.00	67	17.0	13.0	10.0	1.31	1.30	1.70
30	20.5	19.0	10.0	1.08	1.90	2.05	68	12.5	11.0	8.0	1.14	1.38	1.56
31	23.0	21.0	12.5	1.10	1.68	1.84	69	22.0	16.5	12.0	1.33	1.38	1.83
32	22.0	15.0	8.0	1.47	1.88	2.75	70	15.0	12.0	9.5	1.25	1.26	1.58
33	23.5	18.0	10.0	1.31	1.80	2.35	71	24.5	14.0	8.0	1.75	1.75	3.06
34	27.0	19.0	9.0	1.42	2.11	3.00	72	16.0	13.0	6.0	1.23	2.17	2.67
35	22.0	16.0	14.0	1.38	1.14	1.57	73	20.0	16.0	11.0	1.25	1.45	1.82
36	25.0	20.0	17.5	1.25	1.14	1.43	74	23.0	18.0	9.0	1.28	2.00	2.56
37	26.0	19.0	10.0	1.37	1.90	2.60	75	18.0	16.0	9.0	1.13	1.78	2.00
38	18.0	16.0	8.0	1.13	2.00	2.25							
										MEAN	1.32	1.70	2.22
										STD DEV	±0.18	±0.29	±0.39

Measurements of principal axes in mm.

Appendix D

Procedures for cross section construction and retrodeformation using Adobe Illustrator™

Procedures for cross section construction and retrodeformation using Adobe Illustrator™

The following procedures apply to the construction of cross sections and retrodeformed cross sections in Plate III using Adobe Illustrator software for the Macintosh computer.

Cross sections

Step 1-*Scanning*. Scan cross section as line art using Ofoto software, and save as pict file. Be sure to also scan in the scale along with your cross section.

Step 2-*Transferring to Adobe Illustrator™*. Open Adobe Illustrator™ 6.0 and open the scanned pict as a template.

Step 3-*Tracing template*. Trace, using the pen tool, the topographic profile and cross section boundaries (sides and bottom of cross section) as one object (polygon). The rest of the cross section is traced as separate lines. Each stratigraphic unit or structure (fault) has its own line, therefore some lines will overlap. For example, a stratigraphic unit bounded by a fault will have a line representing the stratigraphic unit, and a line representing the fault. Use different stroke weights for lines representing different types of contacts. Stratigraphic contacts are best converted to 0.5-point lines, while fault contacts are left as 1.0-point lines (the default line weight is 1.0-point).

Step 4-*Preserving line art and template*. Open a new file in Adobe Illustrator™ 6.0 and import the line art from the template. This file is used to edit your cross section and to make revisions. Keep the original file containing the line art and template as a backup.

Step 5-*Rotate to horizontal.* In the new file just created, select all (command A) and rotate the base of the cross section to the horizontal. To ensure the base of the cross section is completely horizontal increase, magnification to 800% (using the zoom tool) and rotate section until it is horizontal. Next, make the vertical lines representing the sides of the cross section completely vertical using the direct-selection tool (the open arrow tool). Do not select all here, just select the node(s) you wish to move in order to make the sides of the cross section vertical.

Step 6-*Constructing reference lines ("sticks").* These lines are constructed to represent the thickness of individual units (using the scale scanned in with the cross section), the top of basement, and the ramp angles. These reference lines ensures each stratigraphic unit has constant thickness, and are "installed" precisely normal to bedding. Other reference lines and/or objects may be used at your discretion to ensure constant thickness of stratigraphic units. Make copies of the reference lines representing the thickness of each stratigraphic unit and distribute them throughout the cross section. Reference lines representing the top of basement ensure that each supracrustal unit will have the same dip as basement. Reference lines oriented parallel to ramps ensures stratigraphic units will have the same dip as the ramp. Increase magnification to 800% and make the necessary adjustments to ensure stratigraphic units have constant thickness by first adjusting the "sticks" normal to bedding and then correcting the thickness. It is best to begin with the least deformed part of the section (near basement and, here, westernmost units).

Step 7-*Coloring the cross section using Pantone™ colors.* Copy the lines representing the area you wish to color, removing them as a unit without changing their shape, then connect those lines using either the pen tool or the open arrow tool and command join to make a polygon. Fill each polygon with the color you want, make the line "none", and move the polygon back to the section. Pantone colors are located in the custom colors section of Adobe Illustrator™.

Retrodeformed cross sections

Step 8-*Line-balancing of Valley and Ridge footwall units.* Line-balancing Valley and Ridge footwall units can be accomplished using two techniques. The first technique requires measuring each line (using the measure tool-ruler) of the cross section. Draw a line equal to the length of the line measured in the cross section. Do this for each line to be retrodeformed. The second technique involves copying the line to be retrodeformed and rotating that line to the horizontal. For folded strata, select the entire line and rotate (using rotate tool) the line around the end of the line till the adjacent node is horizontal. Unselect the first node which the line was originally rotated around, and rotate the line around the adjacent node that was just rotate to the horizontal. Repeat this procedure until the entire folded/curved line is horizontal.

Step 9-*Line- and area-balancing of western Blue Ridge hanging-wall units.* Parts of this portion of the cross section is retrodeformed using line- and area-balancing techniques. Units or thrust sheets in the hanging wall that have undergone at least one period of deformation can be line-balanced using the procedure in Step 8. Line-balanced portions of the hanging-wall units include the strata in the Great Smoky and Bullet Mountain thrust sheets. Area-balancing is required for retrodeforming strata that has undergone at least two episodes of deformation. First, copy and isolate the hanging wall strata. Second, copy and isolate individual thrust sheets that comprise the hanging-wall units. Group each thrust sheet after the individual thrust sheets have been isolated. Next, establish a horizontal reference line representing an original flat fault surface (Great

Smoky fault). Each thrust sheet will be rotated to parallel along this horizontal line. Select all of the thrust sheets to be retrodeformed, and rotate each thrust sheet so that the leading edge of the fault is aligned with the horizontal reference line. Rotate the object till the next node is parallel to the horizontal reference line. Continue to rotate the object to the horizontal reference line until the next node is parallel to this line. Select only the nodes of the object that need to be rotated. Unselected nodes will not move. Once you have rotated the object, unselect the nodes of the object that do not need to be rotated. Continue this procedure until the entire thrust sheet is retrodeformed.

Step-10-*Coloring*. Color retrodeformed sections as needed in the same manner as in Step 7.

Vita

Steven Lee Martin was born in Knoxville, Tennessee on April 1, 1963 to Charles Edward and Shirley Drummond Martin. Steves' family moved to Chattanooga, Tennessee in 1965. He attended Alpine Crest Elementary, Hixson Junior High, and Hixson High schools in the Chattanooga public school system, from which he graduated in June, 1981. Steve enrolled at the University of Tennessee at Chattanooga (UTC) in August, 1981. While at UTC, he earned a Bachelor of Science degree in Business Administration with a concentration in Marketing, and played varsity soccer in four years. After Graduating from UTC in May, 1985, he worked as a customer service representative for World Carpets. Inc., in Dalton, Georgia. He was then employed at the Chattanooga Freight Bureau, Inc., where he worked from 1986 to 1989 as a transportation broker and consultant. During this time he became interested in geology. After taking Geology 101 at UTC, Steve decided to return to school for a second undergraduate degree. He enrolled at the University of Tennessee at Knoxville (UTK) in August, 1989, and received a Bachelor of Science degree in Geology in December, 1992. He became a graduate student in the Department of Geological Sciences at UTK in January. 1993. He earned a Master of Science degree in Geology in December, 1996.

PLATE I

Geologic Map of parts of the Tellico Plains, Bald River Falls, Farner, and Unaka 7.5-minute Quadrangles, Tennessee and North Carolina

Steven L. Martin
1996

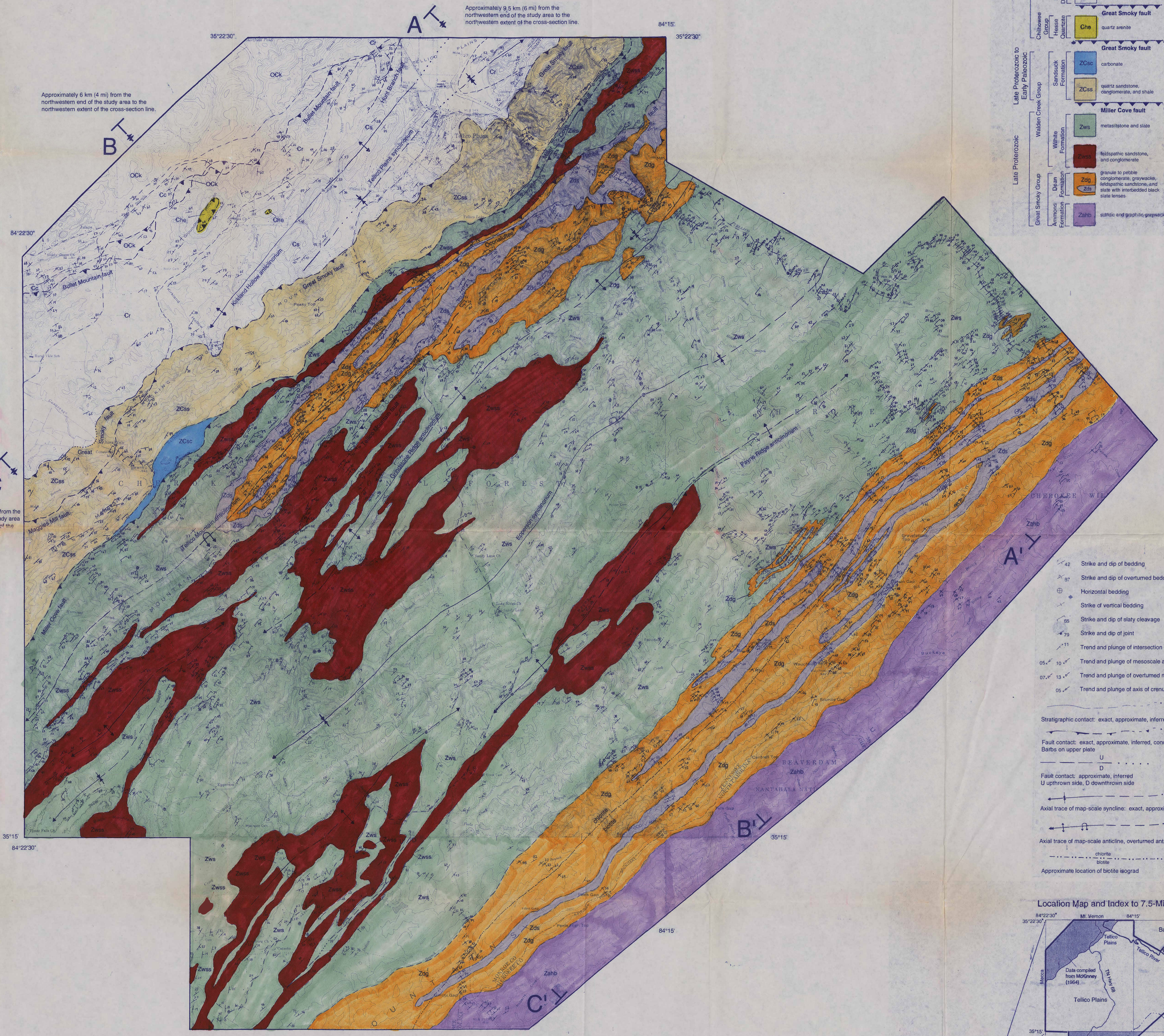

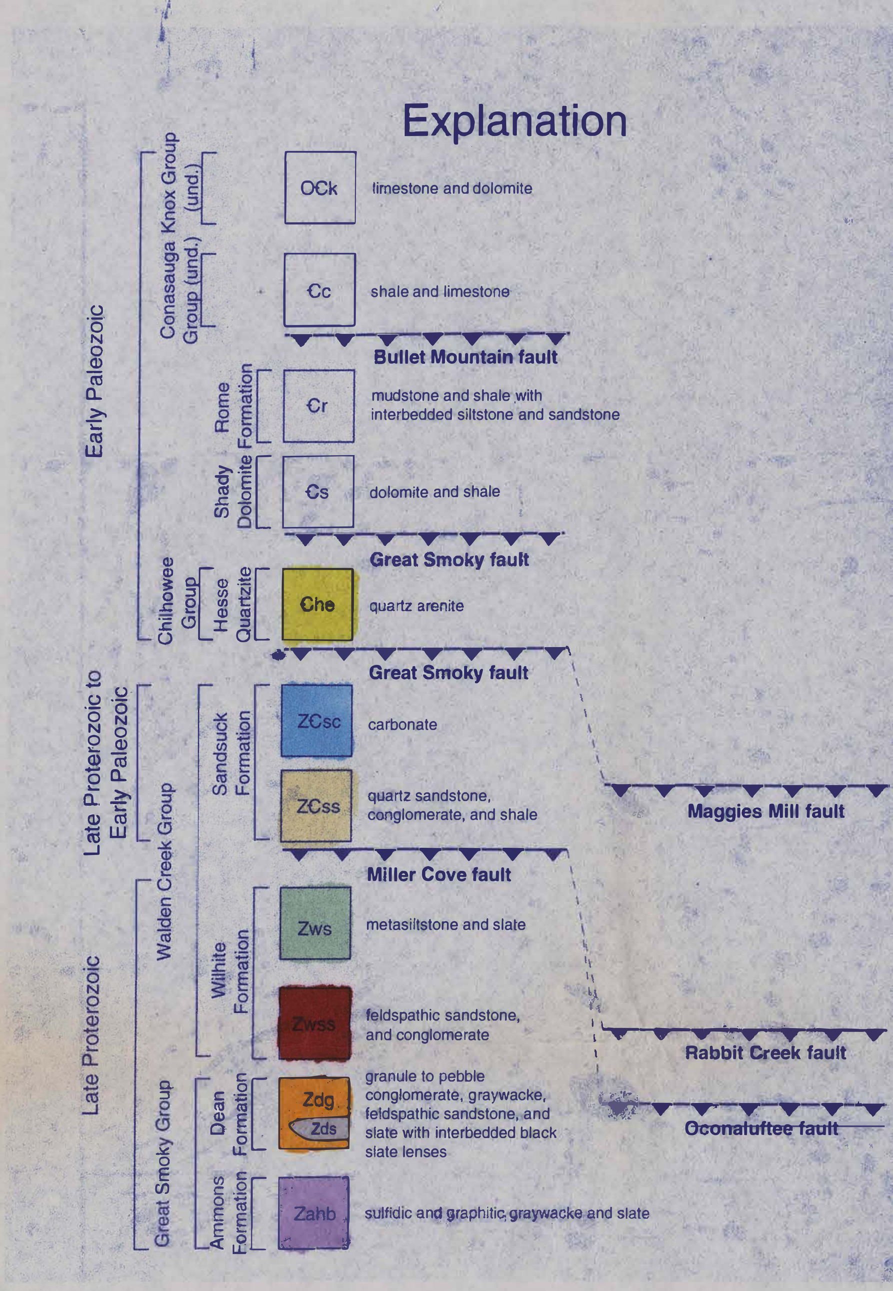

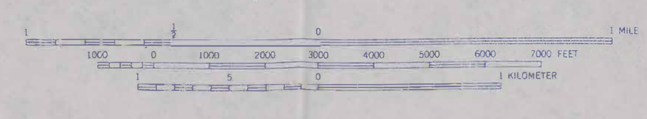

Scale 1:24,000

Location Map and Index to 7.5-Minute Quadrangles

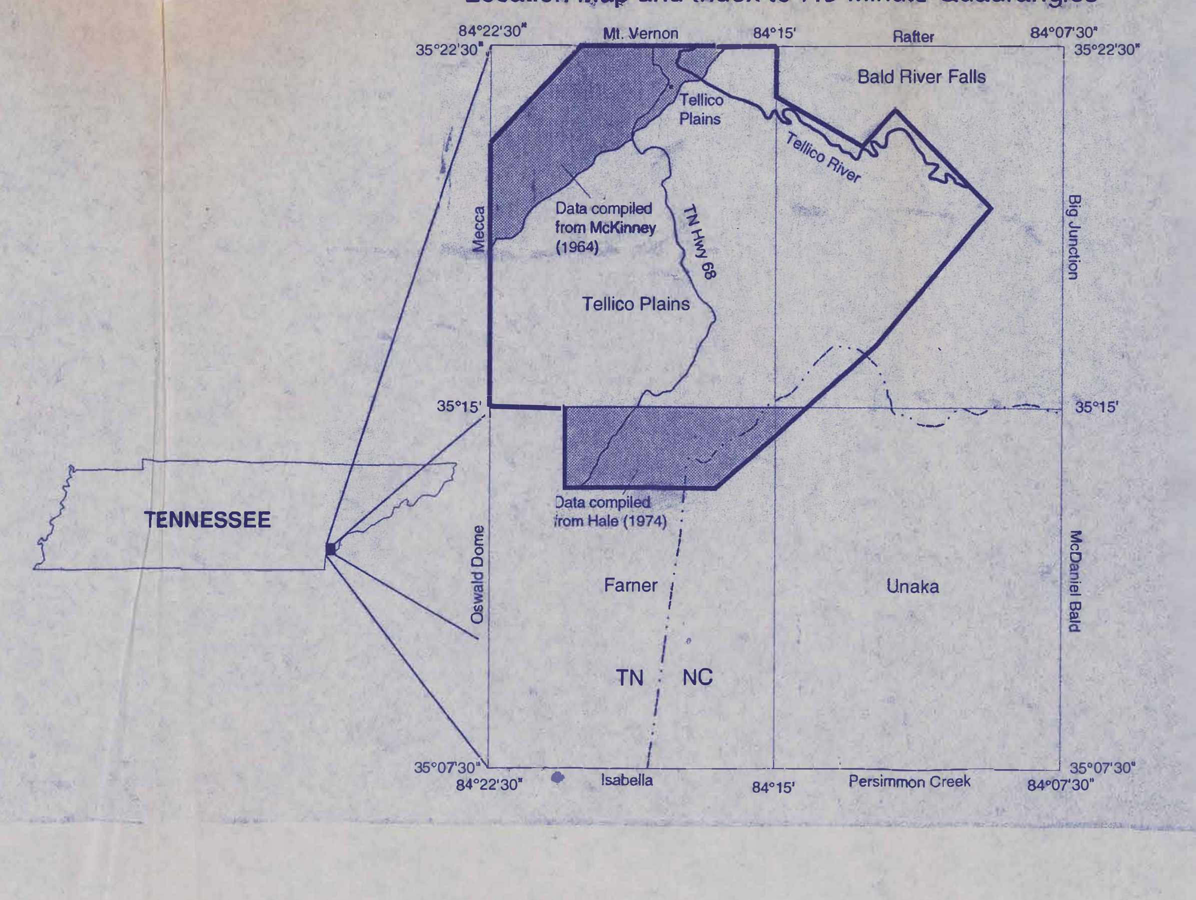

PLATE II
Station Map

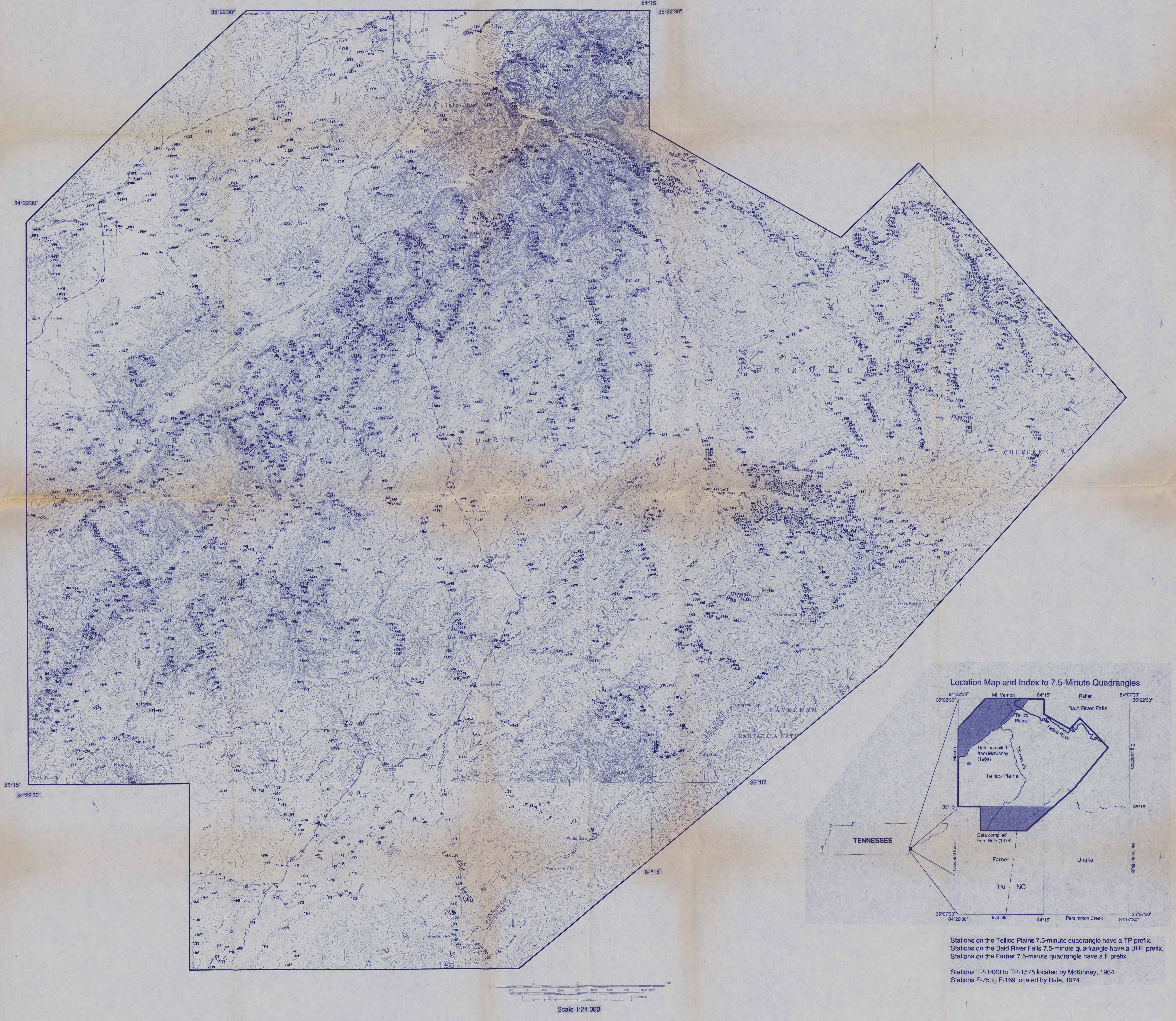

Scale 1:24,000

Stations on the Tellico Plains 7.5-minute quadrangle have a TP prefix.
Stations on the Bald River Falls 7.5-minute quadrangle have a BRF prefix.
Stations on the Farner 7.5-minute quadrangle have a F prefix.

Stations TP-1420 to TP-1575 located by McKinney, 1964.
Stations F-75 to F-169 located by Hale, 1974.

Plate III

Cross sections and retrodeformed sections of the western Blue Ridge Foothills near Tellico Plains, southeasternTennessee and southwestern North Carolina

Cross section A-A'

Line-balanced Valley and Ridge footwall strata, and line- and area-retrodeformed western Blue Ridge hanging-wall strata. X/Z strain ratios as determined by the Rf/φ method.

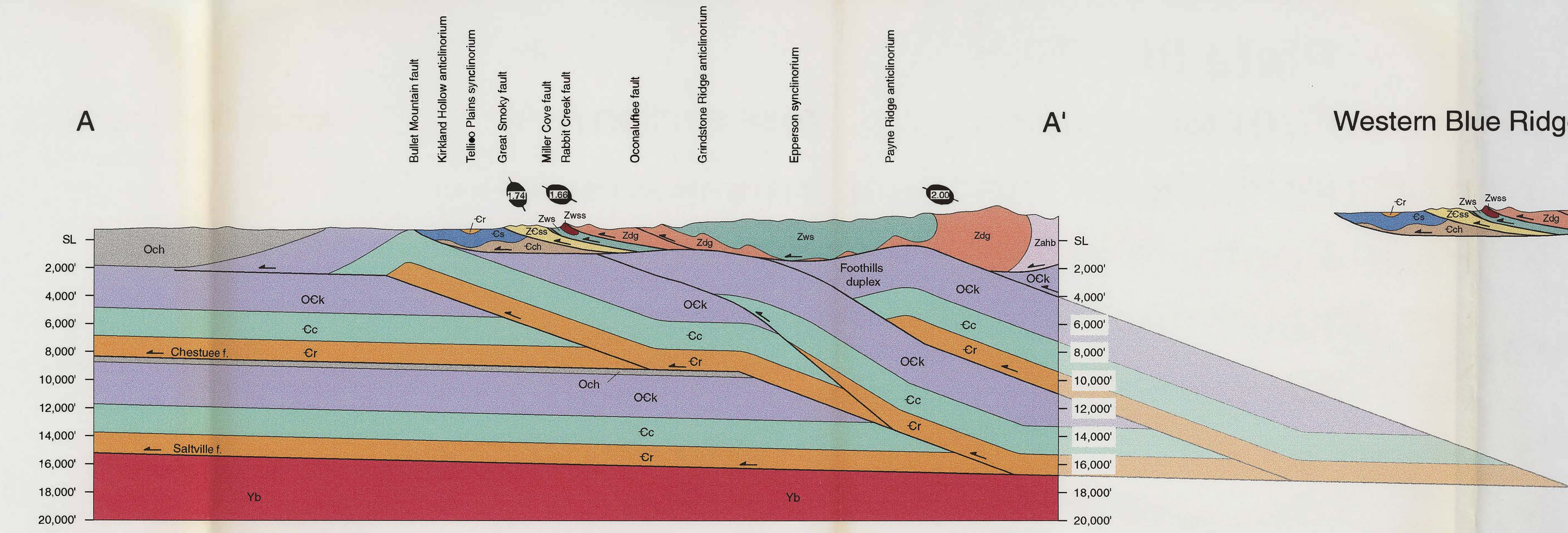

Western Blue Ridge hanging-wall strata, A-A'

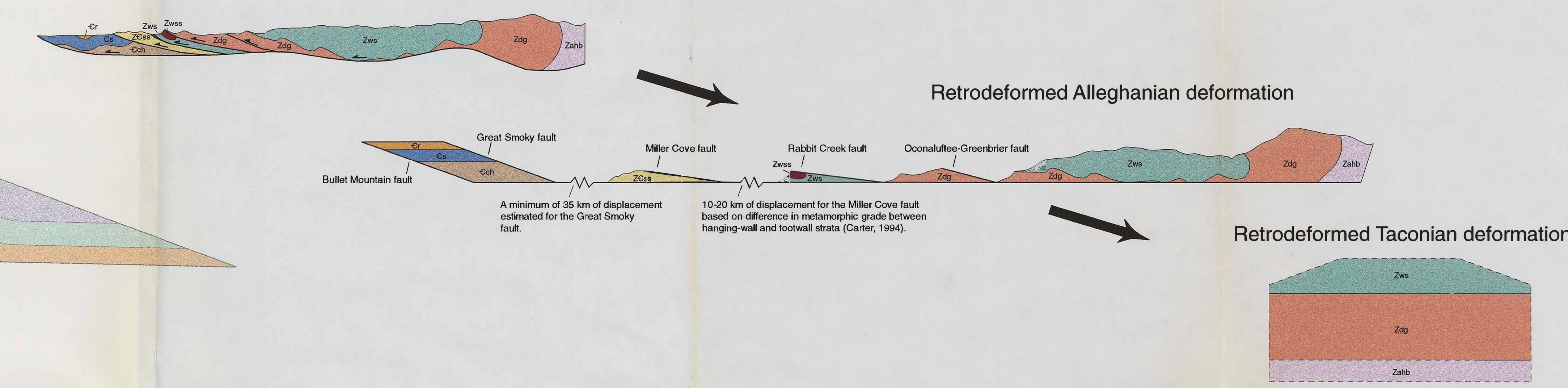

Retrodeformed Valley and Ridge footwall strata, A-A'

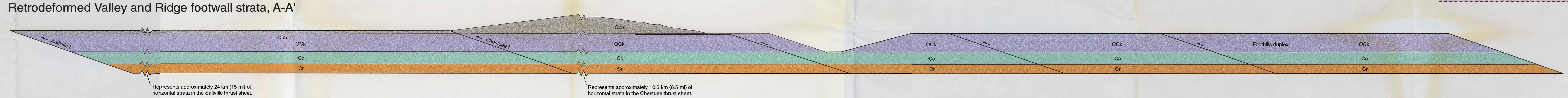

Cross section B-B'

Line-balanced Valley and Ridge footwall strata, and line- and area-retrodeformed western Blue Ridge hanging-wall strata. X/Z strain ratios as determined by the Rf/φ method.

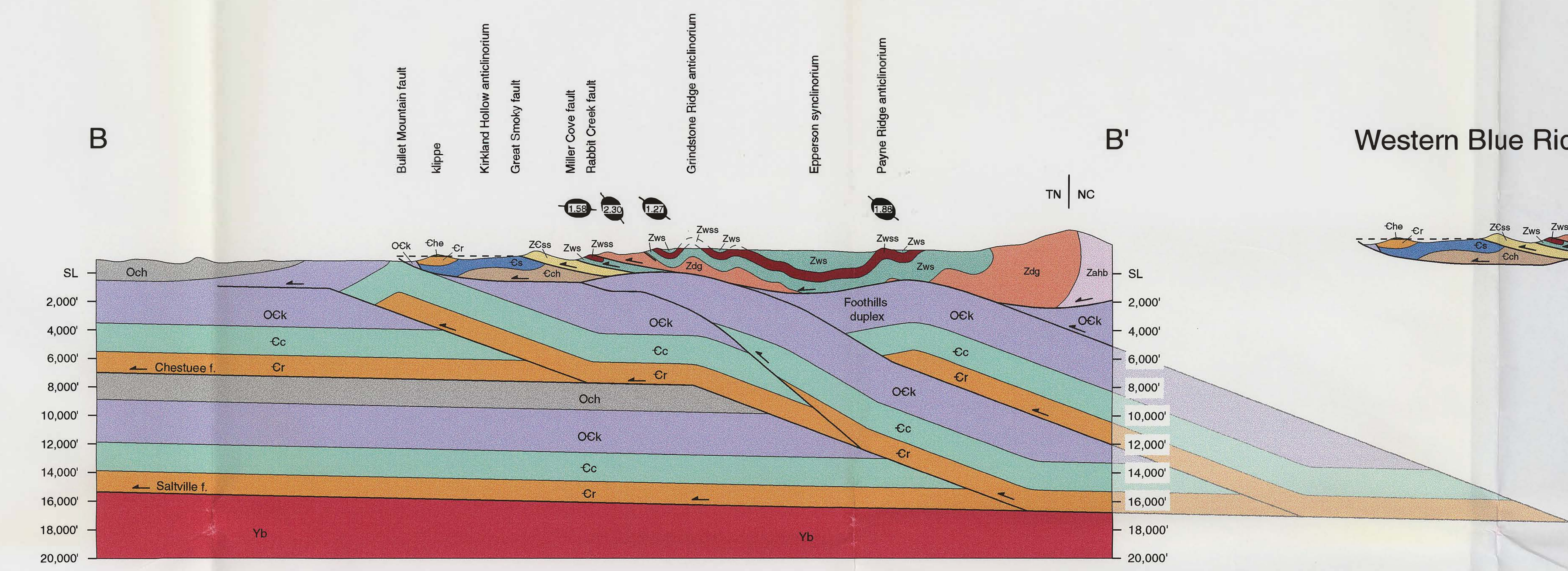

Western Blue Ridge hanging-wall strata, B-B'

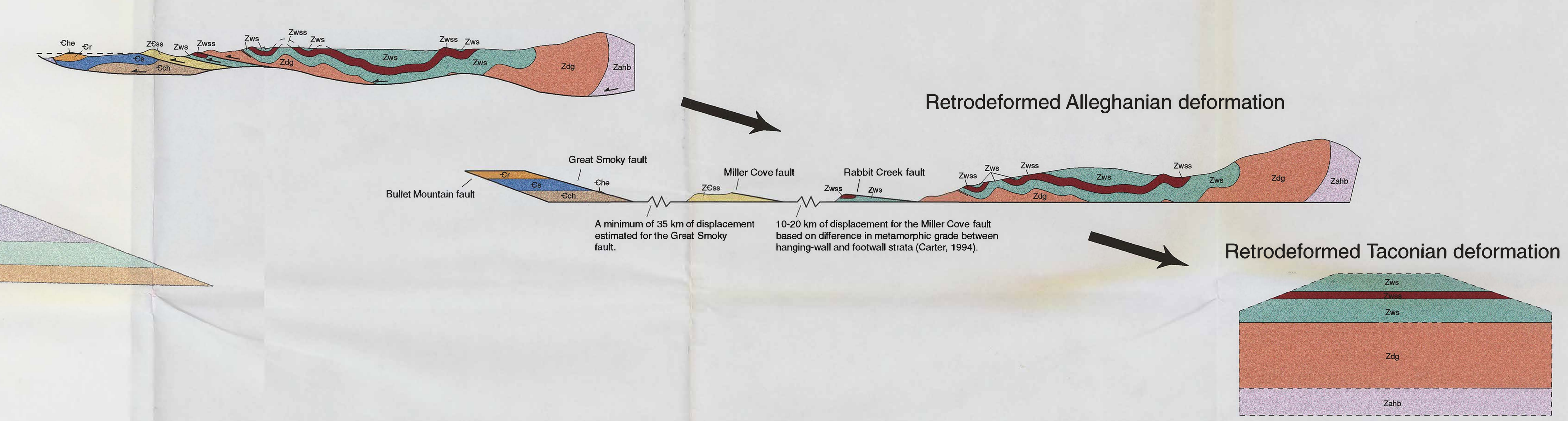

Retrodeformed Valley and Ridge footwall strata, B-B'

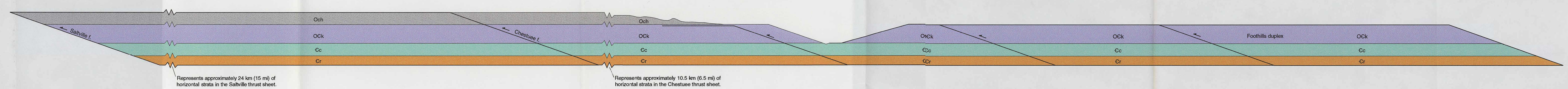

Cross section C-C'

Line-balanced Valley and Ridge footwall strata, and line- and area-retrodeformed western Blue Ridge hanging-wall strata. X/Z strain ratios as determined by the Rf/φ method.

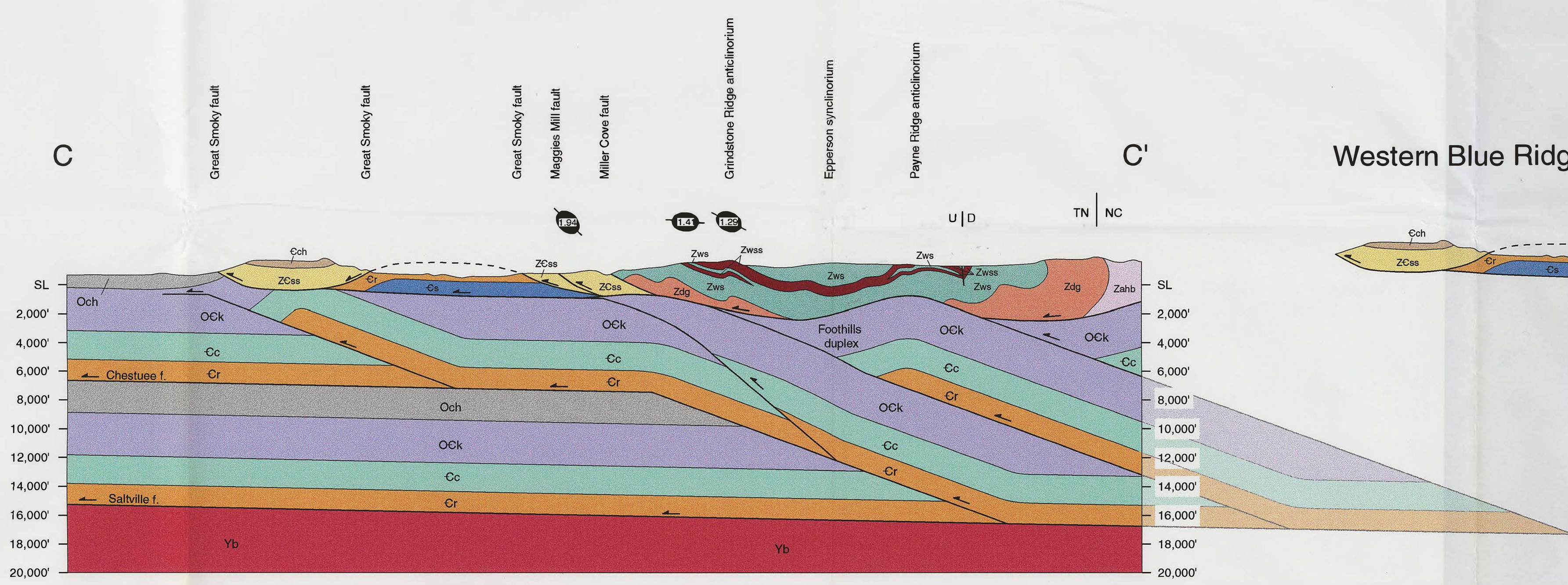

Western Blue Ridge hanging-wall strata, C-C'

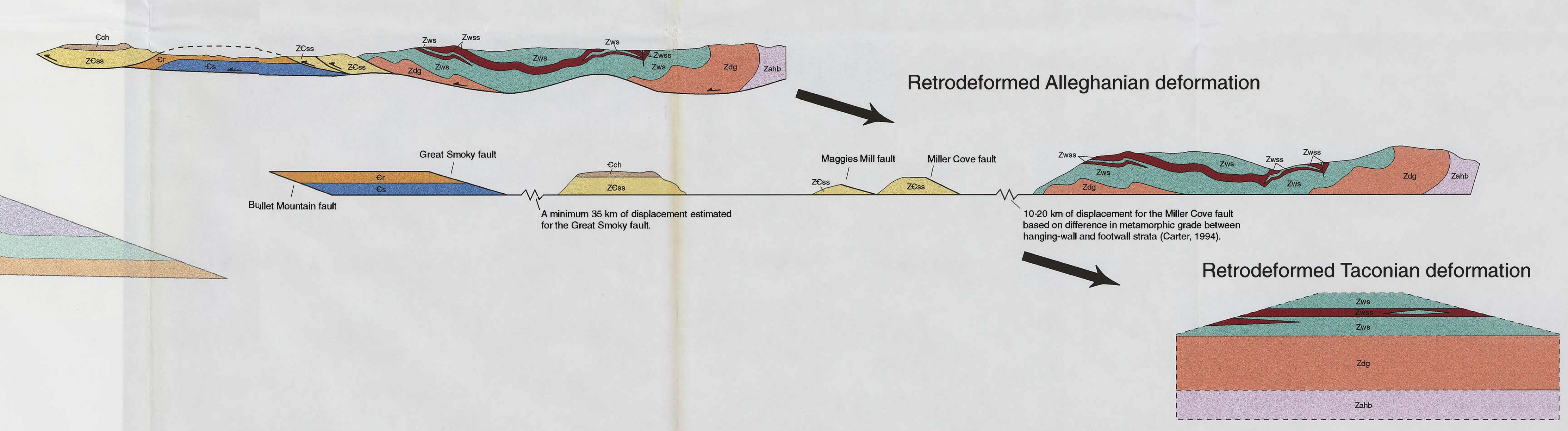

Retrodeformed Valley and Ridge footwall strata, C-C'

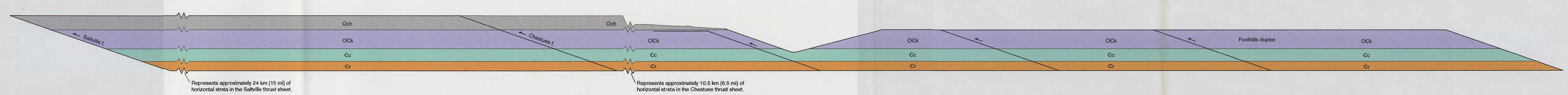

Explanation

Ordovician
- Och — Chickamauga Group
- OCk — Knox Group

Cambrian
- Cc — Conasauga Group
- Cr — Rome Formation
- Shady Dolomite
- Che — Hesse Quartzite
- Cch — Chilhowee Group

Late Proterozoic
- ZCss — Sandsuck Formation - sandstone lithofacies
- Wilhite Formation - sandstone lithofacies
- Zws — Wilhite Formation - metasiltstone lithofacies
- Zdg — Dean Formation
- Zahb — Ammons Formation - Horse Branch member

0 1 2 mi
0 1 2 km
No vertical exaggeration
1:72,000

Plate IIIa
Cross sections

Cross section A-A'

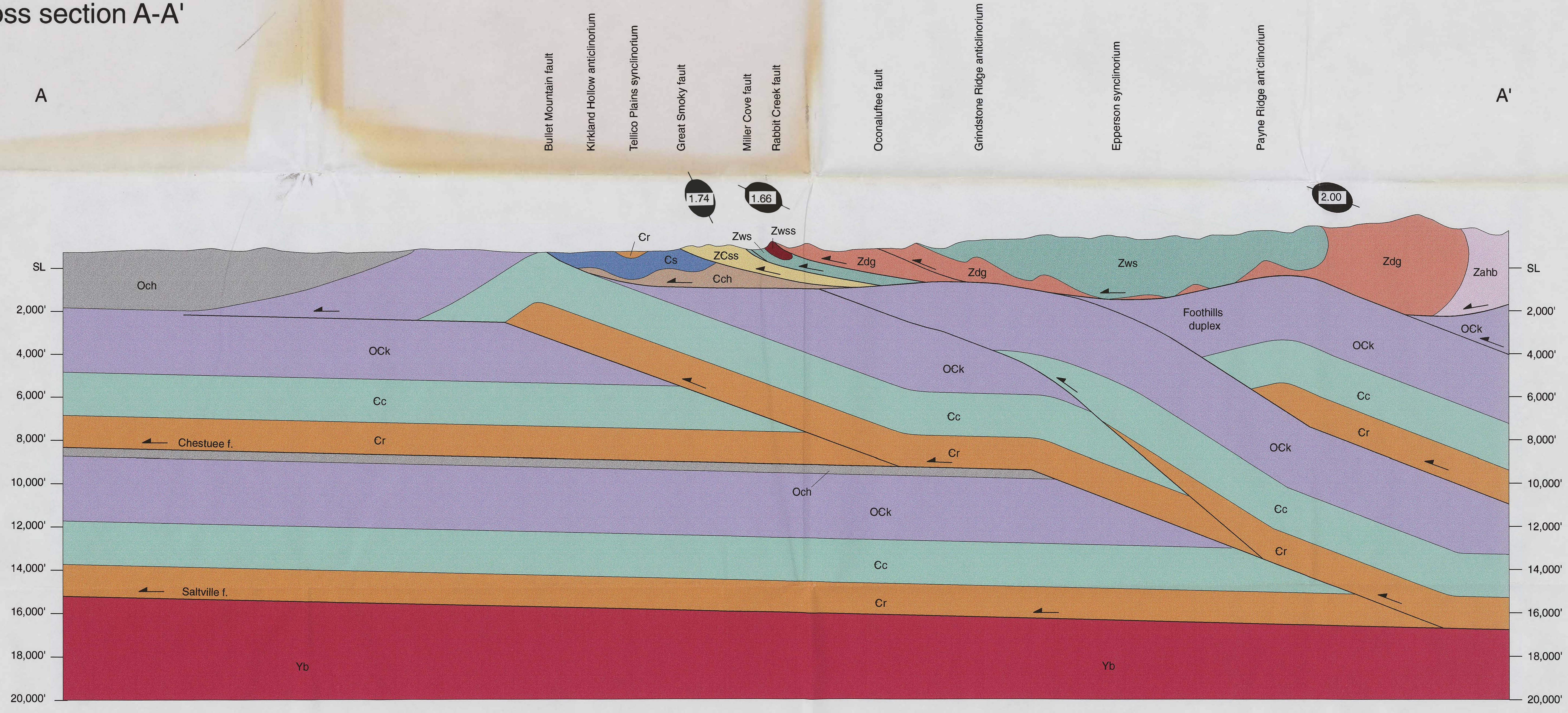

Cross section B-B'

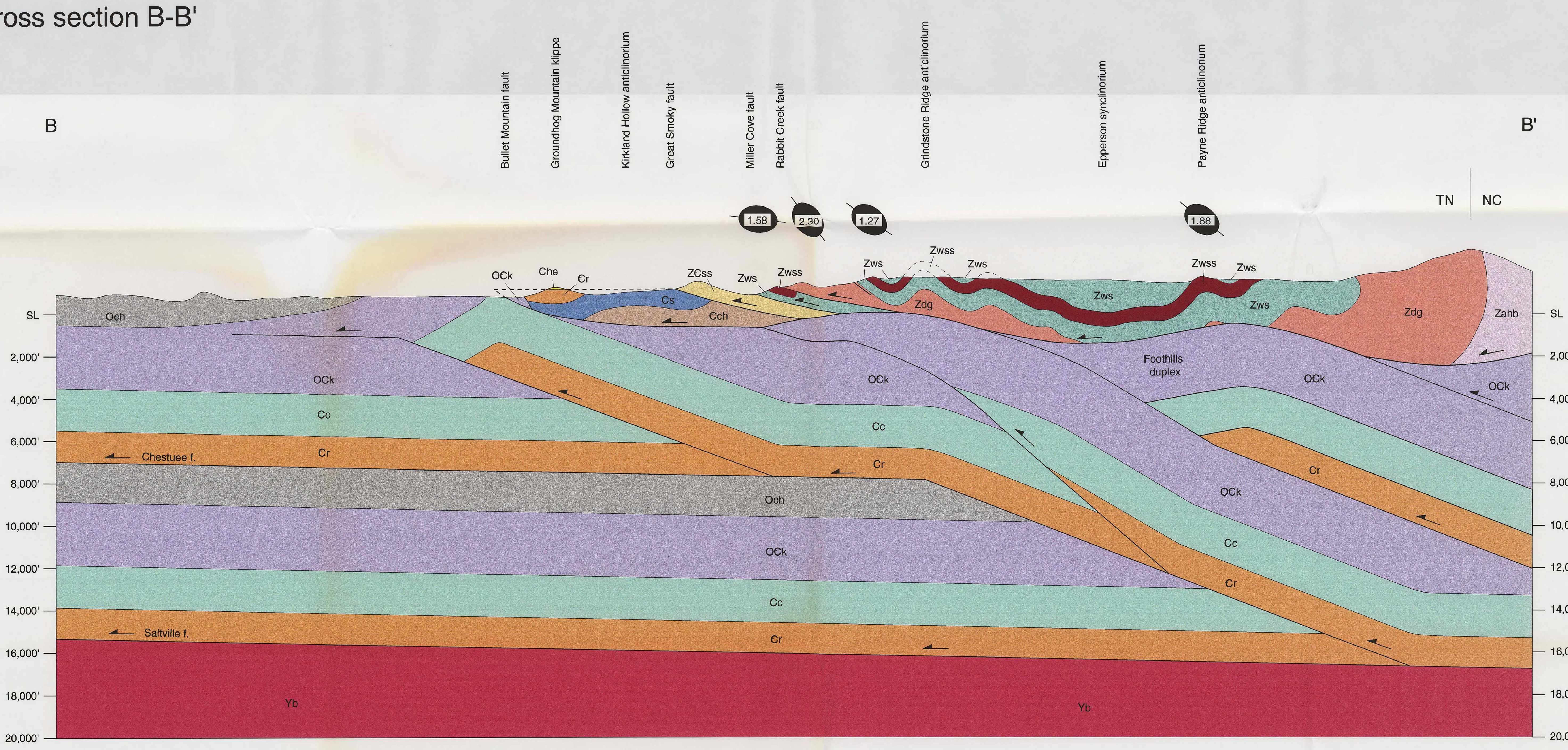

Cross section C-C'

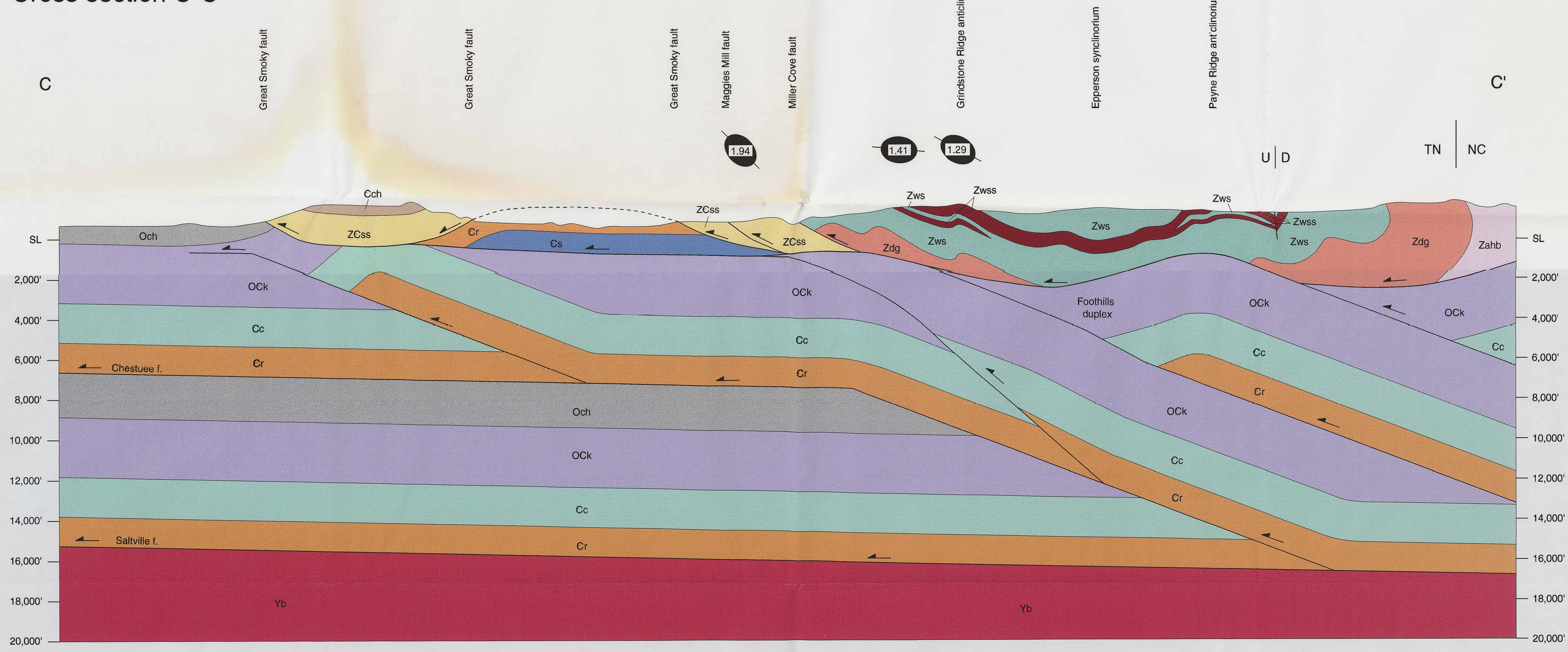

Explanation

Ordovician
- Och — Chickamauga Group
- OCk — Knox Group

Cambrian
- Cc — Conasauga Group
- Cr — Rome Formation
- Shady Dolomite
- Che — Hesse Quartzite
- Cch — Chilhowee Group

Late Proterozoic
- ZCss — Sandsuck Formation - sandstone lithofacies
- Zwss — Wilhite Formation - sandstone lithofacies
- Zws — Wilhite Formation - metasiltstone lithofacies
- Zdg — Dean Formation
- Zahb — Ammons Formation - Horse Branch Member

Scale: 0 — 1 — 2 mi; 0 — 1 — 2 km

No vertical exaggeration

Note: These cross sections are reduced slightly to 1:31,680 from the 1:24,000 map scale.

PLATE IV
Surficial deposits

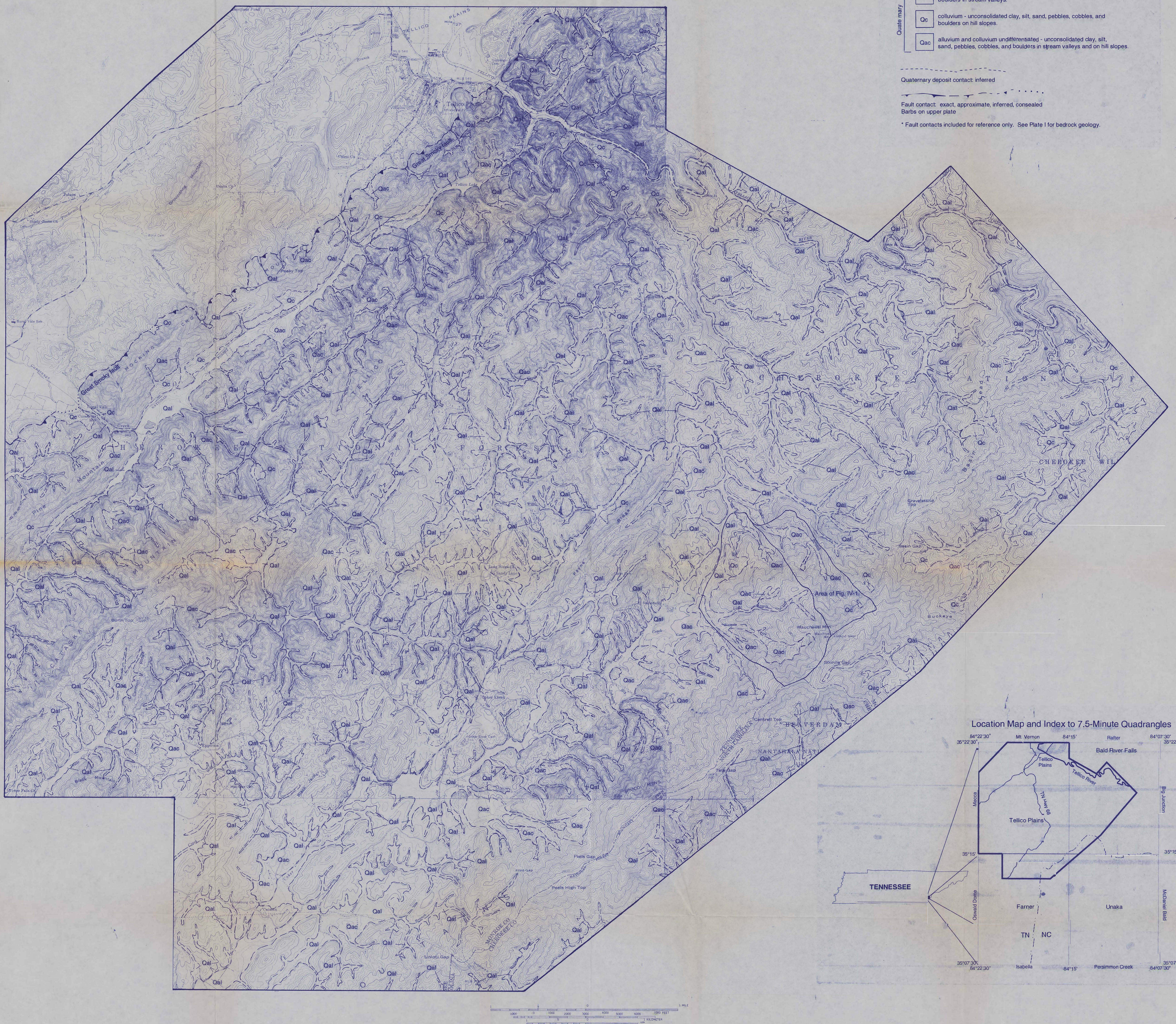

Explanation

Quaternary

- **Qal** alluvium - unconsolidated clay, silt, sand, pebbles, cobbles, and boulders in stream valleys.
- **Qc** colluvium - unconsolidated clay, silt, sand, pebbles, cobbles, and boulders on hill slopes.
- **Qac** alluvium and colluvium undifferentiated - unconsolidated clay, silt, sand, pebbles, cobbles, and boulders in stream valleys and on hill slopes.

Quaternary deposit contact: inferred

Fault contact: exact, approximate, inferred, consealed
Barbs on upper plate

* Fault contacts included for reference only. See Plate I for bedrock geology.